

DOT/FAA/AR-01/55

Office of Aviation Research  
Washington, D.C. 20591

# Probabilistic Design of Damage Tolerant Composite Aircraft Structures

January 2002

Final Report

This document is available to the U.S. public  
through the National Technical Information  
Service (NTIS), Springfield, Virginia 22161.



U.S. Department of Transportation  
Federal Aviation Administration

20020322 146

## NOTICE

This document is disseminated under the sponsorship of the U.S. Department of Transportation in the interest of information exchange. The United States Government assumes no liability for the contents or use thereof. The United States Government does not endorse products or manufacturers. Trade or manufacturer's names appear herein solely because they are considered essential to the objective of this report. This document does not constitute FAA certification policy. Consult your local FAA aircraft certification office as to its use.

This report is available at the Federal Aviation Administration William J. Hughes Technical Center's Full-Text Technical Reports page: [actlibrary.tc.faa.gov](http://actlibrary.tc.faa.gov) in Adobe Acrobat portable document format (PDF).

**Technical Report Documentation Page**

|   |   |   |           |
|---|---|---|-----------|
| 1. Report No.<br><br>DOT/FAA/AR-01/55   | 2. Government Accession No.   | 3. Recipient's Catalog No.  |           |
| 4. Title and Subtitle<br><br>PROBABILISTIC DESIGN OF DAMAGE TOLERANT COMPOSITE AIRCRAFT STRUCTURES  |   | 5. Report Date<br><br>January 2002  |           |
| 7. Author(s)<br><br>A. Ushakov, A. Stewart, I. Mishulin, and A. Pankov  |   | 6. Performing Organization Code   |           |
| 9. Performing Organization Name and Address<br><br>Central Aerohydrodynamic Institute (TsAGI)<br>Zukowski<br>Russia   |   | 8. Performing Organization Report No.                                       |           |
| 12. Sponsoring Agency Name and Address<br><br>U.S. Department of Transportation<br>Federal Aviation Administration<br>Office of Aviation Research<br>Washington, DC 20591   |   | 10. Work Unit No. (TRAIS)<br><br>11. Contract or Grant No.<br><br>NAT-I3413 |           |
| 15. Supplementary Notes<br><br>The FAA William J. Hughes Technical Center Technical Monitor was Mr. Peter Shyprykevich.   |   | 13. Type of Report and Period Covered<br><br>Final Report                   |           |
| 16. Abstract<br><br>The present document describes the efforts under Memorandum of Cooperation between the Federal Aviation Administration (FAA), USA, and the Central Aero-Hydrodynamic Institute (TsAGI), Russian Federation. Under this effort, a methodology for calculating reliability of composite aircraft structures was developed and is contained in software Probabilistic Design of Damage Tolerant Composite Structures (ProDeCompoS). In addition, background data culled from Russian usage of composite aircraft structures was compiled to use with ProDeCompoS. This includes statistical data of damage occurrence, effectiveness of repair, and test data and computational methods to determine residual strength for damaged composite laminate. |   |   |           |
| The methodology and use of ProDeCompoS was demonstrated by calculating the reliability of four composite components: a highly maneuverable MiG-29 fin, a transport TU-204 aileron, a business jet Lear Fan-2100 wing, and an aerobatic SU-29 wing.  |   |   |           |
| To evaluate the robustness of ProDeCompoS, a method to estimate of spread and confidence intervals for failure probability was developed and used in the analysis of the MiG-29 fin. The analysis showed that the reliability estimates are quite stable for the range of expected variations of input data.  |   |   |           |
| 17. Key Words<br><br>Composites, Probabilistic design, Damage tolerance,<br>Durability, Repair  | 18. Distribution Statement<br><br>This document is available to the public through the National Technical Information Service (NTIS) Springfield, Virginia 22161. |   |           |
| 19. Security Classif. (of this report)<br><br>Unclassified  | 20. Security Classif. (of this page)<br><br>Unclassified  | 21. No. of Pages<br><br>200   | 22. Price |

## TABLE OF CONTENTS

|  | <b>Page</b> |
|--|-------------|
| <b>EXECUTIVE SUMMARY</b>   | <b>xvii</b> |
| <b>1. INTRODUCTION</b>   | <b>1-1</b>  |
| 1.1 Occurrence of Random Damage in Composite Aircraft Structures—<br>Statistical Data              | 1-3         |
| 1.1.1 Classification of Mechanical Impacts and In-Service Damage Types                             | 1-4         |
| 1.1.2 Rate of Occurrence of In-Service Damage in Aircraft Structures<br>Made of Polymer Composites | 1-5         |
| 1.1.3 Comparing With Statistical Data From Other Countries   | 1-18        |
| 1.1.4 Initial Data for Analyzing Wing Damage Rates of Lear Fan 2100<br>and SU-29                   | 1-20        |
| 1.1.5 Conclusion   | 1-23        |
| <b>2. EFFICIENCY OF REPAIRS ON AIRFRAMES MADE OF COMPOSITES</b>                                    | <b>2-1</b>  |
| 2.1 Repair of Composite Skin   | 2-1         |
| 2.2 Data From Experiments on Recovering the Skin Strength by Repair                                | 2-2         |
| 2.2.1 Bond-Based Repair With Patches (Batch 1)   | 2-3         |
| 2.2.2 Prepreg-Based Repair for CFRP Skin (Batch 1)   | 2-4         |
| 2.2.3 Methods for Repairing the Polymer Composite Materials in Field<br>Conditions (Batch 2)       | 2-5         |
| 2.3 Repair of Honeycomb Sandwich Structure   | 2-8         |
| 2.3.1 Repairing Group 1 Damage   | 2-8         |
| 2.3.2 Repairing Group 2 Damage   | 2-8         |
| 2.3.3 Repairing Group 3 Damage   | 2-9         |
| 2.4 Experimental Data on Recovering the Sandwich Structure Specimen<br>Strength After Repair       | 2-10        |
| 2.4.1 Shear Strength Test Results  | 2-10        |
| 2.4.2 Results of Testing Under In-Plane Compression  | 2-12        |
| 2.4.3 Results of Testing in Bending  | 2-12        |

|     |  |      |
|-----|--|------|
| 2.5 | Conclusions  | 2-13 |
| 3.  | EXPERIMENTAL DATA ON THE INFLUENCE OF DEFECTS ON RESIDUAL STRENGTH OF COMPOSITE SKIN       | 3-1  |
| 3.1 | Uniaxial Tension of Skin With Circular Hole—The Two-Parameter Model                        | 3-1  |
| 3.2 | Biaxial Tension of Skin With Circular Hole—Residual Strength Criterion                     | 3-5  |
| 3.3 | Uniaxial Tension of Skin With Rectangular Cutout Whose Corners are Rounded With Radius $r$ | 3-7  |
| 3.4 | Uniaxial Compression of Skin With Circular Hole  | 3-8  |
| 3.5 | The Effect of Stress Concentration on Residual Strength                                    | 3-9  |
| 4.  | COMPUTING THE RESIDUAL STRENGTH OF UNSTIFFENED COMPOSITE SKIN                              | 4-1  |
| 4.1 | Algorithm for Evaluating a Skin With Through Damage  | 4-1  |
| 4.2 | Method for Analyzing Compression-Loaded Components With Delamination                       | 4-2  |
| 5.  | METHOD FOR ANALYZING WING STRENGTH   | 5-1  |
| 5.1 | Beam Model Analysis Technique  | 5-1  |
| 5.2 | Computation of Stiffness and Strength of Composite Panels                                  | 5-5  |
| 5.3 | Panel Buckling Critical Loads  | 5-8  |
| 5.4 | Local Buckling Critical Loads for Panel Structures   | 5-9  |
| 6.  | MONTE-CARLO SIMULATION MODULE  | 6-1  |
| 6.1 | General Statement of the Problem   | 6-1  |
| 6.2 | Description of Stressed State of Structure—Finite Set of Loading Cases                     | 6-1  |
| 6.3 | Description of Loads   | 6-2  |
| 6.4 | Description of Defects/Damages   | 6-4  |
| 6.5 | Description of Inspections   | 6-5  |
| 6.6 | Description of Repairs   | 6-6  |
| 6.7 | Methods of Failure Probability Estimation  | 6-6  |
| 6.8 | One Life Simulation  | 6-6  |

|        |  |      |
|--------|--|------|
| 6.9    | The Data Preparation Program PreDaMC for Statistical Simulation<br>(User's Manual) | 6-8  |
| 6.9.1  | Starting the Program—Termination of Work   | 6-8  |
| 6.9.2  | Data Format  | 6-9  |
| 6.9.3  | Set Name Page  | 6-10 |
| 6.9.4  | Load&T Page  | 6-11 |
| 6.9.5  | Damage Page  | 6-14 |
| 6.9.6  | Detection Page   | 6-15 |
| 6.9.7  | Strength Page  | 6-17 |
| 6.9.8  | Repair Page  | 6-18 |
| 6.9.9  | Inspections Page   | 6-20 |
| 6.9.10 | Strength (T) Page  | 6-21 |
| 6.9.11 | Monte Carlo Page   | 6-22 |
| 7.     | DATABASES FOR ProDeCompoS (USER'S MANUAL)  | 7-1  |
| 7.1    | TESTS Database (User's Manual)   | 7-2  |
| 7.1.1  | Requirements for Hardware and System Software Installation                         | 7-2  |
| 7.1.2  | Terms and Definitions  | 7-2  |
| 7.1.3  | Contents of the Database   | 7-3  |
| 7.1.4  | Functions of TESTS Database  | 7-3  |
| 7.1.5  | User's Proficiency Requirements  | 7-4  |
| 7.1.6  | Starting the Program—Termination of Work   | 7-4  |
| 7.1.7  | Main Menu of TESTS Database  | 7-5  |
| 7.1.8  | Data Representation Format   | 7-6  |
| 7.1.9  | Entering the Data—Data Editing Mode  | 7-7  |
| 7.1.10 | Saving Data to a File  | 7-8  |
| 7.1.11 | List of Data in TESTS Database   | 7-9  |
| 7.2    | MATERIALS Database (User's Manual)   | 7-13 |
| 7.2.1  | Requirements for Hardware and System Software Installation                         | 7-14 |
| 7.2.2  | Terms and Definitions Data Structures  | 7-14 |
| 7.2.3  | Contents of Database   | 7-14 |
| 7.2.4  | Functions of MATERIALS Database  | 7-15 |
| 7.2.5  | User's Proficiency Requirements  | 7-15 |
| 7.2.6  | Starting the Program—Termination of Work   | 7-16 |
| 7.2.7  | Main Menu  | 7-16 |
| 7.2.8  | Data Representation Format   | 7-17 |
| 7.2.9  | Entering the Data—Data Editing Mode  | 7-17 |
| 7.2.10 | List of Data in MATERIALS Database   | 7-18 |
| 7.3    | AIRCRAFT Database (User's Manual)  | 7-20 |
| 7.3.1  | Requirements for Hardware and System Software Installation                         | 7-20 |

|        |  |      |
|--------|--|------|
| 7.3.2  | Terms and Definitions                                    | 7-21 |
| 7.3.3  | Contents of Database                                     | 7-21 |
| 7.3.4  | Functions of the AIRCRAFT Database                       | 7-21 |
| 7.3.5  | User's Proficiency Requirements                          | 7-22 |
| 7.3.6  | Starting the Program—Termination of Work                 | 7-22 |
| 7.3.7  | Main Menu  | 7-22 |
| 7.3.8  | Data Representation Format                               | 7-24 |
| 7.3.9  | Entering the Data—Data Editing Mode                      | 7-24 |
| 7.3.10 | List of Data in AIRCRAFT Database                        | 7-25 |
| 7.3.11 | Saving Data to Clipboard                                 | 7-27 |
| 8.     | SYNTHESIS OF DATA IN THE FORM REQUIRED BY ProDeCompoS    | 8-1  |
| 8.1    | MIG-29 Composite Fin Failure Probability Estimation      | 8-1  |
| 8.1.1  | Mechanical Properties of Materials                       | 8-1  |
| 8.1.2  | Mechanical Properties of Skin                            | 8-1  |
| 8.1.3  | Fin Loads  | 8-2  |
| 8.1.4  | Temperature Cumulative Probability Function              | 8-4  |
| 8.1.5  | Defect and Damage Exceedance                             | 8-6  |
| 8.1.6  | Damage   | 8-6  |
| 8.1.7  | Defects  | 8-7  |
| 8.1.8  | Strength Degradation Function for Damaged Skin           | 8-8  |
| 8.1.9  | Probability of Damage Detection                          | 8-10 |
| 8.1.10 | Repairs  | 8-12 |
| 8.1.11 | Static Strength vs Temperature                           | 8-13 |
| 8.1.12 | Result of Calculating the MIG-29 Fin Failure Probability | 8-14 |
| 8.2    | TU-204 Composite Aileron Failure Probability Estimation  | 8-14 |
| 8.2.1  | Aileron Structure Described                              | 8-14 |
| 8.2.2  | Aileron Loads  | 8-16 |
| 8.2.3  | Aileron Strength   | 8-18 |
| 8.2.4  | Mechanical Characteristics of Materials                  | 8-18 |
| 8.2.5  | Aileron Skin Load-Carrying Capacity                      | 8-20 |
| 8.2.6  | Scatter of Mechanical Properties of Materials            | 8-21 |
| 8.2.7  | Strength Degradation Function for Damaged Skin           | 8-21 |
| 8.2.8  | Damage Occurrences                                       | 8-22 |
| 8.2.9  | Repairs  | 8-24 |

|        |   |      |
|--------|---|------|
| 8.2.10 | Results of Calculating the TU-204 Aileron Fracture Probability<br>Within the ProDeCompoS Methodology  | 8-24 |
| 8.2.11 | Parametric Studies Based on TU-204 Aileron Example  | 8-25 |
| 8.2.12 | Uncertainty Due to Load Extrapolation   | 8-25 |
| 8.2.13 | Extent of Damage  | 8-26 |
| 8.2.14 | Estimates for Various Service Life Duration   | 8-26 |
| 8.2.15 | The Influence of Inspection Schedule  | 8-27 |
| 8.2.16 | The Effect of Repair Quality  | 8-28 |
| 8.3    | Lear Fan-2100 Wing Failure Probability Estimation   | 8-28 |
| 8.3.1  | Airplane Under Consideration  | 8-28 |
| 8.3.2  | Spectra Loading   | 8-29 |
| 8.3.3  | Critical Areas  | 8-31 |
| 8.3.4  | Damage Occurrences  | 8-32 |
| 8.3.5  | Residual Strength   | 8-33 |
| 8.3.6  | Residual Strength Degradation of Damaged Panels   | 8-36 |
| 8.3.7  | Probability of Damage Detection   | 8-40 |
| 8.3.8  | Repairs   | 8-40 |
| 8.3.9  | Lear Fan Wing Box Analysis/Results  | 8-40 |
| 8.4    | Sukhoi SU-29 Composite Wing Failure Probability Estimation  | 8-41 |
| 8.4.1  | Airplane Under Consideration  | 8-41 |
| 8.4.2  | Spectra Loading   | 8-42 |
| 8.4.3  | Critical Areas  | 8-43 |
| 8.4.4  | Damage Occurrences  | 8-43 |
| 8.4.5  | Residual Strength   | 8-45 |
| 8.4.6  | Residual Strength Degradation of Damaged Panels   | 8-47 |
| 8.4.7  | Probability of Damage Detection   | 8-49 |
| 8.4.8  | Repairs   | 8-49 |
| 8.4.9  | SU-29 Wing Box Analysis/Results   | 8-50 |
| 9.     | ESTIMATES OF RELIABILITY OF FAILURE PROBABILITY<br>CALCULATION ON THE BASIS OF STATISTICAL SIMULATION | 9-1  |
| 9.1    | Estimate of Failure Probability Computation Reliability for a Particular<br>Statistical Model         | 9-1  |
| 9.1.1  | Confidence Intervals; Determining the Necessary Number of<br>Realizations in Simulation               | 9-1  |

|       |   |      |
|-------|---|------|
| 9.1.2 | Establishing the Parameters of Probabilistic Model  | 9-3  |
| 9.2   | Reliability of Failure Probability Computation Taking Into Account of Variations in Parameters of Statistical Model                       | 9-5  |
| 9.2.1 | Scatter Caused by Selection of the Initial Value for Beginning the Simulation   | 9-5  |
| 9.2.2 | Variability in Failure Probability Due to Uncertainty in Load-Stress Transfer Coefficient   | 9-7  |
| 9.2.3 | Variability in Failure Probability Due to Uncertainty in the Structural-Size Coefficient  | 9-9  |
| 9.2.4 | Variability in Failure Probability Due to Uncertainty in Static Strength  | 9-12 |
| 9.2.5 | Variability in Failure Probability Due to Uncertainties in the Coefficients of Load-Stress Transfer, Structural Size, and Static Strength | 9-14 |
| 10.   | CONCLUSIONS   | 10-1 |
| 11.   | REFERENCES  | 11-1 |

## LIST OF FIGURES

| Figure  | Page |
|---|------|
| 1-1 Chart of ProDeCompoS Software   | 1-2  |
| 1-2 Types of In-Service Damage  | 1-6  |
| 1-3 In-Service Damages That Occurred Upon Mechanical Impacts and Were Found by Inspectors—Histogrammatic Representation | 1-8  |
| 1-4 Exceedance Intensity of Damage to MIG-29 Wing Leading Edge  | 1-10 |
| 1-5 Exceedance Intensity of Damage to MIG-29 Vertical Stabilizer Skin   | 1-11 |
| 1-6 Exceedance Intensity of Damage to MIG-29 Air Inlet Shell  | 1-11 |
| 1-7 Exceedance Intensity of Damage to MIG-29 Engine Fairing   | 1-12 |
| 1-8 Exceedance Intensity of Damage to MIG-29 Lower-Vault Panel  | 1-12 |
| 1-9 Exceedance Intensity of Damage to MIG-29—Averaged Data  | 1-13 |
| 1-10 Exceedance Intensity of Damage to SU-27 Stabilizer Actuator Fairing  | 1-13 |
| 1-11 Exceedance Intensity of Damage to SU-27 Fairing of Nose Strut Wheel  | 1-14 |
| 1-12 Exceedance Intensity of Damage to SU-25 Nose Landing Gear Door   | 1-14 |
| 1-13 Exceedance Intensity of Damage to L-1011 Wing/Fuselage Fairing   | 1-15 |
| 1-14 Exceedance Intensity of Damage to AN-124 Landing Gear Door   | 1-15 |
| 1-15 Exceedance Intensity of Damage to AN-124 Cargo Bay Door  | 1-16 |
| 1-16 Exceedance Intensity of Damage—Exponential Approximation   | 1-21 |
| 1-17 Exceedance Intensity of Damage—Polynomial Approximation  | 1-21 |
| 1-18 Exceedance Intensity of Damage   | 1-22 |
| 2-1 Prepreg-Based Repair  | 2-2  |
| 2-2 Repair With the Use of Patches  | 2-2  |
| 2-3 Repair Effectiveness of Various Methods   | 2-7  |
| 2-4 Repairing a Delamination Area   | 2-8  |
| 2-5 Repairing a Partial Through Hole  | 2-9  |

|      |  |      |
|------|--|------|
| 2-6  | Repairing a Through Hole   | 2-9  |
| 2-7  | Crack Growth During Fatigue Loading  | 2-11 |
| 3-1  | The Two-Parameter Model for Evaluating Stress Concentration                        | 3-2  |
| 3-2  | Comparing Theoretical and Experimental Data for Uniaxial Tension                   | 3-5  |
| 3-3  | Residual Strength of Plates Subjected to Biaxial Stress                            | 3-6  |
| 3-4  | Results of Testing the Tubular Specimens   | 3-7  |
| 3-5  | Residual Strength of Specimens Under Compression                                   | 3-9  |
| 3-6  | Residual Strength of Plates With Holes and Notches                                 | 3-10 |
| 3-7  | Residual Strength of Plates With Through and Partial Through (Superficial) Defects | 3-10 |
| 4-1  | Model of a Damaged Plate   | 4-1  |
| 4-2  | Delamination in Composite Skin   | 4-2  |
| 4-3  | Delamination Propagation Under Torsion   | 4-6  |
| 5-1  | Beam Model of Idealized Wing Structure   | 5-1  |
| 5-2  | Free-Body Diagram of the Wing Structure  | 5-2  |
| 5-3  | Wing Section for Shear Flow Computation  | 5-4  |
| 6-1  | Finite Element Model of a Structural Element                                       | 6-2  |
| 6-2  | Load Exceedance Curves   | 6-3  |
| 6-3  | Damage Exceedance Curves   | 6-4  |
| 6-4  | Probability of Damage Detection Versus Indentation Size                            | 6-5  |
| 6-5  | The Maximum Loads per Interval, $t_3-t_2$ , Are Generated for All DLC              | 6-7  |
| 6-6  | The Set Name Page  | 6-10 |
| 6-7  | The Load&T Page  | 6-11 |
| 6-8  | The Damage Page  | 6-14 |
| 6-9  | The Detection Page   | 6-16 |
| 6-10 | The Strength Page  | 6-17 |

|      |  |      |
|------|--|------|
| 6-11 | The Repair Page  | 6-19 |
| 6-12 | The Inspections Page   | 6-20 |
| 6-13 | The Strength (T) Page  | 6-21 |
| 6-14 | The Monte Carlo Page   | 6-22 |
| 8-1  | Load Exceedance for Subsonic Loading Case                                | 8-3  |
| 8-2  | Load Exceedance for Supersonic Loading Case                              | 8-3  |
| 8-3  | Temperature Exceedance   | 8-5  |
| 8-4  | Defect and Damage Exceedance   | 8-8  |
| 8-5  | Effect of Indentation Diameter on Residual Strength                      | 8-9  |
| 8-6  | Effect of Through-Thickness Gap on Skin Residual Strength                | 8-10 |
| 8-7  | Probability of Indentation Detection vs Damage Size and Inspection Type  | 8-11 |
| 8-8  | Probability of Gap Detection vs Damage Size and Inspection Type          | 8-12 |
| 8-9  | Effect of Test Temperature on Relative Compression Strength of Specimens | 8-13 |
| 8-10 | Schematic Depiction of TU-204 Aileron                                    | 8-15 |
| 8-11 | Relation Between Aileron Force and Aileron Deflection Angle              | 8-17 |
| 8-12 | TU-204 Aileron Deflection Angle (Load) Exceedance Curve                  | 8-18 |
| 8-13 | Relative Strength of Damaged Skin  | 8-22 |
| 8-14 | Damage Exceedances of AN-124 Landing Gear Door                           | 8-23 |
| 8-15 | Load Exceedance Extrapolation  | 8-25 |
| 8-16 | Failure Probability for Different Levels of Damage Rate                  | 8-26 |
| 8-17 | Failure Probability vs Service Life Duration                             | 8-27 |
| 8-18 | Failure Probability vs Visual Inspection Schedule                        | 8-27 |
| 8-19 | Failure Probability vs Strength Restoration Coefficients                 | 8-28 |
| 8-20 | Maneuver/Gust Spectrum Exceedance Curve                                  | 8-30 |
| 8-21 | Maneuver Spectrum Exceedance Curve (Restricted load factor)              | 8-30 |

|      |  |      |
|------|--|------|
| 8-22 | Extrapolation of Exceedance Curve  | 8-31 |
| 8-23 | Critical Panels on Upper Wing Surface  | 8-32 |
| 8-24 | Critical Panels on Lower Wing Surface  | 8-32 |
| 8-25 | Damage Spectra   | 8-33 |
| 8-26 | Area of Chosen Critical Panels, $\text{m}^2$   | 8-33 |
| 8-27 | Schematic of Panel Under Tensile Load  | 8-36 |
| 8-28 | Relative Strength of Damaged Panels, Lear Fan-2100 (Compression panels)  | 8-37 |
| 8-29 | Relative Wing Residual Strength for Upper Skin Panels With Damage (Compression panels)                         | 8-37 |
| 8-30 | Schematic of Panel With Hole Under Tensile Load  | 8-38 |
| 8-31 | Relative Strength of Damaged Panel of Lear Fan-2100 Wing (Tension panels)                                      | 8-39 |
| 8-32 | Relative Wing Residual Strength for Lower Skin Panels With Damage  | 8-39 |
| 8-33 | Maneuver Spectrum Exceedance Curve   | 8-42 |
| 8-34 | Critical Panels on Upper/Lower Wing Surfaces   | 8-43 |
| 8-35 | Damage Spectra   | 8-44 |
| 8-36 | Area of Chosen Critical Panels, $\text{m}^2$   | 8-45 |
| 8-37 | Loading of Panel   | 8-46 |
| 8-38 | Relative Strength of Damaged Panels, SU-29 (Compression panels)  | 8-48 |
| 8-39 | Loading of Open-Holed Panel  | 8-48 |
| 8-40 | Relative Strength of Damaged Panel of Sukhoi SU-29 Composite Wing (Tension panels)                             | 8-49 |
| 9-1  | Load Exceedance Curve  | 9-4  |
| 9-2  | Load Exceedance Curve With Extrapolation When $P^{lim}$ Cannot Be Exceeded                                     | 9-5  |
| 9-3  | Cumulative Distribution Function of the Failure Probability Due to Uncertainty in Initial Value for Simulation | 9-6  |
| 9-4  | Random Load-Stress Transfer Coefficient and Its Respective Failure Probability vs Number of the Realization    | 9-7  |

|      |  |      |
|------|--|------|
| 9-5  | Relationship Between Failure Probability and Load-Stress Transfer Coefficient  | 9-8  |
| 9-6  | Cumulative Distribution Function of Failure Probability Due to Uncertainty in Load-Stress Transfer Coefficient   | 9-8  |
| 9-7  | Random Structural-Size Coefficient and Its Respective Failure Probability vs Number of the Realization   | 9-9  |
| 9-8  | Relationship Between Failure Probability and Structural-Size Coefficient   | 9-10 |
| 9-9  | Cumulative Distribution Function of Failure Probability Due to Uncertainty in Structural-Size Coefficient (Uniform probability scale)                                  | 9-11 |
| 9-10 | Cumulative Distribution Function of Failure Probability Due to Uncertainty in Structural-Size Coefficient (Normal probability scale)                                   | 9-11 |
| 9-11 | Random Static-Strength Coefficient and the Respective Failure Probability vs Number of the Realization   | 9-12 |
| 9-12 | Relationship Between Failure Probability and Static-Strength Coefficient   | 9-13 |
| 9-13 | Cumulative Distribution Function of Failure Probability Due to Uncertainty in Static-Strength Coefficient (Uniform probability scale)                                  | 9-13 |
| 9-14 | Cumulative Distribution Function of Failure Probability Due to Uncertainty in Static-Strength Coefficient (Normal probability scale)                                   | 9-14 |
| 9-15 | Cumulative Distribution Function of Failure Probability Due to Uncertainties in Load-Stress Transfer, Structural Size, and Static Strength (Uniform probability scale) | 9-15 |
| 9-16 | Cumulative Distribution Function of Failure Probability Due to Uncertainties in Load-Stress Transfer, Structural Size, and Static Strength (Normal probability scale)  | 9-15 |

## LIST OF TABLES

| Table  | Page |
|--|------|
| 1-1 Characteristics of Structural Elements in Inspected Airframes  | 1-7  |
| 1-2 Empirical Exceedances of Damage in Inspected Airframes   | 1-9  |
| 1-3 Empirical Exceedances Intensity  | 1-10 |
| 1-4 Exceedance Intensity—Exponential Approximation $H(2L) = H_0 \cdot e^{-\frac{2L}{b}}$                         | 1-17 |
| 1-5 Exponential Approximation Coefficients $H_0$ and $b$ for the Various Groups                                  | 1-18 |
| 1-6 Damage Type Occurrences Taken From Reference 3   | 1-18 |
| 1-7 Empirical Exceedances of Damages Based on 1,000,000 Flight Hours   | 1-19 |
| 1-8 Comparison of Data   | 1-19 |
| 1-9 Comparing Data for Units With Low Damage Rates   | 1-20 |
| 1-10 Empirical Exceedance Intensity (per 1000 Flight Hours per Square Meter)<br>Adopted for Analyzing SU-29 Wing | 1-22 |
| 1-11 Recommended Values of $H_0$ and $b$   | 1-23 |
| 2-1 Results of Testing Batch 1   | 2-3  |
| 2-2 Results of Testing Batch 2   | 2-5  |
| 2-3 Test Results for Repaired Shear Panels Under Static Load   | 2-10 |
| 2-4 Test Results for Repaired Shear Panels in Fatigue  | 2-11 |
| 2-5 Test Results for Intact and Repaired Panels Under Compressive Loading  | 2-12 |
| 2-6 Test Results for Intact and Repaired Panels Under Bending  | 2-13 |
| 2-7 Strength Restoration Factors (SRF)   | 2-14 |
| 2-8 Estimated Data on Strength Restoration Factor  | 2-14 |
| 3-1 Strength of Panel With Circular Hole   | 3-4  |
| 3-2 Strength of Panels With Rectangular Cutouts  | 3-8  |
| 6-1 List of Input Data Into Data Set and PreDaMC Program Pages   | 6-9  |

|      |  |      |
|------|--|------|
| 8-1  | Lamina Properties of C/Epoxy                                   | 8-1  |
| 8-2  | C/Epoxy Skin Laminate Properties                               | 8-2  |
| 8-3  | Load Exceedance per Life for Subsonic Design Loading Case      | 8-2  |
| 8-4  | Load Exceedance per Life for Supersonic Design Loading Case    | 8-3  |
| 8-5  | Temperature Exceedance for Subsonic Design Loading Case        | 8-5  |
| 8-6  | Temperature Exceedance for Supersonic Design Loading Case      | 8-6  |
| 8-7  | Exceedance for In-Service Indentation Damage                   | 8-6  |
| 8-8  | Exceedance for In-Service Hole + Crack Damage                  | 8-7  |
| 8-9  | Exceedance for Manufacturing Defects Indentation Damage        | 8-7  |
| 8-10 | Exceedance for Manufacturing Defects Hole + Crack Damage       | 8-7  |
| 8-11 | Effect of Indentation Size on Skin Residual Strength           | 8-9  |
| 8-12 | Effect of Gap Size on Skin Residual Strength                   | 8-10 |
| 8-13 | Probability P of Damage Detection for Indentation              | 8-11 |
| 8-14 | Probability of Damage Inspection for Gap                       | 8-12 |
| 8-15 | Restoration Factors for Repairs                                | 8-13 |
| 8-16 | Static Strength Versus Temperature With and Without Cracks     | 8-14 |
| 8-17 | MIG-29 Fin Failure Probability per Life                        | 8-14 |
| 8-18 | Aileron Loads  | 8-17 |
| 8-19 | Statistically Analyzed Data of Testing the KMU-4e Layer        | 8-19 |
| 8-20 | Characteristics of Single-Ply Materials KMU-4e and ORGANIT-10T | 8-20 |
| 8-21 | Mechanical Characteristics of Aileron Skin                     | 8-20 |
| 8-22 | Stresses at Danger Points in Critical Cross Section            | 8-21 |
| 8-23 | Empirical Exceedance Intensity of Damage                       | 8-23 |
| 8-24 | Strength Restoration Factors                                   | 8-24 |
| 8-25 | Failure Probability per Life                                   | 8-24 |

|      |   |      |
|------|---|------|
| 8-26 | Cumulative Number of Occurrences per 15,000 Flight Hours per 1 m <sup>2</sup>                                   | 8-32 |
| 8-27 | Failure Load Factor and Coefficient of Variation for Upper Wing Surface Condition—Symmetrical Upbending         | 8-34 |
| 8-28 | Failure Load Factor and Coefficient of Variation for Lower Wing Surface Condition—Symmetrical Upbending         | 8-35 |
| 8-29 | Relative Residual Strength of Upper Panel vs Damage Size  | 8-36 |
| 8-30 | Relative Residual Strength of Lower Panel vs Damage Size  | 8-38 |
| 8-31 | Probabilities of Failure for the Restricted Load Factor   | 8-41 |
| 8-32 | Cumulative Number of Occurrences per 250 Flight Hours per 1 m <sup>2</sup>                                      | 8-44 |
| 8-33 | Failure Load Factor and Coefficient of Variation for Upper/Lower Wing Surface Condition—Symmetrical Upbending   | 8-47 |
| 8-34 | Failure Load Factor and Coefficient of Variation for Upper/Lower Wing Surface Condition—Symmetrical Downbending | 8-47 |
| 8-35 | Relative Residual Strength of Upper Panel vs Damage Size  | 8-47 |
| 8-36 | Relative Residual Strength of Panel Under Tension vs Damage Size  | 8-49 |
| 8-37 | Conditional Probabilities of Wing Skin Failure  | 8-50 |
| 9-1  | Calculated Failure Probabilities Using Different Distribution Properties for Composite Material Strength        | 9-3  |
| 9-2  | Mean Values and Standard Deviations of Failure Probabilities  | 9-6  |

## EXECUTIVE SUMMARY

The present document describes the efforts under Memorandum of Cooperation between the Federal Aviation Administration (FAA), USA, and the Central Aero-Hydrodynamic Institute (TsAGI), Russian Federation. Under this effort, a methodology for calculating reliability of composite aircraft structures was developed and is contained in the software Probabilistic Design of Damage Tolerant Composite Structures (ProDeCompoS). In addition, background data culled from Russian usage of composite aircraft structures was compiled to use with ProDeCompoS. The data includes statistical data of damage occurrence, effectiveness of repair, and test data and computational methods to determine residual strength for damaged composite laminate.

The methodology of the ProDeCompoS evaluates the statistically based probabilistic design to improve structural efficiency of damage tolerant composite aircraft structures. It includes databases and application programs that form an automated complex. The main target is to provide designers, production engineers and analysts with an automated tool for determining and ensuring damage tolerance at all stages of composite aircraft structural life—from preliminary investigation to certification and service. The important goal was to attain specified levels of safety and reliability with simultaneous observance of other feasibility requirements such as structural weight, manufacturing cost, and maintenance cost.

The methodology and use of ProDeCompoS was demonstrated by calculating the reliability of four composite components: a highly maneuverable MIG-29 fin, a transport TU-204 aileron, a business jet Lear Fan-2100 wing, and an aerobatic SU-29 wing.

The robustness of ProDeCompoS was evaluated by a method which estimates the spread and confidence intervals for failure probability in the analysis of the MIG-29 fin. The analysis showed that the reliability estimates are quite stable for the range of expected variations of input data.

## 1. INTRODUCTION.

The present document is the final report of the activities under Memorandum of Cooperation between the Federal Aviation Administration (FAA), USA, and the Central Aero-Hydrodynamic Institute (TsAGI), Russian Federation. The report substantiates background data for calculating reliability of composite aircraft structures by the methodology of Probabilistic Design of Damage Tolerant Composite Structures (ProDeCompoS).

The report includes:

- statistical data on occurrence of random damages in composite aircraft structures;
- classification of repairs to the composite aircraft structures and their effectiveness;
- experimental data evaluating the defect influence on residual strength of composite skins;
- methodologies for computing residual strength of composite skins;
- user's manual for the program PreDaMC that prepares data for the statistical modeling module;
- user's manual for the MontCar program that carries out statistical modeling;
- user's manual on the TEST database that deals with results of experiments for estimating the parameters of composites and structural components;
- user's manual on the AIRCRAFT database with data on structures (including inspection data) and their loading and damage exceedances;
- user's manual on the MATERIALS database with information on characteristics of composite layers for analytical programs;
- analysis of MiG-29 (fin), TU-204 (aileron), Lear Fan-2100 (wing), and SU-29 (wing) failure probability;
- the estimate of spread and confidence intervals for failure probability—in application to the MiG-29 fin.

The methodology of the ProDeCompoS was described in the Final Report [1] under the contract. This methodology was prepared to evaluate and further develop, the statistically based probabilistic design approach to improve structural efficiency of damage tolerant composite aircraft structures. The methodology underlies the ProDeCompoS software (the chart of software is shown in figure 1-1). It includes databases and application programs that form an automated complex. The main target is to provide designers, production engineers, and analysts with automated tools for determining and ensuring damage tolerance at all stages of composite aircraft structural life—from preliminary investigation to certification and service. The important goal is to attain specified levels of safety and reliability with simultaneous observance of other feasibility requirements such as structural weight, manufacturing cost, and maintenance cost.

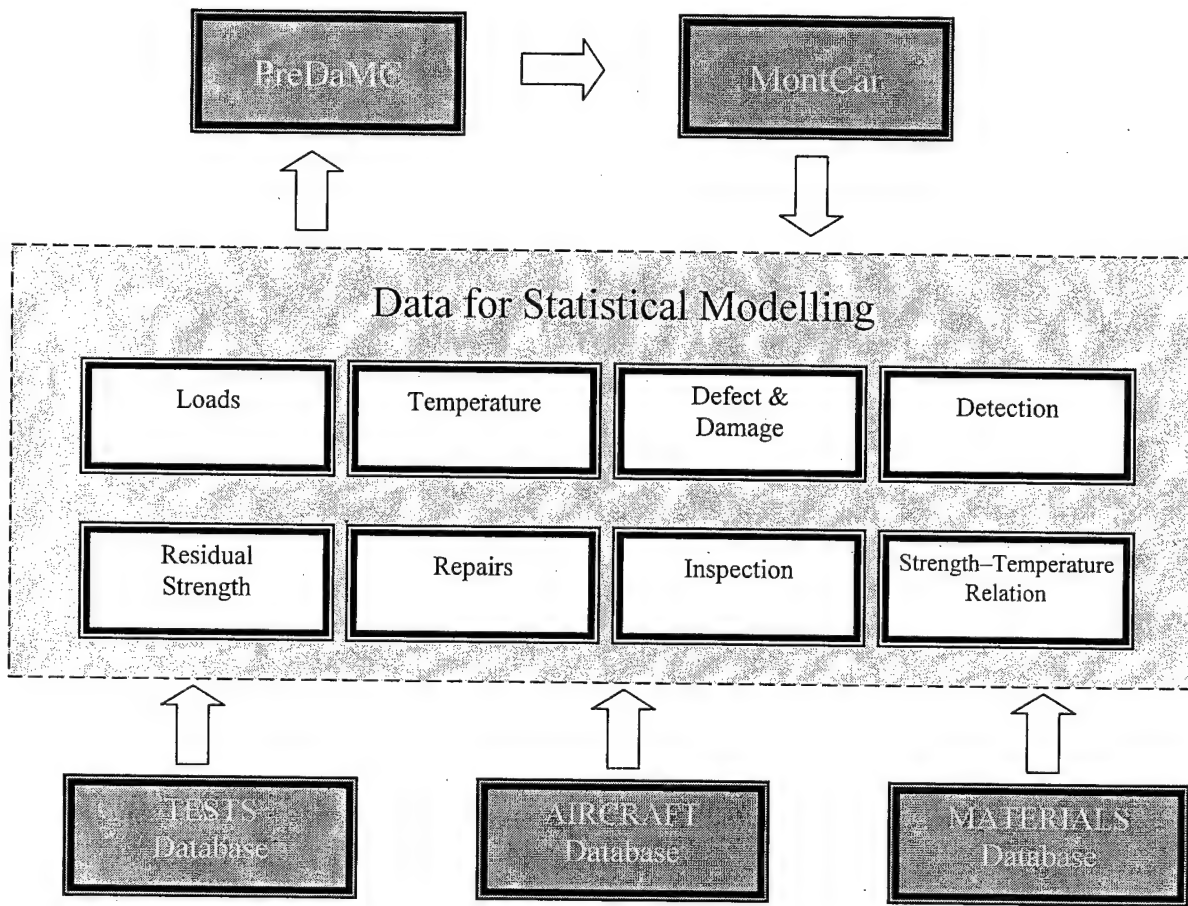


FIGURE 1-1. CHART OF ProDeCompoS SOFTWARE

The structural efficiency of aircraft structures is believed to be improved through the use of polymer matrix composites (PMC) based on thermoset/thermoplastic matrices continuously reinforced with carbon, glass, or ceramic fibers. These materials possess high specific strength/stiffness and high resistance to crack initiation and propagation under cyclic loads. Experience shows that the most hazardous causes of catastrophic failures in composite aircraft structures are the presence of manufacturing flaws not detected in manufacture and mechanical impact damage to composite materials in the course of service. Therefore, the required integrity at high structural efficiency is only attainable through the use of the damage tolerance principle that envisions the composite structures to be serviceable after some damages occurred.

This problem cannot be solved without accounting for the fact that composites are different, that damage tolerance is affected by a set of technology/in-service factors, and that applied loads (including mechanical impacts), environmental conditions, and a scatter in mechanical properties of composite materials are stochastic. This necessitates a multiparameter analysis of a large amount of information:

- mechanical characteristics of composite materials;
- type of manufacturing processes and designs for composite structures;

- results of nondestructive inspection during manufacture, tests, and service;
- data from experimental investigations involving specimens, elements, and full-scale structures, etc.

Such analysis must rely upon the state of art in information science, fracture mechanics, mathematical theory of reliability, methods of the probability theory, and mathematical statistics. Furthermore, this technology must be implemented on up-to-date personal computers. The designer, the industrial engineer, and the analyst must define numerous measures, which are a necessity at design, manufacture, certification, and service stages. Under these conditions, integrated software for ensuring damage tolerance of composite structures is one of the necessary options for implementing the composite materials in the aircraft industry. The challenging problems of increasing the service life and improving the structural efficiency can be solved with such software.

Functional requirements to the software can be formulated in conformity with stages of a composite aircraft structural life. For a damage tolerance prediction to be valid, one must, at all stages, formulate analytical models, involve the results of statistical modeling, and employ data from information databases so as to obtain the following parameters and characteristics:

- types of manufacturing flaws and their statistical distribution in terms of size;
- types of in-service damage and their statistical distribution in terms of size;
- dimensions of damages which occur after typical mechanical impacts;
- estimates of effects of the manufacturing flaws and damages on the residual strength and durability of composite aircraft structures;
- parameters of statistical distribution functions for residual strength and durability, etc.

The above-mentioned parameters and residual structural integrity for each stage can form a basis for predicting structural safety and reliability levels.

### 1.1 OCCURRENCE OF RANDOM DAMAGE IN COMPOSITE AIRCRAFT STRUCTURES—STATISTICAL DATA.

The past experience of operating aircraft structures manufactured of carbon or boron fiber-reinforced plastics or organoplastics shows that processes of initiation and development of damage in polymer composites is totally different from fatigue behaviour of metals. Damage is caused not by periodic loading but by mechanical impacts likely during scheduled inspections and flight operations. However, these damages propagate rather slowly under the usual in-flight loads. The unique composite experience relates to directional strength and toughness properties, impact resistance, both sensitivity in tension and compression and high fatigue resistance. There is a need to develop and refine methods for analysing rate of occurrence of in-service damage in aircraft structures. These methods would be the basis to establish design requirements and

criteria such that aircraft operation safety is guaranteed for load-carrying structure static and fatigue strength. Criteria are defined in the following sequence [2]: failure probability, residual strength, allowable damage, size-inspection interval, and operation condition limitation. Relations between components in this procedure are derived in the reversed sequence:

- in-service statistics are used to investigate the influence of operational conditions on rate of occurrence and size of damage. Theoretical and experimental data are utilized to discover interrelations between damage size and structural residual strength, and
- reliability theory methods are employed in order to estimate the structure failure probability.

The objective of the present chapter is to process the existing data and reveal the laws that describe rate of occurrence of damage in composite structures during service. In general this requires:

- to establish the probability of occurrence of each mechanical impact type usual in the particular structure, and
- to determine types and sizes of composite structure damages while taking into account various structural features.

The damaging factors are numerous and may be characterized by weight, shape, and dimensions of a projectile. There is no existing comprehensive model for computing the composite behavior in the case of mechanical impact. This problem cannot be solved by computation. However, use can be made of the fact that for almost all structures the visible damage size corresponds to the projectile dimensions at wide variation of other impact parameters such as velocity and angle of incidence. If there are statistics of damage to these structures, one can infer the set of projectiles; thereafter, it becomes possible to predict rate of occurrence of damage for different composite structures.

### 1.1.1 Classification of Mechanical Impacts and In-Service Damage Types.

To analyze rate of occurrence of in-service damage to composite structures, one should categorize possible mechanical impacts and types of in-service damages. Depending on the projectile speed ( $V$ ), the mechanical impacts causing damage in composites may be subdivided into low-speed ( $V < 6-8$  m/s) and mid-speed ( $V < 30-200$  m/s) phenomena.

Low-speed impacts occur during assembly and scheduled maintenance due to impacts of falling tools, bolts, and so on. Mid-speed impacts correspond to ice/concrete pieces and stones, (that are thrown by landing gear wheels during takeoffs and landings) hail impacts, bird strikes, uncontained engine failures, etc. In addition to the impacts above one should bear in mind the damages caused by lightning strikes.

Depending on structural features and location within the airframe, each structure has its typical impacts. For instance, the upper-wing panel may be damaged by falling tools, whereas such events are almost impossible for lower panels—but very high probability of damage from a stone

thrown by wheels. A composite structure consisting of elements such as skin cells, ribs, flanges, and spars has different damage probability values for each element. The structural element most vulnerable in terms of mechanical impacts is the skin and, therefore it was the principal study subject.

Unlike metals in which impacts may be absorbed by plastic deformation, polymer composites fail as brittle materials. Therefore, the low-speed and mid-speed impacts are causes of damages to a composite skin which are proposed to be categorized as follows and shown in figure 1-2:

1. Surface damage, scratches, fracture notch, etc. (figure 1-2(a)). Such damages only insignificantly affect the structural load-bearing capability and may be neglected in analyses.
2. Delaminations followed by matrix cracking and fiber failure. These are inside of the composite lay-up. It is usual that the external skin surface is also indented. Among those, one could separate:
  - internal delaminations visually undetectable at both skin surfaces (figure 1-2(b)) and followed by matrix cracking at the side opposite to the impacted surface (figure 1-2(c));
  - delamination visually detectable (due to cracking and fragmentation) at the external skin surface in respect to the impacted surface (figure 1-2(d)).

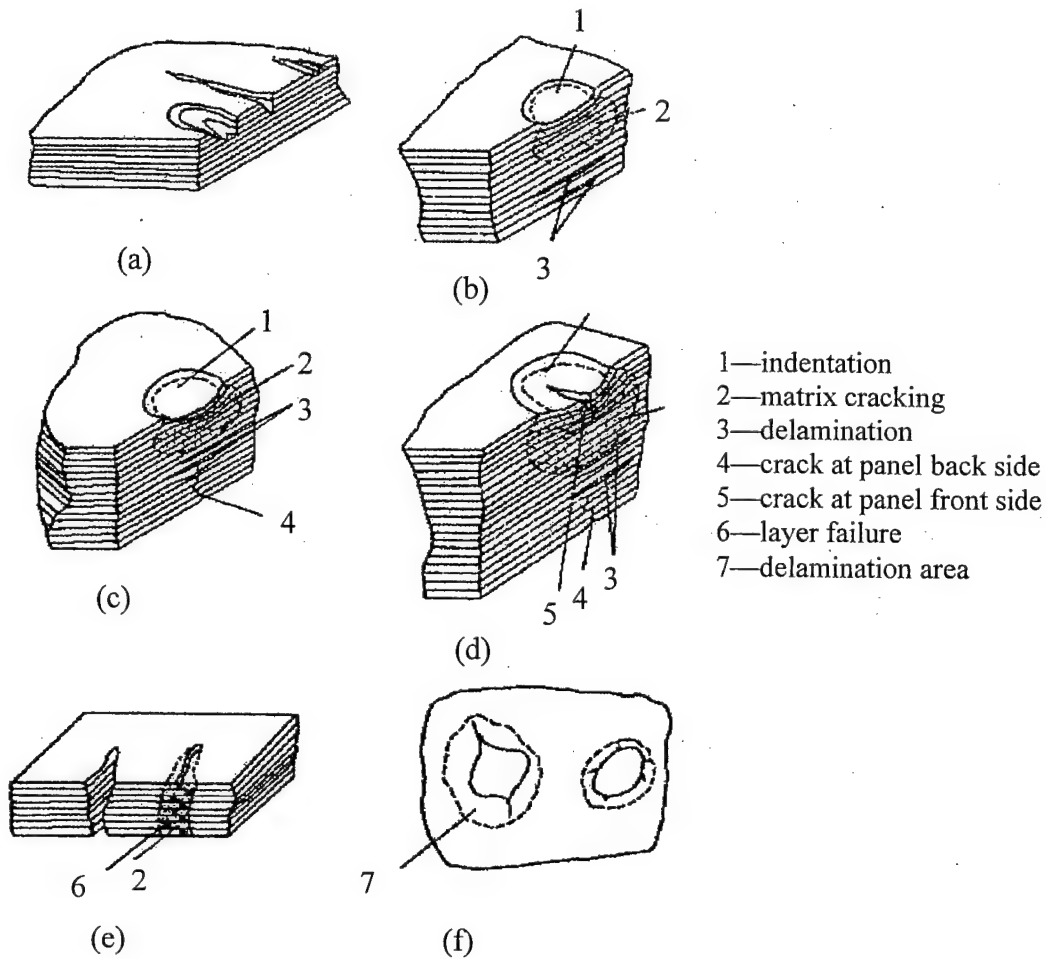
For this type of in-service damages, the failure zone size in internal layers may be much greater than the cracked zone size on external skin surfaces.

3. The through damage—cracks and punctures. In this case, the damage area features failure of layers through the thickness of the composite. The through damages may be characterized as clean hole or damaged material (figure 1-2(e)). Puncture edges usually show delamination and sharp cracks (figure 1-2(f)).

Type 2 and 3 damages are significant factors in reducing load bearing capability of a structure and must be taken into account in analyses.

#### 1.1.2 Rate of Occurrence of In-Service Damage in Aircraft Structures Made of Polymer Composites.

Aircraft manufacturers are using two types of polymer composite structures, honeycomb-core sandwich structures with skin thickness of 0.4 to 3.5 mm and monolithic skins with thickness of 1 to 12 mm. A thinner skin will fail at a lower impact energy, so the rate of occurrence of damage for various structures may differ notably. Nevertheless, the damage area size in general is characteristic of the mechanical impact or size. This allows one to use the inspection results for airframes with identical skin thickness in order to evaluate occurrence probability of the mechanical impacts that cause a damage with a characteristic size  $2L$ , where  $L$  is the characteristic damage radius.



- (a) Surface damage, scratches, fracture notch, etc.
- (b) Internal delaminations visually undetectable at both skin surfaces
- (c) Matrix cracking at the side opposite to the impacted surface
- (d) Delamination visually detectable (due to cracking and fragmentation)
- (e) Through damage—cracks and punctures
- (f) Puncture edges usually show delamination and sharp cracks

FIGURE 1-2. TYPES OF IN-SERVICE DAMAGE

Currently there is no standardized recommendations on inspection intervals and on classification of data on in-service damages. Therefore, the summarized results of specialized visual and instrumented inspections; performed here are the first step in determining the in-service defect rate of occurrence and the interrelation dimensions. The ranges of inspected airframe elements, structural types, skin materials, and thickness are represented in table 1-1.

Composite structures may be installed on an airplane when conducting an inspection in field conditions, or removed from the airplane when inspecting these at factories and technical service centers. In both cases, the main version of assessing the composite structures is the visual inspection, which is intended to reveal through-the-thickness and superficial damages.

TABLE 1-1. CHARACTERISTICS OF STRUCTURAL ELEMENTS IN  
INSPECTED AIRFRAMES

|    | Structural Element          | Aircraft | Flight (hours) | Material      | Skin Version         | Thickness (mm) | Surface Area (m <sup>2</sup> ) |
|----|-----------------------------|----------|----------------|---------------|----------------------|----------------|--------------------------------|
| 1  | Wing leading edge           | MIG-29   | 1495           | CFRP          | Monolithic           | 2.3            | 5.0                            |
| 2  | Vertical stabilizer skin    | MIG-29   | 1495           | CFRP          | Monolithic           | 1.8-3.2        | 11.0                           |
| 3  | Air inlet shell             | MIG-29   | 1495           | CFRP          | Monolithic           | 3.8            | 4.5                            |
| 4  | Engine fairing              | MIG-29   | 1495           | CFRP          | Monolithic           | 3.6            | 2.5                            |
| 5  | Lower-vault panel           | MIG-29   | 1495           | CFRP          | Sandwich (honeycomb) | 1.0            | 2.5                            |
| 6  | Wing skin                   | MIG-29   | 1495           | CFRP          | Monolithic           | 2.3            | 16.2                           |
| 7  | Stabiliser actuator fairing | SU-27    | 2000           | CFRP          | Sandwich (honeycomb) | 0.6            | 1.1                            |
| 8  | Fairing of nose strut wheel | SU-27    | 2000           | CFRP          | Sandwich (honeycomb) | 0.8            | 1.0                            |
| 9  | Nose landing gear door      | SU-25    | 3000           | CFRP          | Sandwich (honeycomb) | 0.6            | 0.8                            |
| 10 | Wing/fuselage fairing       | L-1011   | 79,568         | Organoplastic | Sandwich (honeycomb) | 0.4-0.5        | 5.2                            |
| 11 | Landing gear door           | AN-124   | 1440           | CFRP          | Sandwich (honeycomb) | 0.5-0.8        | 12.2                           |
| 12 | Cargo bay door              | AN-124   | 1440           | CFRP          | Sandwich (honeycomb) | 0.5-0.8        | 5.8                            |

Delamination in both monolithic and sandwich skins may be detected by instrumented inspection with ultrasonic and similar device. However, the instrumented inspection methods require much labor, special equipment, and personnel; so these methods cannot be complete substitutes for visual inspection.

Rate of damage occurrence in a particular structure depends on a number of factors such as design, it's function, location in an airframe, maintenance personnel qualification, and inspection schedule. In general, the parameter is different from that of other structures. In figure 1-3, histograms of the maximum inspection-detected in-service damages caused by mechanical impacts are for the airframe elements as shown in table 1-1 confirm this observation. Here, defects caused by structural assembly errors were not taken into consideration, nor edge delaminations caused by not providing necessary protection. Note that the histograms make it possible to outline two typical sets of damages. The first one, more widespread, includes 5- to 10-mm diameter damages detected in wing leading edges, stabilizer skins, actuator fairing skins, and landing gear doors. These are caused by concrete pieces and stones that impact the structure during takeoffs and landings, the mid-speed impacts as stated before. The second set comprises 3- to 352-mm diameter damages, occurred in the course of ground maintenance and were caused by impacts around structural cutouts (in the fairing and shell) during structure removal and installation (on the landing gear fairing) and operations with stepladders (on wing leading edges). All damages in "wing/fuselage" fairing were associated with scheduled maintenance but have been caused by different events: impacts when removing and installing the fairings during inspection, impacts on internal skins during repair and inspection of airplane hydraulic systems, and impacts on external skins during inspection of surrounding airframe elements.

Data represented in figure 1-3 suggest that sizes of damage to sandwich skins (0.5 to 1 mm) which is caused by both low-speed and mid-speed mechanical impacts correspond to sizes of similar damage to monolithic skins (1.8 to 3.8 mm). This is a sufficient reason to assume that over the above range of thickness, the sizes of damage occurring from low-speed and mid-speed impact do not depend on skin thickness. This makes it possible to summarize and generalize the operational experience and derive analytical probabilistic laws typical of composite structure damage; these laws are necessary for evaluating and ensuring damage tolerance, as well as for planning a dedicated data acquisition for refining the damage-rate parameters.

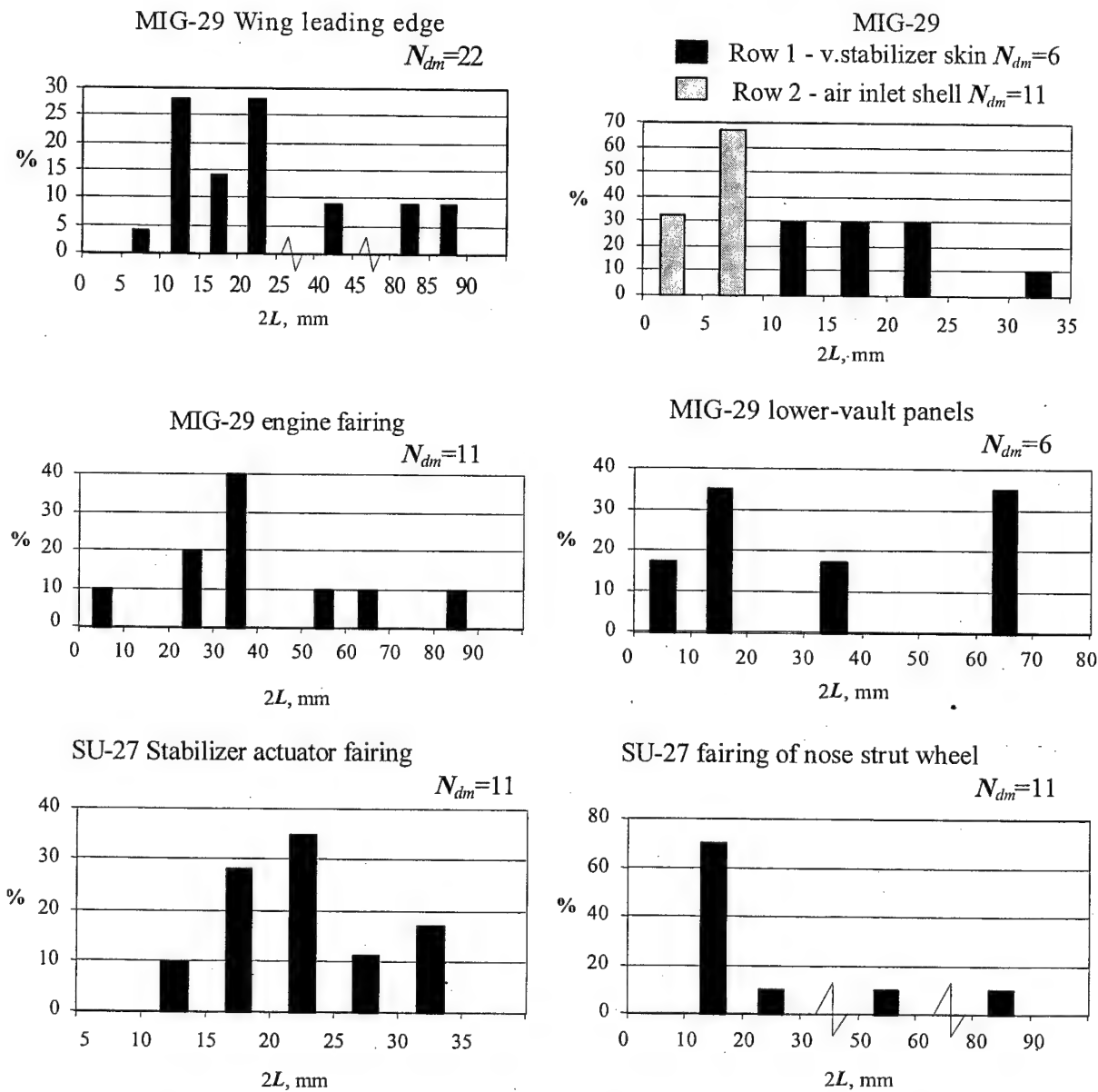


FIGURE 1-3. IN-SERVICE DAMAGES THAT OCCURRED UPON MECHANICAL IMPACTS AND WERE FOUND BY INSPECTORS—HISTOGRAMMATIC REPRESENTATION

In terms of residual strength of airframe components, the most dangerous are through-the-thickness damages such as holes and cracks (in zones mainly loaded with tension) and composites delamination which results in premature buckling of the structure under compression and shear. Table 1-2 provides empirical exceedances of in-service damages to airframes of various airplane types from data that was available to the authors.

TABLE 1-2. EMPIRICAL EXCEEDANCES OF DAMAGE IN INSPECTED AIRFRAMES

|    | Unit                        | Airplane | Flight<br>(hours) | Area<br>sq. m | All Types of Damage*<br>(mm) |         |         | Delaminations<br>(mm) |         |         | Holes and Cracks<br>(mm) |         |         |
|----|-----------------------------|----------|-------------------|---------------|------------------------------|---------|---------|-----------------------|---------|---------|--------------------------|---------|---------|
|    |                             |          |                   |               | 2L > 0                       | 2L > 30 | 2L > 80 | 2L > 0                | 2L > 30 | 2L > 80 | 2L > 0                   | 2L > 30 | 2L > 80 |
| 1  | Wing leading edge           | MIG-29   | 1495              | 5.0           | 22                           | 5       | 3       | 4                     | 3       | 1       | 5                        | 1       | 1       |
| 2  | Vertical stabilizer skin    | MIG-29   | 1495              | 11.0          | 6                            | 3       | 2       | 2                     | 2       | 1       | 3                        | 0       | 0       |
| 3  | Air inlet shell             | MIG-29   | 1495              | 4.5           | 11                           | 1       | 0       | 4                     | 1       | 0       | 0                        | 0       | 0       |
| 4  | Engine fairing              | MIG-29   | 1495              | 2.5           | 10                           | 7       | 1       | 5                     | 4       | 0       | 2                        | 1       | 0       |
| 5  | Lower-vault panel           | MIG-29   | 1495              | 2.5           | 6                            | 3       | 0       | 1                     | 1       | 0       | 3                        | 1       | 0       |
| 6  | Wing skin                   | MIG-29   | 1495              | 16.2          | 1                            | 0       | 0       | 0                     | 0       | 0       | 1                        | 0       | 0       |
| 7  | Stabilizer actuator fairing | SU-27    | 2000              | 1.1           | 11                           | 2       | 0       | 0                     | 0       | 0       | 3                        | 2       | 0       |
| 8  | Fairing of nose strut wheel | SU-27    | 2000              | 1.0           | 11                           | 2       | 1       | 0                     | 0       | 0       | 3                        | 2       | 1       |
| 9  | Nose landing gear door      | SU-27    | 3000              | 0.8           | 7                            | 7       | 2       | 6                     | 6       | 2       | 0                        | 0       | 0       |
| 10 | Wing/fuselage fairing       | L-1011   | 79,568            | 5.2           | 35                           | 11      | 3       | 17                    | 4       | 1       | 12                       | 3       | 2       |
| 11 | Landing gear door           | AN-124   | 1440              | 12.2          | 7                            | 6       | 2       | 4                     | 4       | 1       | 3                        | 2       | 1       |
| 12 | Cargo bay door              | AN-124   | 1440              | 5.8           | 9                            | 5       | 2       | 5                     | 4       | 2       | 2                        | 1       | 0       |

\* Scratches + delaminations + cracks + holes

The information from table 1-2 was utilized to derive empirical exceedance intensity per 1000 flight hours per square meter of damage to the airframe parts inspected. The data reported in table 1-3 and figures 1-4 through 1-15 represent these graphically in semilog plots. One can see that the data may be approximated well by using the exponential function:

$$H(2L) = H_0 \cdot e^{-\frac{2L}{b}} \quad (1-1)$$

which is depicted as a straight line in the semilog plots. Equation 1-1 includes the following notation:

**$H(2L)$** , the exceedance intensity (per 1000 flight hours per square meter);  
 **$H_0, b$** , the approximation function coefficients.

TABLE 1-3. EMPIRICAL EXCEEDANCES INTENSITY (per 1,000 flight hours per sq. m)

|                        | Unit                        | Airplane | All Types of Damage*<br>(mm) |         |         | Delaminations<br>(mm) |          |          | Holes and Cracks<br>(mm) |          |         |
|------------------------|-----------------------------|----------|------------------------------|---------|---------|-----------------------|----------|----------|--------------------------|----------|---------|
|                        |                             |          | 2L > 0                       | 2L > 30 | 2L > 80 | 2L > 0                | 2L > 30  | 2L > 80  | 2L > 0                   | 2L > 30  | 2L > 80 |
| 1                      | Wing leading edge           | MIG-29   | 2.943                        | 0.6689  | 0.4013  | 0.5351                | 0.4013   | 0.1337   | 0.6689                   | 0.1338   | 0.1338  |
| 2                      | Vertical stabilizer skin    | MIG-29   | 0.3649                       | 0.1824  | 0.1216  | 0.1216                | 0.1216   | 0.06081  | 0.1824                   | 0        | 0       |
| 3                      | Air inlet shell             | MIG-29   | 1.635                        | 0.1486  | 0       | 0.5946                | 0.1486   | 0        | 0                        | 0        | 0       |
| 4                      | Engine fairing              | MIG-29   | 2.676                        | 1.873   | 0.2676  | 1.338                 | 1.07     | 0        | 0.5351                   | 0.2676   | 0       |
| 5                      | Lower-vault panel           | MIG-29   | 1.605                        | 0.8027  | 0       | 0.2676                | 0.2676   | 0        | 0.8027                   | 0.2676   | 0       |
| 6                      | Wing skin                   | MIG-29   | 0.04129                      | 0       | 0       | 0                     | 0        | 0        | 0.04129                  | 0        | 0       |
| MIG-29 – averaged data |                             |          | 1.5441                       | 0.7351  | 0.2635  | 0.571                 | 0.401    | 0.09726  | 0.4461                   | 0.223    | 0.1338  |
| 7                      | Stabilizer actuator fairing | SU-27    | 5.0                          | 0.909   | 0       | 0                     | 0        | 0        | 1.364                    | 0.909    | 0       |
| 8                      | Fairing of nose strut wheel | SU-27    | 5.5                          | 1.0     | 0.5     | 0                     | 0        | 0        | 1.5                      | 1.0      | 0.5     |
| 9                      | Nose landing gear door      | SU-25    | 2.917                        | 2.917   | 0.8333  | 2.5                   | 2.5      | 0.8333   | 0                        | 0        | 0       |
| 10                     | Wing/fuselage fairing       | L-1011   | 0.08459                      | 0.02559 | 0.00725 | 0.04108               | 0.00966S | 0.002417 | 0.029                    | 0.007251 | 0.00483 |
| 11                     | Landing gear door           | AN-124   | 0.3985                       | 0.3415  | 0.1138  | 0.2277                | 0.2277   | 0.0592   | 0.1708                   | 0.1138   | 0.05692 |
| 12                     | Cargo bay door              | AN-124   | 1.078                        | 0.5987  | 0.2395  | 0.5987                | 0.4789   | 0.2394   | 0.2395                   | 0.1197   | 0       |

\* Scratches + delaminations +cracks +hole

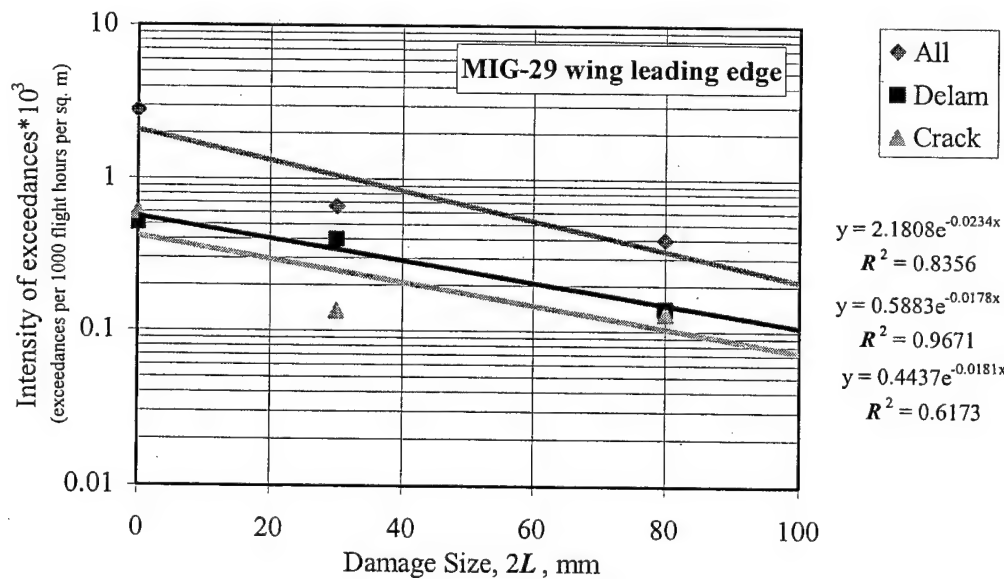


FIGURE 1-4. EXCEEDANCE INTENSITY OF DAMAGE TO MIG-29 WING LEADING EDGE

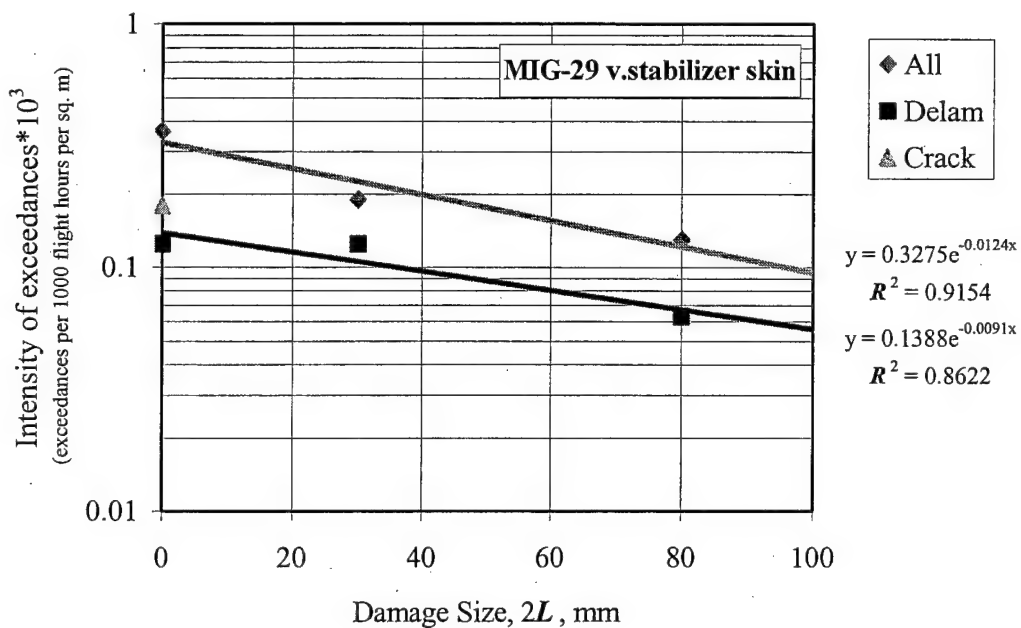


FIGURE 1-5. EXCEEDANCE INTENSITY OF DAMAGE TO MIG-29 VERTICAL STABILIZER SKIN

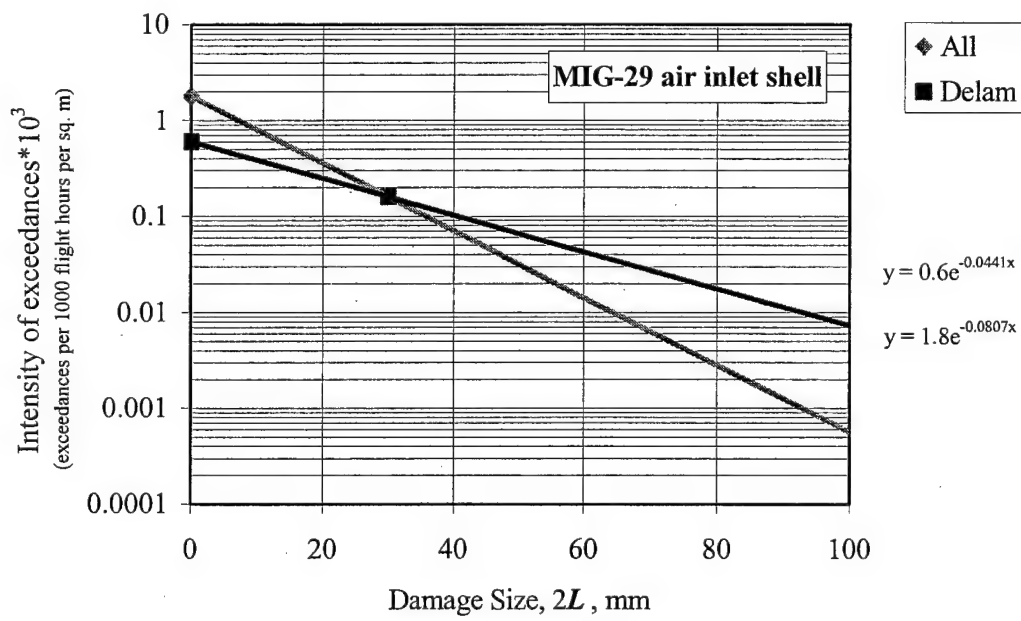


FIGURE 1-6. EXCEEDANCE INTENSITY OF DAMAGE TO MIG-29 AIR INLET SHELL

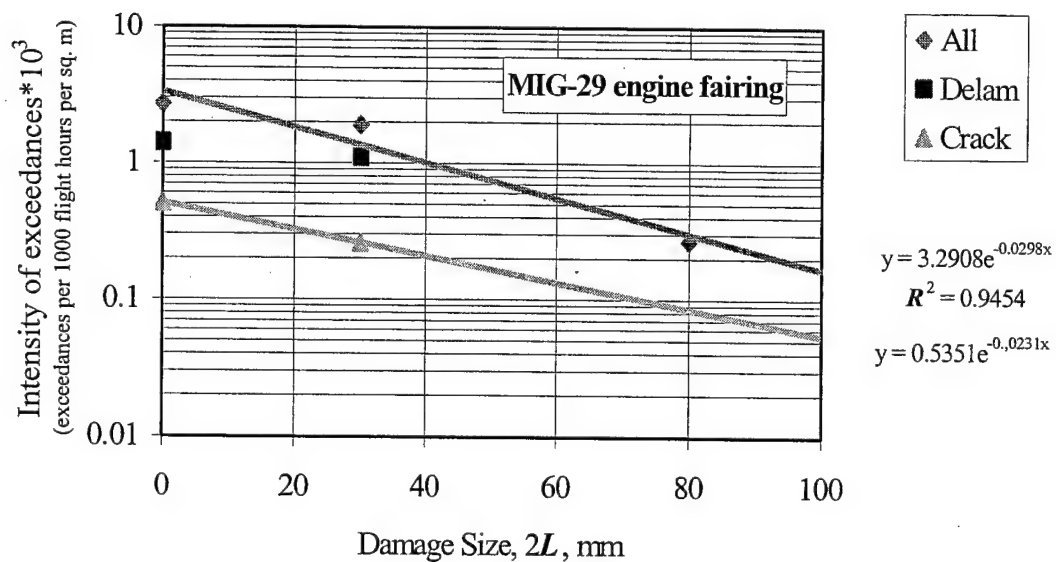


FIGURE 1-7. EXCEEDANCE INTENSITY OF DAMAGE TO MIG-29 ENGINE FAIRING

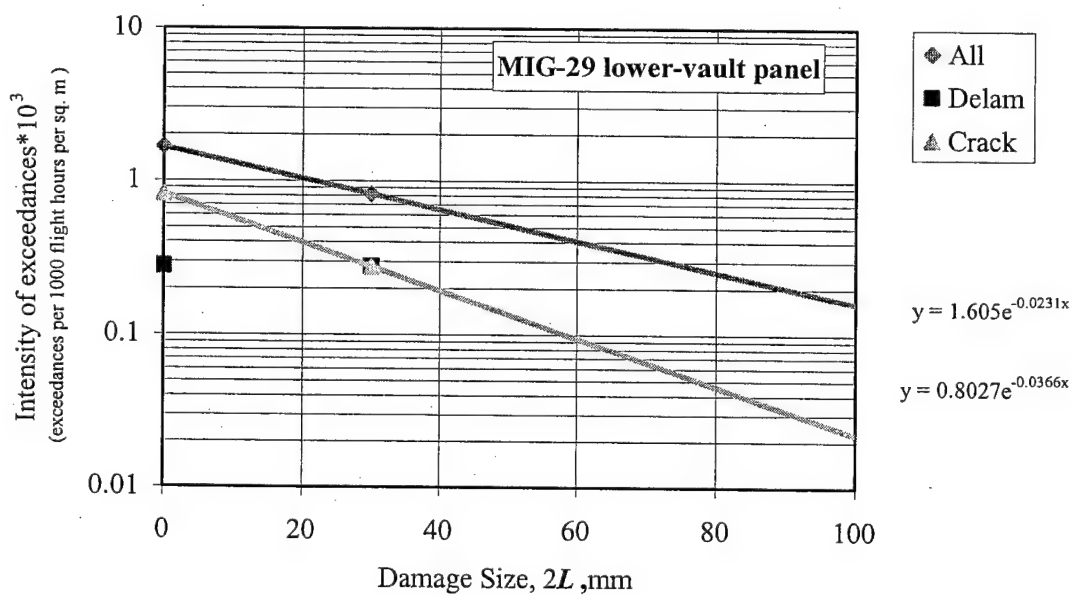


FIGURE 1-8. EXCEEDANCE INTENSITY OF DAMAGE TO MIG-29 LOWER-VAULT PANEL

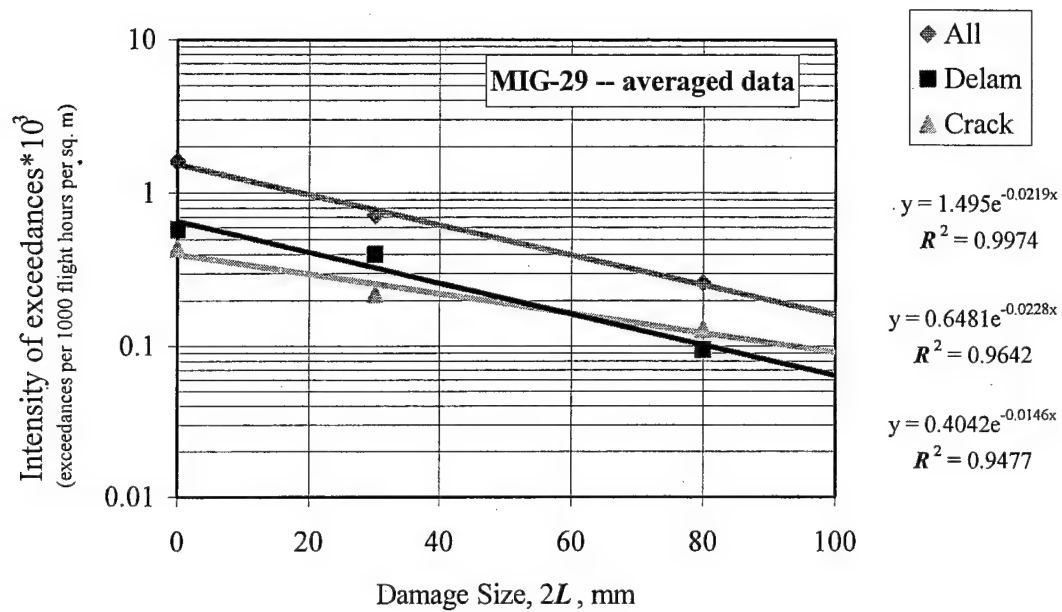


FIGURE 1-9. EXCEEDANCE INTENSITY OF DAMAGE TO MIG-29—AVERAGED DATA

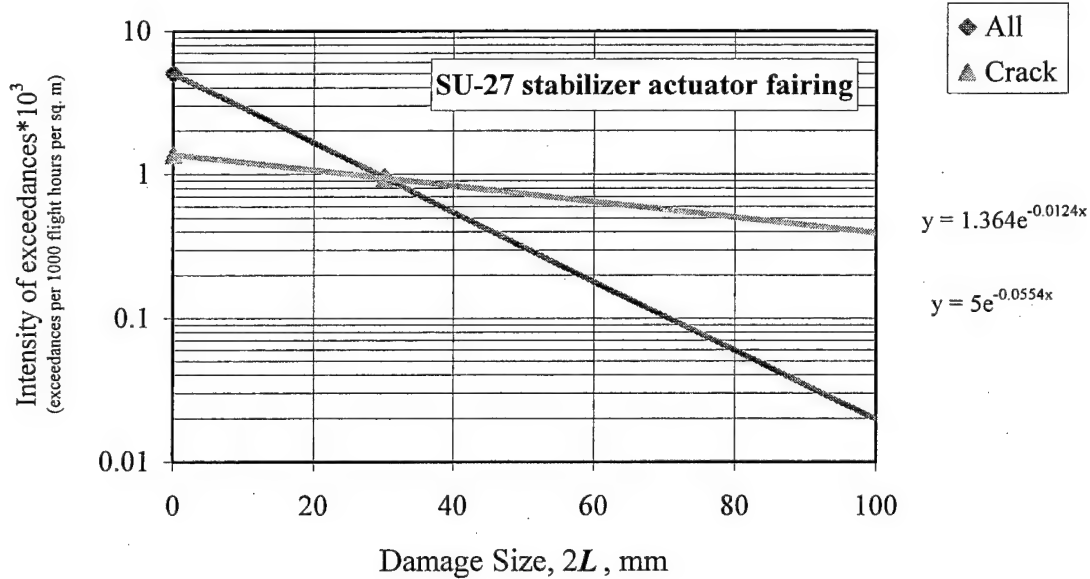


FIGURE 1-10. EXCEEDANCE INTENSITY OF DAMAGE TO SU-27 STABILIZER ACTUATOR FAIRING

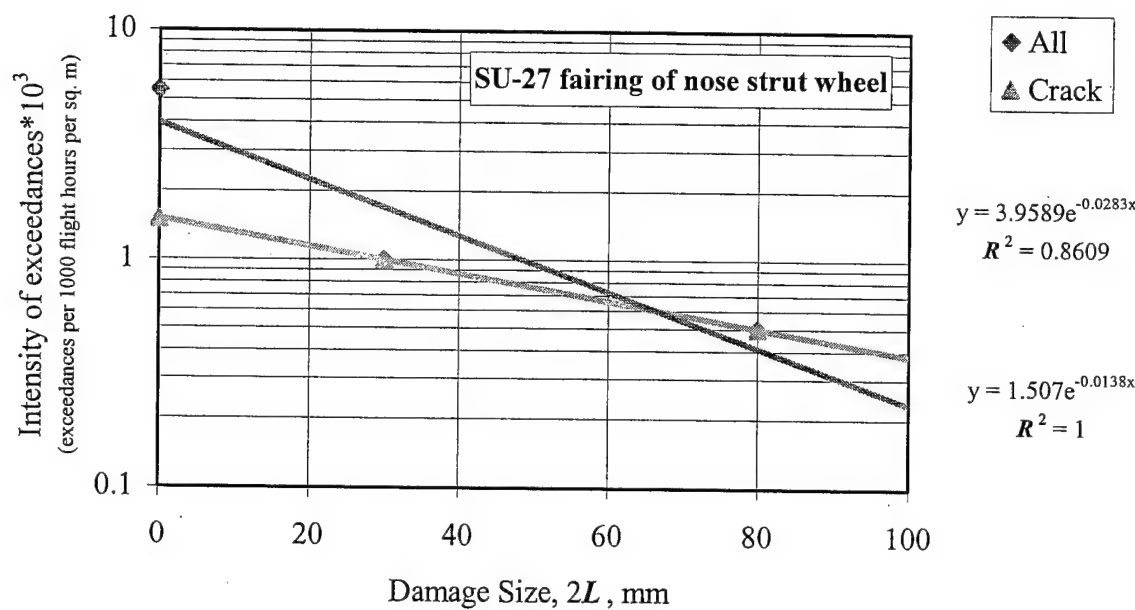


FIGURE 1-11. EXCEEDANCE INTENSITY OF DAMAGE TO SU-27 FAIRING OF NOSE STRUT WHEEL

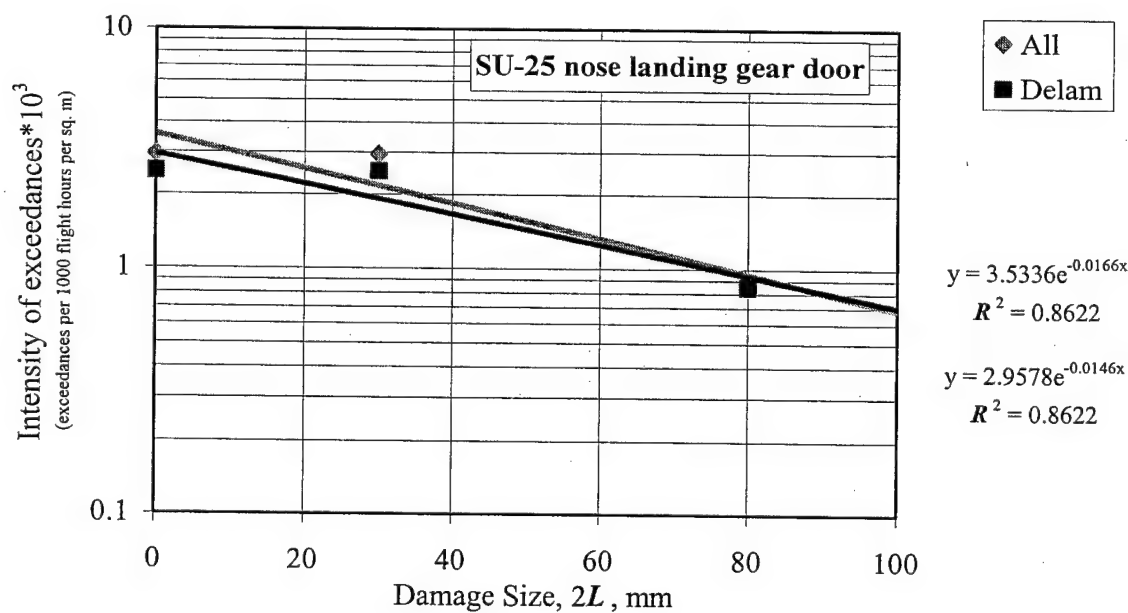


FIGURE 1-12. EXCEEDANCE INTENSITY OF DAMAGE TO SU-25 NOSE LANDING GEAR DOOR

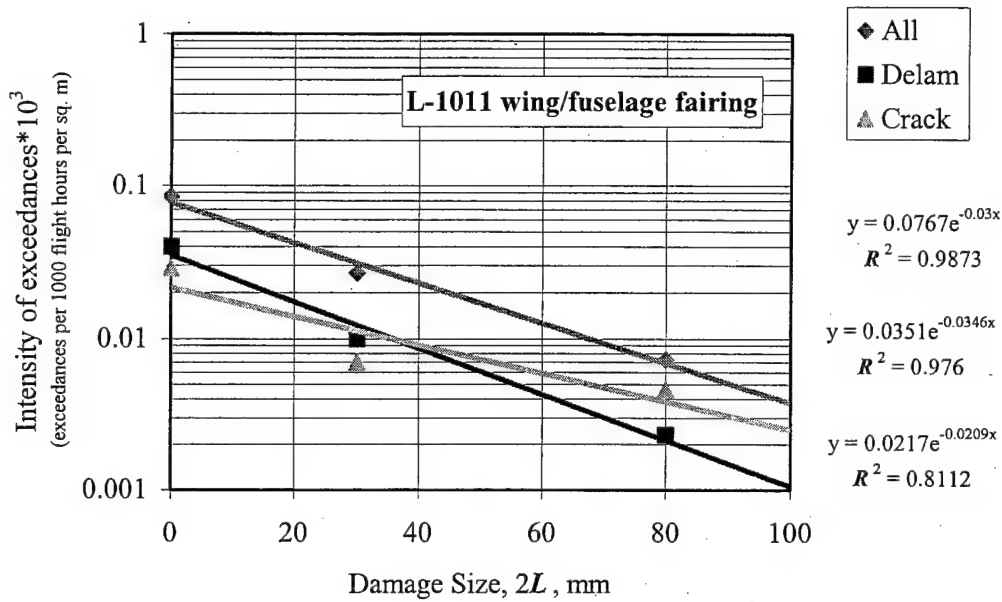


FIGURE 1-13. EXCEEDANCE INTENSITY OF DAMAGE TO L-1011 WING/FUSELAGE FAIRING

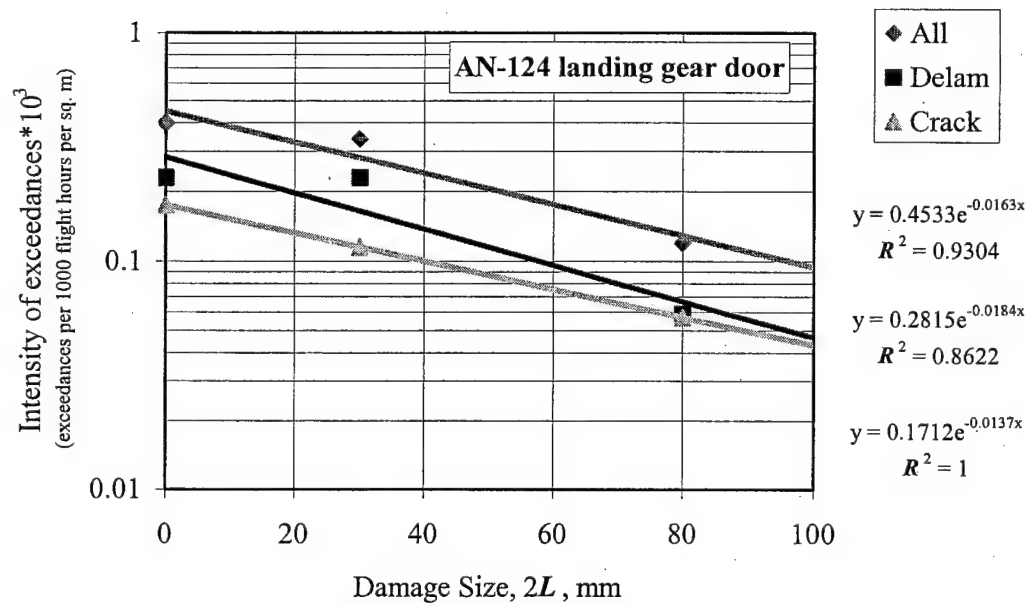


FIGURE 1-14. EXCEEDANCE INTENSITY OF DAMAGE TO AN-124 LANDING GEAR DOOR

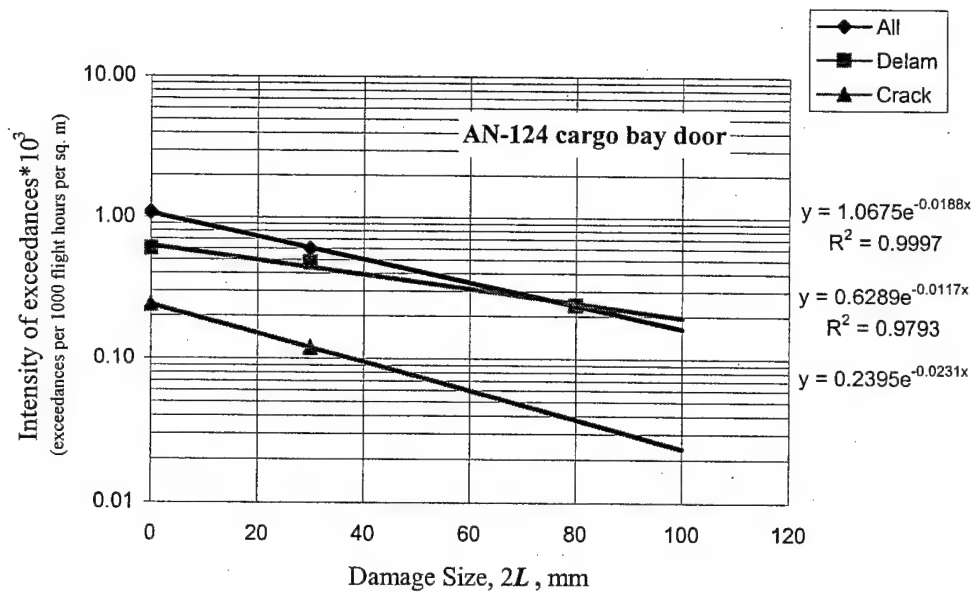


FIGURE 1-15. EXCEEDANCE INTENSITY OF DAMAGE TO AN-124 CARGO BAY DOOR

The approximation function (equation 1-1) coefficients  $H_0$  and  $b$  were determined by using Microsoft Excel. Table 1-4 shows these coefficients and the approximation validity coefficient  $R^2$ . Note that the approximation validity gets higher when the total amount of data acquired grows; this evidences correctness of the approximation equation adopted. For example, the approximation validity coefficient  $R^2$  is maximum when one deals with data on all the MIG-29 units and L-1011 wing/fuselage fairing. These are based on operational experience as long as 79,568 flight hours.

TABLE 1-4. EXCEEDANCE INTENSITY—EXPONENTIAL APPROXIMATION

$$H(2L) = H_0 \cdot e^{-\frac{2L}{b}}$$

|                   | Unit                        | Airplane        | All Types of Damage* |       |          | Delaminations |       |          | Hole + Cracks + Holes |       |          |
|-------------------|-----------------------------|-----------------|----------------------|-------|----------|---------------|-------|----------|-----------------------|-------|----------|
|                   |                             |                 | $H_0$                | $b$   | $R^2$ ** | $H_0$         | $b$   | $R^2$ ** | $H_0$                 | $b$   | $R^2$ ** |
| 1                 | Wing leading edge           | MIG-29          | 2.181                | 42.74 | 0.84     | 0.588         | 56.1  | 0.97     | 0.444                 | 55.2  | 0.62     |
| 2                 | Vertical stabilizer skin    | MIG-29          | 0.325                | 75.84 | 0.91     | 0.135         | 108.7 | 0.86     | 0.182                 | —     | —        |
| 3                 | Air inlet shell             | MIG-29          | 1.635                | 12.51 | —        | 0.594         | 21.65 | —        | —                     | —     | —        |
| 4                 | Engine fairing              | MIG-29          | 3.291                | 33.56 | 0.95     | 1.338         | —     | —        | 0.535                 | 43.29 | —        |
| 5                 | Lower-vault panel           | MIG-29          | 1.605                | 43.29 | —        | 0.2676        | —     | —        | 0.8027                | 27.32 | —        |
| 6                 | Wine skin                   | MIG-29          | 0.04129              | —     | —        | —             | —     | —        | 0.04129               | —     | —        |
| Mean for airplane |                             | Averaged MIG-29 | 1.495                | 45.56 | 0.99     | 0.6481        | 43.86 | 0.96     | 0.4042                | 68.49 | 0.95     |
| 7                 | Stabilizer actuator fairing | SU-27           | 5.0                  | 17.6  | —        | —             | —     | —        | 1.364                 | 74.07 | —        |
| 8                 | Fairing of nose strut wheel | SU-27           | 3.959                | 35.34 | 0.86     | —             | —     | —        | 1.504                 | —     | —        |
| 9                 | Nose landing gear door      | SU-25           | 3.534                | 60.24 | 0.86     | 2.958         | 71.43 | 0.86     | —                     | —     | —        |
| 10                | Wing/fuselage fairing       | L-1011          | 0.0767               | 33.33 | 0.99     | 0.0351        | 28.9  | 0.98     | 0.0217                | 47.85 | 0.81     |
| 11                | Landing gear door           | AN-124          | 0.4533               | 61.35 | 0.93     | 0.2815        | 54.35 | 0.86     | 0.1712                | 72.99 | —        |
| 12                | Cargo bay door              | AN-124          | 1.068                | —     | —        | 0.6289        | 85.47 | 0.98     | 0.2395                | 47.62 | —        |

\* Scratches + delaminations +cracks + holes

\*\* Exponential approximation validity level

Table 1-5 suggests that the airframe units can be subdivided into three groups:

- Group I: units with a high damage rate, such as MIG-29 wing leading edge, MIG-29 engine fairing, SU-27 vertical stabilizer actuator fairing, SU-27 nose landing gear fairing, and SU-25 nose landing gear door.
- Group II: units with an intermediate damage rate, such as MIG-29 air inlet channel, and MIG-29 lower-vault panel.
- Group III: units with a low damage rate, such as MIG-29 vertical stabilizer skin, MIG-29 wing skin, L-1011 wing/fuselage fairing, AN-124 landing gear door, and AN-124 cargo bay door.

Table 1-5 reports the approximation function (equation 1-1) coefficients averaged for the units of various groups. These averaged coefficients may be employed as a basis for analyzing in-service damage rates of other specific but similar units for which no statistics are available.

TABLE 1-5. EXPONENTIAL APPROXIMATION COEFFICIENTS  $H_0$  AND  $b$  FOR THE VARIOUS GROUPS

| Group I: Units With High Damage Rates          |                             |          |                      |       |               |       |                       |       |
|--|-----------------------------|----------|----------------------|-------|---------------|-------|-----------------------|-------|
|  | Unit                        | Airplane | All Types of Damage* |       | Delaminations |       | Hole + Cracks + Holes |       |
|  |                             |          | $H_0$                | $b$   | $H_0$         | $b$   | $H_0$                 | $b$   |
| 1  | Wing leading edge           | MIG-29   | 2.181                | 42.74 | 0.588         | 56.1  | 0.444                 | 55.2  |
| 4  | Engine fairing              | MIG 29   | 3.291                | 33.56 | 1.338         | —     | 0.535                 | 43.29 |
| 7  | Stabilizer actuator fairing | SU-27    | 5.0                  | 17.6  | —             | —     | 1.364                 | 74.07 |
| 8  | Fairing of nose strut wheel | SU-27    | 3.959                | 35.34 | —             | —     | 1.504                 | —     |
| 9  | Nose landing gear door      | SU-25    | 3.534                | 60.24 | 2.938         | 71.43 | —                     | —     |
| Mean for a group                               |                             |          | 3.593                | 37.9  | 1.628         | 63.77 | 0.967                 | 57.72 |
| Group II: Units With Intermediate Damage Rates |                             |          |                      |       |               |       |                       |       |
| 3  | Air inlet shell             | MIG-29   | 1.635                | 12.51 | 0.594         | 21.62 | —                     | —     |
| 5  | Lower-vault panel           | MIG-29   | 1.605                | 43.29 | 0.2676        | —     | 0.8027                | 27.32 |
| Mean for a group                               |                             |          | 1.62                 | 27.9  | 0.4308        | 21.62 | 0.8027                | 27.32 |
| Group III: Units With Low Damage Rates         |                             |          |                      |       |               |       |                       |       |
| 2  | Vertical stabilizer skin    | MIG-29   | 0.325                | 75.84 | 0.135         | 10.87 | 0.182                 | —     |
| 6  | Wing skin                   | MIG-29   | 0.04129              | —     | —             | —     | 0.04129               | —     |
| 10   | Wing/fuselage fairing       | L-1011   | 0.0767               | 33.33 | 0.0331        | 28.9  | 0.0217                | 47.85 |
| 11   | Landing gear door           | AN-124   | 0.4533               | 61.35 | 0.2815        | 54.35 | 0.1712                | 72.99 |
| 12   | Cargo bay door              | AN-124   | 1.068                | —     | 0.6289        | 85.47 | 0.2395                | 47.62 |
| Mean for a group                               |                             |          | 0.3929               | 55.9  | 0.2701        | 69.35 | 0.1311                | 54.71 |

\* Scratches + delaminations + cracks + holes

### 1.1.3 Comparing With Statistical Data From Other Countries.

In reference 3 the characterization of the operational damage was done by analyzing the data obtained during visits to airline maintenance facilities and Naval aviation depots. Data was also obtained from visits to American Airlines, Delta Airlines, United Airlines, the North Island Naval Aviation Depot (NADEP), and from communications with De Havilland Aircraft Inc. Damage report information is summarized in table 1-6. These data seem to be for a "mean airplane" flown by each of the companies above.

TABLE 1-6. DAMAGE TYPE OCCURRENCES TAKEN FROM REFERENCE 3

| Damage Type   | Occurrences per 1,000,000 Flight Hours |                      |                |       |
|---------------|--|----------------------|----------------|-------|
|               | $2L < 1.5$ in.                         | $1.5 < 2L < 3.0$ in. | $2L > 3.0$ in. | Total |
| Holes         | 189                                    | 132                  | 57             | 378   |
| Delaminations | 49                                     | 146                  | 292            | 487   |
| Cracks        | 32                                     | 32                   | 43             | 107   |
| TOTAL         | 270                                    | 310                  | 392            | 972   |

Data presented in table 1-6 make it possible to derive the empirical exceedances shown in table 1-7 with reference to 1,000,000 flight hours. Also, it provides the same kind of data for the MIG-29 (averaged). The MIG-29 exceedance is by a factor of 10 to 20 higher than that of an "average" airplane commercially operated by American companies. This may be explained through the following aspects:

- conditions in which the commercial airplanes and MIG-29s are operated differ,
- composite structures are located in different areas of these airplanes.

TABLE 1-7. EMPIRICAL EXCEEDANCES OF DAMAGES BASED ON 1,000,000 FLIGHT HOURS (For an "averaged" airplane)

| Airplane              | Delaminations + Cracks + Holes |          |         | Delaminations |          |         | Cracks + Holes |          |         |
|-----------------------|--------------------------------|----------|---------|---------------|----------|---------|----------------|----------|---------|
|                       | $2L > 0$                       | > 15 in. | > 3 in. | $2L > 0$      | > 15 in. | > 3 in. | $2L > 0$       | > 15 in. | > 3 in. |
| Data from reference 3 | 972                            | 702      | 392     | 487           | 438      | 292     | 485            | 264      | 100     |
| MIG-29                | $2L > 0$                       | > 30 m   | > 80 mm | $2L > 0$      | > 30 mm  | > 80 m  | $2L > 0$       | > 30 mm  | > 80 m  |
|                       | 20 833                         | 9395     | 2006    | 10 702        | 7357     | 1337    | 9364           | 2006     | 668     |

Data presented in reference 3 do not allow one to compute empirical exceedance intensity because the work does not provide information about airplane/part types, damage location/size, and so on.

Table 1-8 compares exceedances for airplanes dealt with in the present report and data of table 5-5 (damage type frequency) in reference 3.

TABLE 1-8. COMPARISON OF DATA

| $2L$           | > 0  |             | > 1.5 in.     | > 30 mm |             | > 3 in.       | > 80 mm |             |
|----------------|------|-------------|---------------|---------|-------------|---------------|---------|-------------|
|                | [1]  | [2]         |               | [1]     | [2]         |               | [1]     | [2]         |
| Scratches      | 10%  | (I) 27.8%   | Avg.<br>16.5% | —       | —           | —             | —       | —           |
|                |      | (II) 23.9%  |               |         | —           |               |         |             |
|                |      | (III) 2.1%  |               |         | —           |               |         |             |
| Delaminations  | 45%  | (I) 45.3%   | Avg.<br>46.9% | 41%     | (I) 28.3%   | Avg.<br>29.2% | 27%     | (I) 12.9%   |
|                |      | (II) 26.6%  |               |         | (II) 6.6%   |               |         | (II) 0.7%   |
|                |      | (III) 68.7% |               |         | (III) 52.6% |               |         | (III) 25.6% |
| Cracks + holes | 45%  | (I) 26.9%   | Avg.<br>36.6% | 24%     | (I) 16.0%   | Avg.<br>18.4% | 9%      | (I) 6.7%    |
|                |      | (II) 49.5%  |               |         | (II) 16.5%  |               |         | (II) 2.7%   |
|                |      | (III) 33.4% |               |         | (III) 22.8% |               |         | (III) 9.1%  |
| Total          | 100% | —           | 100%          | —       | —           | —             | —       | —           |

Notes:

- [1] data of table 5-5 in reference 3
- [2] data dealt with in present report
- (I) units with a high damage rate
- (II) units with an intermediate damage rate
- (III) units with a low damage rate

#### 1.1.4 Initial Data for Analyzing Wing Damage Rates of Lear Fan 2100 and SU-29.

##### a. Lear Fan 2100

By considering the statistical data provided above, the following has been found:

- wing skins are units with low damage rate—see table 1-5. Exceptions are the leading-edge skins; but the present classification is valid “on the average” for all wing panels. If more data accumulated on separate panels of wings, there may be the possibility to outline some panels featuring higher and lower damage rates.
- statistical data on airplane operation by Western companies show that the damage rate is lower than that on Russian airplanes.

The Lear Fan 2100 wing analysis was based on statistical data of reference 3. However, reference 3 contains data for an average airplane and does not subdivide the data for types/geometry of the units. Therefore, it has been assumed that an average airplane has a 30-sq. m total area of composite structures. Table 1-9 provides information about units with low damage rates to enable comparison with data of reference 3.

TABLE 1-9. COMPARING DATA FOR UNITS WITH LOW-DAMAGE RATES

|   | Unit                     | Airplane                    | All Types of Damage* |                        |                      | Delaminations |                        |                      | Cracks + Holes |                        |                      |
|---|--------------------------|-----------------------------|----------------------|------------------------|----------------------|---------------|------------------------|----------------------|----------------|------------------------|----------------------|
|   |                          |                             | $2L > 0$             | $2L > 30 \text{ mm}$   | $2L > 80 \text{ mm}$ | $2L > 0$      | $2L > 30 \text{ mm}$   | $2L > 80 \text{ mm}$ | $2L > 0$       | $2L > 30 \text{ mm}$   | $2L > 80 \text{ mm}$ |
| 1 | Vertical stabilizer skin | MIG-29                      | 0.3649               | 0.1824                 | 0.1216               | 0.1216        | 0.1216                 | 0.06081              | 0.1824         | —                      | —                    |
| 2 | Wing skin                | MEG-29                      | 0.04129              | —                      | —                    | —             | —                      | —                    | 0.04129        | —                      | —                    |
| 3 | Landing gear door        | AN-124                      | 0.3985               | 0.3415                 | 0.1138               | 0.2277        | 0.2277                 | 0.05692              | 0.1708         | 0.1138                 | 0.05692              |
| 4 | Cargo bay door           | AN-124                      | 1.078                | 0.5987                 | 0.2395               | 0.5987        | 0.4789                 | 0.2394               | 0.2395         | 0.1197                 | —                    |
| 5 | Wing/fuselage fairing    | L-1011                      | 0.08459              | 0.02659                | 0.007251             | 0.04108       | 0.009668               | 0.002417             | 0.029          | 0.007251               | 0.004834             |
| 6 | Data of reference 3      | “Average” airplane in fleet | $2L > 0$             | $2L > 1.5 \text{ in.}$ | $2L > 3 \text{ in.}$ | $2L > 0$      | $2L > 1.5 \text{ in.}$ | $2L > 3 \text{ in.}$ | $2L > 0$       | $2L > 1.5 \text{ in.}$ | $2L > 3 \text{ in.}$ |
|   |                          |                             | 0.036                | —                      | —                    | 0.01623       | 0.0146                 | 0.009733             | 0.01617        | 0.0088                 | 0.00333              |

\* Scratches + delaminations + cracks + holes

Figure 1-16 is a plot of exceedance intensity, which is approximated by exponential functions:

for delaminations

$$H(2L) = 0.0171 \cdot e^{\left(-\frac{2L}{149.3}\right)}$$

for crack + hole

$$H(2L) = 0.0172 \cdot e^{\left(-\frac{2L}{48.31}\right)}$$

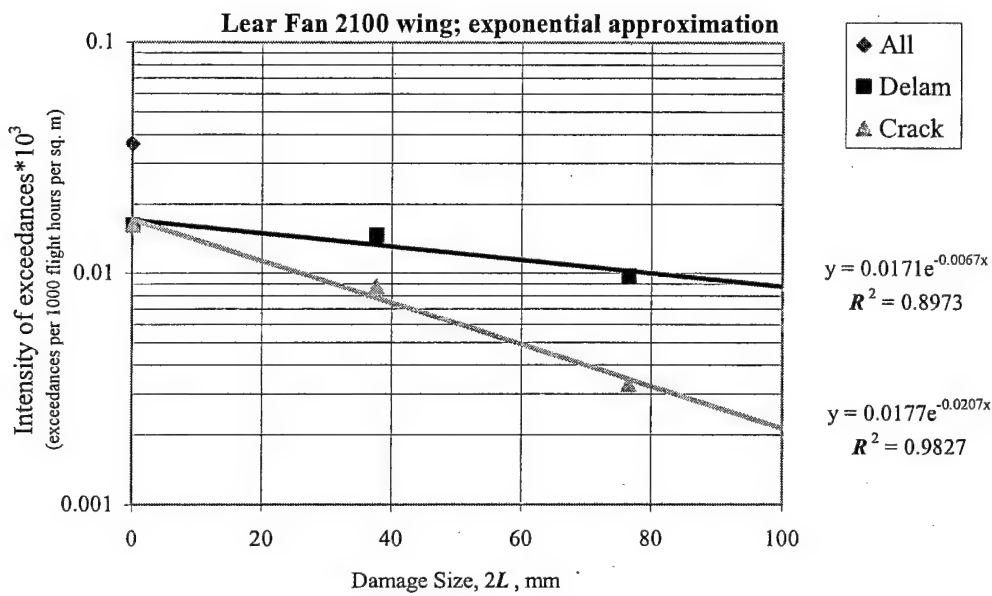


FIGURE 1-16. EXCEEDANCE INTENSITY OF DAMAGE—EXPONENTIAL APPROXIMATION

For comparison's sake, figure 1-17 provides the same kind of plots based on polynomial approximation:

for delaminations

$$H(2L) = -10^{-6} \cdot (2L)^2 - 3 \cdot 10^{-7} \cdot (2L) + 0.0162$$

for crack + hole

$$H(2L) = -7 \cdot 10^{-7} \cdot (2L)^2 - 2 \cdot 10^{-4} \cdot (2L) + 0.0162$$

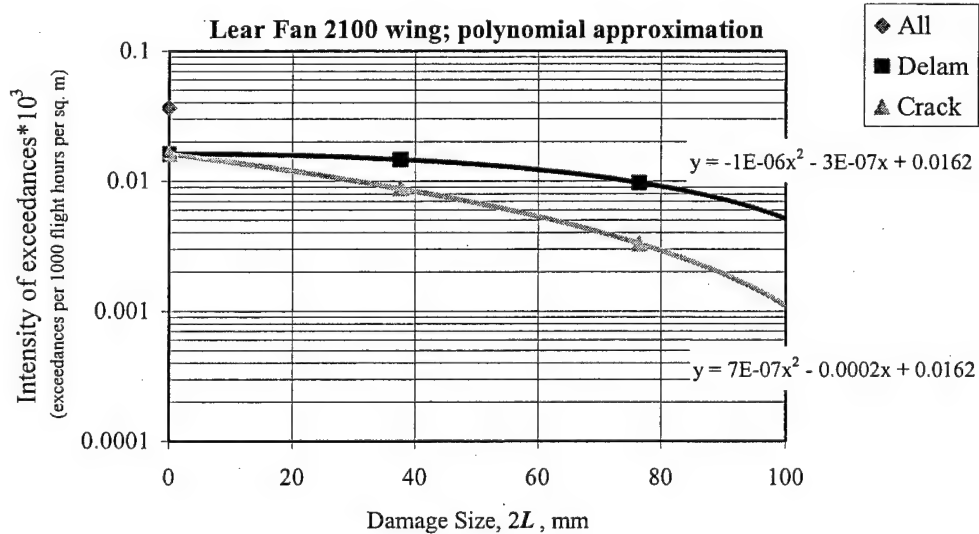


FIGURE 1-17. EXCEEDANCE INTENSITY OF DAMAGE—POLYNOMIAL APPROXIMATION

b. SU-29

The SU-29 damage rate analysis relies on data presented in reference 4. As with the previous case, the assumption was that the crack + hole exceedance is equal to that of delaminations. Table 1-10 reports these data.

TABLE 1-10. EMPIRICAL EXCEEDANCE INTENSITY (PER 1000 FLIGHT HOURS PER SQUARE METER) ADOPTED FOR ANALYZING SU-29 WING

|          | Delaminations | Cracks + Holes |
|----------|---------------|----------------|
| $2L > 0$ | 0.45          | 0.45           |
| > 20 mm  | 0.173         | 0.173          |
| > 60 mm  | 0.051         | 0.051          |
| > 100mm  | 0.0264        | 0.0264         |
| > 140 mm | 0.0136        | 0.0136         |
| > 200 mm | 0.0074        | 0.0074         |
| > 300 mm | 0.0022        | 0.0022         |
| > 400 mm | 0.00066       | 0.00066        |
| > 500 mm | 0.000172      | 0.000172       |

Table 1-10 data and their theoretical approximation are presented graphically in figure 1-18. Used as the theoretical approximation is the function:

$$H(2L) = 0.1724 \cdot e^{\left(-\frac{2L}{69.44}\right)}$$

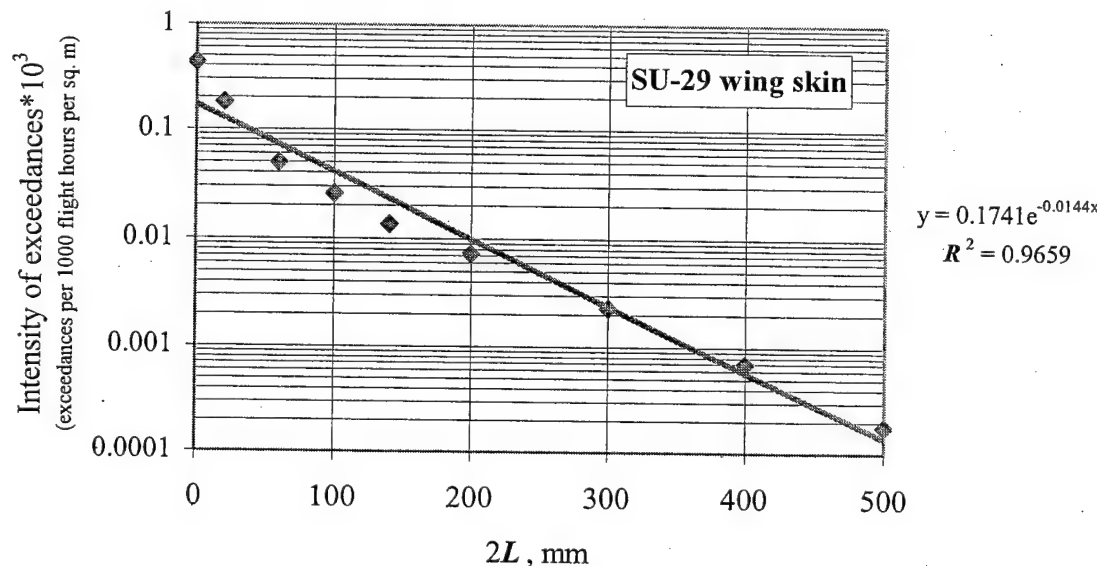


FIGURE 1-18. EXCEEDANCE INTENSITY OF DAMAGE

Values  $H_0 = 0.1741$  and  $b = 69.44$  are close to averaged values for Group III (refer to table 1-5) if one equalizes empirical exceedances for delamination and cracks + holes:

$$H_0 = \frac{0.2701 + 0.1311}{2} = 0.2006$$

$$b = \frac{69.35 + 54.71}{2} = 62.03$$

### 1.1.5 Conclusion.

In general, one may use the above statistics on empirical exceedances for airframe units in order to suggest the following approximation equation describing the damage occurrence rate curves:

$$H(2L) = H_0 \cdot e^{\left(\frac{-2L}{b}\right)}$$

Values  $H_0$  and  $b$  (referred to 1 000 flight hours and sq. m) are stated in table 1-11.

TABLE 1-11. RECOMMENDED VALUES OF  $H_0$  AND  $b$   
(per 1000 flight hours per square meter)

| Group                                 | Unit   | $H_0$               |               |              | $b$                 |               |              |
|---------------------------------------|--|---------------------|---------------|--------------|---------------------|---------------|--------------|
|                                       |  | All Types of Damage | Delaminations | Crack + Hole | All Types of Damage | Delaminations | Crack + Hole |
| I—<br>High<br>damage<br>rate          | <u>Maneuverable airplanes:</u><br>• wing leading edges<br>• engine fairings<br>• vertical stabilizer actuator fairings<br>• nose landing gear fairings,<br>• nose landing gear doors       | 3.6                 | 1.6           | 0.97         | 38                  | 64            | 58           |
| II—<br>Intermediate<br>damage<br>rate | <u>Maneuverable airplanes</u><br>• air inlet channels<br>• lower vault panels  | 1.6                 | 0.43          | 0.81         | 28                  | 22            | 27           |
| III—<br>Low<br>damage<br>rate         | <u>Maneuverable airplanes</u><br>• vertical stabilizer skins<br>• wing skins<br><u>Low-maneuverable airplanes</u><br>• wing/fuselage fairings<br>• landing gear doors<br>• cargo bay doors | 0.33                | 0.27          | 0.13         | 56                  | 69            | 55           |

## 2. EFFICIENCY OF REPAIRS ON AIRFRAMES MADE OF COMPOSITES.

An aircraft structure may suffer from damage in the form of a scratch, indentation, punch, and/or delamination caused by mechanical impacts. In addition, sandwich structures can have skin delamination from honeycomb core because a bond may show inadequate strength or because the structure may lose airtightness, so moisture could penetrate inside the structure. These damages degrade strength. Moreover, delamination areas tend to grow under long-term action of variable loads and environmental attack. Therefore, principal requirements in respect of ensuring in-service reliability of these structures include condition monitoring, timely detection of damage, and repair.

Various manufacturing errors may be detected in the course of nondestructive inspection at factories; in-service damage may be found during scheduled inspection. Repairing these anomalies is a mandatory component for ensuring damage tolerance of airframes. If the production instructions are followed during manufacture, there would be no defects in structures. However, acceptance testing do sometime reveal manufacturing errors, and cognizant engineers for each defect, makes a decision: accept, repair, or not accept the structure. While in service, damages may occur, and detecting these requires a systematic inspection, with involvement of instrumented inspection methods.

The literature available to the authors contains insufficient amount of data on composites strength recovery by repair, so systematization is difficult to carry out. This is due to some specificity of repair processes, which are often developed for a particular structural units, particular operational conditions, and particular repair conditions. Below, results of studying postrepair strengths are provided; principal data have been reported in references 2 and 5.

### 2.1 REPAIR OF COMPOSITE SKIN.

Types of repair work on skins may be classified as follows:

- Prepreg-based repair. The damage area is filled with prepreg layers (see figure 2-1). It is customary to grind the damage area edge to form either a cylinder or a cone.
- Repair with metal/composite patches (see figure 2-2). Repairs may be made with no insert and with a patch at a either side. Patches can be attached by using three methods:
  - method 1: bonding the patch
  - method 2: bonding and fastening the patch
  - method 3: of fixing the patch with fasteners only

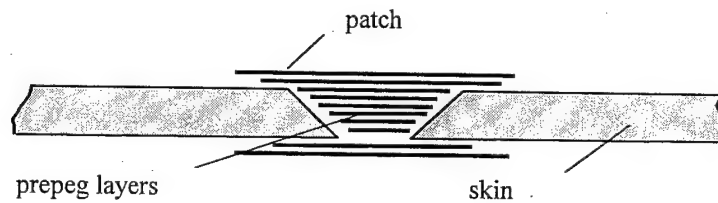


FIGURE 2-1. PREPREG-BASED REPAIR

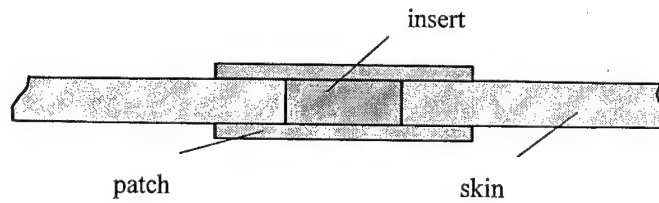


FIGURE 2-2. REPAIR WITH THE USE OF PATCHES

## 2.2 DATA FROM EXPERIMENTS ON RECOVERING THE SKIN STRENGTH BY REPAIR.

The test program included evaluating two batches of specimen made out of KMU-3L carbon fiber reinforced plastic with  $[0^\circ/90^\circ]$  stacking:

- Batch 1. Specimens (with 360-mm by 150-mm in-plane dimensions and 50-mm-diameter cutouts) have been repaired in accordance with recommendations for mass-production factories that possess special-purpose equipment including autoclaves, refrigerators, etc.
- Batch 2. Specimens (with 260 by 80 mm dimensions and 20-mm-diameter holes) have been repaired so as to replicate field conditions.

The tests involved

- repaired specimens,
- specimens with no defects, and
- specimens with defects that were not repaired.

Table 2-1 represents results of static tension tests on Batch 1:

- $P_{rep}$  for the repaired specimens,
- $P$  for specimens with no defects, and
- $P_{hole}$  for specimens with defects that were not repaired.

Table 2-2 reports data for Batch 2. The tables also depict schematics of repair, as well as the repair efficiency indicator  $K = \frac{P_{rep.}^{av.}}{P^{av.}}$  and the residual strength improvement factor  $K_1 = \frac{P_{rep.}^{av.}}{P_{hole}^{av.}}$ ; these are based on mean values of ultimate loads. The test results may be described as follows.

### 2.2.1 Bond-Based Repair With Patches (Batch 1).

To evaluate efficiency of the bonding for repairing the carbon fiber reinforced plastic (CFRP) skin, double-sided circular patches were utilized. In the patch and specimen, the ply angles of the plies contacting with the adhesive film were identical. Table 2-1 shows that the present repair method features the repair efficiency indicator  $K = 63\%$  and the residual strength improvement factor  $K_1 = 2$  defined as strength of repaired specimen divided by the strength of the unrepaired specimen.

TABLE 2-1. RESULTS OF TESTING BATCH 1 (of 360- by 150-mm specimens)

(Loading conditions: static tension; basic material: CFRP; Repair method: prepreg-based repair with treating the damage area edge to form a cone, bonded one-sided patches.)

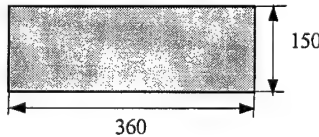
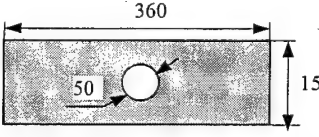
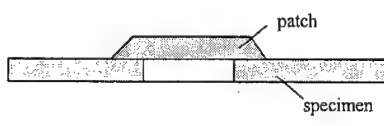
| No. | Specimen/Repair Schematic  | Specimen ID | $P^{ult.}, N$              | $P^{av.}, N$ | $K, \%$ | $K_1$ |
|-----|--|-------------|----------------------------|--------------|---------|-------|
| I   | Intact specimen<br>               | 1           | 76,500                     | 76,500       | —       | —     |
| II  | Specimen with hole<br>            | 2<br>3      | 23,500<br>25,000           | 24,250       | —       | —     |
| III | Bonded one-sided CFRP patches<br> | 4<br>5<br>6 | 48,000<br>55,800<br>40,500 | 48,100       | 63      | 2.0   |

TABLE 2-1. RESULTS OF TESTING BATCH 1  
(of 360- by 150-mm specimens) (Continued)

| No. | Specimen/Repair Schematic    | Specimen ID | $P^{ult.}, N$ | $P^{av.}, N$ | $K, \%$ | $K_1$ |
|-----|------------------------------|-------------|---------------|--------------|---------|-------|
| IV  | Specimen with conical cutout | 7           | 14,000        |              |         |       |
|     |                              | 8           | 16,500        | 15,250       | —       | —     |
| V   | Prepreg-based repair         | 9           | 45,000        |              |         |       |
|     |                              | 10          | 44,000        | 43,000       | 56      | 2.8   |
|     |                              | 11          | 41,000        |              |         |       |
| VI  | Prepreg-based repair         | 12          | 49,500        |              |         |       |
|     |                              | 13          | 59,500        | 54,500       | 71      | 3.57  |
| VII | Prepreg-based repair         | 14          | 71,000        |              |         |       |
|     |                              | 15          | 67,000        | 69,000       | 90      | 4.52  |

### 2.2.2 Prepreg-Based Repair for CFRP Skin (Batch 1).

Efficiency of the method including damage area edge treatment with forming a cone with 1:18 slope—which is advised in literature as optimal for CFRP skins was studied. The damage area was filled with a plug made of KMU-4L composite. The area has been reinforced by applying additional external patches. Also, the influence of roughened patch edges on patch/specimen adhesion strength was estimated. It turned out that increasing the number of layers in the patch from 6 to 9 improves the prepreg-based repair method efficiency from 56% to 90%. Making teeth on the patch edge oriented along the load axis increases the repair efficiency from 56% to 71%.

### 2.2.3 Methods for Repairing the Polymer Composite Materials in Field Conditions (Batch 2).

Two methods to effect field repairs were investigated. One utilized KMU-6-36 composite with VK-36 film adhesive. The second method used KMU-5L-CFRPP (composed of LV-3 CFRP tape and EDA/2 resin). The first method still required autoclave or press forming, but the hole was not filled and the patch was applied on one side only. Table 2-2 shows that this approach to in-service damage repair provides a rather high efficiency  $K = 83\text{--}90\%$ .

Repairs in field conditions using patches made of KMU-5L CFRP requires a moderate cure temperature and does not need high pressure for forming. The tape is impregnated during stacking of the patch on the damage area; thereafter, the structure is heated, while being subjected to local pressure whose value for the specimens was varied from 500 MPa to 3,000 MPa. Experiments show the efficiency to increase from 56% to 67% at higher pressure, refer to table 2-2.

TABLE 2-2. RESULTS OF TESTING BATCH 2 (of 260- by 80-mm specimens)

(Loading conditions: static tension; basic material: CFRP; Repair method: prepreg-based repair with no cone formed on damage area edge, bonded one-sided patches.)

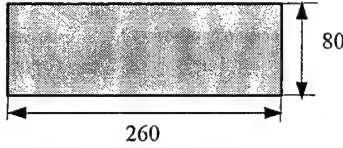
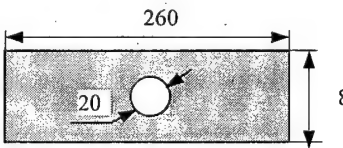
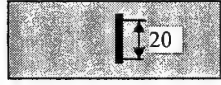
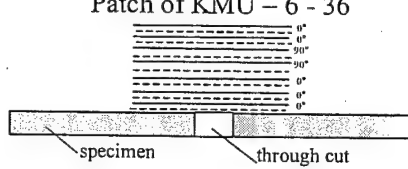
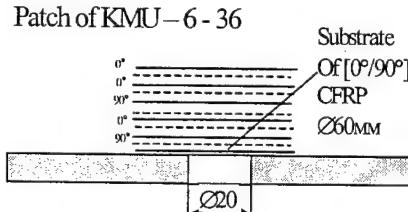
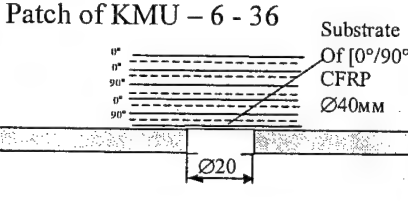
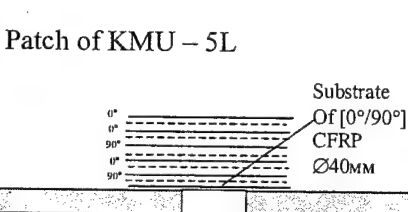
| No. | Specimen/Repair Schematic   | Specimen ID | $P^{ult.}, N$    | $P^{av.}, N$ | $K, \%$ | $K_1$ | Note |
|-----|---|-------------|------------------|--------------|---------|-------|------|
| I   | Intact specimen   | 1<br>2      | 43,000<br>39,000 | 41,000       | —       | —     |      |
|     |  |             |                  |              |         |       |      |
| II  | Specimen with hole  | 3<br>4      | 21,000<br>20,000 | 20,500       | —       | —     |      |
|     |  |             |                  |              |         |       |      |
| III | Specimen with through cut   | 5<br>6      | 17,900<br>16,100 | 17,000       | —       | —     |      |
|     |  |             |                  |              |         |       |      |

TABLE 2-2. RESULTS OF TESTING BATCH 2 (of 260- by 80-mm specimens)  
(Continued)

| No. | Specimen/Repair schematic   | Specimen ID | $P_{ult.}, N$ | $P_{av.}, N$ | $K, \%$ | $K_I$ | Note              |
|-----|---|-------------|---------------|--------------|---------|-------|-------------------|
| IV  | Patch of KMU - 6 - 36<br>  | 7           | 33,500        |              |         |       | 5-mm overlap      |
|     |   | 8           | 33,800        | 34,700       | 84      | 2.0   |                   |
|     |   | 9           | 36,800        |              |         |       |                   |
| V   | Patch of KMU - 6 - 36<br>  | 10          | 34,200        |              |         |       | 5-mm overlap      |
|     |   | 11          | 34,600        | 34,600       | 84      | 1.7   |                   |
|     |   | 12          | 35,000        |              |         |       |                   |
| VI  | Patch of KMU - 6 - 36<br> | 13          | 37,500        |              |         |       | 10-mm overlap     |
|     |   | 14          | 36,000        | 37,000       | 90      | 1.85  |                   |
|     |   | 15          | 37,500        |              |         |       |                   |
|     |   | 16          | 35,200        |              |         |       | 5-mm overlap      |
|     |   | 17          | 33,200        | 34,200       | 83      | 1.70  |                   |
|     |   | 18          | 34,200        |              |         |       |                   |
| VII | Patch of KMU - 5L<br>    | 19          | 24,150        |              |         |       | Pressure 500 MPa  |
|     |   | 20          | 24,000        | 24,000       | 56      | 1.20  |                   |
|     |   | 21          | 25,000        |              |         |       | Pressure 500 MPa  |
|     |   | 22          | 26,200        | 25,600       | 60      | 1.28  |                   |
|     |   | 23          | 30,000        |              |         |       | Pressure 3000 MPa |
|     |   | 24          | 27,600        | 28,000       | 67      | 1.44  |                   |

In terms of strength restoration, the best repair method for skins is the version in which prepreg is utilized and the damage area edge is processed to form a cone. According to the data above (and information in reference 6), the efficiency  $K$  of this method may be as high as 97%. Note, however, that the version needs a relatively great labor consumption (and cost) requirement. One could reject the edge forming stage, thus notably reducing the repair expenses. However, the repair efficiency  $K$  in this case reduces to approximately 90%.

Prepreg-based repair is costly, so references 7 and 8 recommend the field repair teams to rely on patches of aluminum and titanium attached to skins by fasteners. However, the efficiency of these methods is usually as low as 50%. Therefore, the repair with mechanical joints should be considered temporary; it would be followed with more thorough repair at depots or repair stations.

Bond repair methods are relatively efficient, especially those with double-sided patches. According to reference 9, CFRP panels repaired by using adhesives have been restored to 53%-77% by one-sided patches and to 89%-99% by double-sided patches. Additional fasteners make it possible to improve reliability and efficiency of bonded methods, especially when a one-sided patch may only be applied.

The present data on the repair efficiency can be summarized in figure 2-3. However, one should bear in mind that the data are conditional since the efficiency of a particular repair strongly depends on production process used.

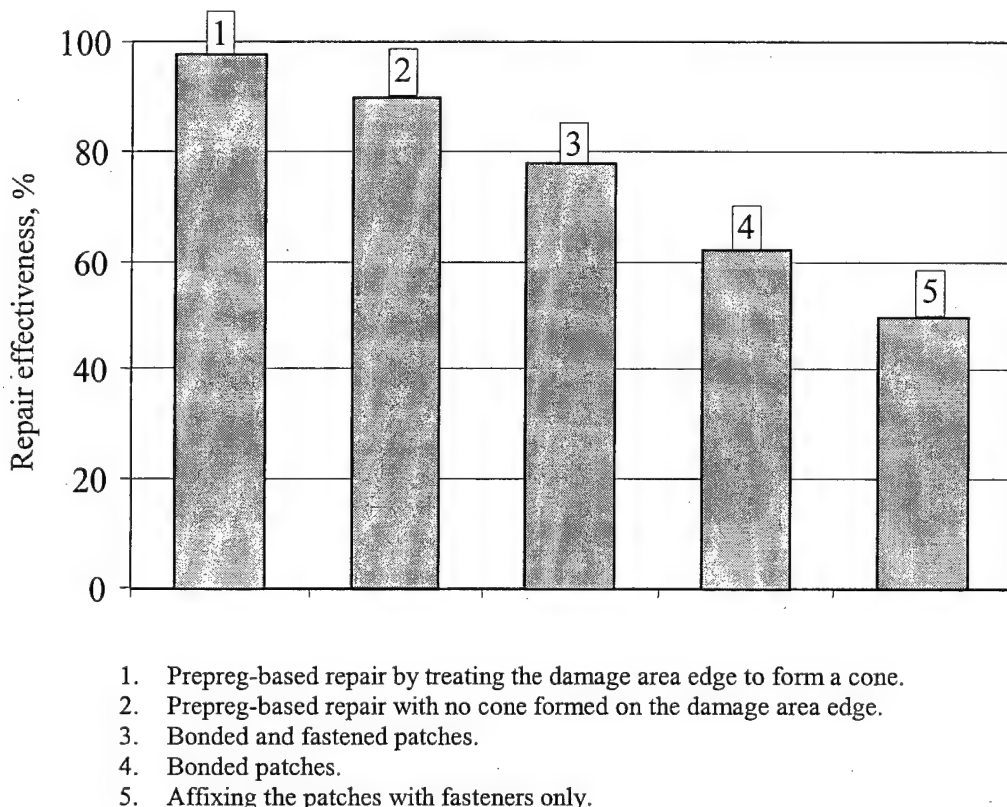


FIGURE 2-3. REPAIR EFFECTIVENESS OF VARIOUS METHODS

## 2.3 REPAIR OF HONEYCOMB SANDWICH STRUCTURE.

The type of repair chosen depends on the extent of damage. The damages to a structure can be subdivided into the following groups:

- Group 1: damage not violating structural integrity—such as indentation, scratch, or skin erosion.
- Group 2: damage resulting in partial violation of structural integrity—such as crack, delamination, punch through a composite ply, or core damage.
- Group 3: damage violating structural integrity—such as through holes or cracks with damage to load-carrying layers.
- Group 4: damage violating structural integrity, so greatly, that separate components or the entire structure must be replaced.

### 2.3.1 Repairing Group 1 Damage.

Indentation, scratch, and superficial cracks in load-carrying layers may be removed by utilizing suitable filler such as epoxy resin. To do so, the damaged area is cleaned, washed, and treated with the filler. Upon hardening, the filler is ground and covered with a protective layer. If the damage to the load-carrying layer can degrade strength (for example, in the case with deep cracks) then the area would be reinforced with patches.

### 2.3.2 Repairing Group 2 Damage.

Applicability of various repair methods depends on damage sizes and structural strength requirements.

Disbonded (or delamination) areas are cured by injecting the adhesives and fillers through holes (see figure 2-4).

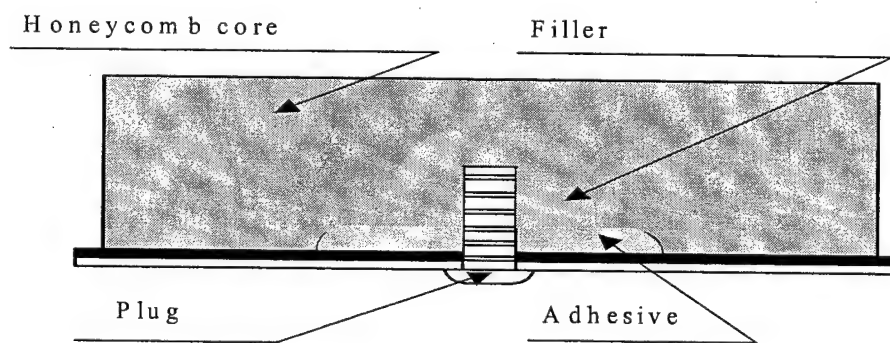


FIGURE 2-4. REPAIRING A DELAMINATION AREA

If the delamination area is rather large, the usual practice is to insert special purpose plugs or fasteners.

When repairing a through hole, both the skin and honeycomb core are removed to form a cylindrical or square hollow (with rounded corners). The honeycomb core may be cut partially (figure 2-5(a)) or completely (figure 2-5(b)). Patches are applied (figure 2-5(b)) for better structural strength recovery.

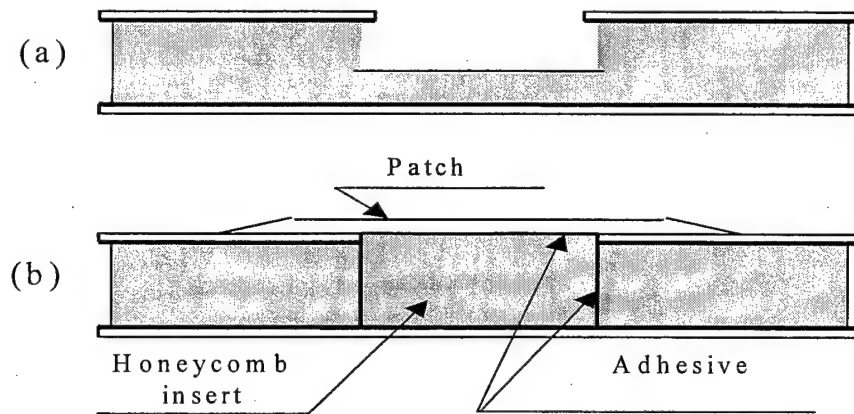


FIGURE 2-5. REPAIRING A PARTIAL THROUGH HOLE

### 2.3.3 Repairing Group 3 Damage.

Damage that is through the thickness can be repaired by using the same approaches as in the Group 2 damage (see figure 2-6). At first, a patch is bonded onto the first skin, then honeycomb core is recovered, and finally the other patch is bonded onto the second skin.

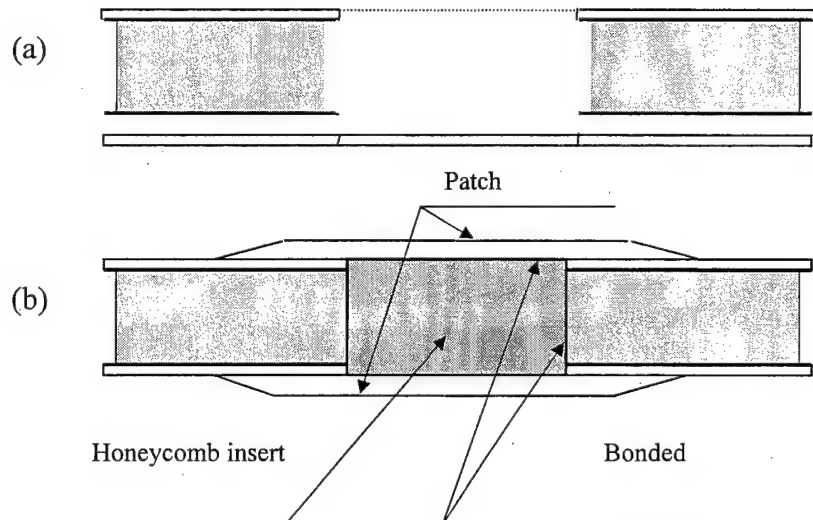


FIGURE 2-6. REPAIRING A THROUGH HOLE

## 2.4 EXPERIMENTAL DATA ON RECOVERING THE SANDWICH STRUCTURE SPECIMEN STRENGTH AFTER REPAIR.

To evaluate the strength recovery factor for sandwich structures bonded with the VK-31 adhesive, the intact and damaged specimens have been tested under various loads. The test results were used to estimate the strength recovery factor for sandwich structures subjected to various repair methods.

### 2.4.1 Shear Strength Test Results.

The shear tests were conducted in a hinged frame with a 330- by 330-mm workspace. Table 2-3 reports the test data. The repaired components almost recover their strength with respect to this kind of loading.

TABLE 2-3. TEST RESULTS FOR REPAIRED SHEAR PANELS UNDER STATIC LOAD

| Dimensions<br>(mm) |                 |                    | Damage/Repair Type         | $\tau_{ult\ mean}^{**}$<br>kg/sq. mm | $K = \tau_{rep}/\tau_{int.}^*$ |
|--------------------|-----------------|--------------------|----------------------------|--------------------------------------|--------------------------------|
| $h$                | $\delta_{skin}$ | $\delta_{wall\ a}$ |                            |                                      |                                |
| 20                 | 0.4             | 0.03-2.5           | Disbonded skin             | 28.4                                 | 96                             |
|                    |                 |                    | Repair type; figure 2-4    | 29.0                                 | 98                             |
|                    |                 |                    | Ø70 mm                     | 28.6                                 | 97                             |
| 20                 | 0.4             | 0.03-2.5           | One-sided damage           | 30.8                                 | 105                            |
|                    |                 |                    | Repair type; figure 2-5(b) |                                      |                                |
| 20                 | 0.4             | 0.03-2.5           | Double-sided damage        | 28.1                                 | 95                             |
|                    |                 |                    | Repair type; figure 2-6(b) |                                      |                                |
| 20                 | 0.4             | 0.04-5             | Disbonded skin             | 28.6                                 | 100                            |
|                    |                 |                    | Repair type; figure 2-4    | 28.4                                 | 99                             |
|                    |                 |                    | Ø70 mm                     | 28.3                                 | 98                             |
| 20                 | 0.4             | 0.04-5             | One-sided damage           | 25.7                                 | 90                             |
|                    |                 |                    | Repair type; figure 2-5(b) |                                      |                                |
| 20                 | 0.4             | 0.04-5             | Double-sided damage        | 26.8                                 | 93                             |
|                    |                 |                    | Repair type; figure 2-6(b) |                                      |                                |

\* the mean ultimate shear stress for specimens with no damage,  $\tau_{int.}$ , is 29.5 kg/sq. mm for panels with honeycomb core (0.03-2.5mm) and 28.6 kg/sq. mm for panels with honeycomb core (0.04-5 mm).

\*\* - mean ultimate shear stress for three specimens with damage repaired.

The repaired specimens were fatigue loaded in shear by sine cycles at  $\tau_{min} = 0.3$  kg/sq. mm and  $\tau_{max} = 14.7$  kg/sq. mm. Load-bearing capability under the fatigue load was compared with that under static load. Repaired specimens were being subjected to the fatigue load until there appeared cracks detectable by the naked eye (i.e., as long as 20 mm); thereafter, residual strength of the specimens was evaluated. Results of the fatigue tests may be seen in table 2-4.

It is clear from table 2-4 that the load-bearing capability of repaired specimens in fatigue degrades by 4% to 28%—depending on the type of damage.

TABLE 2-4. TEST RESULTS FOR REPAIRED SHEAR PANELS IN FATIGUE

| Dimensions (mm) |                 |                         | Damage/Repair Type                                       | Cycles to Crack Detection | $\tau_{residual}$ kg/sq. mm | $K = \tau_{res} / \tau_{static}$ |
|-----------------|-----------------|-------------------------|--|---------------------------|-----------------------------|----------------------------------|
| $h$             | $\delta_{skin}$ | $\delta_{wall \cdot a}$ |  |                           |                             |                                  |
| 20              | 0.4             | 0.03-2.5                | Disbonded skin Ø50 mm<br>Repair type; figure 2-4         | 120,000                   | 28.1                        | 0.96                             |
|                 |                 |                         |  | 118,750                   | 27.1                        |                                  |
|                 |                 |                         |  | 121,300                   | 28.9                        |                                  |
| 20              | 0.4             | 0.03-2.5                | One-sided damage Ø50 mm<br>Repair type; figure 2-5(b)    | 98,800                    | 28.1                        | 0.82                             |
|                 |                 |                         |  | 101,500                   | 26.4                        |                                  |
|                 |                 |                         |  | 140,160                   | 21.3                        |                                  |
| 20              | 0.4             | 0.03-2.5                | Double-sided damage Ø50 mm<br>Repair type; figure 2-6(b) | 120,280                   | 26.3                        | 0.90                             |
|                 |                 |                         |  | 115,300                   | 25.4                        |                                  |
|                 |                 |                         |  | 118,400                   | 24.6                        |                                  |
| 20              | 0.4             | 0.04-5                  | Disbonded skin Ø30 mm<br>Repair type; figure 2-4         | 122,500                   | 24.4                        | 0.82                             |
|                 |                 |                         |  | 117,800                   | 23.1                        |                                  |
|                 |                 |                         |  | 80,900                    | 22.6                        |                                  |
| 20              | 0.4             | 0.04-5                  | One-sided damage Ø50 mm<br>Repair type; figure 2-5(b)    | 127,250                   | 18.4                        | 0.78                             |
|                 |                 |                         |  | 120,850                   | 19.8                        |                                  |
|                 |                 |                         |  | 62,500                    | 21.9                        |                                  |
| 20              | 0.4             | 0.04-5                  | Double-sided damage Ø50 mm<br>Repair type; figure 2-5(b) | 61,500                    | 21.8                        | 0.72                             |
|                 |                 |                         |  | 76,630                    | 17.9                        |                                  |
|                 |                 |                         |  | 90,450                    | 18.8                        |                                  |

Panels with repaired disbonds were fatigue loaded to failure at various maximum levels of shear stress:  $\tau = 10, 12, 14.7$  kg/sq. mm. The tests reveal that cracks occur around the plugs. Development of fatigue cracks depends on total hours of fatigue and the shear stress applied; refer to figure 2-7.

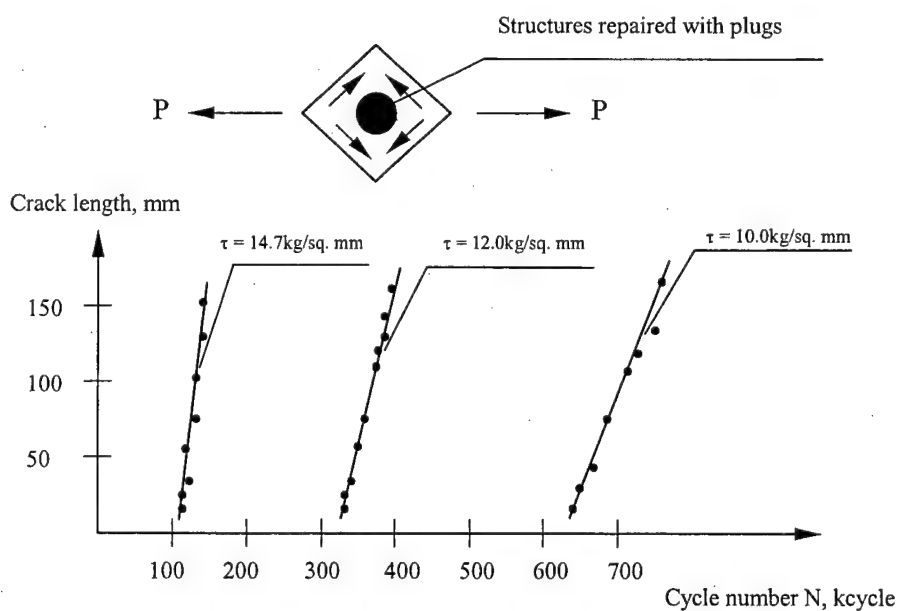


FIGURE 2-7. CRACK GROWTH DURING FATIGUE LOADING

#### 2.4.2 Results of Testing Under In-Plane Compression.

Sandwich panel specimens with length  $l = 300$  mm, width  $b = 140$  mm, and thickness  $h = 20$  mm underwent testing under in-plane compression. A damage area was at the center of each specimen.

Tests results are shown in table 2-5. Panels failed because of skin buckling and honeycomb shear. Panels with disbonding have disbonded under load of approximately 70% of the breaking value for intact panels. Repair of both one-sided and double-sided damages almost completely recover structural in-plane compressive strength.

TABLE 2-5. TEST RESULTS FOR INTACT AND REPAIRED PANELS UNDER COMPRESSIVE LOADING

| Damage Type   | Cell Size | $\sigma_{ult.}$<br>kg/sq. mm | $K = \tau_{rep.} / \tau_{int.}$<br>% |
|---|-----------|------------------------------|--------------------------------------|
| Intact panel  | 2.5-0.03  | 38.3                         | —                                    |
|   | 5-0.04    | 33.3                         | —                                    |
| Skin disbonded from core<br>(repaired*)<br>(diameter 30 mm) | 2.5-0.03  | 24.8                         | 65                                   |
|   | 5-0.04    | 23.0                         | 69                                   |
| Disbonding (repaired*)<br>(diameter 30 mm)                  | 2.5-0.03  | 32.7                         | 85                                   |
|   | 5-0.04    | 32.0                         | 96                                   |
| One-sided damage (repaired*)<br>(diameter 30 mm)            | 2.5-0.03  | 36.3                         | 95                                   |
|   | 5-0.04    | 33.1                         | 100                                  |
| Double-sided damage (repaired*)<br>(diameter 30 mm)         | 2.5-0.03  | 37.3                         | 97                                   |
|   | 5-0.04    | 30.5                         | 92                                   |

\*For repair schematics see table 2-3

$\sigma_{ult.}$  – mean ultimate compressive strength for three specimens

#### 2.4.3 Results of Testing in Bending.

Specimens with length  $l = 500$  mm, width  $b = 100$  mm, and thickness  $h = 20$  mm were tested under four-point bending in a rig with 100 mm distance between support points. In each specimen a damaged area was at the center between the supports. Results for repaired specimens are shown in table 2-6. Specimens with disbonding not repaired have failed under loads less (by 30%-35%) than those for intact specimens. Upon the repair, the specimens have almost completely recovered their strengths.

TABLE 2-6. TEST RESULTS FOR INTACT AND REPAIRED PANELS UNDER BENDING

| Damage Type  | Cell Size | $\sigma_{ult.}$<br>kg/sq. mm | $K = \tau_{rep.} / \tau_{int.}$<br>% |
|--|-----------|------------------------------|--------------------------------------|
| Intact panel   | 2.5-0.03  | 35.0                         | —                                    |
|  | 5-0.04    | 31.2                         | —                                    |
| Skin disbonded from core (unrepaired*)<br>(diameter 30 mm) | 2.5-0.03  | 24.8                         | 71                                   |
|  | 5-0.04    | 20.5                         | 66                                   |
| Disbonding (repaired*)<br>(diameter 30 mm)                 | 2.5-0.03  | 33.9                         | 97                                   |
|  | 5-0.04    | 24.4                         | 78                                   |
| One-sided damage (repaired*)<br>(diameter 30 mm)           | 2.5-0.03  | 34.1                         | 97                                   |
|  | 5-0.04    | 31.0                         | 99                                   |
| Double-sided damage (repaired*)<br>(diameter 30 mm)        | 2.5-0.03  | 34.4                         | 98                                   |
|  | 5-0.04    | 27.0                         | 87                                   |

\*For repair schematics see table 2-3

$\sigma_{ult.}$  – mean ultimate out of plane bending stress in skins

## 2.5 CONCLUSIONS.

It is difficult to generalize the available data on residual strength after repair. The data suggest that the residual strength greatly depends on the repair method employed. Note also a principal difference between statistical data on damage occurrence rates and statistical information on strength restoration factors. The damage rate is a real indicator which is hard to control by human beings. Whereas the strength restoration data can be changed by using advanced repair techniques and by selecting the structures to be repaired. Therefore, when estimating the probability of failure of particular structures, the analyst should adopt a suitable restoration factor, as well as respective strength variance factors. These values should thereafter be inserted in the repair documentation and become the basis for technical inspection after repair.

Proceeding from these considerations, the Lear Fan-2100 and SU-29 wing failure probability analyses were based on the restoration factors and strength variance factors represented in table 2-7.

In general the initial data for statistical modelling may proceed from the values presented in table 2-8.

TABLE 2-7. STRENGTH RESTORATION FACTORS (SRF)

|  | SRF for<br>Tension Mode |                             | SRF for<br>Compression Mode |                             | SRF for<br>Buckling Mode |                             |
|--|-------------------------|-----------------------------|-----------------------------|-----------------------------|--------------------------|-----------------------------|
|  | Mean<br>Strength        | Coefficient<br>of Variation | Mean<br>Strength            | Coefficient<br>of Variation | Mean<br>Strength         | Coefficient<br>of Variation |
| Airfield conditions,<br>holes/cracks   | 0.95                    | 0.1                         | 0.95                        | 0.1                         | 0.95                     | 0.12                        |
| Maintenance facility,<br>holes/cracks  | 1.0                     | 0.1                         | 1.0                         | 0.1                         | 1.0                      | 0.12                        |
| Airfield conditions,<br>delaminations  | 0.95                    | 0.12                        | 0.95                        | 0.12                        | 0.95                     | 0.12                        |
| Maintenance facility,<br>delaminations | 1.0                     | 0.12                        | 1.0                         | 0.12                        | 1.0                      | 0.12                        |

TABLE 2-8. ESTIMATED DATA ON STRENGTH RESTORATION FACTOR

| Repair Method   | Strength Restoration Factor               |
|---|---|
| <u>Composite Skin</u>   |   |
| 1. Prepreg-based repair   |   |
| <ul style="list-style-type: none"> <li>with damage area edge formed as a cone</li> <li>with no cone formed on damage area edge</li> </ul>   | 50... 97%<br>50... 90%                    |
| 2. Repair with patches  |   |
| <ul style="list-style-type: none"> <li>adhesive/fastener joint with one-sided patch</li> <li>adhesive joint <ul style="list-style-type: none"> <li>with one-sided patch</li> <li>with double-sided patch</li> </ul> </li> <li>mechanical joint</li> </ul> | 65... 80%<br>50...80%<br>90...100%<br>50% |
| <u>Sandwich Panel With Honeycomb Core</u>   |   |
| 1. Repairing the skin debonding from honeycomb  | 80...100%                                 |
| 2. Repairing a hole/crack   |   |
| in one skin   | 80...100%                                 |
| in two skins  | 70...95%                                  |

### 3. EXPERIMENTAL DATA ON THE INFLUENCE OF DEFECTS ON RESIDUAL STRENGTH OF COMPOSITE SKIN.

Creating a math model to evaluate fiber-based composites fracture around a stress concentrator of arbitrary shape is a difficult problem that has not been solved by now. Therefore, the current fracture models rely on simplified methods and fracture resistance characteristics that are determined by testing of specimens with through defects such as a narrow cut or a circular hole. From this point of view, the two-parameter model of references 10-17 use such fracture resistance characteristics as:

- critical Stress Intensity Factors (SIFs) for tension compression and in-plane shear ( $K_{Ic}$ ,  $K_{-Ic}$ ,  $K_{IIc}$ ), and
- corrections for cracking around the crack tip ( $a_I$ ,  $a_{-I}$ ,  $a_{II}$ ).

These parameters are mechanical characteristics of the material itself, but depend on a stacking sequence, and are established by unidirectional testing of specimens with central notches.

#### 3.1 UNIAXIAL TENSION OF SKIN WITH CIRCULAR HOLE—THE TWO-PARAMETER MODEL.

In the two-parameter model substantiated in [10, 11, and 17] the cracking zone at a circular hole is modelled with through narrow notches as depicted in figure 3-1.

The breaking stress,  $\sigma_c^\infty$ , for a plate with infinite width may be determined by the equation from reference 16 for symmetric cracks at a hole with radius  $R$ :

$$\sigma_c^\infty = \frac{K_{Ic}}{\sqrt{\pi a_I} \cdot f(a_I/R)} \quad (3-1)$$

Here,  $\sigma_c^\infty$  is the critical stress intensity factor and  $a_I$  is the correction for cracking zone dimensions. The function  $f(a_I/R)$  with  $f = 1/(1 + R/a_I)$  can be introduced by the plot in figure 3-1.

As for a plate with finite width,  $2B$ , the correction function  $f_1(R/B)$  could be used:

$$\sigma_c^\infty = \frac{K_{Ic}}{\sqrt{\pi a_I} \cdot f(a_I/R) \cdot f_1(R/B)} \quad (3-2)$$

where the correction function may be as in reference 18:

$$f_1\left(\frac{R}{B}\right) = \frac{2 + \left(1 - \frac{R}{B}\right)^3}{3 \cdot \left(1 - \frac{R}{B}\right)}.$$

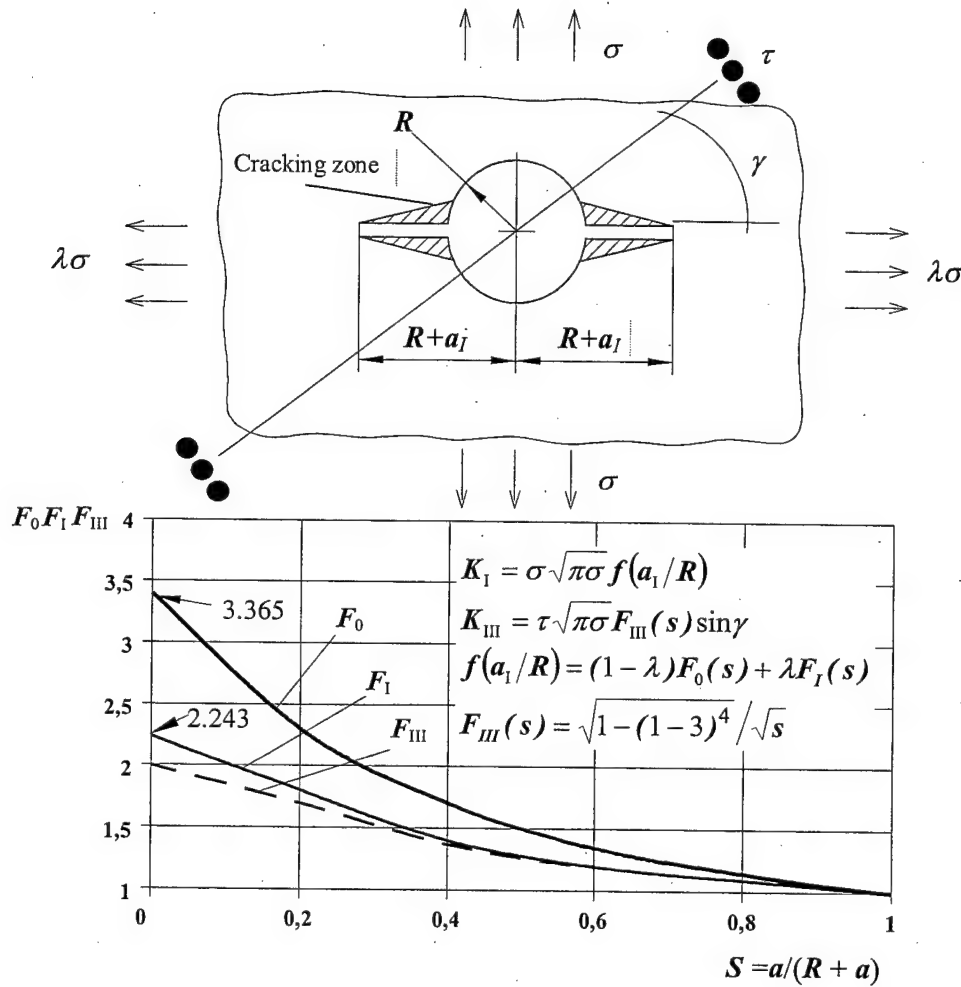


FIGURE 3-1. THE TWO-PARAMETER MODEL FOR EVALUATING STRESS CONCENTRATION

The method for establishing the critical stress intensity factor  $K_{Ic}$  and the crack zone size  $a_I$  may be described as follows. Assuming that two values,  $\sigma_c^{(1)}$  and  $\sigma_c^{(2)}$  were experimentally obtained, then

$$K_{Ic} = \sigma_c^{(1)} \sqrt{\pi a_I} \cdot f\left(\frac{a_I}{R^{(1)}}\right) \cdot f_1\left(\frac{R^{(1)}}{B}\right)$$

$$K_{Ic} = \sigma_c^{(2)} \sqrt{\pi a_I} \cdot f\left(\frac{a_I}{R^{(2)}}\right) \cdot f_1\left(\frac{R^{(2)}}{B}\right)$$

From this equation, the equality is:

$$\sigma_c^{(1)} \sqrt{\pi a_I} \cdot f\left(\frac{a_I}{R^{(1)}}\right) \cdot f_1\left(\frac{R^{(1)}}{B}\right) = \sigma_c^{(2)} \sqrt{\pi a_I} \cdot f\left(\frac{a_I}{R^{(2)}}\right) \cdot f_1\left(\frac{R^{(2)}}{B}\right)$$

If the first value is for the intact material and the second value is for a damaged specimen with radius  $R^{(1)}$ , then

$$\begin{aligned}\sigma_c^{(1)} &= \sigma_b; f\left(\frac{a_I}{R^{(1)}}\right) = 1; f_1\left(\frac{R^{(1)}}{B}\right) = 1; \\ \sigma_c^{(2)} &= \sigma_c^d\end{aligned}$$

Here,  $\sigma_b$  is the ultimate stress for the intact material and  $\sigma_c^d$  is the ultimate stress for a specimen with damage.

This is the basis for determination of the critical  $F_0^s(s)$  value:

$$F_0^s(s) = \frac{\sigma_b}{\sigma_c^d \cdot f_1\left(\frac{R}{B}\right)}$$

Thereafter one could utilize the plot in figure 3-1 to establish the critical value  $s^*$  and the cracking zone size  $a_I$ :

$$a_I = \frac{R \cdot s^*}{1 - s^*}$$

This is sufficient for computing the critical stress intensity factor:

$$K_{Ic} = \sigma_c^d \sqrt{\pi a_I} \cdot F_0^* \cdot f_1\left(\frac{R}{B}\right)$$

Table 3-1 reports results of experimental evaluation of residual strength of KMU-4e plates with various stacking sequences. Here the total number of specimens tested, the mean breaking stress  $\bar{\sigma}_c^{\infty}$  and coefficient of variation  $\gamma$  are provided. In addition, results of computation by the above method are shown. The difference between experimental and theoretical values does not exceed 13%. Figure 3-2 represents these data graphically.

TABLE 3-1. STRENGTH OF PANEL WITH CIRCULAR HOLE (Uniaxial tension; KMU-4e composite)

| Stacking Sequence  | Residual Strength                                   | 2R, mm                                     |  |  |  |  |  |  |  |     |
|--|---|--|--|--|--|--|--|--|--|-----|
|  |   | 8  | 16   | 24   | 30   | 40   | 50   | 72   | 100  | 140 |
| $[0_2 / 90 / \pm 45 / 0 / 90_{1/2}]_s$<br>$K_{Ic} = 995 \text{ N/mm}^{3/2}$<br>$a_l = 1.28 \text{ mm}$ | Experiments<br>$\bar{\sigma}_c^\infty, \text{ MPa}$ | 256<br>$\gamma=9.2\%$<br>$3 \text{ spcns}$ | 208<br>$\gamma=7.5\%$<br>$7 \text{ spcns}$ | 194<br>$\gamma=6.6\%$<br>$3 \text{ spcns}$ | 186<br>$\gamma=3.9\%$<br>$9 \text{ spcns}$ | 181<br>$\gamma=8.5\%$<br>$3 \text{ spcns}$ | 185<br>$\gamma=11\%$<br>$3 \text{ spcns}$  | 154<br>$\gamma=3.7\%$<br>$5 \text{ spcns}$ | 168<br>$\gamma=5.5\%$<br>$2 \text{ spcns}$ |     |
|  | Theory<br>$(\bar{\sigma}_c^\infty)^*, \text{ MPa}$  | 239  | 196  | 180  | 173  | 167  | 163  | 158  | 155  | 152 |
|  | $\bar{\sigma}_c^\infty / (\bar{\sigma}_c^\infty)^*$ | 1.07                                       | 1.06                                       | 1.08                                       | 1.08                                       | 1.08                                       | 1.13                                       | 0.97                                       | 1.08                                       | 1.0 |
|  | Experiments<br>$\bar{\sigma}_c^\infty, \text{ MPa}$ | 277<br>$\gamma=4.8\%$<br>$4 \text{ spcns}$ | 224<br>$\gamma=4.6\%$<br>$5 \text{ spcns}$ | 210<br>$\gamma=2.8\%$<br>$4 \text{ spcns}$ | 182<br>$\gamma=5.4\%$<br>$3 \text{ spcns}$ | 201<br>$\gamma=7.6\%$<br>$6 \text{ spcns}$ | —  | —  | 198<br>$\gamma=5.3\%$<br>$3 \text{ spcns}$ | —   |
|  | Theory<br>$(\bar{\sigma}_c^\infty)^*, \text{ MPa}$  | 269  | 224  | 208  | 200  | 196  | —  | —  | 185  | —   |
|  | $\bar{\sigma}_c^\infty / (\bar{\sigma}_c^\infty)^*$ | 1.03                                       | 1.0  | 1.01                                       | 0.91                                       | 1.03                                       | —  | —  | 1.07                                       | —   |
| $[\pm 20 / \mp 20]_s$<br>$K_{Ic} = 1109 \text{ N/mm}^{3/2}$<br>$a_l = 1.13 \text{ mm}$                 | Experiments<br>$\bar{\sigma}_c^\infty, \text{ MPa}$ | 249<br>$\gamma=3.6\%$<br>$3 \text{ spcns}$ | 195<br>$\gamma=3.7\%$<br>$4 \text{ spcns}$ | —  | 171<br>$\gamma=9.1\%$<br>$4 \text{ spcns}$ | —  | 164<br>$\gamma=3.9\%$<br>$2 \text{ spcns}$ | —  | 153<br>$\gamma=4.9\%$<br>$3 \text{ spcns}$ | —   |
|  | Theory<br>$(\bar{\sigma}_c^\infty)^*, \text{ MPa}$  | 234  | 198  | —  | 180  | —  | 169  | —  | 163  | —   |
|  | $\bar{\sigma}_c^\infty / (\bar{\sigma}_c^\infty)^*$ | 1.06                                       | 0.98                                       | —  | 0.95                                       | —  | 0.97                                       | —  | 0.94                                       | —   |
|  | Experiments<br>$\bar{\sigma}_c^\infty, \text{ MPa}$ | —  | —  | —  | —  | 213<br>$\gamma=2.1\%$<br>$3 \text{ spcns}$ | —  | —  | 204<br>$\gamma=4.0\%$<br>$2 \text{ spcns}$ | —   |
|  | Theory<br>$(\bar{\sigma}_c^\infty)^*, \text{ MPa}$  | —  | —  | —  | 207  | —  | —  | —  | 192  | 186 |
|  | $\bar{\sigma}_c^\infty / (\bar{\sigma}_c^\infty)^*$ | —  | —  | —  | 1.03                                       | —  | —  | 1.06                                       | 0.98                                       | —   |
| $[0_2 / 90 / 0_2 / \pm 45 / 0]_s$<br>$K_{Ic} = 987 \text{ N/mm}^{3/2}$<br>$a_l = 1.14 \text{ mm}$      | Experiments<br>$\bar{\sigma}_c^\infty, \text{ MPa}$ | —  | —  | —  | —  | —  | —  | —  | —  | —   |
|  | Theory<br>$(\bar{\sigma}_c^\infty)^*, \text{ MPa}$  | —  | —  | —  | 207  | —  | —  | —  | 192  | 186 |
|  | $\bar{\sigma}_c^\infty / (\bar{\sigma}_c^\infty)^*$ | —  | —  | —  | —  | —  | —  | —  | —  | —   |
|  | Experiments<br>$\bar{\sigma}_c^\infty, \text{ MPa}$ | —  | —  | —  | —  | —  | —  | —  | —  | —   |
|  | Theory<br>$(\bar{\sigma}_c^\infty)^*, \text{ MPa}$  | —  | —  | —  | —  | —  | —  | —  | —  | —   |
|  | $\bar{\sigma}_c^\infty / (\bar{\sigma}_c^\infty)^*$ | —  | —  | —  | —  | —  | —  | —  | —  | —   |
| $[0_2 / 90 / 0_2 / \pm 45 / 0]_s$<br>$K_{Ic} = 1145 \text{ N/mm}^{3/2}$<br>$a_l = 1.17 \text{ mm}$     | Experiments<br>$\bar{\sigma}_c^\infty, \text{ MPa}$ | —  | —  | —  | —  | —  | —  | —  | —  | —   |
|  | Theory<br>$(\bar{\sigma}_c^\infty)^*, \text{ MPa}$  | —  | —  | —  | 207  | —  | —  | —  | 192  | 186 |
|  | $\bar{\sigma}_c^\infty / (\bar{\sigma}_c^\infty)^*$ | —  | —  | —  | 1.03                                       | —  | —  | 1.06                                       | 0.98                                       | —   |
|  | Experiments<br>$\bar{\sigma}_c^\infty, \text{ MPa}$ | —  | —  | —  | —  | —  | —  | —  | —  | —   |
|  | Theory<br>$(\bar{\sigma}_c^\infty)^*, \text{ MPa}$  | —  | —  | —  | —  | —  | —  | —  | —  | —   |
|  | $\bar{\sigma}_c^\infty / (\bar{\sigma}_c^\infty)^*$ | —  | —  | —  | —  | —  | —  | —  | —  | —   |

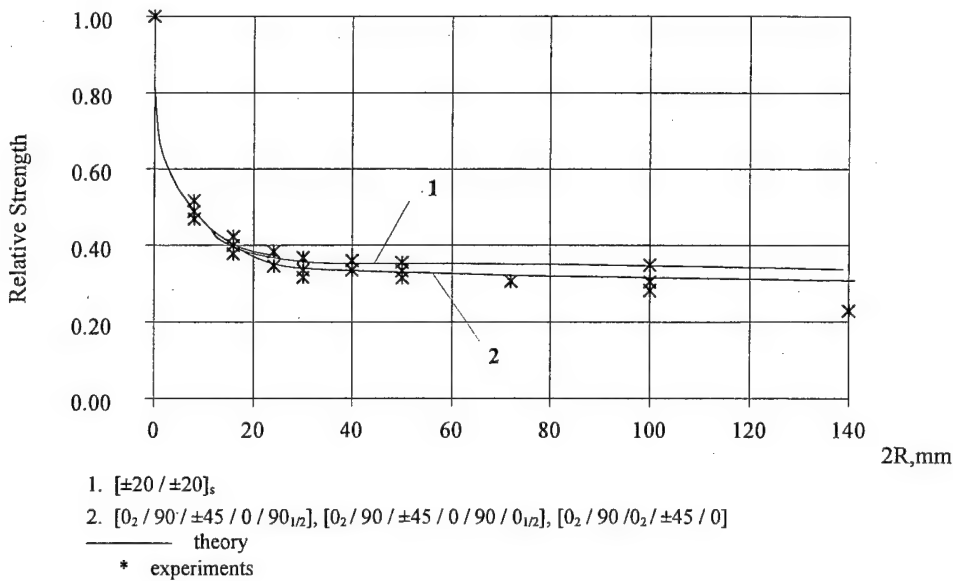


FIGURE 3-2. COMPARING THEORETICAL AND EXPERIMENTAL DATA FOR UNIAXIAL TENSION

### 3.2 BIAXIAL TENSION OF SKIN WITH CIRCULAR HOLE—RESIDUAL STRENGTH CRITERION.

To determine residual strength of a plate with stress concentration under multiaxial loading use could be made of equation 3-1. To do so, the crack resistance characteristics  $K_{lc}$  and  $a_l$ , should be established for the particular stacking sequence and the specific load combination. If these characteristics have not been obtained by experiments, one could define these analytically by employing residual strength criteria. Strength of composite structures subjected to multiaxial loading and having no stress concentration may be calculated through various strength criteria. In particular, the three component in-plane stress (including both tension/compression along two axes and shear) could be analyzed by the Hill-Tsai criterion for a single layer:

$$\frac{\sigma_1^2}{S_1^2} - \frac{\sigma_1 \sigma_2}{S_1^2} + \frac{\sigma_2^2}{S_2^2} + \frac{\tau_{12}^2}{S^2} = 1 \quad (3-3)$$

Here  $S$  is the limit shear stress and  $S_1$  and  $S_2$  are limit normal stresses along and across fibers, respectively. These arcs are defined by the following expressions:

$$S_1 = \begin{cases} X_t & \text{for } \sigma_1 \geq 0; \\ X_c & \text{for } \sigma_1 < 0; \end{cases}$$

$$S_2 = \begin{cases} Y_t & \text{for } \sigma_2 \geq 0; \\ Y_c & \text{for } \sigma_2 < 0; \end{cases}$$

where  $X_t$  and  $X_c$  are the layer longitudinal strengths for tension and compression respectively and  $Y_t$  and  $Y_c$  the corresponding transverse strengths.

The criterion (equation 3-3) may be rewritten in terms of stress intensity factors and the layer residual strength criterion becomes:

$$\left(\frac{K_{Ix}}{K_{Icx}}\right)^2 - \frac{K_{Ix}K_{Iy}}{(K_{Icx})^2} + \left(\frac{K_{Iy}}{K_{Icy}}\right)^2 + \left(\frac{K_{Ixy}}{K_{Icxy}}\right)^2 = 1 \quad (3-4)$$

Relations of this kind enable analysts to compute critical crack-resistance characteristics for any lay-up while proceeding from crack resistance of a uniaxial plate subjected to simple load patterns. Criterion based computation of composite skin residual strength is detailed in the next section.

Figure 3-3 demonstrates experimental data [14] obtained by testing the specimens made of T300/SP286 carbon fiber reinforced plastic. The specimens had quasi-isotropic stacking patterns and circular holes and were loaded with in-plane biaxial tension. Also depicted was the theoretical curve from equation 3-1.

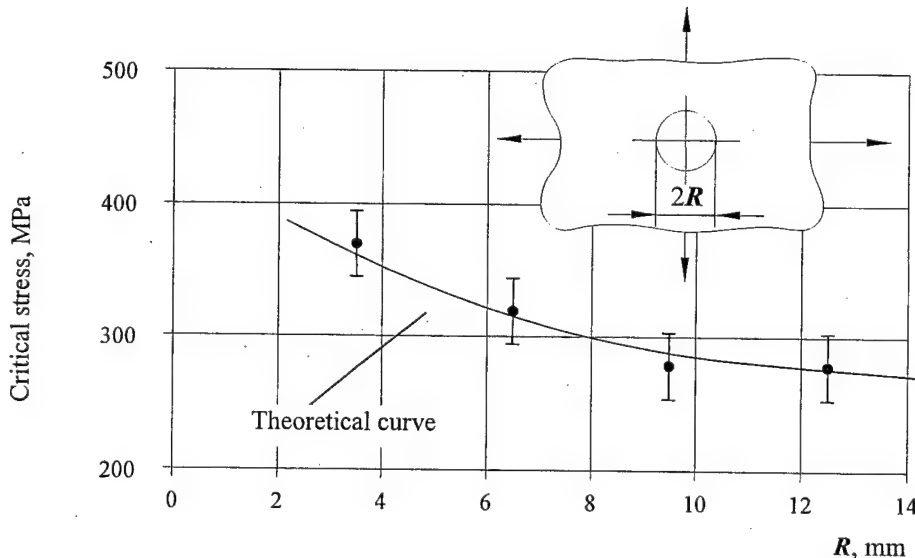


FIGURE 3-3. RESIDUAL STRENGTH OF PLATES SUBJECT TO BIAXIAL STRESS

Validity of the criterion (equation 3-4) for estimating residual strength of composite structures is confirmed by residual strength testing of notched tubular carbon fiber reinforced plastic/glass fiber reinforced plastic (CFRP/GFRP) specimens subjected to pure tension, pure compression, pure shear, and combinations thereof. Figure 3-4 represents loading conditions and failure modes of specimens manufactured of CFRP/GFRP Lu-3/5-211B and T-25VM-78/5-211B with the following stacking sequences:

- No. 1:  $[90_1^g / 0_2^c / 90_1^g / 0_1^c / 90_1^g / 0_2^c / 90_1^c]$  and
- No. 2:  $[0_1^g / \pm 45_1^c / 0_3^g / \mp 45_1^c / 0_1^g]$ ,

glass fabric reinforced plastic T-25VM-78/5-211B with  $[0_3^g / \pm 45_1^g / 0_3^g]$  stacking sequence; (ply thickness are  $\delta^g = 0.27$  mm and  $\delta^c = 0.15$  mm).

The superscripts "g" and "c" indicate GFRP and CFRP, respectively. The solid line in figure 3-4 demonstrates the relation (equation 3-4), and dots are the experimental data.

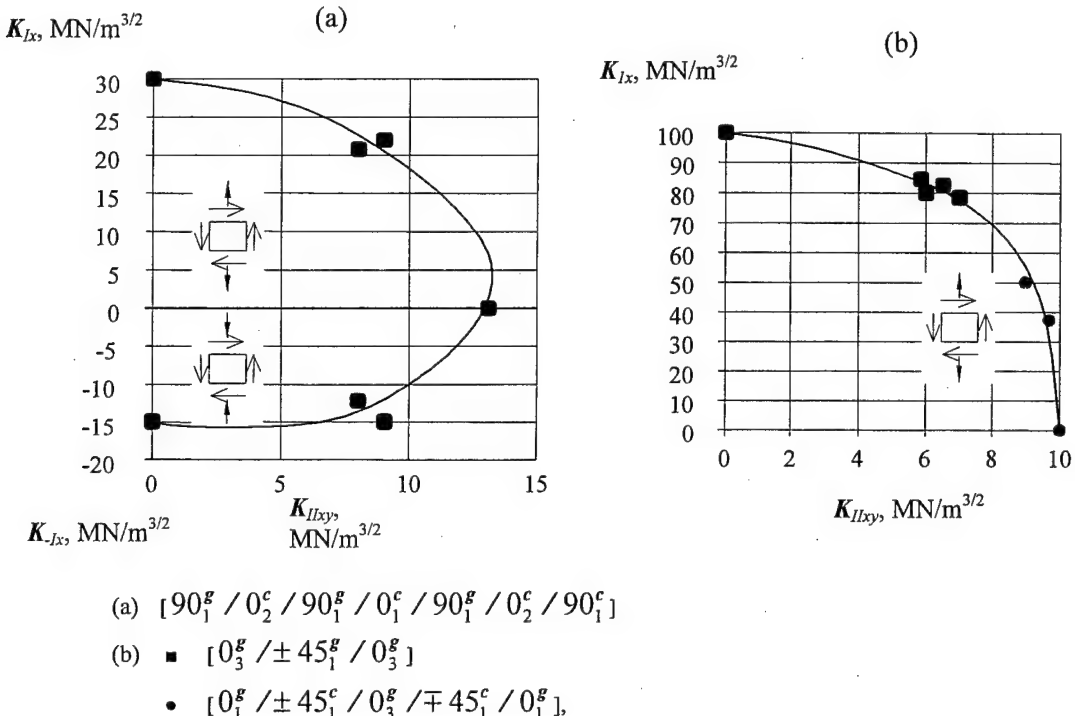


FIGURE 3-4. RESULTS OF TESTING THE TUBULAR SPECIMENS

### 3.3 UNIAXIAL TENSION OF SKIN WITH RECTANGULAR CUTOUT WHOSE CORNERS ARE ROUNDED WITH RADIUS $r$ .

Experiments reveal that a skin with a rectangular cutout fails due to rapid development of cracks in the transverse direction from at least one of the cutout corners. The experimental data may be approximated with equation 3-1 by introducing an additional coefficient to allow for geometric difference between the rectangular rounded cutout and a circular hole. In this case the analytical relation looks like this:

$$\sigma_c^\infty = \frac{K_{Ic}}{\sqrt{\pi a_I} \cdot f\left(\frac{a_I}{R}\right) \cdot f_r\left(\frac{r}{h}, \frac{c}{h}\right)}, \quad (3-5)$$

Here,  $r$  is the corner radius,  $h$  and  $c$  are cutout dimensions, and  $f_r$  is the coefficient to allow for the influence of cutout shape on residual strength. References [10, 11] provide the method on how to determine the coefficient  $f_r$ .

Table 3-2 includes data obtained by testing the plates with rectangular rounded cutouts. The plates have been fabricated from KMU-4e CFRP with various stacking sequences. The cutout width  $h$  was 100 mm for all specimens.

TABLE 3-2. STRENGTH OF PANELS WITH RECTANGULAR CUTOUTS  
(Uniaxial tension; KMU-4e composite)

| Stacking Sequence  | $c$<br>(mm)                    | $r$<br>(mm)                | $P_c$<br>(kN)                  | $\sigma_c$<br>(Mpa)             | $f(a/r)$                            | $f(r/h, c/h)$                         | $\sigma_c^*$<br>(Mpa)           | $\sigma_c^* / \sigma_c^*$            |
|--|--------------------------------|----------------------------|--------------------------------|---------------------------------|-------------------------------------|---------------------------------------|---------------------------------|--------------------------------------|
| $[0_2 / 90 / \pm 45 / 0 / 90 / 0_{1/2}]_s$ ,<br>$K_{Ic} = 987 \text{ N/mm}^{3/2}$<br>$a_I = 1.14 \text{ mm}$ | 100<br>100                     | 10<br>10                   | 122<br>130                     | 135.6<br>144.4                  | 2.7<br>2.7                          | 1.263<br>1.263                        | 146.5<br>146.5                  | 0.92<br>0.95                         |
| $[0_2 / 90 / \pm 45 / 0 / 90_{1/2}]_s$<br>$K_{Ic} = 995 \text{ N/mm}^{3/2}$<br>$a_I = 1.28 \text{ mm}$       | 100<br>100<br>40<br>100<br>101 | 20<br>20<br>20<br>30<br>30 | 124<br>125<br>82<br>128<br>119 | 159<br>160<br>105<br>163<br>152 | 3.0<br>3.0<br>3.0<br>3.076<br>3.076 | 1.06<br>1.06<br>1.387<br>0.96<br>0.96 | 149<br>149<br>114<br>160<br>160 | 1.07<br>1.07<br>0.92<br>1.02<br>0.95 |
| $[\pm 10 / \mp 10]_s$<br>$K_{Ic} = 1238 \text{ N/mm}^{3/2}$<br>$a_I = 1.09 \text{ mm}$                       | 100                            | 30                         | 106                            | 220.8                           | 3.13                                | 0.96                                  | 212                             | 1.04                                 |
| $[\pm 20 / \mp 20]_s$<br>$K_{Ic} = 1109 \text{ N/mm}^{3/2}$<br>$a_I = 1.13 \text{ mm}$                       | 101                            | 30                         | 86                             | 179                             | 3.13                                | 0.96                                  | 186                             | 0.96                                 |
| $[\pm 30 / \mp 30]_s$<br>$K_{Ic} = 960 \text{ N/mm}^{3/2}$<br>$a_I = 1.25 \text{ mm}$                        | 101                            | 30                         | 60                             | 124.5                           | 3.08                                | 0.96                                  | 130                             | 0.95                                 |

### 3.4 UNIAXIAL COMPRESSION OF SKIN WITH CIRCULAR HOLE.

Unlike metals, the composites subjected to compression fail as brittle materials. This circumstance serves as the basis to employ the two-parameter model [11] in analyzing composite skin compressive strength.

Composites are known to exhibit two failure modes in compression (1) interlaminar shear when compressive strength of fibers is reached and (2) local buckling of fibers in the matrix.

When using the two-parameter model, one should bear in mind these features.

Assume that stress/strain fields around the stress concentrator in compression is the same as in tension; then calculation may use equation 3-1 in the form

$$\sigma_c^\infty = \frac{K_{-Ic}}{\sqrt{\pi a_{-I}} \cdot f\left(\frac{a_{-I}}{R}\right)} \quad (3-6)$$

where the coefficient  $f\left(\frac{a_{-I}}{R}\right)$  is from figure 3-1;  $K_{-Ic}$  and  $a_{-I}$  are crack resistance characteristics for compression.

Figure 3-5 shows results of compressive testing (carried out at TsAGI) of 1.6-mm-thick KMU-4e CFRP specimens that had centrally located concentrators in the shape of a circular hole, notched hole, and notch. Under compression these specimens failed because of local fiber buckling. The information shows that the concentration area shape is not of importance when failure modes are identical.

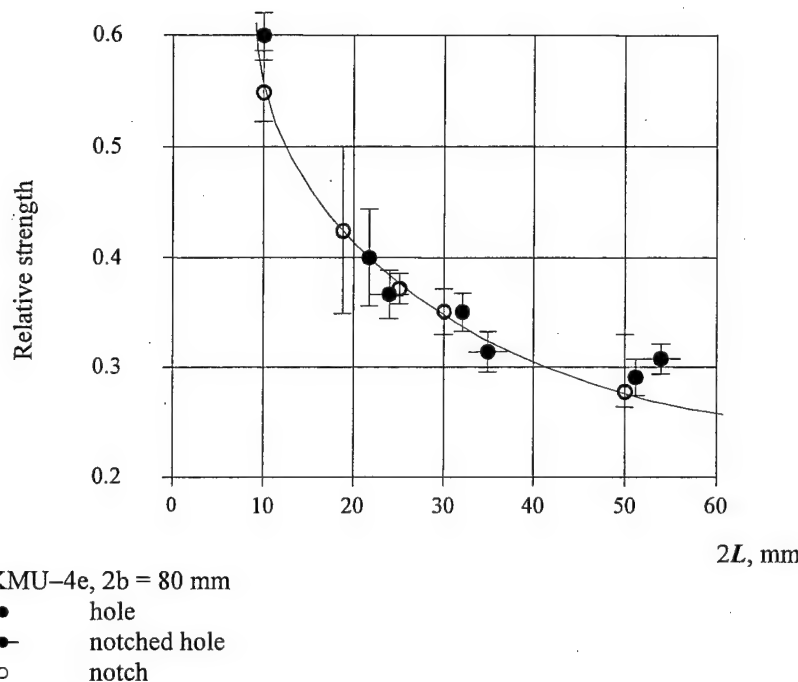


FIGURE 3-5. RESIDUAL STRENGTH OF SPECIMENS UNDER COMPRESSION

### 3.5 THE EFFECT OF STRESS CONCENTRATION ON RESIDUAL STRENGTH.

In appearance the occasional penetrations seen in service because of mechanical impact (such as fall of a stone, or repair tool) differs from a regular hole artificially introduced in a specimen. However, the high-strength composites (in particular, carbon fiber reinforced plastics) are brittle, and this essentially eliminates the above difference, as there is a rather uncertain cracking area around any hole. Within the simplified approach to probabilistic modelling of aircraft service, a single method to simulate behavior of material with an occasional penetration and a through hole can be used. Experiments performed at TsAGI by A. Ushakov and Yu. Trunin [11] evidence that strength degradation of composite plates is mainly influenced by damage sizes. Figure 3-6 presents the results of tensile testing of CFRP plates with through defects that were either circular holes or sharp narrow notches.

The other kind of likely in-service defects is a partial through damage caused by impact of a low-speed thing such as tool, ladder, hail, and runway concrete fragment. Figure 3-7 compares data on how partial through damage (due to an impact by the rounded side of a steel disk) and a through damage (such as a sharp narrow notch) affect KMU-4l CFRP characteristics.

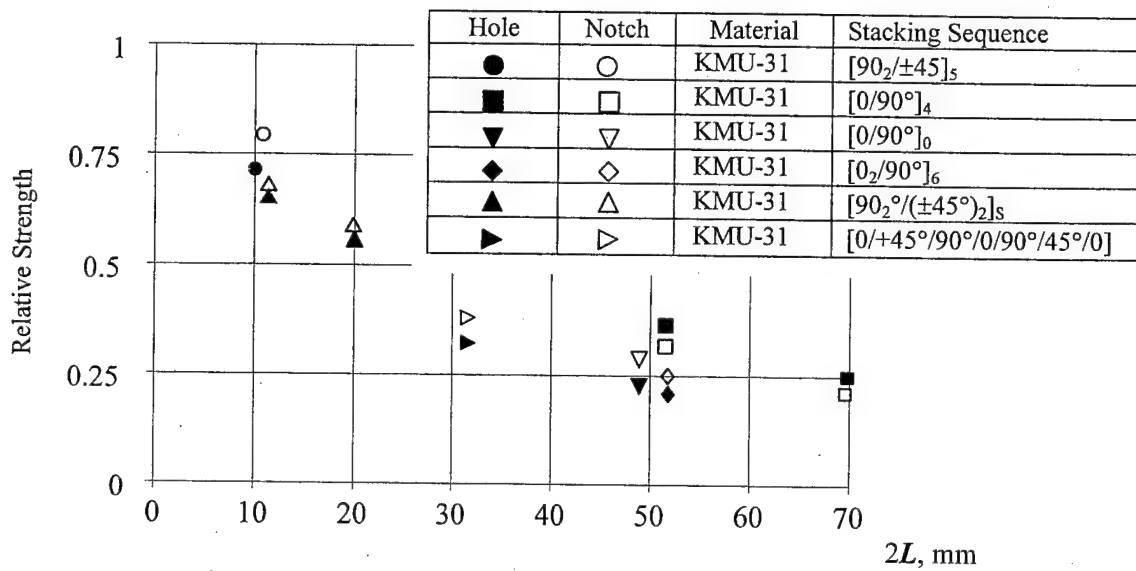


FIGURE 3-6. RESIDUAL STRENGTH OF PLATES WITH HOLES AND NOTCHES

It is rather clear that equal size defects of various types do degrade strength to almost equal extent. For further consideration it can be assumed that in-service damage to a sufficient accuracy degree be represented by a through crack with a certain characteristic size.

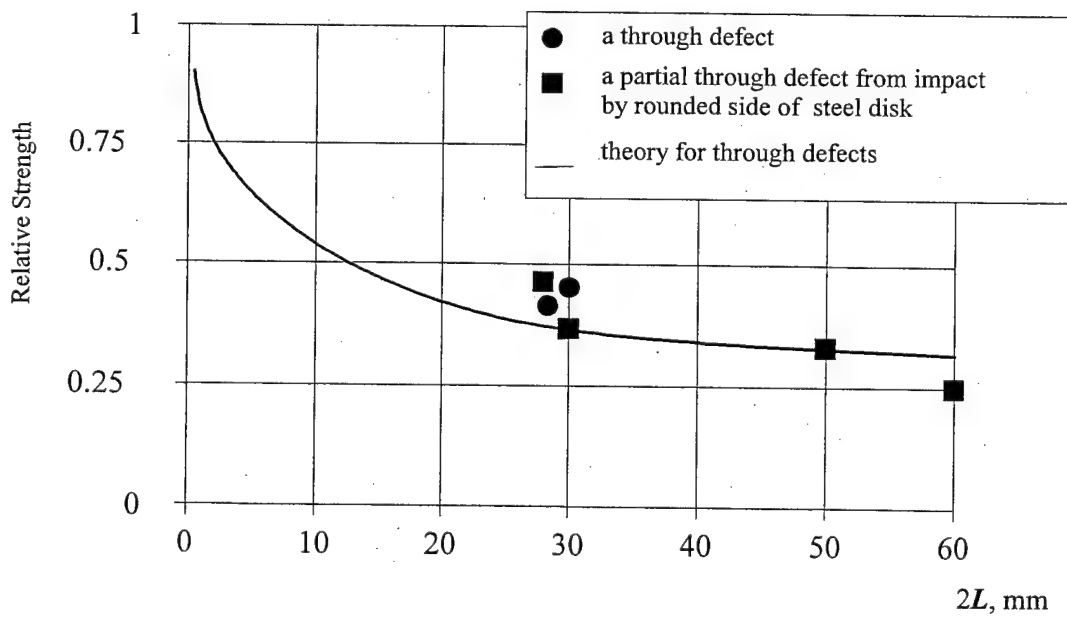


FIGURE 3-7. RESIDUAL STRENGTH OF PLATES WITH THROUGH AND PARTIAL THROUGH (SUPERFICIAL) DEFECTS

#### 4. COMPUTING THE RESIDUAL STRENGTH OF UNSTIFFENED COMPOSITE SKIN.

At various locations of structural component, the residual strength for composite structure needs to be calculated and compared to stresses caused by loads in order to assess the probability of failure. For areas of the structure where no damage exists the probability will be very low and will not contribute to the overall probability of failure. Thus, the methods for the residual strength calculations need only be developed for composite structure with damage. The two critical damages that need only be considered are a through hole or slit for tensile, shear, and compressive loads and delamination for compressive and shear loads. The methods of analyses suggested in the sections that follow are not a part of ProDeCompoS. However, they provide guidance how the residual strength of composite structure can be calculated.

##### 4.1 ALGORITHM FOR EVALUATING A SKIN WITH THROUGH DAMAGE.

To calculate the residual strength of a damaged composite skin, the simplified approach has been selected. It is based on the two-parameter fracture model similar to equation 3-1, and is explicitly shown below.

$$\sigma_c^\infty = \frac{K_{Ic}}{\sqrt{\pi a_I \cdot f}}$$

As shown in section 3, this model gives good agreement between theoretical analyses and experimental data obtained in tests under various conditions and for various concentrations area shapes. In this case, the residual strength is mainly influenced by the damage size with the damage concentration shape considered of minor importance. Identical-size damages of various causes do result in almost identical degradation of skin strength.

The model assumes that the damage (refer to figure 4-1) in a skin bearing the normal stresses  $\sigma_x$  and  $\sigma_y$ , and the in-plane shear stresses  $\tau_{xy} = \tau_{yx}$  may be simulated with cracks whose lengths  $2L_x$  and  $2L_y$  correspond to projections of the damage onto x and y axes, and the residual strength may be calculated on the basis of the linear elastic fracture mechanics (LEFM).

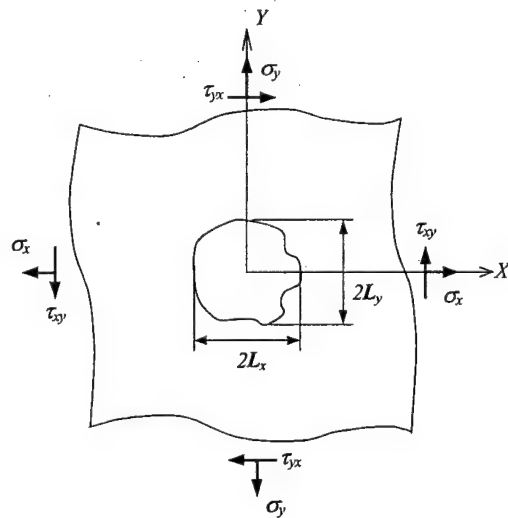


FIGURE 4-1. MODEL OF A DAMAGED PLATE

#### 4.2 METHOD FOR ANALYZING COMPRESSION-LOADED COMPONENTS WITH DELAMINATION.

Delamination is the typical detect/damage in polymeric composites. It is known that the most serious are the delaminations spread over the entire width of the specimen  $t = b$  (figure 4-2). Here the specimen having such an initial damage is considered. It is assumed that the damage exists in a form of sublamine, and the interlaminar bond is absent over initial delamination length  $l$ .

The debonded sublamine buckles under the compressive load and this can trigger the laminate fracture. Four main modes of fracture can be considered:

1. Buckling of the sublamine without the delamination length growth
2. Buckling of the sublamine with simultaneous delamination growth
3. Complete specimen delamination over the entire specimen length
4. Delamination up to one end of the specimen.

The fracture mode will occur when the criteria of minimum released energy is met depending on the loading conditions. The analysis of the behavior of the specimen damage is based on energy criterion according to which the difference between the potential energy of stress field just before the buckling,  $U_0$ , and that after buckling of the sublamine (strip) above delamination,  $U_*$ , is sufficient to produce a work  $R$  required for delamination failure:

$$U_0 - U_* > R.$$

It is assumed that failure is associated with normal separation, i.e.,  $R = 2\gamma\xi t$ ; where  $\gamma$  is the specific energy of normal separation,  $2\xi$  is the additional separation/delamination length, and  $t$  is the delaminated area width (figure 4-2).

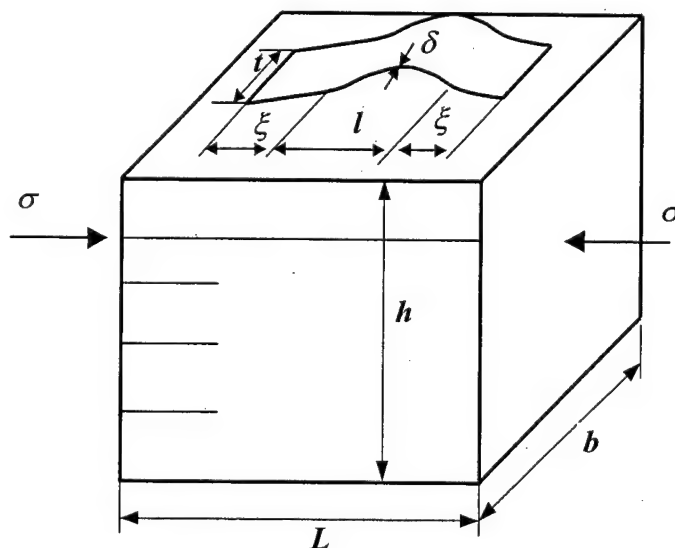


FIGURE 4-2. DELAMINATION IN COMPOSITE SKIN

To determine the critical value of acting stress and critical parameters of the damage, the beam approximation version is used. Taking into account the potential energy of compression and flexure of the delaminated strip having a thickness  $\delta$ , the energy criterion enables to obtain:

$$\delta = \frac{E\delta^2\pi^2}{12(l+2\xi)^2} + 2\sqrt{\frac{\gamma\xi E}{(l+2\xi)\delta}}, \quad (4-1)$$

where  $E$  is the sublamine modulus of elasticity.

The lateral strains over specimen width can also be taken into account. In this case, modulus of elasticity  $E$  in equation 4-1 should be replaced with value  $E/(1-\nu_{xy}\cdot\nu_{yx})$ , where  $\nu_{xy}$ ,  $\nu_{yx}$  are the Poisson's ratios. Elastic constants  $E, \nu_{xy}, \nu_{yx}$  in the sublamine/strip depend on sublamine structure, i.e., by monolayer number and layup orientation in sublamine and properties of elementary monolayer.

First of all, one could consider the failure related to buckling of layers where delamination does not reach the ends of specimen. This case refers to the sufficiently long specimens. Solving the equation  $d\sigma/d\xi = 0$ , one could find the value of additional delamination length  $\xi$  corresponding to the minimum stress. It can be shown that by assuming homogeneity of specimen and sublamine properties, the equation  $d\sigma/d\xi = 0$  has the solution,

$$(1+X)^3 = aX,$$

where

$$a = \frac{86.6E\delta^5}{\gamma l^4}, \quad X = 2\xi/l.$$

One could determine damage critical size  $L$  and appropriate stress value if failure occurs according to the first type (without the additional delamination). Assuming  $a = 6.75$ , the formula for critical length of the buckling area can be derived by:

$$l_* = \left( \frac{86.6 \cdot E\delta^5}{6.75\gamma} \right)^{\frac{1}{4}}. \quad (4-2)$$

Substituting  $l_*$  in equation 4-1 (at  $\xi = 0$ ), critical stress becomes

$$\sigma_* = \frac{\pi^3}{3} \left( \frac{6.75\gamma E}{86.6\delta} \right)^{\frac{1}{2}}. \quad (4-3)$$

In making computations by equations 4-2 and 4-3, it should be taken into account that the sublamine can have only the integer number of layers, and the elastic sublamine parameters are defined by the layup arrangement.

The corresponding calculation algorithm stated below enables one to also determine the permissible depth of delamination.

In recalculation of delamination characteristics, one can take into account the well-known formulas for stiffness of the laminate containing  $n$  layers of given thickness with known layup angles. These formulas are valid for laminates exposed to planar stresses in plane xyz, where the x axis is a load direction that coincides with the longitudinal specimen axis. The lamina angle is measured from the axis x. It is assumed that the layup orientation in the sublamine which is expected to buckle is known. Let  $\delta_l$  be a layer thickness. One could assume that  $\delta = \delta_l$ . As the elastic characteristics of the first layer at the specimen surface are known, it is possible to find values  $l_*$  and  $\sigma_*$  for one delaminated layer with equations 4-1 and 4-2.

Taking into account the known layup sequence, one could increase the thickness  $\delta$  assuming that  $\delta = m\delta_l$ ,  $m = 1, 2, \dots$ . Computing the characteristics of the sublaminates, it is possible to find successively a series of values  $l_*$ , and  $\sigma_*$ . As a result, the graphs of functions  $l_*(\delta)$  and  $\sigma_*(\delta)$  can be plotted. The obtained curves enable one to easily solve the problem of determination of the allowable damage length and depth and also the problem of determination of the critical load for the given damage and given specimen layup.

One could consider the case of failure according to the second type when buckling is accompanied by delamination over length  $l_{**}$ . According to analysis of the solution of equation 4-1, if  $a$  becomes greater than 6.75, then the failure mode should change. Let  $R > 16$ . There is only one solution meeting the condition of the existence of additional delamination and condition  $2\xi \geq 1.5l$ . Taking into account equation 4-1, one could find the critical stress value  $\sigma_{**}$  and the critical value of damage length  $l_{**}$ .

The critical parameters should be calculated by equation 4-1, according to the above procedure:

$$\sigma_{**} = \sigma_*(l_{**}) + 2\sqrt{\frac{\gamma\xi E}{l_*\delta}}, \quad (4-4)$$

where

$$l_{**} = (l + 0.75) \sqrt{\frac{86.6E\delta^5}{16\gamma}},$$

$$\xi = 0.75 \sqrt{\frac{86.6E\delta^5}{16\gamma}}.$$

To describe the strength of the damage-free specimen, it should be assumed that  $l = 0$  in equation 4-1 when initiated delamination spreads over the entire specimen. Therefore, it should be assumed that  $2\xi = L$ .

Taking shear into account one could obtain:

$$\sigma_0 = \frac{\pi^2(t - \tanh(t))E\delta^2}{4E^2t^3} + \sqrt{\frac{2\gamma E}{\delta}}$$

The minimum strength corresponds to the critical delamination thickness  $\delta_0$ :

$$\delta_0 \approx (L^4\gamma)^{\frac{1}{5}} \left[ 4\pi^2 E \frac{t - \tanh(t)}{t^3} \right]^{-\frac{1}{5}}$$

The appropriate value of the critical stresses is founded by substituting  $\delta_0$  into above mentioned formula for  $\sigma$ .

Two other types of failure are possible in the rods of finite length. Buckling with the simultaneous delamination over the entire length is one and delamination up to the end of the specimen is another.

If the specimen delaminates over the entire length, it should be assumed in equation 4-4 that  $l_{**} = L$  and  $2\xi = L - 1$ . As a result, it was found that:

$$\sigma_{\text{III}} = \frac{\pi^2 E \delta^2}{12L^2} + \sqrt{\frac{2E\gamma(L-l)}{L\delta}} \quad (4-5)$$

Here the modulus of elasticity  $E$  depends on both delamination thickness and its feature. Therefore, the value  $\sigma_{\text{III}}$  depends on the depth of the delamination (damage) in a complicated manner. To find the critical stress and critical depth of the delamination the computation procedure stated above can be used.

The fourth type of failure deals with the initial delamination propagating to one of the ends is considered in a similar manner. Let the damage be located symmetrically relative to the end. Then the critical stress is determined from:

$$\sigma_{\text{IV}} = 6.72 \frac{E\delta^2}{L^2(1+y)^2} + \sqrt{\frac{2E\gamma(1-y)}{\delta(1+y)}}, \quad (4-6)$$

where

$$y = l/L.$$

In compression and tension of a specimen with thin surface film, the latter is likely to separate if the initial damage like a crack at the interface takes place. The critical stress at which the film delaminates can be found by:

$$\sigma = E_x \sqrt{\frac{4\gamma_f(1-\nu_{xy}\nu_{yx})}{(1-\nu_1\nu_2)hE_1}}, \quad (4-7)$$

where  $E_x$ ,  $\nu_{xy}$ , and  $\nu_{yx}$  are the specimen elastic constants,  $E_1$ ,  $\nu_1$ , and  $\nu_2$  are the elastic constants of film (layer),  $h$  is the film thickness, and  $\gamma_f$  is the adhesion specific energy.

It is assumed that the adhesion bond determines the failure mode. If the film critical strain is known, the equation relating the critical delamination stress and the critical strain characterizing the film rupture is as follows:

$$\sigma = \sqrt[3]{\frac{4\gamma_f E_x^2 (1-\nu_{xy}\nu_{yx})}{(1-\nu_1\nu_2)hE_1}}. \quad (4-8)$$

The specimen and film (layer) characteristics which can have the laminated structure are computed according to the above described algorithm.

Delamination propagating from the damage in specimen under torsion can also be studied on the bases of the energy criterion. It is assumed that the initial delamination propagates over the entire specimen width (figure 4-3).

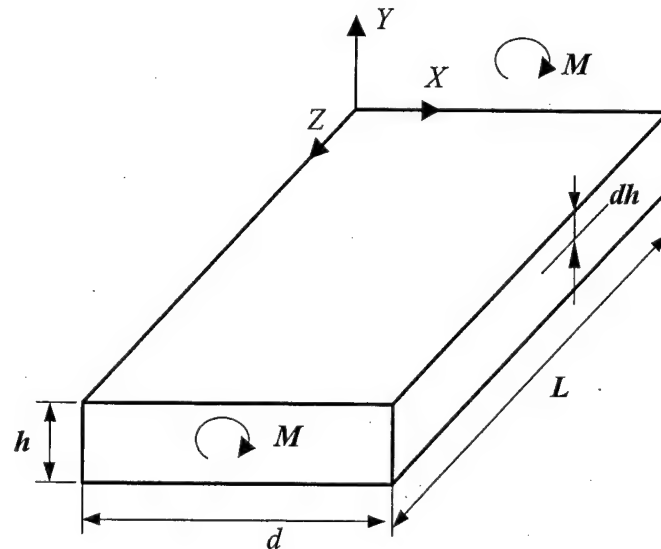


FIGURE 4-3. DELAMINATION PROPAGATION UNDER TORSION

The critical torque value is determined by:

$$M = \sqrt{\frac{2G_{xy}I_0ak(1-\varepsilon)}{(k-1)[1-\varepsilon(k-L)+\varepsilon^2(1-k)]}}, \quad (4-9)$$

where

$$\begin{aligned} \varepsilon &= \frac{1}{h}, \quad k = \frac{I_0}{I_1}, \quad I_0 = \beta(c)dh^3, \quad a = \frac{Ah}{h}, \\ I_1 &= dh^3 \left\{ \beta\left(\frac{c}{a}\right)a^3 + \beta\left(\frac{c}{1-a}\right)(1-a)^3 \right\}, \\ c &= \frac{d}{L}, \quad g = \frac{G_{xy}}{G_{yz}}. \end{aligned}$$

If the specimen is damage-free ( $l = 0$ ), delamination spreads over the entire specimen and the critical torque equals to:

$$M = \sqrt{\frac{2G_{xy}I_0^2\gamma a}{I_0I_1}}. \quad (4-10)$$

It is easy to demonstrate that the extreme  $M$  value is attained at  $a = 1/2$ , i.e., the specimen is divided into equal parts. The maximum torque is computed by equation 4-8:

$$M = 2aL^2\beta(c)\sqrt{\frac{2\gamma G_{xy}}{h[4\beta(c)-\beta(2c)]}}. \quad (4-11)$$

Now it is easy to determine the critical damage size using equations 4-9 and 4-11:

$$\varepsilon^* = \left(1 - \frac{\kappa-1}{\kappa} \cdot \frac{\kappa_1}{\kappa_{1-1}}\right) \cdot \frac{(\kappa-1)^2}{\kappa} \cdot \frac{\kappa_1}{\kappa_{1-1}},$$

where

$$\kappa_1 = 4 \frac{\beta(c)}{\beta(2c)}$$

## 5. METHOD FOR ANALYZING WING STRENGTH.

Within the ProDeCompoS the reliability of a large unit such as an airplane wing is estimated on the basis of strength degradation of this unit in case some of components (such as wing panels) are damaged. The wing strength analysis method underlying the BOX-C program is described below. The latter has been employed to analyze the residual strength of damaged wings of the Lear Fan and SU-29.

The model is based on the beam modelling technique of reference 19. This beam model of a structure is divided into sections by drawing some basic cuts (figure 5-1). Geometry of every basic contour is specified by the coordinates of basic points. Between every two pairs of the basic points on two adjacent cuts a panel of one type is situated. The program envisages the use of uniaxially stiffened panels of six types. The panel can be modelled by a system of structures such as the cover skin, stringer webs, and flanges. Each element of a panel is a multidirectional system comprised of composite material layers.

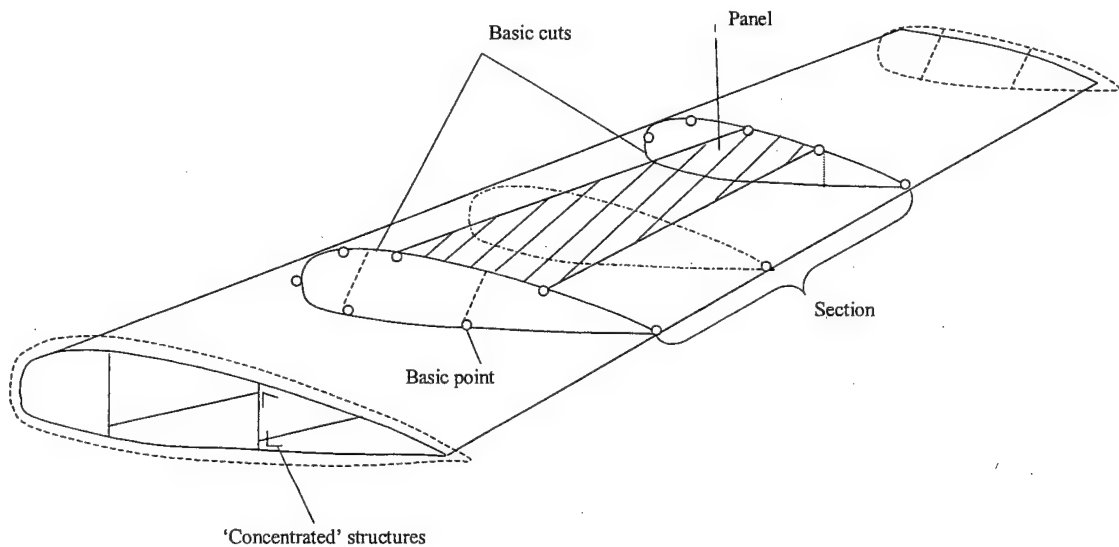


FIGURE 5-1. BEAM MODEL OF IDEALIZED WING STRUCTURE

At the first stage, the effective stiffness of the panels are calculated and later used in analysis as a single-ply structure. Concentrated structures may be introduced, such as spar flanges and beams, that carry compression/tension forces only.

### 5.1 BEAM MODEL ANALYSIS TECHNIQUE.

Consider an inhomogeneous thin-walled beam (figure 5-2). Let the  $r$  axis run along the beam axis and the  $x$  and  $y$  axes are fixed in the beam cross-section. (Assume diagrams of the bending moments  $M_x$ ,  $M_y$ , the torsion moment  $M_z$ , the transverse forces  $Q_x$ ,  $Q_y$ , and the axial force  $Q_z$  are known.)

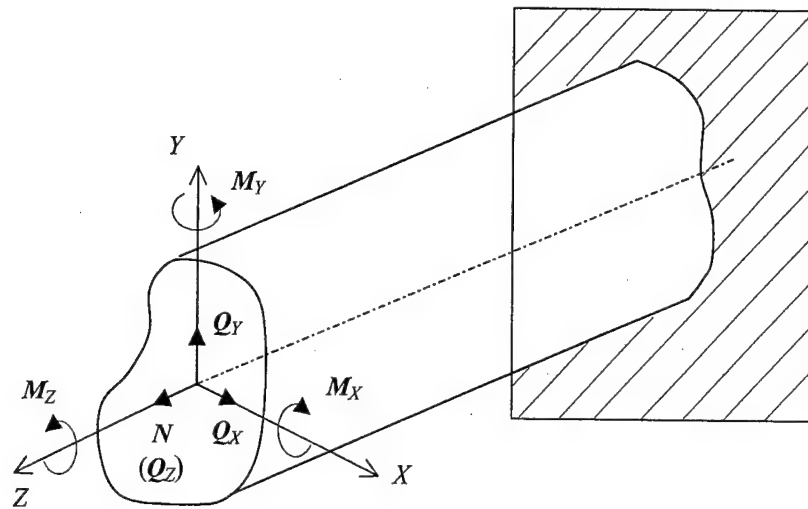


FIGURE 5-2. FREE-BODY DIAGRAM OF THE WING STRUCTURE

To compute the normal stresses in the cross-section of an inhomogeneous beam whose material does not follow the Hook's law, use should be made of the successive approximation method. The axial strain  $\varepsilon_x$  can be written as

$$\varepsilon_z = \varepsilon_{zo} - \kappa_y(Y + v_y) + \kappa_x(X + v_x), \quad (5-1)$$

where  $\varepsilon_{zo}$  is the axial strain in the section centroid,  $v_x$  and  $v_y$  are coordinates of the centroid, and  $\kappa_x$  and  $\kappa_y$  are curvatures of the beam elastic axis.

The normal stress-strain relation may be as follows:

$$\sigma_z = E_c(\varepsilon_z - \alpha_z T), \quad (5-2)$$

where  $\alpha_z$  is the linear expansion coefficient for the z axis,  $T$  is the temperature, and  $E_c$  is the secant modulus.

From the equilibrium equations

$$Q_z = \int_F \sigma_z dF;$$

$$M_X = - \int_F \sigma_z (Y + v_y) dF;$$

$$M_Y = \int_F \sigma_z (Y + v_x) dF,$$

( $F$  is the cross sectional area) one determine the parameters for equation 5-1:

$$\begin{aligned}\varepsilon_{zo} &= \frac{Q_z + Q_T}{A_0}; & v_Y &= -\frac{A_x}{A_0}; & v_x &= \frac{A_y}{A_0}; \\ \aleph_y &= \frac{M_x - M_{XT}}{B_x}; & \aleph_x &= \frac{M_Y - M_{YT}}{B_Y}\end{aligned}\quad (5-3)$$

In the latter the new symbols mean:

$$\begin{aligned}A_0 &= \int_F E_c \cdot dF; & A_X &= \int_F E_c \cdot Y dF; & A_Y &= \int_F E_c \cdot X dF; \\ B_X &= \int_F E_c (Y + v_Y)^2 \cdot dF; & B_Y &= \int_F E_c (X + v_X)^2 \cdot dF; \\ Q_T &= \int_F \alpha_Z T E_c \cdot dF; & M_{YT} &= \int_F \alpha_Z T (X + v_X) E_c \cdot dF; \\ M_{XT} &= \int_F \alpha_Z T (Y + v_Y) E_c \cdot dF.\end{aligned}\quad (5-4)$$

The successive approximation technique consists in the following. An arbitrary deformation state (i.e.,  $\varepsilon_{Z_0}^{(0)}$ ,  $v_Y^{(0)}$ ,  $v_x^{(0)}$ ,  $\aleph_x^{(0)}$ ,  $\aleph_y^{(0)}$ ) should be specified. These are utilized to compute the strain at the first step:

$$\varepsilon_Z^{(1)} = \varepsilon_Z^{(0)} - \aleph_Y^{(0)} (Y + v_Y^{(0)}) + \aleph_X^{(0)} (X + v_X^{(0)}).$$

By using the stress strain curves of the panels and the bars, find stresses as functions of the strains:

$$\sigma_Z^{(1)} = f(\varepsilon_Z^{(1)} - \alpha_Z T).$$

Now determine the secant modulus for the first approximation:

$$E_c^{(1)} = \frac{\sigma_Z^{(1)}}{\varepsilon_Z^{(1)} - \alpha_Z T},$$

and, using equation 5-4, determine the deformation state parameters for the first approximation. They are taken for the following approximation. The successive approximation process is repeated until strains at two subsequent stages are identical, to a minor (prescribed) error. With the successive approximations completed, the normal stress field in the cross-section should be obtained.

Thereafter, it is necessary to compute the shear stresses in the section (figure 5-3). Consider a multiple-connected thin-walled section composed of closed contours. One can assume the shear stress to be uniform through the thickness of the wall. The curvilinear coordinate axis is introduced, running along the midline in the section. By cutting every contour, make the section open. Denote the shear stress flows in the portions of the cuts as  $q_i$  ( $i=1,2,\dots,n$ ).

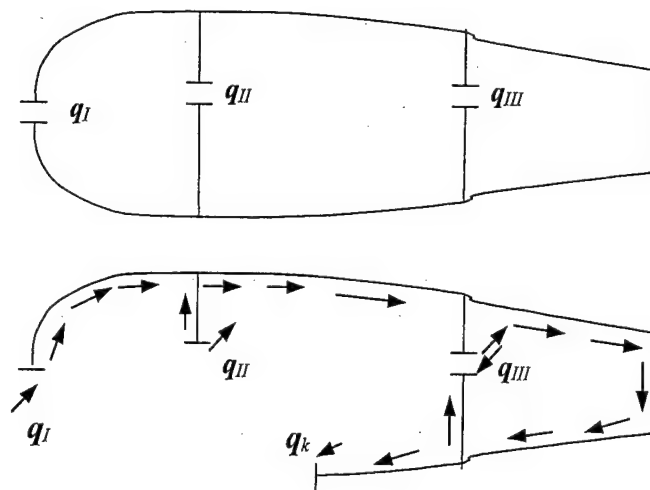


FIGURE 5-3. WING SECTION FOR SHEAR FLOW COMPUTATION

The flow is the product of the shear stress and the wall thickness:

$$q = \tau \cdot \delta.$$

Draw an additional, arbitrarily placed, cut which separates a part of the section with the area  $\omega$ . The equilibrium equation for the part of length  $dz$  and of cross-sectional area  $m$  may be written as:

$$\int_W \sigma_Z \cdot dF - \int_W (\sigma_Z - d\sigma) \cdot dF + q dz - \sum_W q_i dz = 0, \quad (5-5)$$

where  $q$  is the flow at the cut location,  $\sum_W q_i$  is the sum of the flows in the cut points that fall into the part  $\omega$ , under consideration.

From equation 5-5, get:

$$q = \sum_{\omega} q_i + \int_{\omega} \frac{d\sigma_Z}{dZ} \cdot dF = \sum_{\omega} q_i + q_0, \quad (5-6)$$

where

$$q_0 = \int_{\omega} \frac{d\sigma_Z}{dZ} \cdot dF.$$

For determining the flows  $q_i$  ( $i = 1, 2, \dots, n$ ), use may be made of the Bredt theorem:

$$\oint_i \frac{\mathbf{q} ds}{G\delta} = 2\xi \Omega_i, (i = 1, 2, \dots, n) \quad (5-7)$$

where  $G$  is the shear modulus,  $\xi$  is the twist angle per unit length, and  $\Omega_i$  is the  $i^{\text{th}}$  contour area.

Integration in equation 5-7 is performed over the  $i^{\text{th}}$  closed contour. Substituting equation 5-6 into equation 5-7; obtain the system of  $n$  equations for unknowns  $q_i$  and  $\xi$ :

$$\sum_{k=1}^n q_k \int_k \frac{ds}{G\sigma} - 2\xi \Omega_i = - \oint_i \frac{q_0}{G\delta} ds. \quad (5-8)$$

Close the set (equation 5-8) by the equilibrium equation after summarizing the moments of all forces with respect to the longitudinal axis  $z$ :

$$\sum_{i=1}^k \oint_i q r ds = M_z. \quad (5-9)$$

Where  $r$  is the length or the normal drawn from the coordinate system origin to the tangent to the midline. Substituting equation 5-6 into equation 5-9; write  $n+1$  equations:

$$2 \sum_{i=1}^n q_i \cdot \Omega_i = M_z - \sum_{i=1}^n \oint_i q_0 r ds. \quad (5-10)$$

The system of  $n+1$  in equations 5-1 and 5-10 makes it possible to compute the shear stress flows in the cut points, thereafter, the shear stress is at an arbitrary point of the section (using equation 5-8).

## 5.2 COMPUTATION OF STIFFNESS AND STRENGTH OF COMPOSITE PANELS.

Consider a regular panel that is comprised of rectangular plates (width  $b_i$ , thickness  $t_i$ ) made of  $n_i$  orthotropic plies of composite materials with differing orientation angles  $\varphi_i$ . The index  $i$  identifies the number of the rectangular element of the panel.

The loads per unit length ( $N$ ) <sub>$i$</sub> , the moments ( $M$ ) <sub>$i$</sub> , the strains ( $\varepsilon^0$ ) <sub>$i$</sub> , and the curvatures ( $\kappa$ ) <sub>$i$</sub>  are interrelated as follows:

$$\begin{pmatrix} N \\ M \end{pmatrix}_i = [K]_i \begin{pmatrix} \varepsilon^0 \\ \kappa \end{pmatrix}_i = \begin{bmatrix} A & B \\ C & D \end{bmatrix}_i \begin{pmatrix} \varepsilon^0 \\ \kappa \end{pmatrix}_i, \quad (5-11)$$

where

$$[\mathbf{A}]_i = \sum_{j=1}^{k_i} [\mathbf{C}]_j (\mathbf{Z}_{ij} - \mathbf{Z}_{i,j-1}),$$

$$[\mathbf{B}]_i = \frac{1}{2} \sum_{j=1}^{k_i} [\mathbf{C}]_j (\mathbf{Z}_{ij}^2 - \mathbf{Z}_{i,j-1}^2),$$

$$[\mathbf{D}]_i = \frac{1}{3} \sum_{j=1}^{k_i} [\mathbf{C}]_j (\mathbf{Z}_{ij}^3 - \mathbf{Z}_{i,j-1}^3).$$

Here one denotes:

$[\mathbf{A}]_i$ ,  $[\mathbf{B}]_i$ , and  $[\mathbf{D}]_i$  the matrices of the inplane stiffness bending/torsion stiffness and interaction respectively;

$[\mathbf{C}]_i$  the stiffness matrix of the layer (in coordinates related to the  $i^{\text{th}}$  rectangular element);

$\mathbf{Z}_{ij}$  the distance from the upper plane of the  $j^{\text{th}}$  layer to the mid surface of the  $i^{\text{th}}$  element.

The stiffness matrix of the  $j^{\text{th}}$  layer is determined from the relation:

$$[\mathbf{C}]_j = [\mathbf{T}]_j^{-1} [\mathbf{Q}] [\mathbf{T}]_j^T,$$

where  $[\mathbf{Q}]$  is the stiffness matrix of the layer in the principal axes,  $[\mathbf{T}]_j$  is the matrix of tensor multipliers for rotation of coordinate axes, symbol  $[\cdot]^T$  identifies transposition.

The ultimate breaking loads for the panel are determined using the ply failure criterion:

$$\frac{\sigma_1^2}{S_1^2} - \frac{\sigma_1 \sigma_2}{S_1^2} + \frac{\sigma_2^2}{S_2^2} + \frac{\tau_{12}^2}{S_{12}^2} = 1, \quad (5-12)$$

where

$$S_1 \begin{cases} S_1^t \text{ if } \sigma_2 \geq 0, \\ S_1^c \text{ if } \sigma_2 < 0, \end{cases} \quad S_2 \begin{cases} S_2^t \text{ if } \sigma_2 \geq 0, \\ S_2^c \text{ if } \sigma_2 < 0, \end{cases}$$

$\sigma_1$ ,  $\sigma_2$ , and  $\tau_{12}$  are the stresses in the layer,

$S_1^t$ ,  $S_1^c$ ,  $S_2^t$ ,  $S_2^c$ , and  $S_{12}$  are the strengths of the layer in tension and compression along fibers, across fibers, in shear, respectively.

The stress resultants applied to the panel can be represented as:

$$(\mathbf{q}) = \begin{pmatrix} q_X \\ q_{XY} \end{pmatrix} = \begin{pmatrix} \varphi_X \\ \varphi_{XY} \end{pmatrix} \cdot \mathbf{q}_0 = (\Psi) \cdot \mathbf{q}_0. \quad (5-13)$$

The load-to-failure corresponding to the primary failure is determined from equation:

$$q_0^I = \min_{i,j} (q_0^{ij}), \quad (5-14)$$

where  $q_0^{ij}$  is the ultimate load for which the criterion equation 5-12 predicts failure of the  $i^{\text{th}}$  ply in the  $j^{\text{th}}$  element of the panel:

$$q_0^{ij} = \left( \frac{\bar{\sigma}_{1,ij}^2}{S_1^2} - \frac{\bar{\sigma}_{1,ij}\bar{\sigma}_{2,ij}}{S_1^2} + \frac{\bar{\sigma}_{2,ij}^2}{S_2^2} + \frac{\bar{\sigma}_{12,ij}^2}{S_{12}^2} \right)^{-\frac{1}{2}}, \quad (5-15)$$

where

$$\begin{pmatrix} \bar{\sigma}_1 \\ \bar{\sigma}_2 \\ \bar{\sigma}_3 \end{pmatrix} = [\mathbf{T}]_{ij} [\mathbf{C}]_{ij} \{ \mathbf{E} - Z_{ij}^0 [\mathbf{B}]_i [\mathbf{D}]_i^{-1} \} \mathbf{A}_i - [\mathbf{B}]_i [\mathbf{D}]_i^{-1} [\mathbf{B}]_i \}^{-1} \cdot (\varphi_i). \quad (5-16)$$

Here

$Z_{ij}^0$  is the distance from the mid-surface of the  $j^{\text{th}}$  layer of the  $i^{\text{th}}$  element to the mid-surface of this element;

indices  $j$  and  $i$ ; signify correspondence of the matrix to the  $i^{\text{th}}$  layer of the  $j^{\text{th}}$  element;

$(\varphi_i)$  is the vector of undimensionalized stress resultants in the  $j^{\text{th}}$  element;

$[\mathbf{E}]$  is the unit matrix.

It is assumed that the loads are distributed among the structures in proportion to stiffness of the structures.

If the material of the panel is isotropic (for example, a metallic panel), the load-to-failure is determined by equation 5-14. For fibrous composites one must calculate the load-to-failure corresponding to the secondary failure  $q_0^{II}$ . The secondary load-to-failure is the load for the composite where one or several layers have failed, according to equation (5-14). The final load-to-failure is the maximum of the two values:

$$q_{ne} = \max(q_0^I, q_0^{II}). \quad (5-17)$$

### 5.3 PANEL BUCKLING CRITICAL LOADS.

Consider an orthotropic plate that is equivalent with respect to the bending/torsion stiffness  $D_1$ ,  $D_2$ , and  $D_3$  to the uniaxially stiffened panel under study. The bending rigidity of the equivalent plate is determined as:

$$D_1 = \frac{1}{2} \sum_{i=1}^{n_e} E_{Xi} b_i t_i \left[ (Z_i - Z_c)^2 + \frac{1}{2} (b_i^2 \cdot \cos^2 Q_i + t_i^2 \cdot \sin^2 Q_i) \right], \quad (5-18)$$

where  $n_e$  is the total number of panel structures,

$$Z_c = \frac{\sum_{i=1}^{n_e} E_{Xi} b_i t_i Z_i}{\sum_{i=1}^{n_e} E_{Xi} b_i t_i},$$

is the coordinate of the panel section centroid.

For open-profile stiffeners, the stiffness  $D_2$  and  $D_3$  are determined as stiffness of structures lying in the plane of the skin.

The critical load  $q^b$  is described by:

$$q_0^b = \begin{cases} \frac{1}{2} N_0^{-1} \cdot at & \varphi_{XY} \neq 0, \\ (N_{XY}^0)^2 \left( -N_o + \sqrt{N_o^2 + \frac{\varphi_{XY}^2}{(N_{XY}^0)^2}} \right) \Big/ \varphi_{XY}^2 & at \quad \varphi_{XY} \neq 0, \end{cases} \quad (5-19)$$

where  $N_0 = \varphi_X / 2N_X^0$ ;

$N_X^0$  and  $N_{XY}^0$  are the critical loads for cases of separate application of axial compression and shear respectively.

The latter may be calculated using the equations

$$N_X^0 = \left[ \frac{1}{D_1} \left( \frac{l}{\pi} \right)^2 + \frac{b}{GF} \right]^{-1}, \quad \text{where} \quad D_0 = \frac{\sqrt{D_1 D_2}}{D_3} \quad (5-20)$$

$$\begin{cases} \left(\frac{2}{\ell}\right)^2 D_1 \sqrt{\frac{D_2}{D_1} \left(8.125 + \frac{5.05}{D_o}\right)}, & \text{if } D_o \geq 1 \\ \left(\frac{2}{\ell}\right)^2 \sqrt{D_1 D_3} \left(11.7 + 0.53 D_o + 0.938 D_o^2\right), & \text{if } D_o < 1 \end{cases}$$

Here,  $l$  is panel length and  $GF$  is the stiffness of webs (taking into account the effect of shear of stiffeners).

#### 5.4 LOCAL BUCKLING CRITICAL LOADS FOR PANEL STRUCTURES.

The panel is assumed to be composed of long plates, each of which either having both edges simply supported or having any one edge supported and the other free. The local buckling critical stress resultant  $N_b^l$  is defined as the minimum for all the plates:

$$N_b^l = \min(N_b^i), \quad i = 1, 2, \dots, k, \quad (5-21)$$

where  $N_b^i$  is critical load at buckling of the  $i^{\text{th}}$  plate.

This value is governed by the relations:

$$N_b^i = \left[ \frac{\varphi_{X,i}}{2N_{X,o}^i} + \sqrt{\left(\frac{\varphi_{X,i}}{2N_{X,o}^i}\right)^2 + \left(\frac{\varphi_{XY,i}}{N_{XY,i}^i}\right)^2} \right] \cdot \left(\frac{N_{XY,o}^i}{N_{XY,i}^i}\right)^2 - \text{simple support on both edges at}$$

$$\varphi_{XY,i} \neq 0$$

$$N_b^i = \frac{N_{X,o}^i}{\varphi_{X,i}} - \text{simple support on both edges at } \varphi_{XY,i} = 0 \quad (5-22)$$

$$N_b^i = \frac{\pi^2 \sqrt{D_{11,i} \cdot D_{22,i}}}{b_i^2} \left[ \frac{G_{XY,i} \cdot h_i^3}{\pi^2 \sqrt{D_{11,i} \cdot D_{22,i}}} + \left(\frac{b_i}{\ell_i}\right)^2 \sqrt{\frac{D_{11,i}}{D_{22,i}}} \right] \cdot \frac{1}{\varphi_{X,i}} - \text{panel with one edge free.}$$

Here  $N_{X,o}^i$  and  $N_{Y,o}^i$  are the critical stress resultants for a simply supported plate of a composite material under axial compression and shear, respectively, to be determined from

$$N_{X,o}^i = \frac{2\pi^2}{b_i^2} \sqrt{D_{11,i} \cdot D_{22,i}} \left( 1 + \frac{D_{3i}}{\sqrt{D_{11,i} \cdot D_{22,i}}} \right),$$

$$N_{Y,o}^i = \begin{cases} \left( \frac{2}{b_i} \right)^2 \left( 8.125 + \frac{5.05}{\theta} \cdot \sqrt[4]{D_{11,i} D_{22,i}^3} \right) & \text{at } \theta \geq 1 \\ \left( \frac{2}{b_i} \right)^2 \left( 11.7 + 0.532\theta + 0.938\theta^2 \right) \cdot \sqrt{D_{22,i} D_{3i}} & \text{at } \theta < 1 \end{cases} \quad (5-23)$$

where

$\theta = \frac{\sqrt{D_{11,i} \cdot D_{22,i}}}{D_{3i}}$ ,  $D_{k\ell,i}$  ( $k = 1, 2, 6$ ;  $\ell = 1, 2, 6$ ) are the cylindrical stiffness, and  $\ell_i$  is the length of the  $i^{\text{th}}$  plate.

As to homogeneous orthotropic panels, the expressions for cylindrical stiffness are of the following form:

$$D_{11,i} = \frac{E_{X,i} \cdot h_i^3}{12(1 - \mu_{XY,i} \cdot \mu_{YX,i})}, \quad D_{22,i} = \frac{E_{Y,i} \cdot h_i^3}{12(1 - \mu_{XY,i} \cdot \mu_{YX,i})},$$

$$D_{k,i} = G_{XY,i} \cdot h_i^3 / 12 = D_{66}, \quad D_{3,i} = D_{11,i} \cdot \mu_{XY,i} + 2D_{k,i},$$

$$D_{3,i} = D_{12,i} + 2D_{66,i}$$

where  $E_{X,i}$ ,  $E_{Y,i}$ ,  $G_{XY,i}$ ,  $\mu_{XY,i}$ , and  $\mu_{YX,i}$  are averaged elastic modulus and Poisson's ratios for the  $i^{\text{th}}$  plate.

## 6. MONTE-CARLO SIMULATION MODULE.

### 6.1 GENERAL STATEMENT OF THE PROBLEM.

Ideally, the task can be formulated as a flight-by-flight numerical Monte-Carlo simulation of combined stressed state of the considered structure in service, taking into account diverse random sources of loads. In each time instant, this state is compared with strength critical state, which is also simulated for both initial strength of a structure and random variation of strength in operation (random residual strength history). Such comparison determines the local failure of the structure. The analysis of global strength is then conducted. If the local failure results in the global failure (the analysis of global failure is out of the scope of present work), this failure is counted. When  $N$  load histories and residual strength histories are simulated using Monte Carlo and  $M$  failures are observed, the probability of failure is evaluated as:

$$\beta \approx \frac{M}{N} \quad (6-1)$$

It is possible to select  $N$  so that the error of  $\beta$  estimation does not exceed the acceptable value. Obtained value of  $\beta$  and appropriate error level are the final goals of simulation. By changing the initial conditions of simulation (safety factor or margins of safety, frequency and schedule and method of inspection, structural repair technique), the user can select the rational parameters of structure and/or maintenance to satisfy the reliability/cost requirements. Such direct simulation would take a very long time, primarily because of the lack of information sufficient for multicomponent load random generators. Besides the time of simulation, even with modern computers, is too high for parametric analysis.

In order to solve this problem, it is necessary to introduce significant simplified assumptions. The general idea of these assumptions is to replace the infinite continuous space of states of nature by finite countable set of states. Main countable sets assumed here are listed below:

- Set of external load/weights distributions over the airplane and the corresponding set of stress-strain states of structure.
- Set of states of structure, resulting from the impact damages.
- Set of inspection and repair procedures.

At present time it seems possible to obtain enough information for prediction of probability of failure of structural components both on design phase and certification phase. Certainly the accuracy of these predictions depends on the accuracy of initial data.

### 6.2 DESCRIPTION OF STRESSED STATE OF STRUCTURE—FINITE SET OF LOADING CASES.

In accordance with the majority of current structural strength practices, the analysis of strength/rigidity of an airplane is carried out for a finite set of conditions (specified maneuvers, gust conditions, landing conditions, etc.). They are called design load cases (DLC). There are many

load cases, but for each particular structure it is possible to select only a few critical cases. These cases are used for structural sizing. Usually this set of design cases is selected by comparing the external loads (bending moment, torque, shear force). Further, the selected set of cases is verified by using finite element models. Thus, on the global finite element model (FEM), it is possible to obtain the stressed state at least for element of skin with stiffeners or for several such elements (panel). Such a model is shown in figure 6-1.

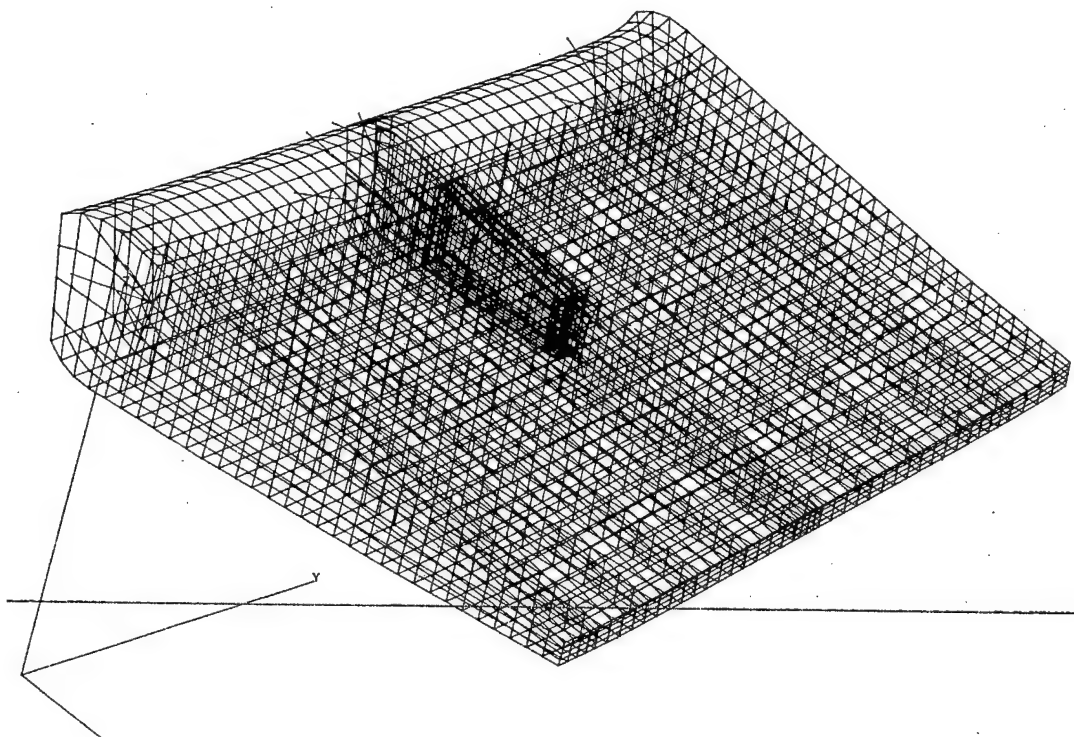


FIGURE 6-1. FINITE ELEMENT MODEL OF A STRUCTURAL ELEMENT

As a rule, FEM information is available in certification phase. In design phase, usually some approximate FEM are available. Such data can also be used for description of local structural behavior, if an impact damage occurs. This damage usually covers only one element. Therefore, the failure probability model is based on the selected design cases taken from strength analysis.

### 6.3 DESCRIPTION OF LOADS.

The structural loads should be described in a probabilistic manner, which should correspond with the description of strength (for comparison), and should be able to determine the maximum expected value of load for arbitrary time of operation (if no-damage-growth concept is used).

In a modern practice of fatigue analysis, a prediction of fatigue life of most fatigue critical sites of structure is carried out by comparing the number of cycles (time) to crack initiation as obtained in laboratory fatigue tests of specimens, with cumulative damage in operation. This cumulative damage is predicted on the statistical basis as cumulative load occurrence, versus

exceedance curve (figure 6-2). It is not easy to obtain adequate statistical information (flight measurements) on the loads (stresses) for all structural sites of interest. In this case, the cumulative damage is predicted by using probabilistic description of governing flight parameters (e.g., maneuver load factors) or probabilistic description of atmosphere (gust) or sinking speed at landing, etc. These parameters are well studied so that their frequency of occurrence can be predicted, if the typical missions are known. However, the local stressed state is determined by the combination of flight parameters (load factor with speed, Mach number, etc). Two distinct load cases are shown in figure 6-2.

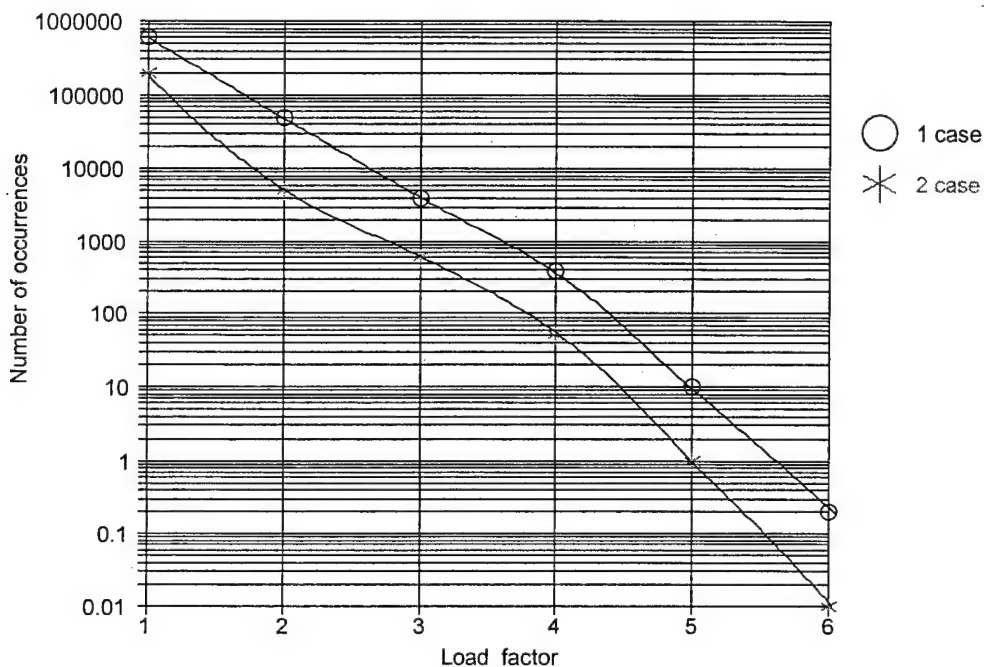


FIGURE 6-2. LOAD EXCEEDANCE CURVES

This problem is usually solved in a following way:

- All mission profiles of aircraft are divided into flight segments so that the load distribution during the one flight segment is approximately constant and load variation can be described by one governing parameter. Usually static design case load distributions are attributed (in conservative manner) to these segments, e.g., pull-up maneuver, load distribution is used together with maneuver load factor (governing parameter) and frequency of occurrence. Rough air loads are described by gust velocity (governing parameter), exceedance curve, and corresponding load distribution (cruise, flaps-down configuration, etc). Landing loads are described by sinking speed occurrence together with corresponding two-point landing load distribution.
- The linear relationships between the governing load parameter and the stress in a considered location is determined from stress analysis for the corresponding design case. Applying some relevant strength criterion, the occurrence of site loads can be obtained.

- If the exceedance curve for some governing load parameter is obtained on the basis of available data, one cannot describe accurately the rare occurrences of high values of this parameter, which mostly contribute to the probability of failure. Then the extrapolation of exceedance curve is a problem [20].

**IMPORTANT:** Linear extrapolation of all initial data is used in simulation, in particular, for sampling high loads approaching ultimate load. The exceedance curves are extrapolated linearly in semilogarithm scale (log-scale for number of exceedances and linear scale for load parameter). If the user implies another type of extrapolation, one should extrapolate the exceedance curve in a manner that is desired, at least up to the ultimate load.

#### 6.4 DESCRIPTION OF DEFECTS/DAMAGES.

Available statistical data, as well as relevant mathematical models, derived on the basis of these data can be used for probabilistic description of defects/damages. This information should be compressed similarly to the load information by introduction of finite set of damage types. Different types of defect/damage are known through damage, delamination, surface dents, etc. The user may use his own classification. For ProDeCompoS application, this classification should be related to the availability of methods of prediction of residual strength depending on the size of damage. The selection of damage types depends also on the type of load realized in the considered site, e.g., if only tension stress takes place there, primary attention should be paid to through damage, and delamination is of minor importance. Further, the damages are described by the frequency of occurrence (exceedance) of damages of various sizes of  $H_{dj}$  ( $2L$ ), derived for each  $j^{\text{th}}$  type of damage (see figure 6-3). This description is very similar to the description of loads.

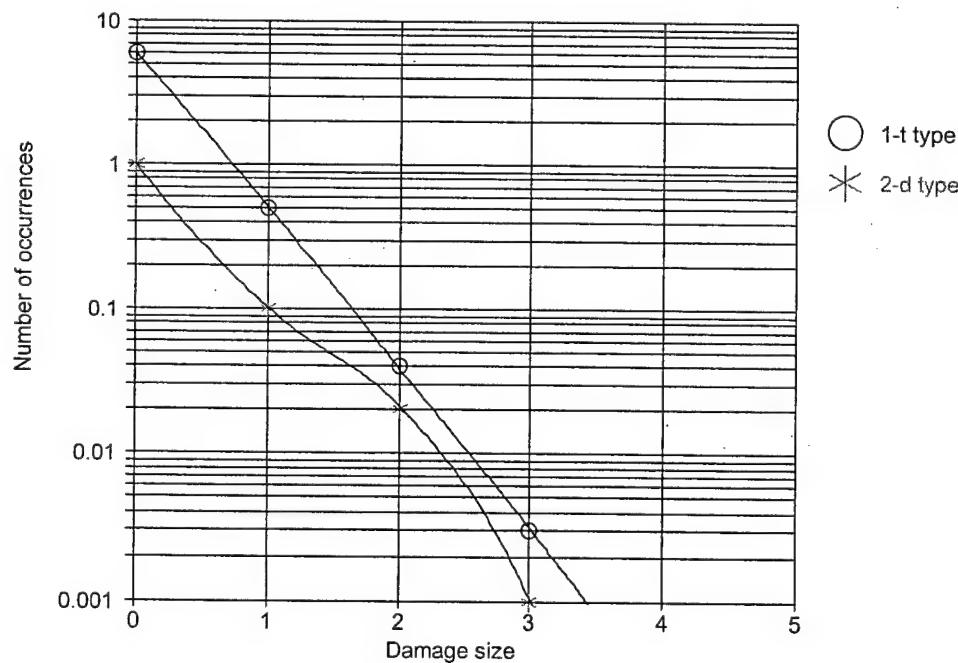


FIGURE 6-3. DAMAGE EXCEEDANCE CURVES

ProDeCompoS uses two classes of mechanical damages: manufacturing defects and operational damages. The damage types within these classes may be the same, e.g., through damage and delamination. Defects and damages are described by similar exceedance curves, but these curves are used in different ways. Manufacturing defect is generated randomly together with initial strength in time instant  $t = 0$ . Operational damages are randomly scattered over the life. The pseudorandom numbers of damages of both classes are generated using Poisson distribution. Mean of the Poisson distribution is an intercept of exceedance curve (mean number of damages per life). The time instants when operational damages appear are generated using uniform probability distribution. The pseudorandom size of defect/damage is generated according to the exceedance curve.

### 6.5 DESCRIPTION OF INSPECTIONS.

The efficiency of inspection should be described by the probability to detect the damage of a given type and given size. This probability is shown in figure 6-4. Only a few attempts to identify this function are known from the literature. As a rule, special tests are needed to obtain this probability. This can be done by having representative experts inspect, by the appropriate methods, different zones of a structure having damages of different size and type. The probability of detection is determined as the ratio of a number of successful inspections to their total number. It is also possible to determine the detection probability by comparing the empirical probability function of detected damages with theoretical one, assuming that the difference between mentioned functions is the probability for detection for various sizes of damage.

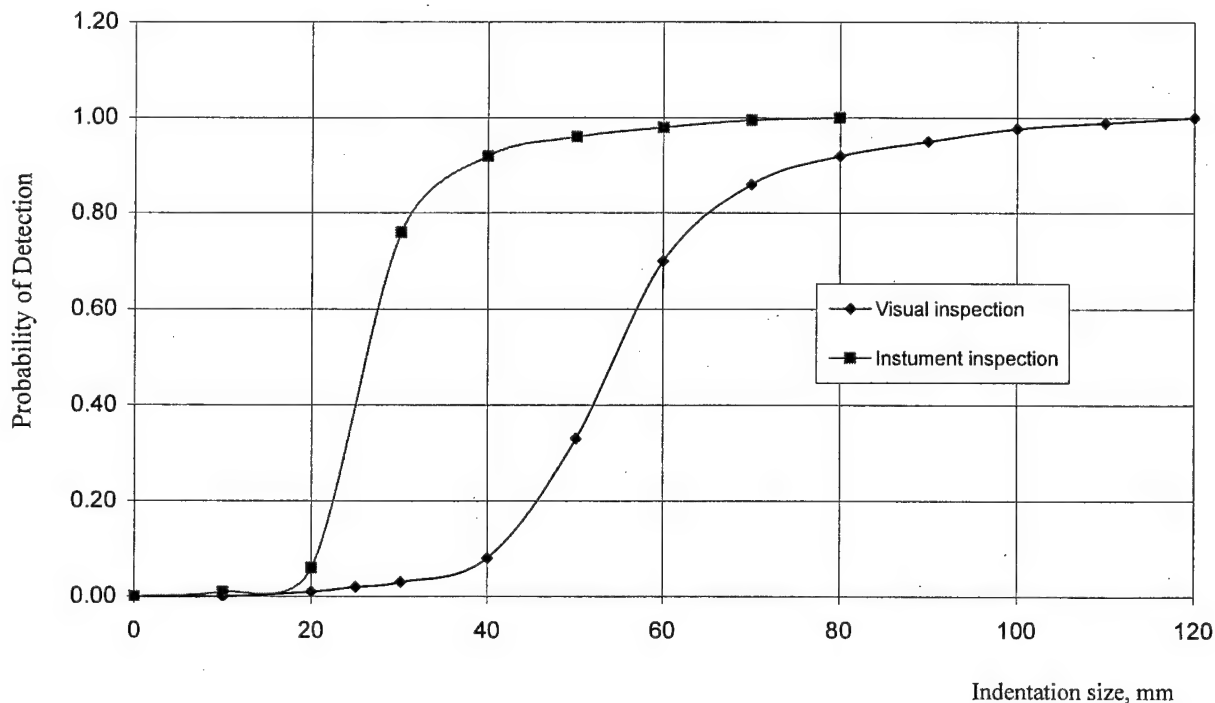


FIGURE 6-4. PROBABILITY OF DAMAGE DETECTION VERSUS INDENTATION SIZE

## 6.6 DESCRIPTION OF REPAIRS.

The logic of making a decision in the case of damage detection seems to be a difficult problem from the point of view of formalization for programming. At present, the simplest logic is realized in ProDeCompoS. If the damage is detected, it should be repaired at once. The method of repair is directly determined by the type of inspection, which has resulted in the detection of damage. The degree of strength restorations after repair is also determined by the type of inspection. It is hoped that this logic does not strongly influence the final result.

## 6.7 METHODS OF FAILURE PROBABILITY ESTIMATION.

If no damages are expected and the structure is operated only at normal temperature, the probability of failure per life is

$$\beta_z = 1 - \prod_{i=1}^{N_{dlc}} (1 - \beta_i), \quad (6-2)$$

Where  $\beta_i$  is the failure probability of site for  $i^{\text{th}}$  design loading case. For the evaluation of this probability for  $i^{\text{th}}$  design case the following well-known relation is used:

$$\beta = \int_0^{\infty} f_{l_{max}i}(x) F_{p_i}(x) dx = 1 - \int_0^{\infty} f_{p_i}(x) F_{l_{max}i}(x) dx \quad (6-3)$$

where  $F_{p_i}(x)$  is a probability distribution function of load-bearing capacity (strength) of site in  $i^{\text{th}}$  design case,  $F_{l_{max}i}(x)$  is a probability distribution function of maximum load per life. This load is distributed according to  $i^{\text{th}}$  design case. It is assumed that  $F_p(x)$  does not depend on time.  $f_{l_{max}i}(x)$  and  $f_p(x)$  are probability densities corresponding to  $F_{l_{max}i}(x)$  and  $F_p(x)$  respectively.

If damages and temperature are to be considered, the probability of failure is assessed by Monte-Carlo simulation. Initially, the simulation is carried out until the occurrence of five failures. Then the failure probability is estimated as  $p = 5/N$ , where  $N$  is a number of iteration when five failures occur. It is known that the variation coefficient  $C_v$ , of the parameter of Bernoulli's distribution  $p$ , is inversely proportional to the square root of the number of tests ( $N$ ). To obtain  $\beta$  with the accuracy,  $C_v$  is necessary to make, as a minimum,  $N_I = p / C_v^2$  iterations. After completion of  $N_I$  iterations,  $\beta$  is finally estimated by equation 6-1.

## 6.8 ONE LIFE SIMULATION.

Figure 6-5 shows the example random time histories generated at simulation.

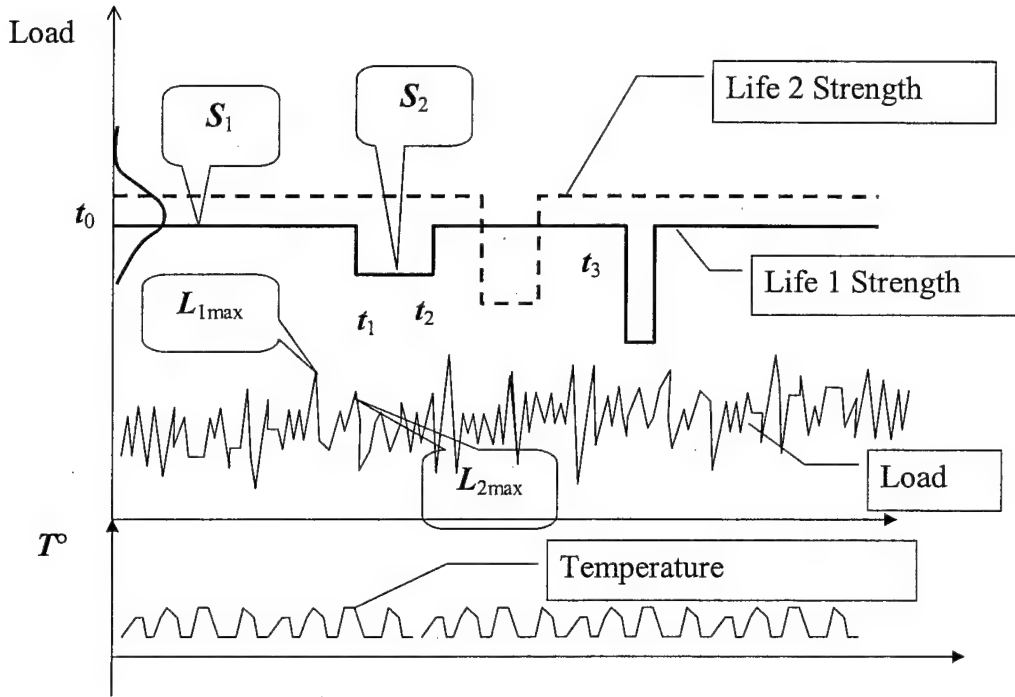


FIGURE 6-5. THE MAXIMUM LOADS PER INTERVAL,  $t_3-t_2$ , ARE GENERATED FOR ALL DLC (Steps 8 and 9 are repeated for residual strength  $s_3$ , and so on.)

Simulation proceeds in a following order:

1. Each iteration begins with the generation of initial strength values ( $t_0=0$ ) for each considered DLC, which is supposed to have Gauss or Weibull probability distribution.
2. At the same instant,  $t_0$ , the number and sizes of manufacturing defects (if any) of all types are generated, followed by generation of residual strength values,  $S_{li}$ , for all DLC. The manufacturing defects are listed in a damage list and after that treated as operational damages occurring at  $t_0=0$ .
3. The numbers of operational damages are generated for all damage types.
4. If no manufacturing defects and operational damages occur during this life, the maximum loads per life are generated for all DLC. At the instants of maximum load occurrence, random temperatures of structure are generated for all DLC. The residual strength values,  $S_{li}$ , are corrected depending on temperature and compared with corresponding loads. If any of these loads exceed the corresponding strength, structural failure is recorded and  $M = M + 1$ , see relation in equation 6-1.
5. Operational damages are scattered over the life using a uniform distribution generator. In fact, the time instants,  $t_l$ , are generated and added to the list of damages.
6. The values of damage size are generated in compliance with proper exceedance curve.

7. The values of residual strength at time instant,  $t_1$ , are generated.

For each damage, the “time of detection” or “time of repair” is randomly generated using the probability of detection and inspection schedule. As it has been stated above, the time of detection and the time of repair are considered to be same. In fact, the random numbers of inspections of different types of damage detection using geometric probability distribution are generated, and then find these inspections in the inspection schedule. A geometric deviate can be interpreted as the number of trials until the first success (including the trial in which the first success is obtained). The probability distribution function is

$$f(x) = P(1 - P)^{x-1}$$

for  $x = 1, 2, \dots$  and  $0 < P < 1$

The “time of detection” is the shortest time between randomly simulated times for different types of inspection. In this way it determines time instants  $t_2$ .

8. The maximum loads per interval,  $t_2 - t_1$ , are generated for all DLC. At the instants of maximum load occurrence, random temperatures of structure are generated for all DLC. The residual strength values,  $S_{2i}$ , are corrected depending on temperature and compared with corresponding loads. If any of these loads exceed the corresponding strength, structural failure is recorded and  $M = M + 1$ , see relation in equation 6-1.
9. At time  $t_2$ , the strength values of repaired structure are randomly generated using the same generators as in step 7.

## 6.9 THE DATA PREPARATION PROGRAM PreDaMC FOR STATISTICAL SIMULATION (USER'S MANUAL).

The PreDaMC is a part of the complex of programs for designing the composite structures. It is used to prepare all input data and to start the statistical simulation program MontCar; thereafter, control is returned to PreDaMC.

In addition to the work within the modelling software complex, the PreDaMC together with MontCar program may be used by organizations that develop and study the composite structures without running the complex ProDeCompoS.

### 6.9.1 Starting the Program—Termination of Work.

To start the PreDaMC program, one should:

- run the *ProDeCompoS.exe* executable module;
- click the item Reliability in the menu bar (which is located at the window top) and the pull-down menu is shown;

- click the subitem Reliability in the pull-down menu.

To terminate the PreDaMC program, one should close the program windows.

### 6.9.2 Data Format.

The input data of the MontCar program are explicitly described in the preceding chapter. As a result of execution of the program PreDaMC for each variant of calculation, nine files (a “data set”) are created. Names of the files have the following format:

*Set\_Name.Ei*, where

Set\_name—name of the data set;

i—number of the parameter of input data.

The “i” parameter varies from 0 to 8. The dependence between the type of input data and the “i” parameter is described in table 6-1.

The dialog window of the program contains nine pages. The user selects a page by clicking the page’s tab that appears at the top of the window. Page 1, Set Name, is designed to choose the name of the data set; pages 2 through 9 are designed to enter and edit the data. In addition, the start button of the MontCar program is on page 9, Monte Carlo. Many objects on the pages have hints with brief help, which can appear when the user keeps the mouse pointer over a particular object for a short length of time. Detailed manuals for the program pages are provided below.

TABLE 6-1. LIST OF INPUT DATA INTO DATA SET AND PreDaMC  
PROGRAM PAGES

| i | Type of Input Data  | Number and Title of Page   |
|---|---|----------------------------|
| 0 | Service data  |                            |
| 1 | Accuracy and type of item probability function.<br>Load exceedances.      | 2. Load&T<br>9. MonteCarlo |
| 2 | Temperature exceedances   | 2. Load&T                  |
| 3 | Defect and damage size exceedances  | 3. Damage                  |
| 4 | Damage detection probability  | 4. Detection               |
| 5 | Residual strength and variation coefficient as<br>function of damage size | 5. Strength                |
| 6 | Recovery coefficient and strength variation after<br>repair               | 6. Repairs                 |
| 7 | Inspections schedule  | 7. Inspections             |
| 8 | Strength vs temperature   | 8. Strength (T)            |

### 6.9.3 Set Name Page.

The Set Name page is used to choose the current data set. The page is represented in figure 6-6. The page carries the name of a current data set: Data set to work; the name of the work directory: Work directory, (in which all files of the data set are located); and the description panel: Brief description of set and the following buttons:

Open—opens the existing data set. Press the button and the MS Windows 95/98 dialog box is displayed for you to choose the name of the set. This name is identified with the symbol string with extension of E0 in the work directory. Choose the data set name and press the OK button. The program checks the presence of all files (with extensions of E0 through E8) and loads data in appropriate pages.

Copy—copies the current data set to the specified one with a new name. After copying, the new set becomes the current one. Works as the Open button.

New—creates a new data set. All parameters obtain default values. After creation, the new set becomes the current one. Works as the Open button.

Rename—renames the current data set. Works as the Copy button.

Delete—deletes the current data set.

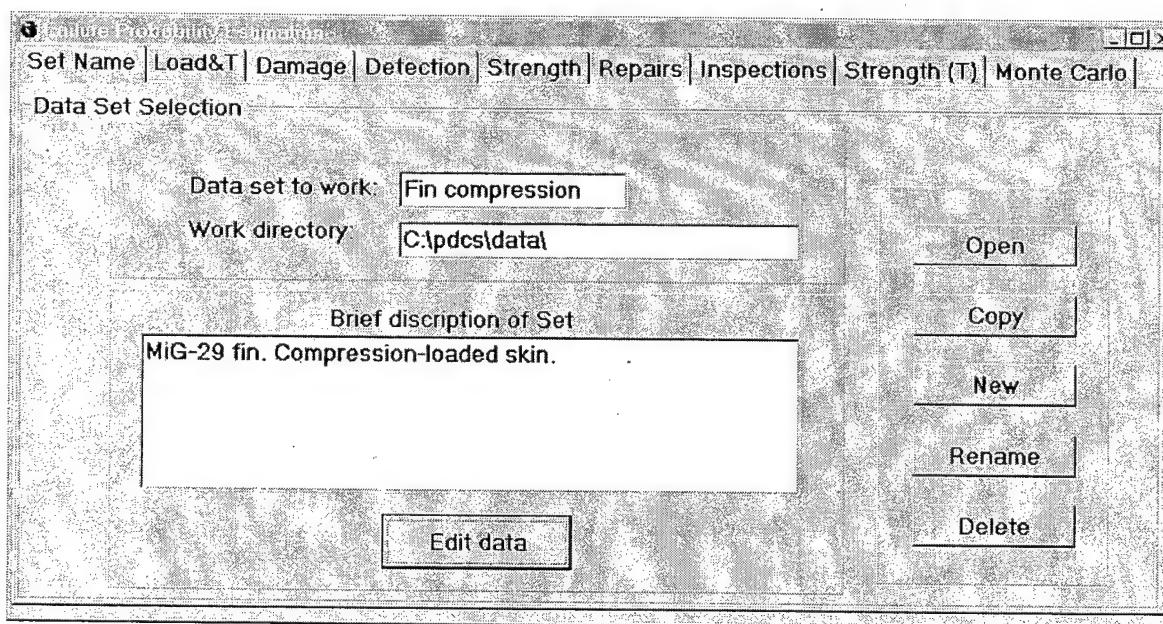


FIGURE 6-6. THE SET NAME PAGE

The Data set to work and Work directory boxes show the current data set name and the work directory name (all files of the current data set must be located in this work directory). Both boxes may not be edited. The Brief description of set panel shows description of the current data set. Click the Edit data button to enter or edit the description.

When you start the program, the data set will open. When the program was previously closed, it opened again.

- Messages for the Set Name Page

*File nmfdemts.dat doesn't exist:* the root directory of the ProDeCompoS does not include file with name *nmfdemts.dat*. This file should contain the name of the data set opened when PreDaMC was previously closed. Click the OK button to continue the work. The Set Name page will offer only two buttons: Open and New.

*File Name in nmfdemts.dat is absent:* in *nmfdemts.dat* there is no data set name. Click the OK button to continue the work. The Set Name page will offer only two buttons: Open and New.

*Input set\_name.Ei file doesn't exist:* there is no file with name *set\_name.Ei* (where i is a digit ranging from 0 to 8) in the work directory. Select other set or open a new one.

*Do you really want to delete the current set?* You should respond with Yes or No.

#### 6.9.4 Load&T Page.

The Load&T page is used to enter the load and temperature exceedances for different design loading cases and to create a new design loading case (parameter DLC) or to edit the existing one. The appearance of the page is shown in figure 6-7. There are three main objects on the page: *Grid* (left), *Graphics* (central), and *Panel* (right).

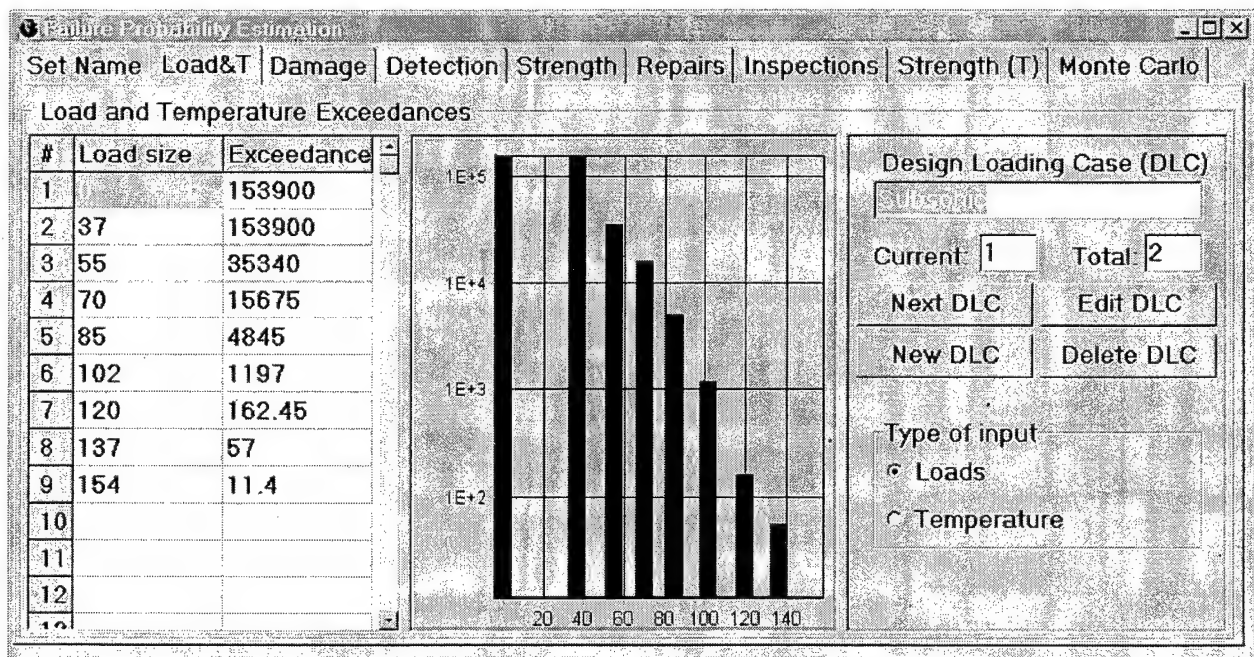


FIGURE 6-7. THE LOAD&T PAGE

The *Panel* object is used to choose the value to be edited. At the top, the buttons and boxes for editing the design loading case are located: the edited text box Design Loading Case (DLC), boxes Current and Total, and buttons Next DLC, Edit DLC, New DLC and Delete DLC.

The Design Loading Case (DLC) box shows the title of the design loading case. The title can be inserted or edited during the editing mode.

The Current and the Total boxes show the current number of the design loading case and the total number of the cases in the set. The Current may range from 1 to the Total, and the Total, from 1 to 15. These parameters cannot be changed directly in the boxes. The parameter, Current, is varied by using the button Next DLC, whereas the Total is changed by buttons New DLC and Delete DLC.

Click the Next DLC button to increase the number of the current design loading case (Current) by 1. If Current becomes greater than Total then it is set to 1.

Click the Edit DLC button to switch the program to the editing mode. In this case, the color of text characters in the editable objects (i.e., the *Grid* object and Design Loading Case (DLC) box) is changed from black to blue, and one can edit and enter values in these objects. Besides, a new window appears above the *Panel* object. It is used to specify the scale factor for exceedances and loads (input the scale factor value into the box, click the Multiply button, and all data in the *Grid* object will be multiplied by this factor) and to terminate the editing mode (by utilizing the End Edit button). After clicking the End Edit button, the standard Windows 95/97 box is displayed with the Save changes? question. There are three buttons: Yes, No, and Cancel. Click Yes to store all changes in the data files, No to exit without storage, and Cancel to remain in the editing mode.

At the bottom of the *Panel* object, two radio buttons are located: Loads and Temperature. Only one radio button in a set can be selected at a time. Click the Loads button to display/edit the load exceedances, or the Temperature button to display/edit the temperature exceedances in the current design loading case.

The *Grid* object is used to display and edit the data in the current design loading case. When in the displaying mode, one can use only standard movement keys: arrows, Page Up, Page Down, Home, End, Ctrl Home, and Ctrl End to see data in the *Grid* object. During the editing mode, one can use buttons Backspace, Delete, Left, Right, Home, and End to edit the data in cells of the *Grid* object to input the floating-point values into cells. The user can operate with the following keys: digits from 0 to 9, point ("."), "+" and "-" signs, and characters "E" and "e."

For entering a new value into a cell, one should click Tab/Shift Tab keys or press and release the left-hand mouse button when the mouse pointer is over the cell. The cell becomes a currently selected one. Enter floating-point values into cells. All earlier data in the cells will be overwritten.

For editing a value in a cell, one should click the left mouse button when the mouse pointer is over the cell (and the cell becomes the selected one). The cell will have an input focus. Edit the

value. When a cell has the input focus, one can work with the Clipboard. Click the right mouse button with the mouse pointer being over the cell (and the latter will feature the input focus) to display the standard Pop-up menu. The following buttons are available on the menu:

- Undo—to undo your most recent actions;
- Cut—to remove the selected items from their current positions and place them on the Clipboard;
- Copy—to place an exact copy of the selected text on the Clipboard and leave the original untouched; Copy replaces the current Clipboard contents with the selected items;
- Paste—to insert the contents of the Clipboard into the selected cell;
- Delete—to delete the selected text;
- Select All—to select all the text in the active cell.

The Clipboard can contain more than one digit (when the user fills the Clipboard from other programs or files). To input many digits into the *Grid*, one must select the first cell for input and click the right mouse button with the mouse pointer over the cell. If the Clipboard contains correctly written numbers, one will be asked: Paste from Clipboard? The digits are then sent into the *Grid* in the columnar manner. Thereafter, the user will be informed of how many digits were inputed, and the last changed cell will be currently selected. Digits in the Clipboard may be written in an arbitrary format. Characters such as space, tab, comma (,), and semicolon (;) can be used as separators.

Attention! Do not forget to end your editing mode and to save changes before moving to other pages in PreDaMC.

The *Graphic* object is used to show the values entered. The changes of data in the *Grid* object are presented graphically after pressing the End Edit button. Click the mouse pointer on a graphics to select the point data cell in the *Grid* object (at both view and edit mode).

- Messages for the Load&T page
  - *Error reading file set\_name.E0.* Can arise upon damage of the data file with extension of E0.
  - *Error reading file set\_name.E1.* Can arise upon damage of the data file with extension of E1.
  - *Error reading file set\_name.E2.* Can arise upon damage of the data file with extension of E2.
  - *Number of loading case must be less than 16.* The number of design loading cases varies from 1 to 15.

- *You can't delete last set.* The number of design loading cases should be greater than 0. The message appears after an attempt to delete the last data set.
- *Insufficient points in design load case.* The number of data points in a design loading case should be greater than 1.
- *Delete design loading case  $i$ ?* The user is asked if he or she really wants to delete the  $i^{\text{th}}$  design loading case. It is necessary to answer with Yes or No.
- *XXX is not a valid floating-point value.* The message appears when the input number has an invalid format. Click any key to return into the edit mode. The cell with error will be currently selected.
- *Loads must be positive or 0 for first.* The load value should be positive, except for the first value, which can be 0.
- *Exceedance must be positive.* The load and temperature exceedance values should be positive.
- *Load and Temperature must be strictly in the increasing order!*
- *Exceedances might not increase with sizes!*

#### 6.9.5 Damage Page.

The Damage page is used to input the defect and damage exceedances for different damage types and to create new damage types (the parameter DT) or to edit the existing ones. The appearance of the page is shown in figure 6-8. The main objects of the page, the work modes, and the technique of editing/entering data is very similar to the technique described for the Load&T page.

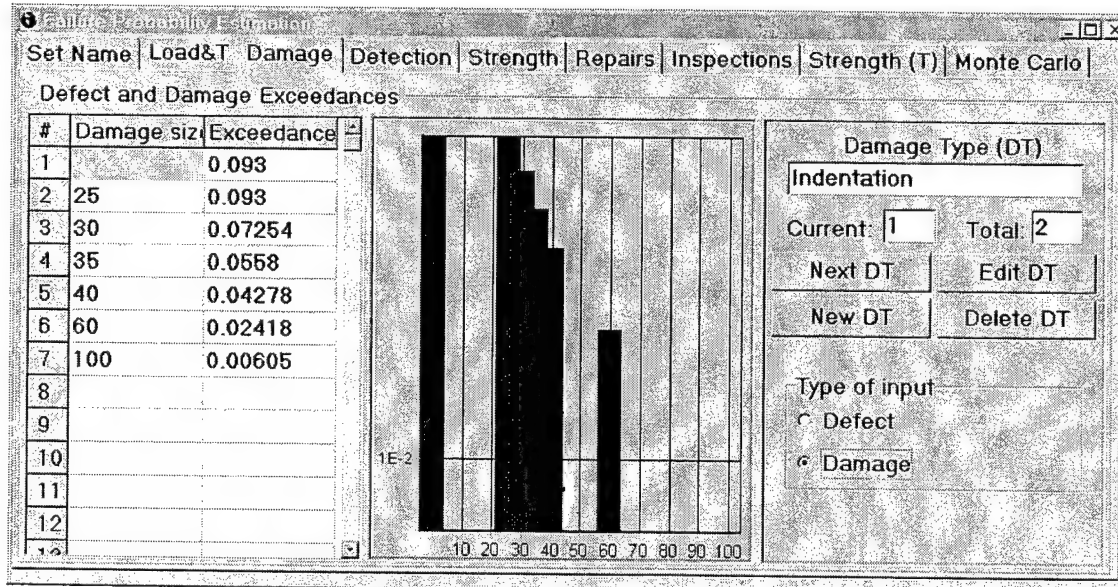


FIGURE 6-8. THE DAMAGE PAGE

- Messages for the Damage page

- *Error reading file set\_name.E0.* Can arise upon damage of the data file with extension of E0.
- *Error reading file set\_name.E3.* Can arise upon damage of the data file with extension of E3.
- *Number of damage type must be less than 16.* The number of damage types varies from 1 to 15.
- *You can't delete last set.* The number of damage types should be greater than 0. The message appears after an attempt to delete the last data set.
- *Insufficient points in design load case.* The number of data points in a damage type should be greater than 1.
- *Delete damage type i?* The user is asked if he/she really wants to delete the  $i^{\text{th}}$  damage type. It is necessary to respond with Yes or No.
- *XXX is not a valid floating-point value.* The message appears when the input number has an invalid format. Click any key to return into the edit mode. The cell with error will be currently selected.
- *Damage size must be positive or 0 for first.* The damage size value should be positive, except for the first value, which can be 0.
- *Exceedance must be positive value.* The defect and damage exceedance values should be positive.
- *Sizes must be strictly in the increasing order!*
- *Exceedances might not increase with sizes!*

#### 6.9.6 Detection Page.

The Detection page is used to input the defect/damage detection probability function at the defect/damage size for a particular damage type (the parameter IT) and to create new inspection types or to edit the existing ones. The appearance of the page is shown in figure 6-9. There are three main objects on the page: *Grid* (left), *Graphics* (central), and *Panel* (right). The *Grid* and *Graphics* objects are similar to those described for the Load&T page.

The *Panel* object is used to choose the value for editing. At the top, the buttons and boxes for editing the inspection type number are located: text box Inspection Type (IT), boxes Current and Total, and buttons Next IT, Edit IT, New IT and Delete IT. These are similar to those described for Load&T page. If one presses the Edit IT button the Next IT, Edit IT, New IT, and Delete IT buttons will be invisible, and the End Edit button remains.

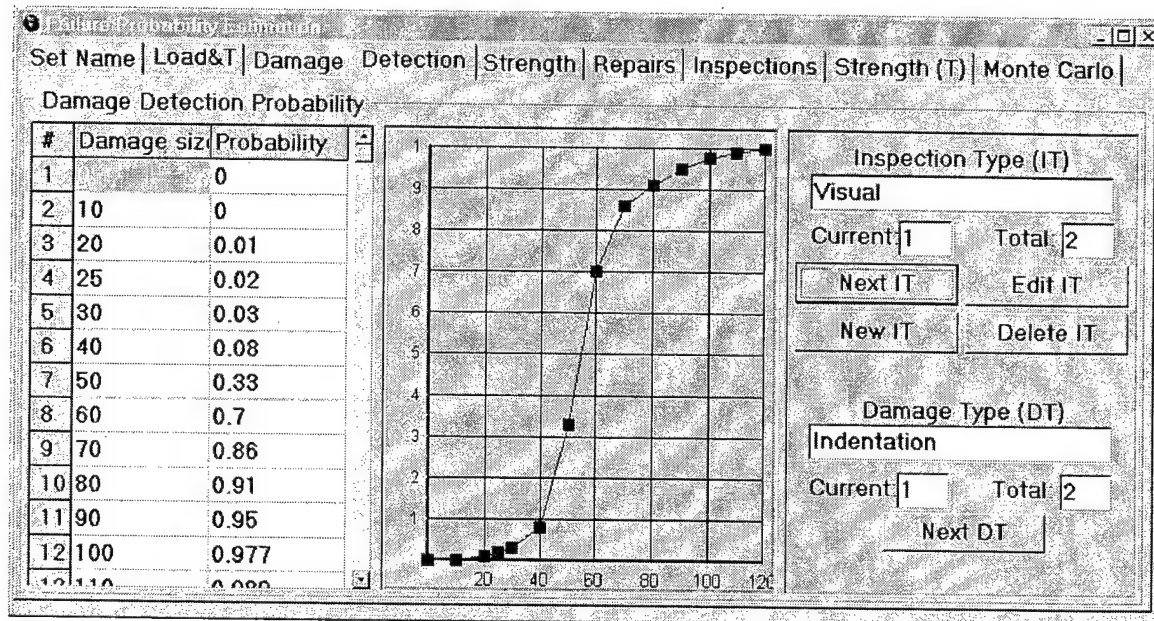


FIGURE 6-9. THE DETECTION PAGE

At the bottom of the *Panel* object the buttons for damage type selection are located.

- Messages for the Detection page
  - *Error reading file set\_name.E0.* Can arise upon damage of the data file with extension of E0.
  - *Error reading file set\_name.E4.* Can arise upon damage of the data file with extension of E4.
  - *Number of inspection types must be less than 16.* The number of inspection types varies from 1 to 15.
  - *You can't delete last set.* The number of inspection types should be greater than 0. The message appears after an attempt to delete the last data set.
  - *You can't delete first set.* The first inspection type must be the preflight check. It can not be deleted.
  - *Insufficient points in inspection type.* The number of data points in an inspection type should be greater than 1.
  - *Delete inspection type i?* One is asked if he/she is really wanting to delete the  $i^{\text{th}}$  inspection type. It is necessary to respond with Yes or No.
  - *XXX is not a valid floating-point value.* The message appears when the number entered has an invalid format. Click any key to return into the editing mode. The cell with error will be the currently selected one.

- *Damage size must be positive or 0 for first.* The damage size value should be positive, except for the first value, which can be 0.
- *Probability of damage varies from 0 to 1.*
- *Probability must increase with sizes!* The function of defect/damage detection probability must increase with the damage size.
- *Damage sizes must be strictly in the increasing order!*

#### 6.9.7 Strength Page.

The Strength page is used to input the function of static strength and static strength variation, depending on the damage size. The appearance of the page is shown in figure 6-10. There are three main objects on the page: *Grid* (left), *Graphics* (central), and *Panel* (right). The *Grid* and *Graphics* objects are similar to those described for Load&T page.

The *Panel* object is used to choose the value for editing. At the top, the buttons and boxes for editing the design loading case number are: text box, Design Loading Case (DLC); the boxes Current and Total; and the Next DLC button. These are similar to those described for the Load&T page.

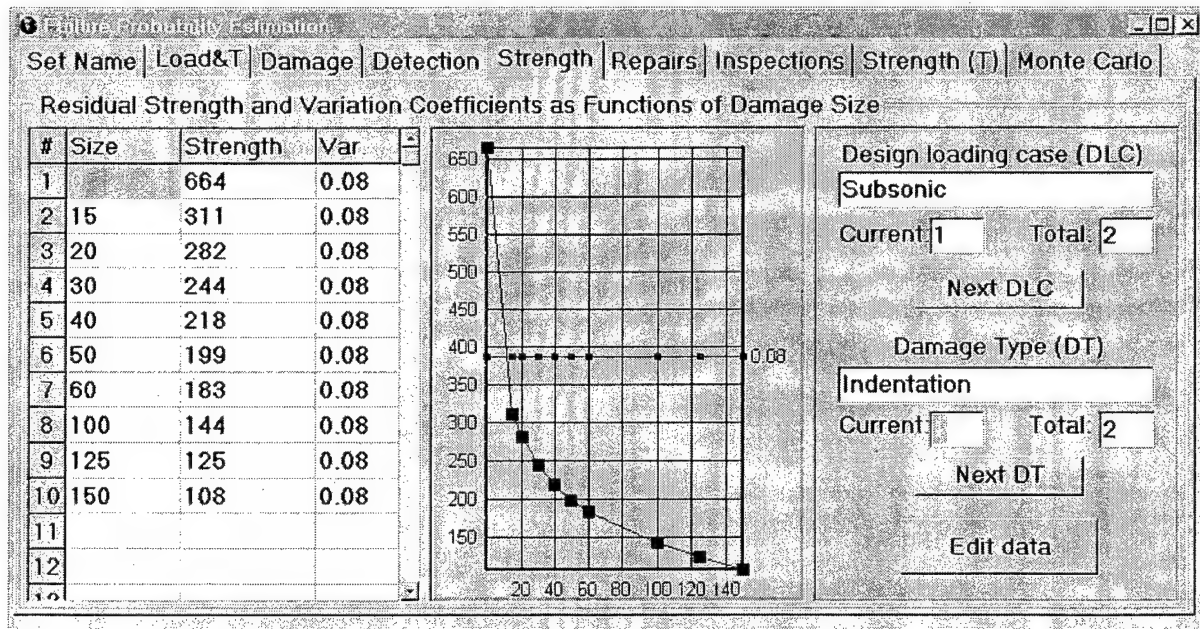


FIGURE 6-10. THE STRENGTH PAGE

In the lower part of the *Panel* object, the buttons and boxes to select the current damage type are the text box, Damage Type (DT); the boxes Current and Total; and the Next DT button. These ones are similar to those described for the Load&T page.

The Edit data button is placed at the bottom of the *Panel* object, which is used for editing the function of static strength and static strength variation (depending on the damage size). In the editing mode, a new window appears above the *Panel* object. It is used to input the scale factor for the function (the user should input the scale factor into the box, click the Multiply button, and all data in the Strength row of the *Grid* object will be multiplied by this factor) and to terminate the editing mode (by pressing the End Edit button). The editing mode is similar to that described for the Damage page.

- Messages for the Strength page
  - *Error reading file set\_name.E5.* Can arise upon damage of the data file with extension of E5.
  - *Insufficient points in residual strength and variation.* The number of data points in both parameters should be greater than 1.
  - *XXX is not a valid floating-point value.* The message appears when the new number has an invalid format. Click any key to return to editing. The cell with error will be the currently selected one.
  - *Damage size must be positive or 0 for first.* The damage size value should be positive, except for the first value which can be 0.
  - *Residual strength must be positive value.*
  - *Strength might not increase with sizes!*
  - *Residual strength variation must not be negative.*
  - *Damage sizes must be strictly in the increasing order!*

#### 6.9.8 Repair Page.

The Repair page is used to enter the static strength recovery coefficient and the static strength variation after repair. The appearance of the page is shown in figure 6-11. There are three main panels on the page to select: the current design loading case, the damage type, and the inspection type. The description boxes Current and Total and the Next button are inserted therein. These buttons and boxes are similar to their counterparts described for preceding pages.

Failure Probability = 0.000000

Set Name | Load&T | Damage | Detection | Strength | Repairs | Inspections | Strength (T) | Monte Carlo

Recovery Coefficients and Strength Variation after Repair

|                                 |                           |                      |
|---------------------------------|---------------------------|----------------------|
| Recovery type                   | Design Loading Case (DLC) | Inspection Type (IT) |
|                                 | Subsonic                  | Visual               |
| Recovery coefficient            | Current: 1 Total: 2       | Current: 1 Total: 2  |
|                                 | Next DLC                  | Next IT              |
| Strength variation after repair | Damage Type (DT)          |                      |
| 0.1                             | Indentation               | Edit data            |
|                                 | Current: 1 Total: 2       |                      |
|                                 | Next DT                   |                      |

FIGURE 6-11. THE REPAIR PAGE

There are three boxes for editing at the left:

- a. Recovery type—the repair title or description.
- b. Recovery coefficient—the strength recovery coefficient; it is the ratio of static strength after repair to static strength before repair.
- c. Strength variation after repair—the coefficient of static strength variation after repair.
- d. Click the Edit data button located in the right lower corner to edit these boxes. During the editing mode, the Edit data button is changed to End Edit. The editing mode are similar to that described for the Load&T page.
- Messages for the Repair page
  - *Error reading file set\_name.E6.* Can arise upon damage of the data file with extension of E6.
  - *XXX is not a valid floating-point value.* The message appears when the new number has an invalid format. Click any key to return to editing. The cell with error will be the selected one.
  - *Recovery coefficients must be positive.*
  - *Strength variation must be positive.*

### 6.9.9 Inspections Page.

The Inspections page is used to input the inspection schedule. The appearance of the page is shown in figure 6-12. There are three main objects on the page: *Grid* (left), *Graphics* (central), and *Panel* (right). The *Grid* and *Graphics* objects are similar to those described for the Load&T page.

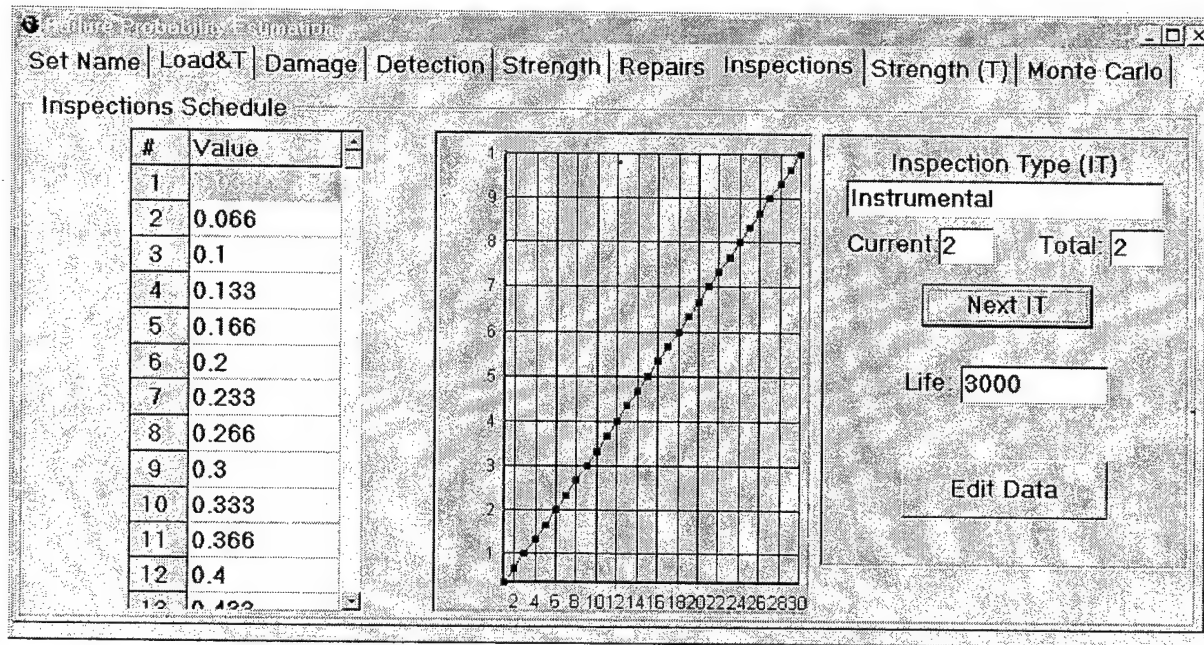


FIGURE 6-12. THE INSPECTIONS PAGE

The *Panel* object is used to choose the value to be edited. At the top, the following buttons and boxes to select the current inspection type are located: the Inspection Type (IT) and Current and Total boxes; and the Next DLC button. These buttons and boxes are similar to those described for the Load&T page.

The Life window for input of design service life (in flights) is available. In this version of the program, the inspection type 1 is for pre- or post-flight surveys; therefore, when the current value of IT is 1, the Life value is entered only. Grid and Graphics objects are not used.

At the bottom of the *Panel* object, the button Edit data for editing the inspection schedule and life is located. The editing mode is similar to that described for the Load&T page.

- Messages for the Inspections page
  - *Error reading file set\_name.E8.* Can arise upon damage of the data file with extension of E8.
  - *Insufficient points in inspection schedule.* The number of data points should be greater than 1.

- *XXX is not a valid floating-point value.* Appears when the new number has an invalid format. Click any key to return to editing. The cell with error will be currently selected.
- *Life must be from 10 to 150 000.* Design life should be from 10 to 150 000.
- *Value must be from 0 to 1.*
- *Values must be strictly in the increasing order!*

#### 6.9.10 Strength (T) Page.

The Strength (T) page is used to input the static strength versus temperature relation. The appearance of the page is shown in figure 6-13. There are three main objects on the page: *Grid* (left), *Graphics* (central), and *Panel* (right). These objects are similar to ones on the Load&T page.

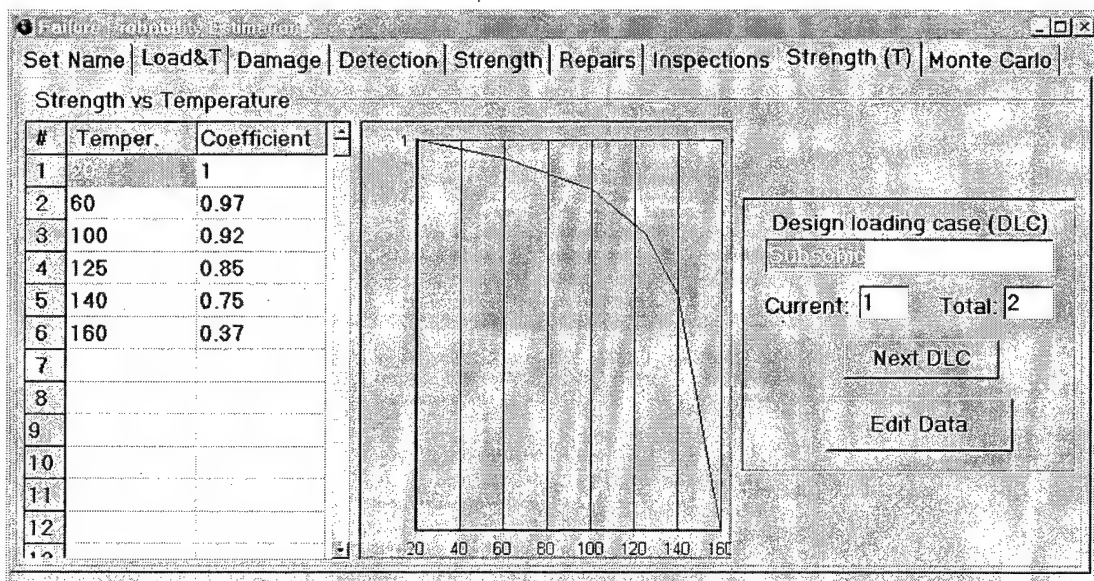


FIGURE 6-13. THE STRENGTH (T) PAGE

- Messages for Strength (T) page
  - *Error reading file set\_name.E7.* Appears upon damage of the data file with extension of E7.
  - *Insufficient points in strength-temperature relation.* The number of data points should be greater than 1.
  - *XXX is not a valid floating-point value.* Appears when the new number has an invalid format. Click any key to return to editing. The cell with error will be currently selected.

- *Coefficient must be from 0 to 2. The coefficient of the static strength vs. temperature relation varies from 0 to 2.*
- *Temperatures must be strictly in the increasing order!*
- *Coefficient might not increase with sizes!*

#### 6.9.11 Monte Carlo Page.

The Monte Carlo page is used to enter the accuracy of the item probability function (Accuracy box), type of item probability function (Type of Probability Function radio button), calculate the failure probability by the statistical simulation (Monte Carlo) method (Run button), and show the result of calculation. The appearance of the page is shown in figure 6-14.

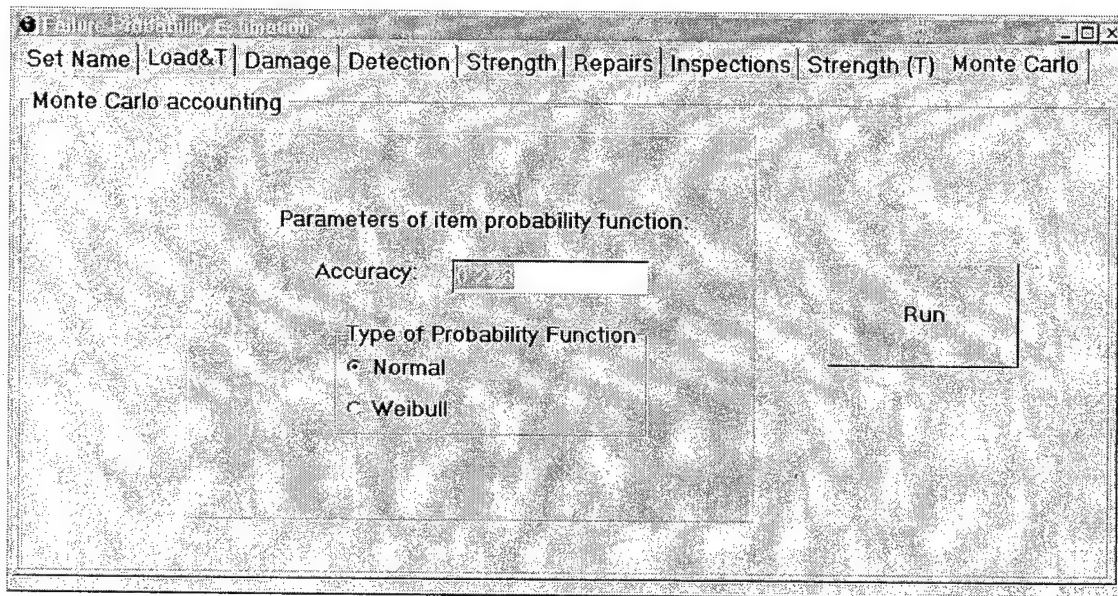


FIGURE 6-14. THE MONTE CARLO PAGE

- Messages for the Monte Carlo page
  - *MontCar Failed. "ErrorMessage"* There occurred an error named ErrorMessage during program execution. See the MontCar program description.
  - *XXX is not a valid floating-point value.* Appears if the input number has an invalid format. Click any key to return to editing. The cell with error will be currently selected.
  - *Accuracy must not be null.* Accuracy must be from 0 to 0.5.

## 7. DATABASES FOR ProDeCompoS (USER'S MANUAL).

The structural efficiency of aircraft structures is believed to be improved through the use of the polymer matrix composites (PMC), based on thermoset/thermoplastic matrices continuously reinforced with carbon, glass, or ceramic fibers. These materials possess high specific strength/stiffness and high resistance to crack initiation and propagation under cyclic loads. Widespread implementation of composite materials in various industries (aerospace, shipbuilding, and automotive) requires the "three-in-one" problem to be solved, on developing materials with high production characteristics and suitable in-service behavior, efficient and high-output manufacturing processes, and methodology of design taking into account features of the composite materials.

Integrated database of the program complex "Probability design of damage tolerant composite aircraft structures" will accelerate access of designers, process engineers, and analysts to the necessary information, ensure completeness and reliability of this information, simplify development of an applications software for analyzing the composite structures, and improve the convenience for users.

The designer, the industrial engineer, and the analyst must define numerous measures, which are a necessity at design, manufacture, certification, and service stage. Under these conditions, integrated software for ensuring damage tolerance of composite structures is one of the necessary options for implementing composite materials in the aircraft industry.

The user for input/editing purposes may access all data in the databases. Of the latter, each has its own database management system. A part of the data (mainly the statistical characteristics) is written to a file for using in other programs. Databases of the complex are created by using Borland Delphi database management system.

The databases can be used not only in the program complex, but also autonomously in organizations developing, studying, and operating composite structures.

This chapter includes description of the following databases:

- TESTS database;
- MATERIALS database; and
- AIRCRAFT database;

which includes information about:

- composite materials and their main characteristics;
- the usage of composites in airframes and other relevant designers;
- the manufacturing processes for composite structures;
- methods of nondestructive inspection and repair;
- the manufacturing defects;
- in-service damages; and
- the results of testing the specimens, structural members, and full-scale structures.

## 7.1 TESTS DATABASE (USER'S MANUAL).

The TESTS database is a part of the complex of programs for designing the composite structures and performs functions of collection, storage, and preprocessing of the data obtained during experimental evaluation of composites strength.

In addition to the work within the modelling software complex, the TESTS database may be used "off-line" in organizations that develop and study the composite structures.

### 7.1.1 Requirements for Hardware and System Software Installation.

The TESTS database is designed to be operated on Windows 98 and later. A minimal configuration of hardware is sufficient; however, in order to implement all options prepared for the user, the computer should have a mouse. In addition, one should take into account that if the RAM is less than 32 MB, the total number of simultaneously open windows may turn out to be limited, and the overall speed of response may be slower. It is recommended that a 64-MB RAM be used.

The relevant data files are to be installed in a separate directory on a hard disk with path Math\_path\BED\BAZA. (File bde.zip should be unzipped in the directory Math\_Path.) Here, Math\_path is the directory name where the executable module *ProDeCompoS.exe* is located.

The Math\_path\BDKM\BAZAKM directory should incorporate

- Database files: Bed.dbf, Bed.dbt, Bed.mdx;
- Service data: Bedout.dbf, Bedout.dbt, Bedout.mdx;  
    Fld\_rez.dbf, Fld\_rez.dbt, Fld\_rez.mdx;  
    Fld\_rkon.dbf, Fld\_rkon.dbt, Fld\_rkon.mdx;  
    Dop\_wrem.dbf, Dop\_wrem.dbt,  
    Dop\_wrem.mdx;
- Temporary files: Tmp.db, Tmp.mb;  
    Bedout1.dbf, Bedout1.dbt, Bedout1.mdx.

The TESTS image files are to be installed in a separate directory on a hard disk with path Math\_path\BED\IMAGE.

### 7.1.2 Terms and Definitions.

- Data field (or field)—an indivisible element of the database
- Record—a set of attributes describing one copy of an information entity

- Window—a display screen containing information of one section or subsection; as a rule, a window can appear or be removed as a whole; in certain situations window dimensions can be varied by a user.
- Bold label—the label that can be seen on the display during working of programs.

#### 7.1.3 Contents of the Database.

From the user's point of view, the database contains the following information on composite specimens:

- general information (a registered number, a test date, a tester organization, test type, etc.);
- data on the structure/semitinished item from which the specimen has been cut out and a location on the structure where the specimen has been cut out;
- specimen dimensions;
- size of stress concentrator or damage area;
- lay-up sequence;
- test conditions; and
- type and results of tests.

One record in the database corresponds to one specimen and one experiment with this specimen.

#### 7.1.4 Functions of TESTS Database.

This section briefly describes main operations with data in the database. All the functions that can be grouped are in the following categories:

- on-screen review;
- input, editing; and
- output to files for the analytical programs to use.

ON-SCREEN REVIEW. All data in the database can be sent to a display screen for inspection and survey. Two types of output are used: in Table Brief review and in screen Forms Detailed view. For switching between the Brief review mode and the Detailed view mode, one can use “+” or “-” buttons which are located in the blue panel at the window top.

Each line of the table contains the most widely used information about one record. The number of simultaneously provided lines (and, respectively, records) depend on which display screen field is specified by the user. The table is the most convenient facility for survey-type analyses.

As for screen Forms, a window of prescribed size is getting all fields, but only for one record at a time.

In this version, the database has options for sorting, searching, and filtering the data (so as to output the requested data only).

INPUT/EDITING of data while working with the TESTS database is performed at the moment when information is represented in the forms. Editing is initiated by selecting Edit in the NAVIGATOR menu (the latter is located in the blue panel at the window top). At the moment of selection, if the data were displayed in the table, the program will automatically change over to data representation in the Forms.

Data of each data field are sent to the database once (but can continuously be edited). For example, data on a testing of a particular structural assembly may at the initiatory stage be input partly (if data are not complete by the recording time) and thereafter edited and complemented if more correct information becomes available.

OUTPUT TO FILES. The major function of the TESTS database is to provide initial information for aircraft reliability analysis programs. The information is transferred to files, described later using Main menu "Report" item, and can be processed in order to obtain statistical characteristics of the parameters by utilizing standard software (such as STATISTICA for Windows 5.0) or another program.

#### 7.1.5 User's Proficiency Requirements.

The database is designed for being used by specialists who have taken at least a minimal training in the field of automatic data processing. The user is expected to be

- capable of handling the PC hardware and peripherals;
- familiar with Windows 98 or later, including the file system;
- familiar with Borland Delphi user interface principles since these are employed in the TESTS database (the Delphi interface is much similar to the MS Windows interface that has been a world's standard).

#### 7.1.6 Starting the Program—Termination of Work.

To start the TESTS database, one should:

- run the *ProDeCompoS.exe* executable module;
- click the item Databases in the menu bar (the latter is located at the window top), and the pull-down menu is shown;
- click the subitem TESTS in the pull-down menu.

To terminate work with the TESTS database, one should close program windows or click the subitem Exit in the Main menu item File.

### 7.1.7 Main Menu of TESTS Database.

Considered as the major option for navigation in the TESTS database is the Main TESTS menu. It appears promptly after starting the system and remains accessible throughout a session. The menu comprises of

- a menu bar at the window top; and
- a pull-down menu with columns of items.

The user selects items and subitems (by mouse or keyboard) to initiate the corresponding operations of the system.

To utilize menus while in the keyboard control mode, one should

- click the left mouse button when the system is waiting for commands and the mouse cursor is under a menu button;
- use the arrow keys to place the cursor on the item required;
- press <Enter>.

The fastest option for working with menus is the mouse. To select an item, it suffices to click the mouse button when the cursor is on the item.

The TESTS database Main menu comprises the following items:

- File—to use the service functions and to quit the program
- Subitems
  - Product select group—to select a product group;
  - Brief review—to show the table with the most widely used information about records. You can search, select records, and write data to a file;
  - Detailed view—to show the forms with all information about one record. You can edit data, prepare new records, or delete unnecessary data;
  - Exit—to exit from the program.
  - Search—to search for a field-specific value and highlight first occurrence in the table.
- Subitems
  - Test number—for the field test number
  - Product name—for the field product name
  - Specimen number—for the field specimen number

- Batch number—for the field batch number
- Type of test—for the field type of test
- Select—to select the records in the table. In this case the user is provided with only those records that meet the “select” conditions.
- Subitems
  - Test number—for the field test number
  - Product name—for the field product name
  - Specimen number—for the field specimen number
  - Batch number—for the field batch number
  - Type of test—for the field type of test
  - Test data—for the field test data
  - Type of load—for the field type of load
  - Material—for the field material
  - Manufacturer—for the field manufacturer
  - Undo last selection.
- Report—to save the data of the current table (after selection) to a file
- Subitems
  - New data—to save only current table
  - Old data—to view and choose data from last sessions of report
  - Old + new data—to add the current table records to old data
  - Old data + current record—to add one current record to old data

The next sections of the manual detail all the operations supported by the menu and other TESTS database control options.

#### 7.1.8 Data Representation Format.

The TESTS database offers two methods for representing the data: as tables and as screen forms. Each table line corresponds to one record. Of course, a finite-width screen cannot display all fields of a record. The tables are used to review, search for, and select data for saving to a file. Only nine fields are shown.

A forms shows all fields, but for only one record. The forms are used to thoroughly review, input, and edit data.

Upon starting the system, data are represented in the table. For changing over, click the “+” button which is in the blue panel at the window top.

### 7.1.9 Entering the Data—Data Editing Mode.

The table-represented data are in the *review only* mode, and the database contents cannot be changed. To add and/or change the data, one should switch to form representation and use the Database Navigator object, located in the blue panel at the window top. The Database Navigator is used to move through the data in a database and perform auxiliary operations with the data, such as inserting a blank record or posting a record.

When the user chooses one of the navigator buttons, the appropriate action is carried out in the database the navigator is linked to. For example, if the user clicks the Insert button, a blank record appears in the database.

The Navigator shows the following buttons:

- First—sets the current record to the first record in the database, disables the First and Prior buttons, and enables the Next and Last buttons if they are disabled.
- Prior—sets the current record to the previous record and enables the Last and Next buttons if they are disabled.
- Next—sets the current record to the next record and enables the First and Prior buttons if they are disabled.
- Last—sets the current record to the last record in the database, disables the Last and Next buttons, and enables the First and Prior buttons if they are disabled.
- Insert—inserts a new record before the current record, and sets the database into Insert and Edit modes.
- Delete—deletes the current record and makes the next record the current record.
- Edit—puts the database into Edit mode so that the current record can be modified.
- Post—writes changes in the current record to the database.
- Cancel—cancels edits to the current record, restores the record display to its condition prior to editing, and turns Insert and Edit modes if they are active.
- Refresh—refreshes the buffered data in the associated database.

When in the Forms mode, one can use the following buttons (located in the blue panel at the window top):

- Copy in buffer—for copying the current record into the buffer.
- Paste from buffer—for the text preliminarily copied into the buffer to be inserted in a new record. One must enter a unique Registration number for the new record. The latter becomes the current record.

Jump to a field in a record is effected by clicking a mouse button on the field required (and arbitrary jump is allowed) or by pressing the following keys:

- Tab—for jump to the next field; or
- Shift + Tab—for jump to the previous field.

The method for entering and changing the data in a field is similar to the MS Windows interface that has been a world's standard now.

#### 7.1.10 Saving Data to a File.

To prepare saving, one should select data from the table. Old data can be utilized by clicking the subitem Old data in the Main menu Report item. New windows and the table with data from last sessions of Report will be shown. You can view and edit table or enter another set of data from a file with extension .sts by clicking the Load from file button at the window top. Click the Cancel button for returning to the Main table.

For adding new data, click the Main menu Report item and choose New data, Old + new data, or Old data + current record. The window for saving is shown on the display. You can view and edit table or save data to a file with extension .sts by clicking the Save to file button at the window top. Program saves the following data:

Data saved in file for all types of tests.

1. Test No.
2. Product
3. Specimen No.
4. Batch No.
5. Type of test
6. Type of load
7. Mass
8. Thickness
9. Length
10. Width

Data saved for only one type of test.

- Static strength
  1. Rate of loading
  2. Young's modulus
  3. Ultimate load
  4. Load at proportional limit or load of 6% ellipticity of holes subjected to bearing stresses

- 5. Strain at ultimate load
- 6. Ultimate stress
- 7. Proportional limit stress
- 8. Poisson's ratio
- Creep strength
  - 1. Loading
  - 2. Time to failure
- Fatigue tests
  - 1. Load frequency
  - 2. Maximum cycle load
  - 3. Stress ratio of a cycle
  - 4. Cycles to failure

#### 7.1.11 List of Data in TESTS Database.

- a. Main data
  - 1. Product (craft)
  - 2. Batch number
  - 3. Type of test (static/creep/fatigue strength)
  - 4. Specimen number
  - 5. Registration number (No. of testing)
  - 6. Test date
  - 7. Note
- b. General sample data (Tab General)
  - 1. Loads (tension, compression, shear, contact load, multiaxial in-plane load, bending, torsion)
  - 2. Concentrator (without hole, central notch, side notch, square cutout, rectangular cutout, elliptic cutout, impact damage)
  - 3. Data for reference book
  - 4. Documentation
  - 5. Test image
  - 6. Date of input

c. Product description (Tab Product)

1. Product group (civil aircraft, military aircraft, helicopters, rockets, other crafts)
2. Manufacturer
3. Product No.
4. Delineation
5. Unit No.
6. Certificate No.

d. Sample description (Tab Sample)

1. Sample type (cut from structure, made simultaneously with the structure, laboratory test specimen)
2. Sample geometry (flat, tubular, complex)
3. Documentation
4. Number in batch
5. Length
6. Width or external diameter of the main part
7. Thickness of the main part
8. Sample image

e. Zone of unit—structural location where the specimen was cut out. (Tab Zone)

1. Structural zone where the specimen was cut out
2. Thickness of structure
3. Coordinate x of the area where the specimen was cut out
4. Coordinate y of the area where the specimen was cut out
5. Angle between specimen axis and structure x axis

f. Concentrator description (Tab Concentrator)

Dimensions written below are used with the shown concentrator only.

• Central notch

1. Coordinate x of concentrator center
2. Coordinate y of concentrator center
3. Slope angle of axis (angle between concentrator main axis and specimen x axis)
4. Half-length of the central notch

• Side notch

1. Length of the first notch
2. Coordinate x of the tip of the first notch
3. Coordinate y of the tip of the first notch

- 4. Slope angle of notch No. 1 (angle between first notch main axis and specimen x axis)
- 5. Length of the second notch
- 6. Coordinate x of tip of the second notch
- 7. Coordinate y of tip of the second notch
- 8. Slope angle of notch No. 2 (angle between second notch main axis and specimen x axis)
- Hole (notched or unnotched)
  - 1. Coordinate x of concentrator center
  - 2. Coordinate y of concentrator center
  - 3. Slope angle of axis (angle between concentrator main axis and specimen x axis)
  - 4. Hole radius
  - 5. Length of the first notch (if any)
  - 6. Length of the second notch (if any)
- Square cutout
  - 1. Coordinate x of concentrator center
  - 2. Coordinate y of concentrator center
  - 3. Slope angle axis (angle between concentrator main axis and specimen x axis)
  - 4. Side of square
  - 5. Radius of rounded corner
- Rectangular cutout
  - 1. Coordinate x of concentrator center
  - 2. Coordinate y of concentrator center
  - 3. Slope angle axis (angle between concentrator main axis and specimen x axis)
  - 4. Major side of rectangle
  - 5. Minor side of rectangle
  - 6. Radius of rounded corner
- Elliptic cutout
  - 1. Coordinate x of concentrator center
  - 2. Coordinate y of concentrator center
  - 3. Slope angle of axis (angle between concentrator main axis and specimen x axis)
  - 4. Major axis
  - 5. Minor axis

- Impact damage area
  - 1. Coordinate x of concentrator center
  - 2. Coordinate y of concentrator center
  - 3. Slope angle of axis (angle between concentrator main axis and specimen x axis)
  - 4. Projectile radius
  - 5. Impact energy
  - 6. Max transverse dimension of impact damage area
  - 7. Min transverse dimension of impact damage area
  - 8. Damage surface area
  - 9. Depth of part-through damage
  - 10. Verbal description of damage
  - 11. Damage surface area evaluation method
  - 12. Kind of instrumented inspection
  - 13. Method of instrumented inspection
  - 14. Code of device

g. Material of sample (Tab Material)

1.-5. The name of material number i used in sample (i from 1 to 5)

You can view the parameter of the material from MATERIALS database by clicking the button View material i.

h. Microstructure of composite (Tab Layup)

1. Microstructure formula (axial single-ply, transverse single-ply, cross-ply, angle-ply, quasi-isotropic)
2. Layup angle (from 1 to 9)
3. Number of layers (from 1 to 9)
4. Material of layers (from 1 to 9)
5. Fiber weight fraction, %
6. Matrix weight fraction, %
7. Porosity, %

i. Test conditions (Tab Conditions)

1. Test laboratory
2. Test equipment
3. Medium (air, water, fuel, kerosene, gasoline)
4. Temperature

5. Relative humidity
6. Information on preliminary tests

j. Test result (Tab Result)

Data are shown for all types of tests.

1. Failure size (size 1, size 2, size 3, size 4)
2. Failure image
3. Note

Data are shown only for one type of tests.

- Static strength
  1. Rate of loading
  2. Young's modulus
  3. Ultimate load
  4. Load at proportional limit or load of 6% ellipticity of holes subjected to bearing stresses
  5. Strain at ultimate load
  6. Ultimate stress
  7. Proportional limit stress
  8. Poisson's ratio
- Creep strength
  1. Loading
  2. Time to failure
- Fatigue tests
  1. Load frequency
  2. Maximum cycle load
  3. Stress ratio of a cycle
  4. Cycles to failure

## 7.2 MATERIALS DATABASE (USER'S MANUAL).

The automated information-retrieval system, MATERIALS database, is a part of the complex for designing the composite structures. It provides information on characteristics of composite

layers for analytical programs. In addition, the MATERIALS database can be employed in order for designers and analysts dealing with composite structures to be quickly given information on properties and characteristics of the materials.

#### 7.2.1 Requirements for Hardware and System Software Installation.

The MATERIALS database is designed to be operated on IBM PCs compatible with MS Windows 95 and later. A minimal configuration of hardware is sufficient; however, in order to implement all options prepared for the user, the computer should have a mouse. In addition, one should take into account that if the RAM is less than 32 MB, the total number of simultaneously open windows may turn out to be limited, and the overall speed of response may be slower. It is recommended a 64-MB RAM be used.

The MATERIALS database data files are to be installed in a separate directory of a hard disk with path Math\_path\BDKM\BAZAKM. (File bde.zip should be unzipped in the directory math\_path.) Math\_path is the directory name where executable module *ProDeCompoS.exe* is located.

- The Math\_path\BDKM\BAZAKM directory should incorporate
- Database files: Marki.dbf, Marki.dbt, Marki.mdx, and
- Temporary files: tmp.db, tmp.mb.

#### 7.2.2 Terms and Definitions Data Structures.

- Data field or field—an indivisible element of the database.
- Record—a set of attributes describing one copy of an information entity.
- Window—a display screen part containing information of one section or subsection; as a rule, a window can appear or be removed as a whole; in certain situations the window dimensions can be varied by a user.
- Bold label—the label you can really see on display when operating the program.

#### 7.2.3 Contents of Database.

From the user's point of view the database contains the following information on composite specimens:

- General description (brand, type, class and type of delivery, input date, etc.);
- physical properties (density, thickness, diffusion factors, porosity, etc.);
- mechanical properties (elastic modulus, Poisson's ratios, ultimate stresses; stress intensity factors, etc.); and
- thermal properties (expansion factor, heat conductivity, thermal diffusivity, diffusion factor, etc.).

#### 7.2.4 Functions of MATERIALS Database.

All functions that the MATERIALS database applies to data may be categorized in the following groups:

- data input/editing;
- data view.

ON-SCREEN REVIEW—All data in the database for inspection and survey can be sent to a display screen. Two types of output are envisaged: Brief review table and Detailed view screen forms. For switching between them, you can use buttons “+” and “-” which are located in the blue panel at the window top.

Each line of the table contains the most widely needed information about one record. The number of simultaneously provided lines (and, respectively, records) depends on the display screen field specified by the user. Tables are the most convenient facility for survey-type analyses.

As for screen Forms, windows of prescribed size are getting all fields, but only for one record at a time.

In this versions the databases have options for sorting, searching, and filtering the data.

INPUT/EDITING of data while working with the MATERIALS database is performed at the moment when information is represented in the Forms mode. Editing is initiated by selecting Edit in the NAVIGATOR menu (which is in the blue panel at the window top). Data of each data field are entered into the database once (but can continuously be edited).

The special data from the MATERIALS database for analytical programs are retrieved by special programs intended for data preparation.

#### 7.2.5 User's Proficiency Requirements.

The database is designed for specialists who have taken at least a minimal training in automatic data processing. The user is expected to be

- capable of handling the PC hardware and peripherals;
- familiar with MS Windows 95 or later, including the file management system; and
- familiar with Borland Delphi user interface principles since these are employed in the MATERIALS database (the Delphi interface is much similar to the MS Windows interface that has been a world's standard).

### 7.2.6 Starting the Program—Termination of Work.

To start the MATERIALS database the user should

- run the *ProDeCompoS.exe* executable module;
- click the item Databases in the menu bar (the latter is located at the window top), and pull-down menus are shown; and
- click the subitem MATERIALS in the pull-down menu.

To terminate the MATERIALS database operation, one should close program windows or click the subitem Exit in Main menu item File.

### 7.2.7 Main Menu.

Considered as the main option for navigation in the MATERIALS database is the Main MATERIALS menu. It appears promptly after starting the system and remains accessible throughout a session. The menu comprises of

- a menu bar at the windows top; and
- a pull-down menu with columns of items.

The user selects items and subitems (by mouse or keyboard) to initiate the corresponding operations of the system. To utilize menus while in the keyboard control mode, one should

- click the left mouse button when the system is waiting for commands and the mouse cursor is at a menu button;
- use the arrow keys to place the cursor on the item required; and
- press <Enter>.

The fastest option for working with menus is the mouse. To select an item, it suffices to click the mouse button when the cursor is on the item.

The MATERIALS database menu comprises the following items:

- File—the auxiliary service functions and quit
- Subitems
  - Material group—select a product group.
  - Brief review—click to show the table with the most widely used information about records; you can search and select records.

- Detailed view—click to show the forms with all information about one record; you can edit data, prepare new records, or delete unnecessary data.
- Exit—exit program.
- Search—to search for value of field and highlight first occurrence in the table.
- Subitems for searching
  - Brand—for field brand of material
  - Select—elects the records in the table. When selecting is applied to the table, only those records that meet select conditions are available to the user.
- Subitems
  - Brand—for field brand of material
  - Type—for field type of material
  - Class—for field class of material
  - Delivery type—for field delivery type
  - Specification—for field specification
  - Date—for field Input data.

Undo last selection.

The next sections of the manual detail the use of all operations supported by the menu and other MATERIALS database control options.

#### 7.2.8 Data Representation Format.

The MATERIALS database offers two options for representing the data: Table and screen Forms. Each line of the Table corresponds to one record. Of course, a finite-width screen cannot display all fields of a record. Tables are used to review and search for data and to select data for saving to a file, it shows only nine fields.

A Form shows all fields, but for only one record. The Forms are used for thorough review and data input/editing.

When starting the system, data are represented in the Table. For changing over, click button “+” which is located in the blue panel at the window top.

#### 7.2.9 Entering the Data—Data Editing Mode.

Data in the Table representation is in the *review only* mode; the database contents cannot be changed. To input and/or change the data, the user should switch to Forms representation and use the Database Navigator object, the latter being in the blue panel at the window top. The database Navigator is used to browse through the data in a database and perform operations on

the data, such as inserting a blank record or posting a record (as described in TESTS database section).

In the Forms mode, the user can use buttons located in the blue panel at the window top:

- Copy in Clipboard—for copying the current record into a buffer.
- Paste from Clipboard—for the text preliminarily copied into the buffer to be inserted in a new record. The user must input a unique Brand number for a new record, and the latter will be the current record.

Movement to a field in a record is effected by clicking the mouse button on the field required (here, arbitrary movement is allowed) or by pressing the following keys:

- Tab—for movement to the next field or
- Shift + Tab—for movement to the previous field.

The method for entering and changing the data in a field is similar to the MS Windows interface that has been a world's standard now.

#### 7.2.10 List of Data in MATERIALS Database.

- a. Main data
  1. Specifications
  2. Class of material
  3. Input date
  4. Name of material (unique)
  5. Type of material
  6. Note
- b. General data on material (Tab General)
  1. Process of manufacturing (pressing, vacuum forming, autoclave forming, vacuum autoclave forming, mechanical machining, adhesion, other)
  2. Application of material (low loading structures, middle loading structures, high loading structures, turbine blades, structural parts, other)
  3. In-service condition (water proof, moisture proof)
  4. Type of forming
- c. Physical properties of lamina (Tab Physical)
  1. Density
  2. Fiber fraction, %
  3. Moisture diffusion factor

4. Fuel diffusion factor
5. Layer thickness
6. Porosity, %

d. Mechanical properties of lamina (Tab Mechanical)

- Longitudinal properties
  1. Elastic modulus
  2. Poisson's ratio
  3. Strain at ultimate load
  4. Proportional limit stress
  5. Ultimate stress
  6. Tensile and compression critical stress intensity factor (SIF)
  7. Tensile and compression cracking zone
- Transverse properties
  1. Elastic modulus
  2. Poisson's ratio
  3. Ultimate stress
  4. Tensile and compression critical SIFs;
  5. Tensile and compression cracking zone
- Shear properties
  1. Elastic modulus
  2. Shear strength
  3. Shear critical SIF
  4. Shear cracking zone
- Other properties
  1. Temperature of tests

e. Thermal properties of lamina (Tab Thermal)

1. Temperature, minimum in-service
2. Temperature, maximum in-service
3. Thermal expansion factor
4. Specific heat conductivity
5. Thermal diffusivity
6. Specific thermal diffusivity

### 7.3 AIRCRAFT DATABASE (USER'S MANUAL).

The AIRCRAFT database is a part of the complex for modelling of reliability of composite structures. It is intended to support the modelling with data on structures (including inspection data) and their loading and damage exceedances.

The AIRCRAFT database accumulates, stores, and views the following set of information on composite airframes:

- data on aircraft, types and particular structures manufactured of composites (aircraft information, materials, structural design, load exceedances for different design loading case, possible damage types, and damage statistical properties);
- lists of defects and damages detected during inspections of the units made out of composites.

In addition to the planned operation within the modelling program complex, the AIRCRAFT database can be employed autonomously in organizations that develop, evaluate, and use composite structures.

#### 7.3.1 Requirements for Hardware and System Software Installation.

The AIRCRAFT database is designed to be operated on IBM PCs compatible with the MS Windows 95 and later. A minimal configuration of hardware is sufficient. However, in order to implement all options prepared for the user, the computer should have a mouse. In addition, one should take into account that if the RAM is less than 32 MB, the total number of simultaneously open windows may turn out to be limited, and the overall speed of response may be slower. It is recommended that a 64-MB RAM be used.

The AIRCRAFT database data files are to be installed in a separate directory of a hard disk with path Math\_path\BDLA\BAZALA. (File bde.zip should be unzipped in the directory Math\_path.) Here, Math\_path is the directory name where executable module *ProDeCompoS.exe* is placed.

The Math\_path\BDKM\BAZAKM directory should include

- Database files: La\_tip—Main database;
  - Zone—Zone database
  - Load—Load database
  - Damage—Damage database
  - (all files with extensions *dbf*, *dbt*, *mdx*) and
- Temporary files: *tmp.db*, *tmp.mb*.

The AIRCRAFT image files are to be installed in a separate directory on a hard disk with path Math\_path\BDLA\IMAGELA.

### 7.3.2 Terms and Definitions.

- Data field or field—an indivisible element of the database
- Record—a set of attributes describing one copy of an information entity
- Window—a display screen part containing information of one section/subsection; as a rule, a window can appear or be removed as a whole; in certain situations window dimensions can be varied by a user.
- Bold label—the label you can really see on display during work with program

### 7.3.3 Contents of Database.

From the user's point of view the AIRCRAFT database comprises the following sections corresponding to the information objects above:

- description of aircraft types
- list of aircraft copies
- description and properties of composite units
- list of defects revealed in the composite units
- load and damage exceedances for the composite units

### 7.3.4 Functions of the AIRCRAFT Database.

The present subsection briefly describes main operations on data that are carried out by the AIRCRAFT database. All operations that the AIRCRAFT database performs on data may be categorized into the following groups:

- input/editing
- review on display screen
- writing to Clipboard for the reliability modelling programs to use

ON-SCREEN REVIEW is the data available in the AIRCRAFT database can be displayed for checkout and analysis. The database offers three types of data review options: Main table—Brief review, screen Forms—Detailed view, and Editing tables.

In the Main table each line will contain the most frequently needed information from a particular record. The number of lines provided simultaneously (and, respectively, of records) depends on a user-specified screen window size. The Main table is most convenient for familiarization with data. While in the Forms mode, a fixed-size window receives all fields, but for only one record at a time. A screen can simultaneously show both windows with Main table and Forms. For switching from Brief review mode to Detailed view mode you can use buttons "+" and "-" which are located in the blue panel at the window top. Main table of the AIRCRAFT database is used for sorting, searching for, and filtering the data.

Editing tables are used for input/editing of data from other databases, which are related to the Main AIRCRAFT database by means of Registration number (unique) field.

INPUT/EDITING of data while working with the AIRCRAFT database is carried at the moment when information is represented in the Forms and in Editing tables. Editing is initiated by selecting Edit in the NAVIGATOR menu (which is located in the blue panel at the window top for the form and near a table for Editing tables). If by the time instant of selection of the data were displayed in Main table, the program will automatically change over to data representation in the Forms and the Editing tables.

OUTPUT TO CLIPBOARD is the major function of the AIRCRAFT database and provide the initial information for aircraft reliability modelling programs (more specifically, PreDaMC and MontCar programs). The information is transferred to Windows Clipboard.

#### 7.3.5 User's Proficiency Requirements.

The database is designed for specialists who have taken at least a minimal training automatic data processing. The user is expected to be

- capable of handling the PC hardware and peripherals;
- familiar with MS Windows 95 or later, including the file management system;
- familiar with Borland Delphi user interface principles since these are employed in the AIRCRAFT database (the Delphi interface is much similar to the MS Windows interface that has been a world's standard).

#### 7.3.6 Starting the Program—Termination of Work.

To start the AIRCRAFT database, one should

- run the *ProDeCompoS.exe* executable module;
- click the item Databases in the menu bar (the latter is located at the window top), and pull-down menu is shown;
- click the subitem AIRCRAFT in the pull-down menu.

To terminate the AIRCRAFT database, one should close program windows or click the subitem Exit in the Main menu item File.

#### 7.3.7 Main Menu.

Considered as the main option for navigation in the AIRCRAFT database is the Main menu. It appears immediately after starting the system and remains accessible throughout a session. The menu comprises of

- a menu bar at the screen top and
- a pull-down menu with columns of items.

The user selects items and subitems to initiate the corresponding operations of the system.

To utilize menus while in the keyboard control mode, one should

- click the left mouse button when the system is waiting for commands and mouse cursor is at the menu button;
- use the arrow keys to place the cursor on the item required; and
- press <Enter>.

The fastest option for working with menus is the mouse. To select an item, it suffices to click the mouse button when the cursor is on the item.

The AIRCRAFT database menu comprises the following items:

- File—the auxiliary service functions and quit
- Subitems
  - Product group—select product group
  - Brief review—to show the table with the most widely used information about records; you can search for and select records.
  - Detailed view—to show the forms with all information about one record; you can edit data, prepare new records or delete unnecessary data.
  - Exit—exit program
  - Search—to search for a value of a field and highlight first occurrence in the table
- Subitems for searching
  - Registration No.—for field test number
  - Product name—for field product name
  - Product No.—for field product No.
  - Unit name—for field unit name
  - Unit No.—for field unit No.

Select—to select the records in the table. When selecting is applied to the table, only those records that meet select conditions are available to the user.

- Subitems
  - Registration No.—for field test number
  - Product name—for field product name
  - Product No.—for field product No.
  - Unit name—for field unit name
  - Unit No.—for field unit No.

- Product group—for field product group
- Product type—for field product type
- Material—for field material
- Manufacturer—for field manufacturer
- Input date—for field input date
- Damage date—for field damage date
- Draft No.—for field draft No.

---

Undo last selection.

The next sections of the manual describe in detail the use of all operations, supported by the menu and other AIRCRAFT database control options.

#### 7.3.8 Data Representation Format.

The AIRCRAFT database offers three options for representing the data: Main table, screen Forms, and Editing tables. Each line of the Main table corresponds to one record. Clearly, a finite-width screen cannot display all fields of a record. Main tables are used to review and search for data and select data for saving to a file; it shows only nine fields.

The Forms show all fields of the AIRCRAFT database, but for only one record. The Forms are used for thorough review and data input and editing.

The Editing tables show fields from other databases, which are related to the Main AIRCRAFT database by means of Registration number (unique) field. The tables are used for thorough review and data input and editing.

When starting the system, data are represented in the Main table. For changing over, click the “+” button which is in the blue panel at the window top.

#### 7.3.9 Entering the Data—Data Editing Mode.

Data in the Main table representation are in the review only mode. In this case the database contents cannot be changed. To input and/or change the data, the user should switch to Forms representation and use the Database Navigator object, the latter being located in the blue panel at the window top. The database navigator is used to go through the data in a database and perform operations on the data, such as inserting a blank record or posting a record (as described in the TESTS database section).

Movement to a field in a record is carried out by clicking the mouse button on the field required (arbitrary movement is allowed) or by pressing the following keys:

- Tab for movement to the next field
- Shift + Tab for movement to the previous field

The method for entering and changing the data in a field is similar to the MS Windows interface that has been a world's standard now.

There are three Editing tables in Form representation:

1. Table "Zone" for zone description (Tab Zone)
2. Table "Load" for design loading case description (Tab Loads)
3. Table "Damage" for damage description (Tab Damage)

There are distinct Navigator objects for every Editing tables.

#### 7.3.10 List of Data in AIRCRAFT Database.

a. Main data

1. Registration No., unique in database
2. Product name (aircraft name)
3. Unit name
4. Unit No.
5. Manufacturer
6. Damage date
7. Note

b. General data on Product/Unit (Tab General)

1. Product No.
2. Product group (civil aircraft, military aircraft, helicopters, rockets, other aircraft)
3. Product class (passenger, commercial, business, transport, ambulance, long-range, dusting, search, communication, agricultural, tourist, glider, high-speed, short takeoff, sporting, acrobatic, high-altitude, reconnaissance, folding-wing, stratospheric, remotely controlled, drone, fighter, interceptor, bomber, ground-attack, trainer, torpedo-carrier)
4. Basic material
5. Certificate No.
6. Data source
7. Service life (in hours)
8. Flights as per life
9. Input/update date

c. General data on zones (Tab Zone) is data on a "uniform" part of a structure for which reliability is to be analyzed. For input/editing of data, the other table (named Zone) is used. This table is related to the Main AIRCRAFT database table by means of the Registration number (unique) field. Table Zone has a Navigator object for input and

editing of data (see the description in TESTS database section). Below is the list of items in the table Zone:

1. Zone name
2. Zone length
3. Zone width
4. Surface area
5. Location
6. Accessibility
7. Structer type
8. Composite formula
9. Concentrator type
10. Core formula
11. Core thickness

d. Load exceedance (Tab Loads) is data on a loading condition of the unit/zone of a structure for which reliability is to be analysed by means of PreDaMC and MontCar programs. For input/editing data, the other table (named Load) is used. This table is related to the Main AIRCRAFT database table by means of the Registration number (unique) field. Table Loads has a Navigator object for input/editing of data (as described in TESTS database section). Here is the list of items in the page Zone:

1. Loading time
2. Principal loading factor
3. Principal load (items in the Load table)
4. Exceedances (items in the Load table)

e. Damage exceedance (Tab damage), data on damage exceedance in the unit/zone for which reliability is to be analysed by means of PreDaMC and MontCar programs. For input/editing of data, the other table (named Damage) is used. This table is related to the Main AIRCRAFT database table by means of the Registration number (unique) field. The Table Damage has a Navigator object for input/editing of data (refer to the description in the TESTS database section). Here is the list of items in the page Damage:

1. Service period
2. Damage area
3. Damage name
4. Damage sizes (items in the Damage table)
5. Exceedances (items in the Damage table)

f. Unit draft (Tab Draft)

1. Main size of unit 1
2. Main size of unit 2
3. Main size of unit 3

4. Main size of unit 4
5. Draft image (All image files are to be installed in a separate directory on a hard disk with path Math\_path\BDLA\IMAGELA).

#### 7.3.11 Saving Data to Clipboard.

The major function of the AIRCRAFT database is to provide initial information for aircraft reliability modelling programs (i.e., PreDaMC and MontCar programs). The information is transferred to Windows Clipboard. In this version of the program, the load and damage exceedances can be saved to the Clipboard. For saving, click the Save to Clipboard buttons located in Load exceedances and Damage exceedances pages of the Form; all data in the Editing table will be saved to the Clipboard.

## 8. SYNTHESIS OF DATA IN THE FORM REQUIRED BY ProDeCompoS.

In this section, four useful examples of data synthesis and utilization using ProDeCompoS are described. In these four problems, failure probability is calculated for MIG-29 (fin), TU-204 (aileron), Lear Fan-2100 (wing), and SU-29 (wing) airframes.

### 8.1 MIG-29 COMPOSITE FIN FAILURE PROBABILITY ESTIMATION.

The composite portion of the fin is a sandwich with a metallic honeycomb core and carbon fiber reinforced plastic (CFRP) skins. The CFRP is KMU-4e: ELUR-0.1p and ENFB epoxy resin. The volume fractions of plies with orientation angles  $0^\circ$ ,  $90^\circ$ , and  $\pm 45^\circ$  are 50%, 10%, and 40% respectively for the fin root zone (where maximum stresses occur).

#### 8.1.1 Mechanical Properties of Materials.

Lamina properties are presented in table 8-1.

TABLE 8-1. LAMINA PROPERTIES OF C/EPOXY

|  |         |
|--|---------|
| Elastic modulus along fibers under tension, MPa      | 135,000 |
| Elastic modulus along fibers under compression, MPa  | 125,000 |
| Elastic modulus across fibers under tension, MPa     | 9,200   |
| Elastic modulus across fibers under compression, MPa | 8,500   |
| Shear modulus, MPa                                   | 5,200   |
| Poisson's ratio                                      | 0.3     |
| Ultimate Tensile stress along fibers, MPa            | 800     |
| Ultimate Compressive stress along fibers, MPa        | -1,250  |
| Ultimate Tensile stress across fibers, MPa           | 34      |
| Ultimate Compressive stress across fibers, MPa       | -210    |
| Ultimate Shear stress, MPa                           | 65      |
| Lamina thickness, mm                                 | 0.11    |

#### 8.1.2 Mechanical Properties of Skin.

Theoretical mechanical properties of skin are presented in table 8-2.

TABLE 8-2. C/EXPOXY SKIN LAMINATE PROPERTIES

|   |        |
|---|--------|
| Elastic modulus along fin under tension, MPa      | 74,900 |
| Elastic modulus along fin under compression, MPa  | 74,300 |
| Elastic modulus across fin under tension, MPa     | 32,900 |
| Elastic modulus across fin under compression, MPa | 30,600 |
| Shear modulus, MPa                                | 16,500 |
| Poisson's ratio                                   | 0.414  |
| Ultimate Tensile stress along fin, MPa            | 470    |
| Ultimate Compressive stress along fin, MPa        | -664   |
| Ultimate Tensile stress across fin, MPa           | 170    |
| Ultimate Compressive stress across fin, MPa       | -305   |
| Ultimate Shear stress, MPa                        | 163    |
| Cracking zone correction under tension, mm        | 1.8    |
| Cracking zone correction under compression, mm    | 2.2    |

### 8.1.3 Fin Loads.

The fin service life is 3000 flights, with the average flight duration being 1 hour. There are two design load cases: subsonic and supersonic (95% of the entire service life is at subsonic loads and 5% at supersonic loads). The fin is mainly loaded with forces directed to the aeroplane symmetry axis (loads of opposite sign are infrequent and low-level, cannot damage the structure, and are, therefore, not taken into account). Stresses in the external and internal surfaces do differ in their algebraic sign only; so it can be presumed that the external surface is loaded with tension, and the internal one, with compression. With this, the fin failure probability was evaluated on the basis of estimates for the surfaces considered separately. Also, the probability of loads exceeding the maximum tension value (see table 8-3) is assumed to be zero. Statistical data on measured occurrence rates during service life of the MIG-29 fin root zone are demonstrated in tables 8-3 and 8-4 and figures 8-1 and 8-2.

TABLE 8-3. LOAD EXCEEDANCE PER LIFE FOR SUBSONIC DESIGN LOADING CASE

| Loads<br>(stress in MPa) | Exceedance per<br>1 Flight Hour | Exceedance per<br>Life |
|--------------------------|---------------------------------|------------------------|
| 0                        | 54                              | 153,900                |
| 37                       | 54                              | 153,900                |
| 55                       | 12.4                            | 35,340                 |
| 70                       | 5.5                             | 15,675                 |
| 85                       | 1.7                             | 4,845                  |
| 102                      | 0.42                            | 1,197                  |
| 120                      | 0.057                           | 162                    |
| 137                      | 0.02                            | 57                     |
| 154                      | 0.004                           | 11.4                   |

TABLE 8-4. LOAD EXCEEDANCE PER LIFE FOR SUPERSONIC DESIGN LOADING CASE

| Loads<br>(stress in MPa) | Exceedance per<br>1 Flight Hour | Exceedance per<br>Life |
|--------------------------|---------------------------------|------------------------|
| 0                        | 3                               | 450                    |
| 20                       | 3                               | 450                    |
| 35                       | 2.9                             | 435                    |
| 50                       | 2.6                             | 390                    |
| 65                       | 0.2                             | 30                     |
| 70                       | 0.1                             | 15                     |
| 85                       | 0.05                            | 7.5                    |

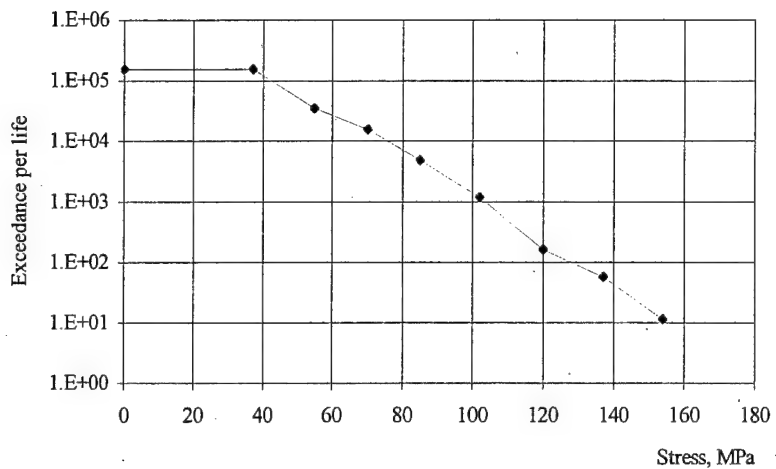


FIGURE 8-1. LOAD EXCEEDANCE FOR SUBSONIC LOADING CASE

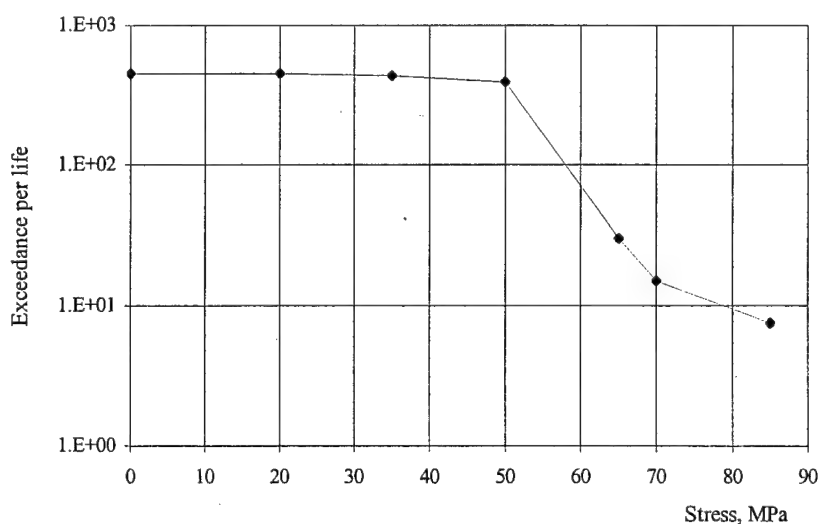


FIGURE 8-2. LOAD EXCEEDANCE FOR SUPERSONIC LOADING CASE

#### 8.1.4 Temperature Cumulative Probability Function.

The temperature cumulative probability function was estimated using *M-H* (Mach-altitude) records of aircraft under considerations. The skin temperature was calculated as:

$$T = T_0(H)(1 + 0.18M^2),$$

where  $T_0$  is a standard temperature at altitude  $H$ .

The obtained function is rather close to the temperature probability function given in reference 4 for maximum Mach number = 2.35.

According to reference 4, this function consists of two branches: the first is common for all planes, which characterizes the frequency of low temperatures, and the second depends on the maximum Mach number  $M_{max}$  of a given plane. This function can be approximated by the formula:

$$F(T) = 0.5 + \Phi_0 \left[ \frac{T - T_0}{\sigma_T} \right]$$

where:

$$T_0 = 310\text{K}; \sigma_T = 25\text{K} \text{ at } T < T_p$$

$$T_0 = 0\text{K}; \sigma_T = 61 + 11 M_{max} \text{ at } T > T_p.$$

Here:

$$T_p = \frac{310 \cdot (61 + 11 \cdot M_{max}^2)}{36 + 11 \cdot M_{max}^2}$$

$\Phi_0$  is tabulated Gauss-Laplace function;  $T$  is a boundary-layer temperature in Kelvin.

The temperature occurrence rate for the fin structure may be seen in figure 8-3 and tables 8-5 and 8-6.

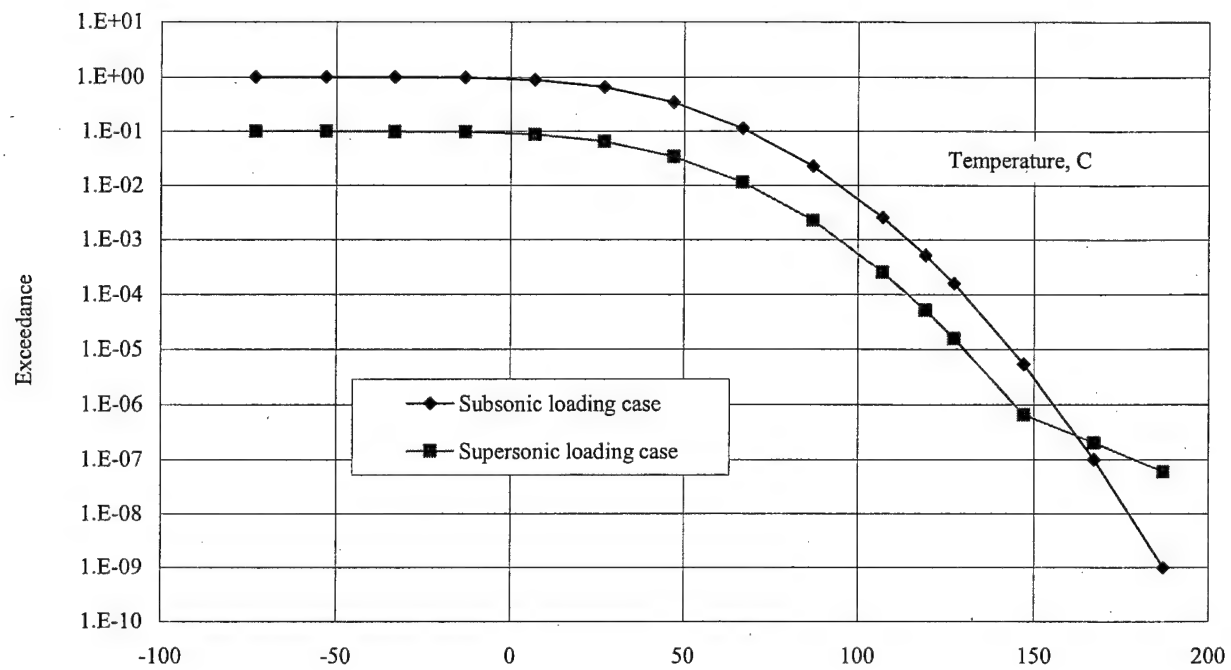


FIGURE 8-3. TEMPERATURE EXCEEDANCE

TABLE 8-5. TEMPERATURE EXCEEDANCE FOR SUBSONIC DESIGN LOADING CASE

| Temperature (C°) | Exceedance |
|------------------|------------|
| -73              | 1          |
| -53              | 0.9998     |
| -33              | 0.9974     |
| -13              | 0.9772     |
| 7                | 0.8849     |
| 27               | 0.6554     |
| 47               | 0.3446     |
| 67               | 0.1151     |
| 87               | 0.02275    |
| 107              | 0.002555   |
| 119              | 5.191E-04  |
| 127              | 1.591E-04  |
| 147              | 5.417E-06  |
| 167              | 9.983E-08  |
| 187              | 9.901E-10  |
| 207              | 5.262E-12  |

TABLE 8-6. TEMPERATURE EXCEEDANCE FOR SUPERSONIC DESIGN LOADING CASE

| Temperature (C°) | Exceedance |
|------------------|------------|
| -73              | 0.1        |
| -53              | 0.09998    |
| -33              | 0.09974    |
| -13              | 0.09772    |
| 7                | 0.08849    |
| 27               | 0.06554    |
| 47               | 0.03446    |
| 67               | 0.01151    |
| 87               | 2.275E-03  |
| 107              | 2.555E-04  |
| 119              | 5.191E-05  |
| 127              | 1.591E-05  |
| 147              | 6.635E-07  |
| 167              | 2.033E-07  |
| 187              | 5.915E-08  |
| 207              | 1.635E-08  |

8.1.5 Defect and Damage Exceedance.

8.1.6 Damage.

In-service fin inspection data were processed to obtain damage exceedance (per flight hour per square meter) for two types of defects:

- delamination or indentation (table 8-7) and
- hole+crack (table 8-8).

The latter tables and figures 8-4 and 8-5 represent in-service damage occurrence rates for the structural part in question, the fin root zone, where the maximum stresses are applied to a portion with 0.31-sq. m surface area.

TABLE 8-7. EXCEEDANCE FOR IN-SERVICE INDENTATION DAMAGE

| Diameter (mm) | Exceedance $\cdot 10^5$ per Hour (Flight) per $m^2$ | Exceedance per Life per 0.31 $m^2$ |
|---------------|---|------------------------------------|
| 0             | 10  | 0.093                              |
| 25            | 10  | 0.093                              |
| 30            | 7.8   | 0.07254                            |
| 35            | 6   | 0.0558                             |
| 40            | 4.6   | 0.04278                            |
| 60            | 2.6   | 0.02418                            |
| 100           | 0.65  | 0.00605                            |

TABLE 8-8. EXCEEDANCE FOR IN-SERVICE HOLE + CRACK DAMAGE

| Diameter (mm) | Exceedance $\cdot 10^5$ per Hour (Flight) per $m^2$ | Exceedance per Life per $0.31 m^2$ |
|---------------|---|------------------------------------|
| 0             | 5   | 0.0465                             |
| 10            | 5   | 0.0465                             |
| 25            | 2   | 0.0186                             |
| 30            | 1.3   | 0.01209                            |
| 35            | 1   | 0.0093                             |
| 40            | 0.8   | 0.00744                            |
| 60            | 0.4   | 0.00372                            |
| 100           | 0.1   | 0.00093                            |

8.1.7 Defects.

Expert opinion and reference 4 data have been the basis for adopting the probability of the manufacturing defects in the fin structure under study. Values are provided in tables 8-9 and 8-10 and in figure 8-4.

TABLE 8-9. EXCEEDANCE FOR MANUFACTURING DEFECTS INDENTATION DAMAGE

| Diameter (mm) | Exceedance per 1000 Hour per $m^2$ | Exceedance per Life per $0.31 m^2$ |
|---------------|------------------------------------|------------------------------------|
| 0             | 0.027527                           | 0.0256                             |
| 37.5          | 0.014946                           | 0.0139                             |
| 75            | 0.005667                           | 0.00527                            |

TABLE 8-10. EXCEEDANCE FOR MANUFACTURING DEFECTS HOLE + CRACK DAMAGE

| Diameter (mm) | Exceedance per 1000 Hour per $m^2$ | Exceedance per Life per $0.31 m^2$ |
|---------------|------------------------------------|------------------------------------|
| 0             | 0.004581                           | 0.00426                            |
| 37.5          | 0.002495                           | 0.00232                            |
| 75            | 0.000944                           | 0.000878                           |

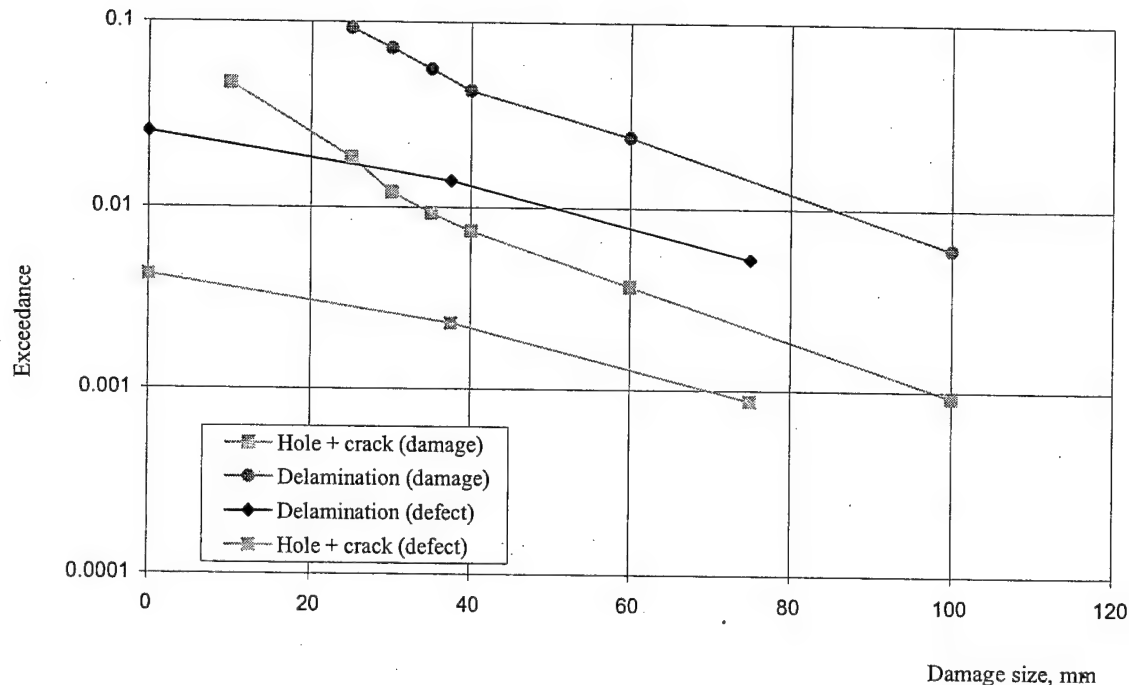


FIGURE 8-4. DEFECT AND DAMAGE EXCEEDANCE

#### 8.1.8 Strength Degradation Function for Damaged Skin.

The computer programs have been used to evaluate the strength degradation function for the fin skin. Two types of impact damage have been considered:

- indentation with crack on the backside (the “Indentation” damage type for modelling),
- through-the-thickness gap (the “Hole + Crack” damage type for modelling).

Relative sizes of damages (referred to as the diameter  $D$ ) are as follows:

- $H/D = 0.01$  for indentation depth,
- $2L/D = 0.4$  for crack length in indentation,
- $h/D = 0.02$  for depth crack in indentation,
- $D_0/D = 0.8$  for hole diameter of notch, where  $D$  is the diameter of the notch together with the cracking zone around a hole.

The calculation results may be seen in figures 8-5 and 8-6 and tables 8-11 and 8-12 for normal temperature and subsonic design loading case.

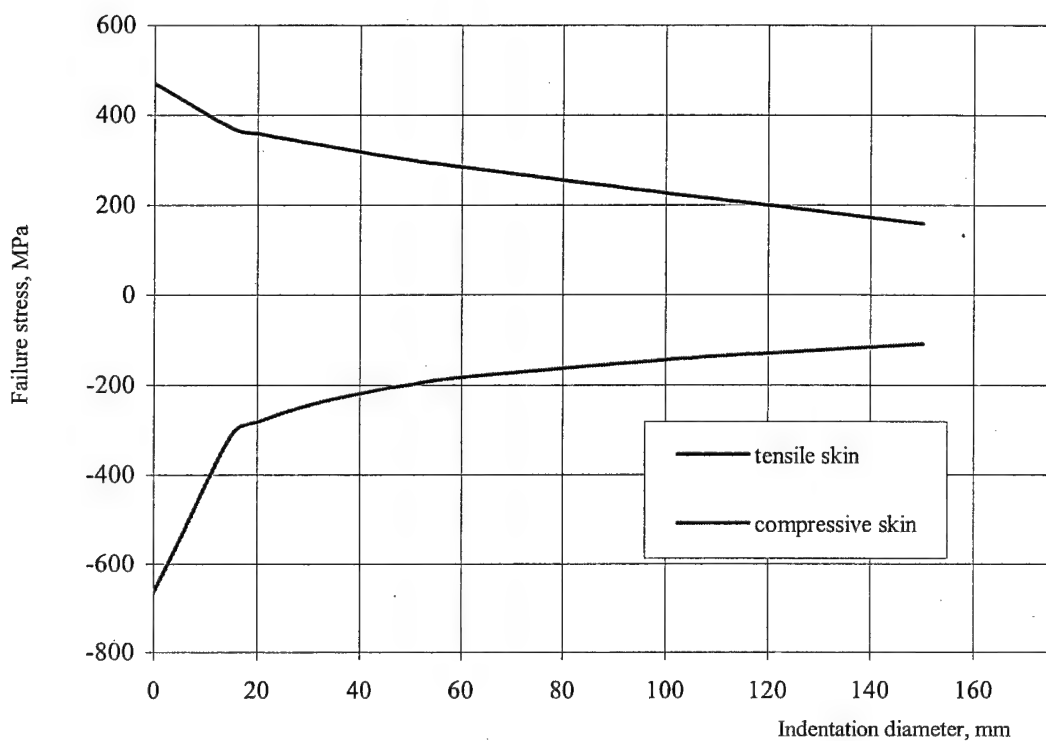


FIGURE 8-5. EFFECT OF INDENTATION DIAMETER ON RESIDUAL STRENGTH

TABLE 8-11. EFFECT OF INDENTATION SIZE ON SKIN RESIDUAL STRENGTH

| Indentation Size (mm) | Tension-Loaded Skin (MPa) | Compression-Loaded Skin (MPa) |
|-----------------------|---------------------------|-------------------------------|
| 0                     | 470                       | -664                          |
| 15                    | 371                       | -311                          |
| 20                    | 359                       | -282                          |
| 30                    | 338                       | -244                          |
| 40                    | 319                       | -218                          |
| 50                    | 301                       | -199                          |
| 60                    | 285                       | -183                          |
| 100                   | 227                       | -144                          |
| 125                   | 193                       | -125                          |
| 150                   | 159                       | -108                          |

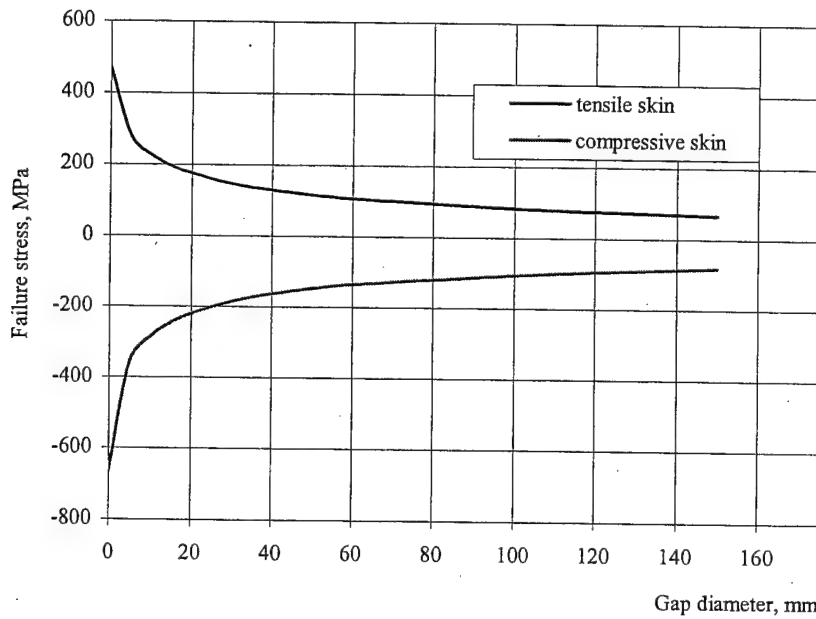


FIGURE 8-6. EFFECT OF THROUGH-THICKNESS GAP ON SKIN RESIDUAL STRENGTH

TABLE 8-12. EFFECT OF GAP SIZE ON SKIN RESIDUAL STRENGTH

| Hole + Crack Diameter (mm) | Tension-Loaded Skin (MPa) | Compression-Loaded Skin (MPa) |
|----------------------------|---------------------------|-------------------------------|
| 0                          | 470                       | -664                          |
| 5                          | 282                       | -355                          |
| 10                         | 228                       | -287                          |
| 15                         | 196                       | -246                          |
| 20                         | 175                       | -220                          |
| 30                         | 147                       | -185                          |
| 40                         | 129                       | -162                          |
| 50                         | 117                       | -146                          |
| 60                         | 107                       | -134                          |
| 100                        | 83                        | -105                          |
| 125                        | 75                        | -92                           |
| 150                        | 67                        | -82                           |

#### 8.1.9 Probability of Damage Detection

It was assumed that two basic methods of inspection are used for each type of damage:

- preflight visual inspection and
- special inspection method applied during maintenance.

The second method's use period was 100 hours of aircraft operation.

Probabilities of damage detection for notch and indentation are shown in figures 8-7 and 8-8 and tables 8-13 and 8-14.

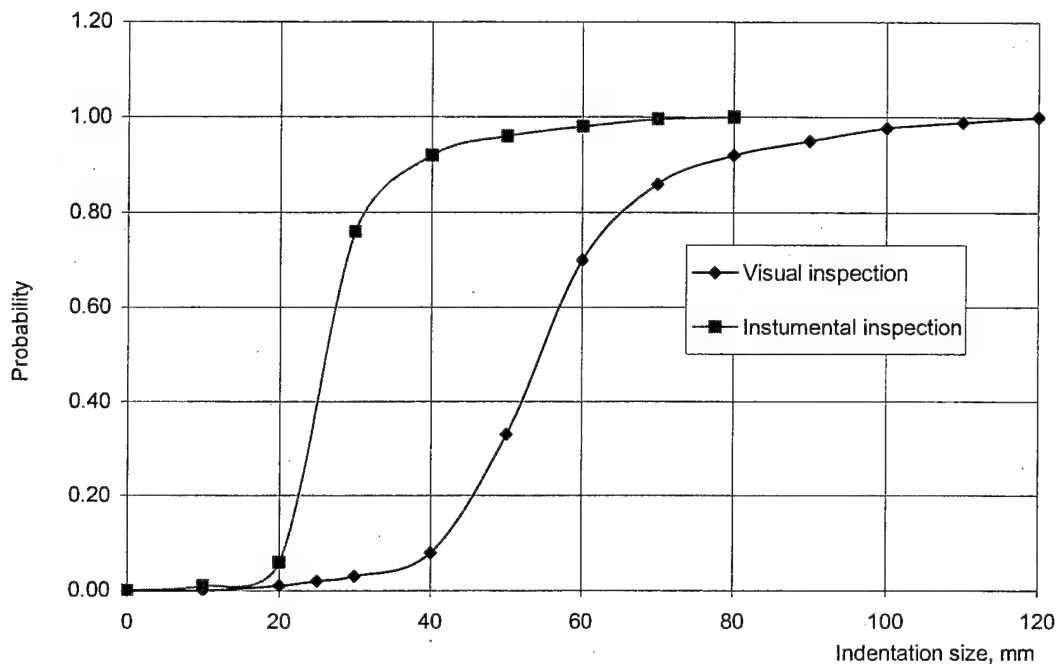


FIGURE 8-7. PROBABILITY OF INDENTATION DETECTION VS DAMAGE SIZE AND INSPECTION TYPE

TABLE 8-13. PROBABILITY P OF DAMAGE DETECTION FOR INDENTATION

| Indentation Diameter (mm) | P, Visual Inspection | Indentation Diameter (mm) | P, Instrumental Inspection |
|---------------------------|----------------------|---------------------------|----------------------------|
| 0.00                      | 0.00                 | 0.00                      | 0.00                       |
| 10.00                     | 0.00                 | 10.00                     | 0.01                       |
| 20.00                     | 0.01                 | 20.00                     | 0.06                       |
| 25.00                     | 0.02                 | 30.00                     | 0.76                       |
| 30.00                     | 0.03                 | 40.00                     | 0.92                       |
| 40.00                     | 0.08                 | 50.00                     | 0.96                       |
| 50.00                     | 0.33                 | 60.00                     | 0.98                       |
| 60.00                     | 0.70                 | 70.00                     | 1.00                       |
| 70.00                     | 0.86                 | 80.00                     | 1.00                       |
| 80.00                     | 0.91                 |                           |                            |
| 90.00                     | 0.95                 |                           |                            |
| 100.00                    | 0.98                 |                           |                            |
| 110.00                    | 0.99                 |                           |                            |
| 120.00                    | 1.00                 |                           |                            |

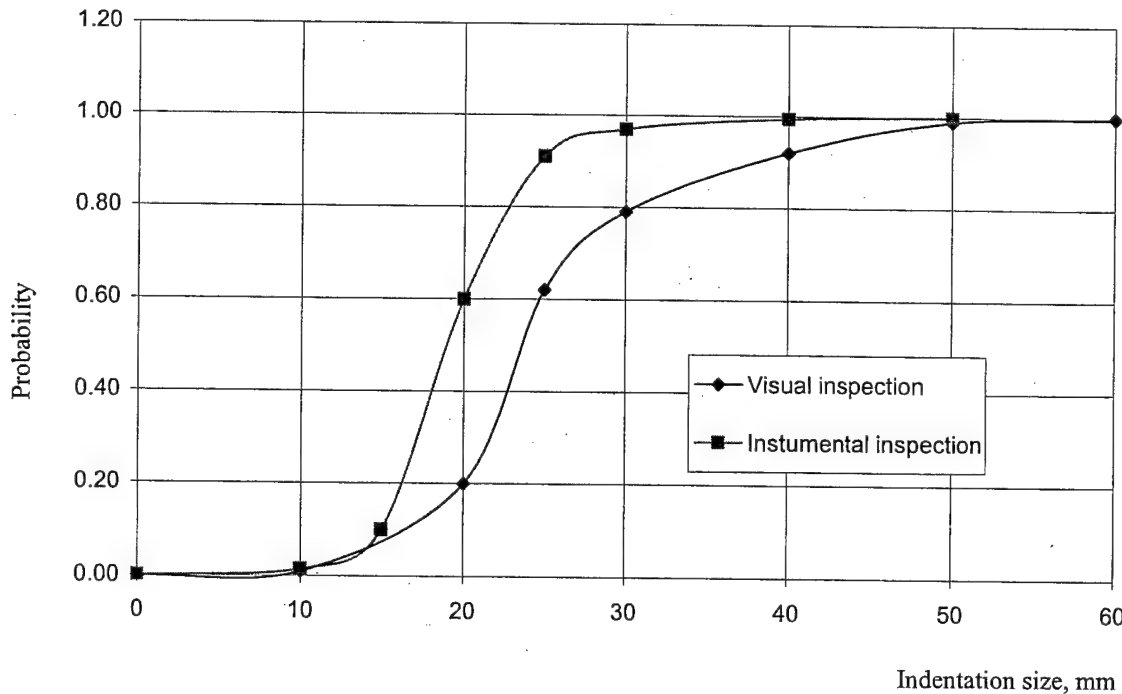


FIGURE 8-8. PROBABILITY OF GAP DETECTION VS DAMAGE SIZE AND INSPECTION TYPE

TABLE 8-14. PROBABILITY OF DAMAGE INSPECTION FOR GAP

| Hole + Crack Diameter (mm) | P, Visual Inspection | Hole + Crack Diameter (mm) | P, Instrumental Inspection |
|----------------------------|----------------------|----------------------------|----------------------------|
| 0.00                       | 0.00                 | 0.00                       | 0.00                       |
| 10.00                      | 0.01                 | 10.00                      | 0.02                       |
| 20.00                      | 0.20                 | 15.00                      | 0.10                       |
| 25.00                      | 0.62                 | 20.00                      | 0.60                       |
| 30.00                      | 0.79                 | 25.00                      | 0.91                       |
| 40.00                      | 0.92                 | 30.00                      | 0.97                       |
| 50.00                      | 0.99                 | 40.00                      | 1.00                       |
| 60.00                      | 1.00                 | 50.00                      | 1.00                       |

### 8.1.10 Repairs.

Two basic methods of repair are assumed to be used for each damage type:

- simplified repair applied in airfield conditions and
- special repair at airline maintenance facilities.

The second method is applied if some damage is detected during maintenance (carried out at the interval of 100 hours of aircraft operation).

The strength restoration factors and variation coefficients for indentation and hole + crack are shown in table 8-15. These values were estimated by using typical data obtained at TsAGI as a result of testing the composite structures after repairs.

TABLE 8-15. RESTORATION FACTORS FOR REPAIRS

|              | Field Facility | Maintenance Facility | Variation Coefficient |
|--------------|----------------|----------------------|-----------------------|
| Indentation  | 0.95           | 1                    | .1                    |
| Hole + Crack | 0.95           | 1                    | 0.12                  |

#### 8.1.11 Static Strength vs Temperature.

The temperature effect on compressive strength of specimens with and without crack is shown in figure 8-9 and table 8-16. The temperature effect on tensile strength is taken to be the same as for compression, this is a conservative estimate.

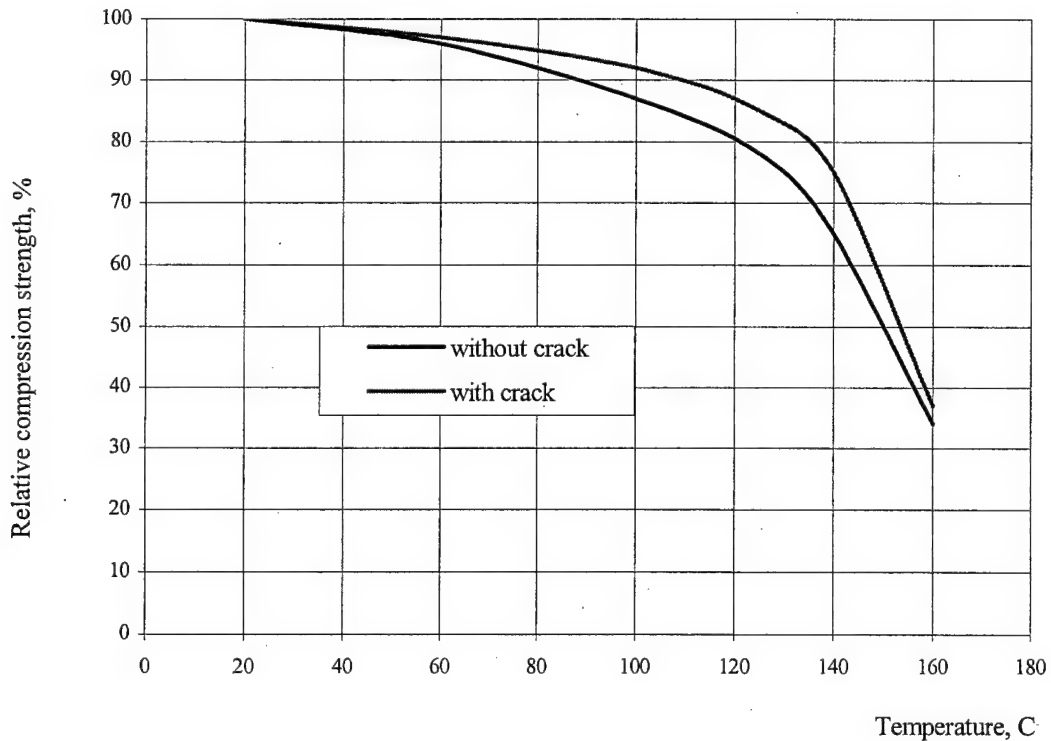


FIGURE 8-9. EFFECT OF TEST TEMPERATURE ON RELATIVE COMPRESSION STRENGTH OF SPECIMENS

TABLE 8-16. STATIC STRENGTH VERSUS TEMPERATURE WITH AND WITHOUT CRACKS

| Temperature (°C) | Without Crack | With Crack |
|------------------|---------------|------------|
| 20               | 1.00          | 1.00       |
| 60               | 0.96          | 0.97       |
| 100              | 0.87          | 0.92       |
| 125              | 0.78          | 0.85       |
| 140              | 0.65          | 0.75       |
| 160              | 0.34          | 0.37       |

8.1.12 Result of Calculating the MIG-29 Fin Failure Probability.

The failure probability was computed for the external and internal surfaces loaded in tension and compression, respectively; note that the internal surface is the one nearer to the airplane symmetry axis. The allowable error was assumed to be 0.0223 and the probability distribution law was Gaussian. Table 8-17 shows the results of calculating the fin failure probability.

TABLE 8-17. MIG-29 FIN FAILURE PROBABILITY PER LIFE

|                         |         |
|-------------------------|---------|
| Compression-loaded skin | 0.0122  |
| Tension-loaded skin     | 0.00763 |

Thus, the fin failure probability is governed with load-carrying capability of the internal (compression-loaded) surface and equals 0.0198.

8.2 TU-204 COMPOSITE AILERON FAILURE PROBABILITY ESTIMATION.

8.2.1 Aileron Structure Described.

The aileron is depicted schematically in figure 8-10. It is attached to the wing by three hinges. Its upper and lower surfaces are symmetric, with each surface area being 2.42 sq. m.

The composite portion of the aileron (see figure 8-10) is a sandwich with a honeycomb core and load-bearing skins made of a hybrid material consisting of carbon and aramide fibers. The graphite-based material is KMU-4e: FLUR-11-0,1 carbon fiber tape and UP-2227 epoxy resin. The aramide-based material is ORGANIT-10T: SVM synthetic fabric and UP-2227 epoxy resin. The honeycomb is of PSP paper and has 2.5 mm diameter cells.

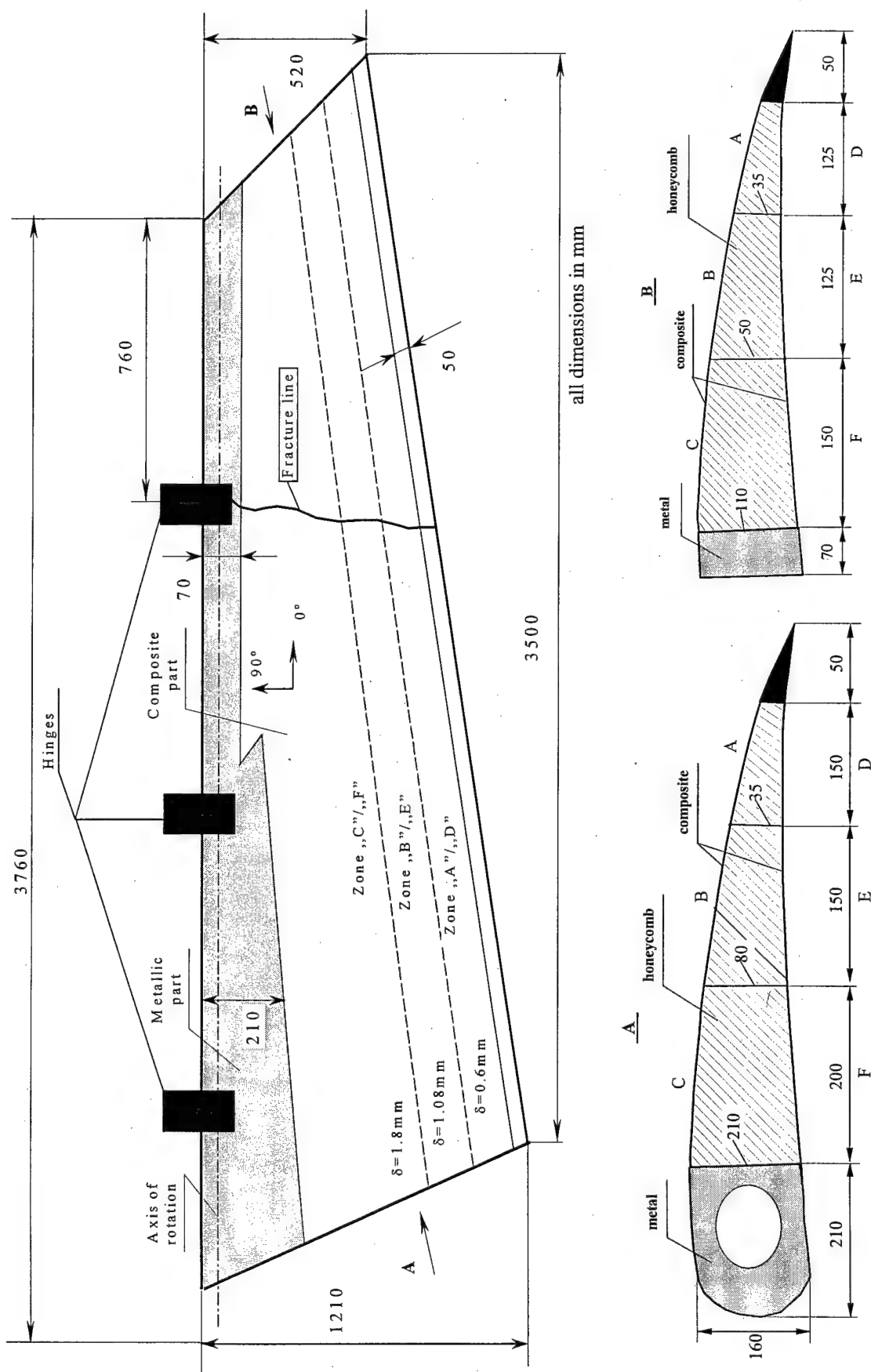


FIGURE 8-10. SCHEMATIC DEPICTION OF TU-204 AILERON

Stacking sequences in the skin are different over three zones (refer to figure 8-10):

- Zone A:  $[0^{\text{ar}}/45^{\text{ar}}/45^{\text{ar}}/0^{\text{ar}}]$ , that is, the aramide/epoxy only; the rated skin thickness is 0.6 mm.
- Zone B:  $[0^{\text{ar}}/45^{\text{ar}}/\mp 45^{\text{ar}}/\pm 45^{\text{ar}}/45^{\text{ar}}/0^{\text{ar}}]$ ; the nominal skin thickness is 1.08 mm.
- Zone C:  $[0^{\text{ar}}/45^{\text{ar}}/\mp 45^{\text{gr}}/90^{\text{gr}}/0^{\text{gr}}/\mp 45^{\text{gr}}/0^{\text{gr}}/90^{\text{gr}}/\pm 45^{\text{gr}}/45^{\text{ar}}/0^{\text{ar}}]$  the nominal skin thickness is 1.8 mm.

Here, symbols “ar” and “gr” stand for aramide and graphite, respectively; the 0-degree direction is depicted in figure 8-10.

### 8.2.2 Aileron Loads.

Maximum aileron deflection angles (as measured from the neutral position) are  $\varphi_{dn} = 25^\circ$  for the downward direction and  $\varphi_{up} = 20^\circ$  for the upward direction. When the aileron is deflected by  $\varphi_{dn} = 25^\circ$  down, it is subjected to the limit force  $P_{lim} = 5228$  kg (due to pressure  $p_{lim} = 2160$  kg/sq. m). The aileron deflected by  $20^\circ$  up is subjected to the limit force  $P_{lim}^{up} = 1876$  kg (due to pressure  $p_{lim}^{up} = 775$  kg/sq. m). When in the neutral setting ( $\varphi = 0^\circ$ ), the force applied is  $P_0 = 1621$  kg (under pressure  $p_0 = 670$  kg/sq. m).

These data allow one to plot the dependence of the force on the aileron deflection angle (see figure 8-11). Also, the latter presents points corresponding to ultimate forces  $P_{ult}^0$  and  $P_{ult}$ . ultimate and limit values are interrelated as,

$$P_{ult}^0 = f \cdot P_{lim} ; P_{ult} = f \cdot f_1 \cdot P_{lim}$$

where  $f = 1.5$  is the factor of safety and  $f_1 = 1.25$  is the additional factor of safety.

Aileron loads are summarized in table 8-18.

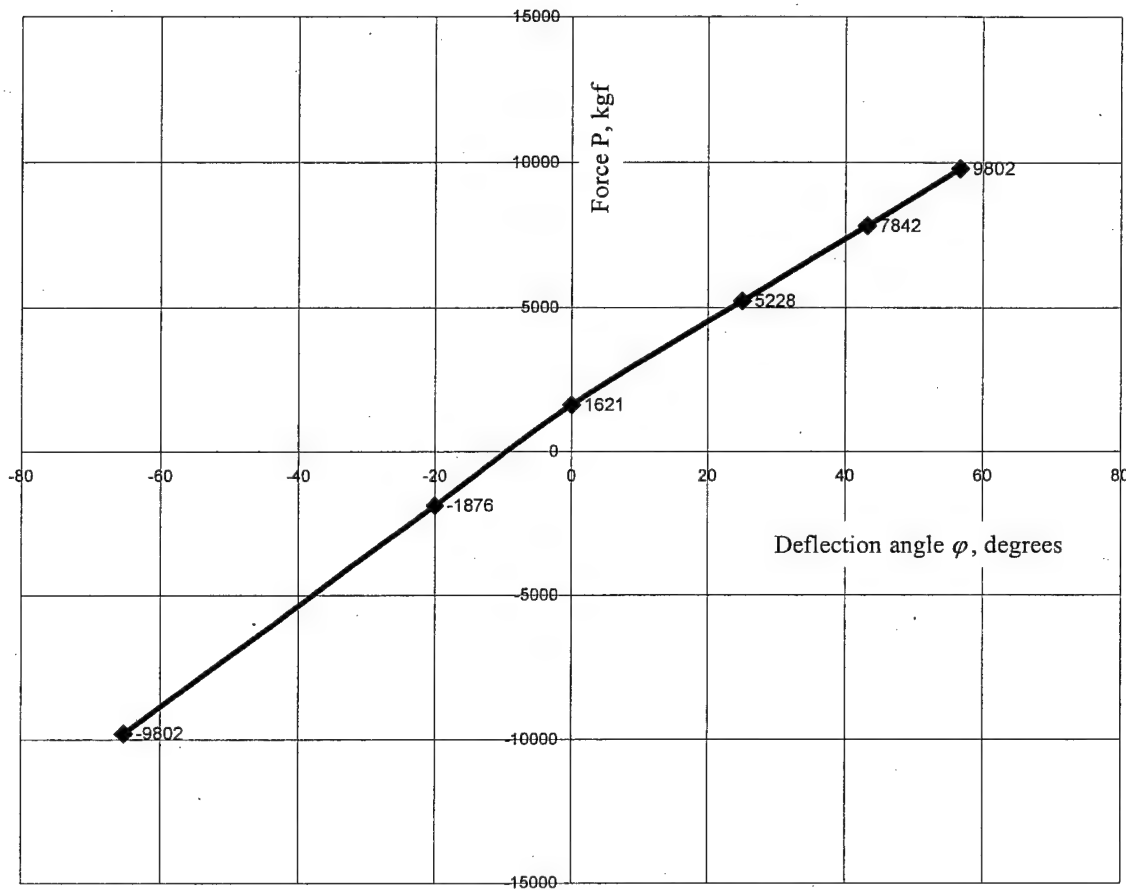


FIGURE 8-11. RELATION BETWEEN AILERON FORCE AND AILERON DEFLECTION ANGLE

TABLE 8-18. AILERON LOADS

|                    | Up                                    |                | $P_0$     | Down       |                               |                                       |
|--------------------|---------------------------------------|----------------|-----------|------------|-------------------------------|---------------------------------------|
|                    | $P_{ult} = f \cdot f_1 \cdot P_{lim}$ | $P_{lim}^{up}$ |           | $P_{lim}$  | $P_{ult}^0 = f \cdot P_{lim}$ | $P_{ult} = f \cdot f_1 \cdot P_{lim}$ |
| $P_0$ , kgf        | 9802                                  | 1876           | 1621      | 5228       | 7842                          | 9802                                  |
| $\varphi$ , degree | $65.33^\circ$                         | $20^\circ$     | $0^\circ$ | $25^\circ$ | $43.12^\circ$                 | $56.71^\circ$                         |

Statistical data on measured occurrence rates of TU-204 aileron deflection angles are demonstrated in figure 8-12. The data are for deflection angles  $-12 \leq \varphi \leq +12$ . Occurrence rates of upward and downward aileron deflection are identical. With the aileron structure symmetric, one could presuppose that aileron failure probability for upward deflection will be much less than that for downward deflection. However, the probability is nonzero and contributes to the total probability. Therefore, the analysis must take into account two load cases: with aileron deflected down and up.

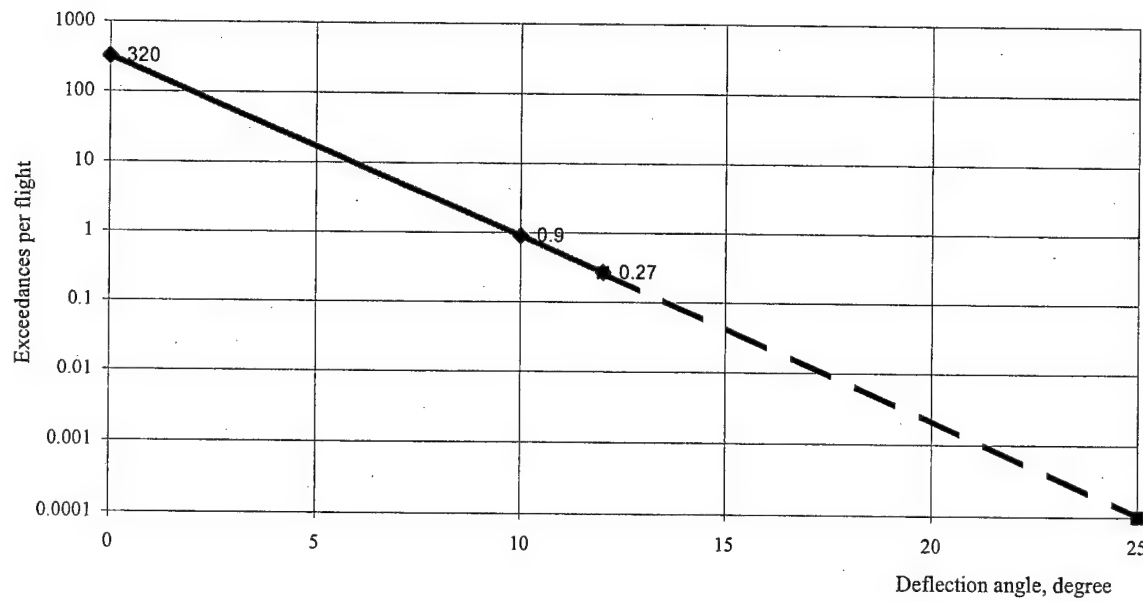


FIGURE 8-12. TU-204 AILERON DEFLECTION ANGLE (LOAD)  
EXCEEDANCE CURVE

In compiling the data for determining the aileron failure probability, one can consider the aileron deflection angle to be the primary argument. In so doing, it is assumed that the angle  $\varphi$  is an abstract mathematical entity related to the force  $P$  by functions depicted in figure 8-2, that is, the angle above  $25^\circ$  is meaningless.

It is assumed that the aileron service life is 10,000 flights, with the average flight duration being 2.5 hours.

### 8.2.3 Aileron Strength.

### 8.2.4 Mechanical Characteristics of Materials.

The composite skin of the aileron includes two materials: KMU-4e carbon/epoxy and ORGANIT-10T aramide/epoxy. Characteristics of KMU-4e layer have been obtained by experiments in a TsAGI materials laboratory. The results of processing the data on KMU-4e layer are reported in table 8-19. ORGANIT-10T layer characteristics have been taken from the relevant certificate.

The KMU-4e and ORGANIT-10T layer characteristics used in analyses are presented in table 8-20.

Theoretical mechanical properties of materials used in various zones of the aileron skin are shown in table 8-21. The index “ $x$ ” in this table corresponds to the 0-degree direction depicted in figure 8-10.

TABLE 8-19. STATISTICALLY ANALYZED DATA OF TESTING THE KMU-4e LAYER

|   | Number of Samples | Min Value | Max Value | Mean Value | Standard Deviation | Variation Coefficient (%) | Confidence Interval ( $P = 0.9$ ) |         |       |
|---|-------------------|-----------|-----------|------------|--------------------|---------------------------|-----------------------------------|---------|-------|
|   |                   |           |           |            |                    |                           | Mean Value                        | Min     | Max   |
| Elastic modulus along fibers $E_1$ , MPa                    | 3                 | 155,010   | 159,280   | 157,470    | 2,211              | 1.4                       | 153,750                           | 161,200 | 1,227 |
| Elastic modulus across fibers $E_2$ , MPa                   | 3                 | 9,970     | 10,820    | 10,340     | 436.8              | 4.2                       | 9,600                             | 11,070  | 252   |
| Shear modulus $G_{12}$ , MPa                                | 4                 | 4,230     | 7,230     | 5,962      | 1,252              | 21.0                      | 4,489                             | 7,434   | 775   |
| Poisson's ratio $\nu_{12}$                                  |                   |           |           | 0.274      |                    |                           |                                   |         |       |
| Ultimate tensile stress along fibers $\sigma'_1$ , MPa      | 6                 | 835       | 1,198     | 1,066      | 132                | 12.4                      | 958                               | 1,175   | 89    |
| Ultimate compressive stress along fibers $\sigma'_1$ , MPa  | 10                | 505       | 818       | 706        | 90.2               | 12.8                      | 654                               | 758     | 66    |
| Ultimate tensile stress across fibers $\sigma'_2$ , MPa     | 7                 | 16        | 44        | 25         | 10.3               | 41.8                      | 17                                | 32      | 7.2   |
| Ultimate compressive stress across fibers $\sigma'_1$ , MPa | 9                 | 90        | 152       | 127        | 17.4               | 13.7                      | 116                               | 137     | 12.5  |
| Ultimate shear stress $\tau_{21}$ , MPa                     | 5                 | 24        | 32        | 28         | 2.99               | 10.3                      | 25                                | 31      | 1.9   |
| Lamina thickness $\delta_m$ , mm                            | 32                | 0.081     | 0.9       | 0.087      | 0.059              | 2.6                       | 0.086                             | 0.088   | 0.049 |
|   |                   |           |           |            |                    |                           |                                   |         | 0.075 |

TABLE 8-20. CHARACTERISTICS OF SINGLE-PLY MATERIALS KMU-4e AND ORGANIT-10T

|  | Graphite/Epoxy<br>KMU-4e | Aramid/Epoxy<br>ORGANIT-10T |
|--|--------------------------|-----------------------------|
| Elastic modulus along fibers $E_1$ , MPa                     | 158,000                  | 26,000                      |
| Elastic modulus across fibers $E_2$ , MPa                    | 10,300                   | 25,000                      |
| Shear modulus $G_{12}$ , MPa                                 | 5,960                    | 2,300                       |
| Poisson's ratio $\nu_{12}$                                   | 0.274                    | 0.14                        |
| Ultimate tensile stress along fibers $\sigma_1^t$ , MPa      | 1,060                    | 650                         |
| Ultimate compressive stress along fibers $\sigma_1^c$ , MPa  | 706                      | 230                         |
| Ultimate tensile stress across fibers $\sigma_2^t$ , MPa     | 25                       | 400                         |
| Ultimate compressive stress across fibers $\sigma_2^c$ , MPa | 127                      | 97                          |
| Ultimate shear stress $\tau_{21}$ , MPa                      | 28                       | 36                          |
| Lamina thickness $\delta_m$ , mm                             | 0.09                     | 0.15                        |

TABLE 8-21. MECHANICAL CHARACTERISTICS OF AILERON SKIN

|   | Zone<br>A/D | Zone<br>B/E | Zone<br>C/F |
|---|-------------|-------------|-------------|
| Longitudinal modulus $E_x$ , MPa                            | 18,760      | 20,730      | 40,350      |
| Transverse modulus $E_y$ , MPa                              | 18,320      | 20,530      | 40,170      |
| Shear modulus $G_{xy}$ , MPa                                | 6,750       | 19,550      | 16,840      |
| Poisson's ratio $\nu_{xy}$                                  | 0.377       | 06          | 0.374       |
| Ultimate longitudinal tensile stress $\sigma_x^t$ , MPa     | 425         | 2,720       | 238         |
| Ultimate longitudinal compressive stress $\sigma_x^c$ , MPa | 1,720       | 150         | 159         |
| Ultimate transverse tensile stress $\sigma_y^t$ , MPa       | 303         | 220         | 231         |
| Ultimate transverse compressive stress $\sigma_y^c$ , MPa   | 74          | 149         | 143         |
| Ultimate shear stress $\tau_{xy}$ , MPa                     | 73          | 171         | 151         |

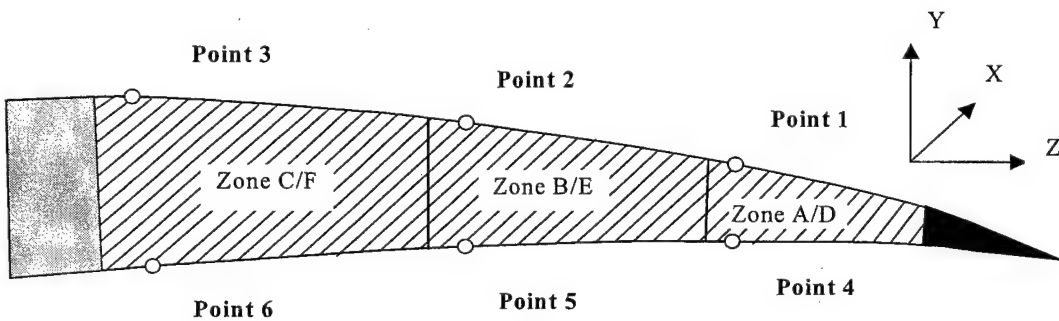
### 8.2.5 Aileron Skin Load-Carrying Capacity.

Static strength tests conducted at TsAGI have revealed that the aileron fails at the cross section drawn through the left-right hinge (see figure 8-10). This cross section is considered to be critical.

Table 8-22 compares experimental and theoretical data on stresses at critical points of the section. Experiments included strain-gaging on the aileron loaded with  $P_{lim} = 5228$  kg (due to pressure  $p_{lim} = 2160$  kg/sq. m;  $\varphi_{dn} = 25^\circ$ ). The theoretical analysis applied the Finite Element Method to structure whose surface was loaded with  $P_{lim} = 6412$  kg (due to pressure  $p_{lim} = 2710$  kg/sq. m;  $\varphi_{dn} = 25^\circ$ ).

TABLE 8-22. STRESSES AT DANGER POINTS IN CRITICAL CROSS SECTION

| Zone         | Stress MPa           |            |             |                         |            |             | Strength Coefficient | Ultimate Stress, (MPa) |  |  |
|--------------|----------------------|------------|-------------|-------------------------|------------|-------------|----------------------|------------------------|--|--|
|              | Static Strength Test |            |             | Finite Element Analysis |            |             |                      |                        |  |  |
|              | $\sigma_x$           | $\sigma_z$ | $\tau_{xz}$ | $\sigma_x$              | $\sigma_z$ | $\tau_{xz}$ |                      |                        |  |  |
| A<br>Point 1 |                      |            |             | -14.7                   | -13.0      | -7.1        | 242                  | 116                    |  |  |
| B<br>Point 2 |                      |            |             | -24.5                   | -12.9      | -26.0       | 129                  | 103                    |  |  |
| C<br>Point 3 | -89.0                | +14.0      | -19.0       | -85.0                   | +9.0       | -25.5       | 54.6                 | 152                    |  |  |
| D<br>Point 4 |                      |            |             | +15.8                   | +13.3      | +6.0        | 850                  | 438                    |  |  |
| E<br>Point 5 |                      |            |             | +25.1                   | +13.4      | +25.0       | 224                  | 183                    |  |  |
| F<br>Point 6 | +74.0                | +8.8       | +18.0       | +67.1                   | +7.1       | +25.0       | 111                  | 243                    |  |  |



#### 8.2.6 Scatter of Mechanical Properties of Materials.

Experimental and theoretical evaluation of the aileron strength variation factors is very difficult to carry out because the cost of such efforts is high and there are no reliable analytical tools. Usually the strength variation factors for complex structures are adopted from tests on smaller specimens. Table 8-23 provides the results of statistically analyzing the test data on specimens made out of KMU-4e with specific stacking sequence. From this table it is clear that the maximum value of the strength variation factor for this material is 9.5%. As the KMU-4e composite is the primary load-bearing material, that determines the strength of the composite aileron skin, the value of 9.5% is assumed for residual strength variation.

#### 8.2.7 Strength Degradation Function for Damaged Skin.

The computer programs have been used to evaluate the strength (load-carrying capability) degradation functions for aileron skins. There are two types of damage considered:

- skin delamination or indentation and
- through-the-thickness holes and cracks.

In the zones where longitudinal stresses are positive (i.e., tensile), the skin delamination from honeycomb core was assumed not to degrade strength (load-carrying capability).

Results of calculating the strength degradation function for the skin with the through damages may be seen in figure 8-13.

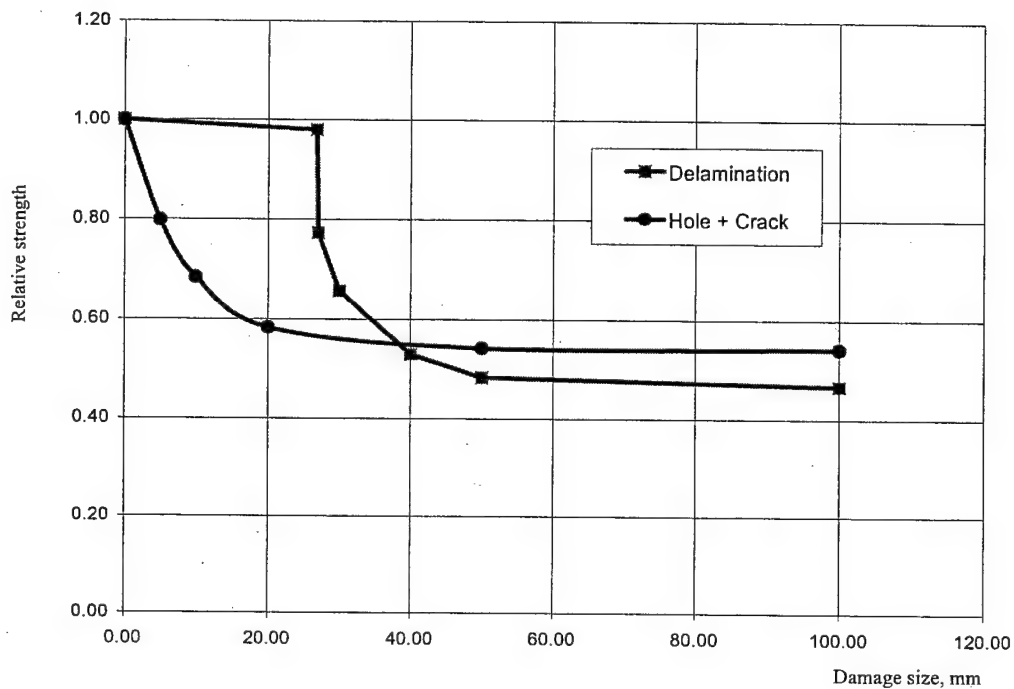


FIGURE 8-13. RELATIVE STRENGTH OF DAMAGED SKIN

For the failure probability calculation, the relative residual strength as a function of damage area size was multiplied by the residual strength of the intact structure:

$$\sigma_i^0 = \frac{\sigma_i^{ult}}{\sigma_i} \cdot 25 \cdot \frac{p_{fem}}{p_{test}};$$

where,  $\sigma_i^{ult}$  and  $\sigma_i$  are the ultimate and limit stress for the point (see table 8-22);

$25^\circ$  is the aileron deflection angle, for which the stress field was derived; and  $p_{fem}$  and  $p_{test}$  are aileron surface pressures adopted in analysis and test, respectively.

Values of  $\sigma_i^0$  for each structural zone stated in rightmost column of table 8-22.

#### 8.2.8 Damage Occurrences.

In fact, the damaging factors are very numerous. Comprehensive models for computing the composites behavior in the case of mechanical impact does not exist. However, if there are statistics of damage to some structures, it becomes possible to predict the rate of occurrence of damage in various composite structures.

Studies carried out at TsAGI have shown that passenger airplane ailerons can be classified as structural units featuring a low damage rate. The ProDeCompoS database includes information on damage rates of units belonging to the group:

- wing/fuselage fairing of L-1011 airplane
- landing gear door of AN-124 airplane
- cargo bay door of AN-124 airplane

Table 8-23 provides data on empirical exceedance intensity for these units.

TABLE 8-23. EMPIRICAL EXCEEDANCE INTENSITY OF DAMAGE  
(per 1,000 flight hours per sq. m)

| Unit                  | Airplane | Hole + Cracks |         |         | Delaminations |         |         |
|-----------------------|----------|---------------|---------|---------|---------------|---------|---------|
|                       |          | >0            | >30 mm  | >80 mm  | >0            | >30 mm  | >80 mm  |
| Wing/fuselage fairing | L-1011   | 0.029         | 0.00725 | 0.00483 | 0.0411        | 0.00967 | 0.00242 |
| Landing gear door     | AN-124   | 0.171         | 0.114   | 0.0569  | 0.228         | 0.228   | 0.0592  |
| Cargo bay door        | AN-124   | 0.240         | 0.120   | 0.0     | 0.599         | 0.479   | 0.239   |

Used as the basis for the aileron, were data about exceedance for AN-124 landing gear door. The basic operation amount was 25,000 flight hours; the surface area is taken to be  $0.15 \times 0.15 = 0.0225$  sq. m. The resulting damage exceedances curve (the cumulative number of occurrences) taken into account is shown in figure 8-14.

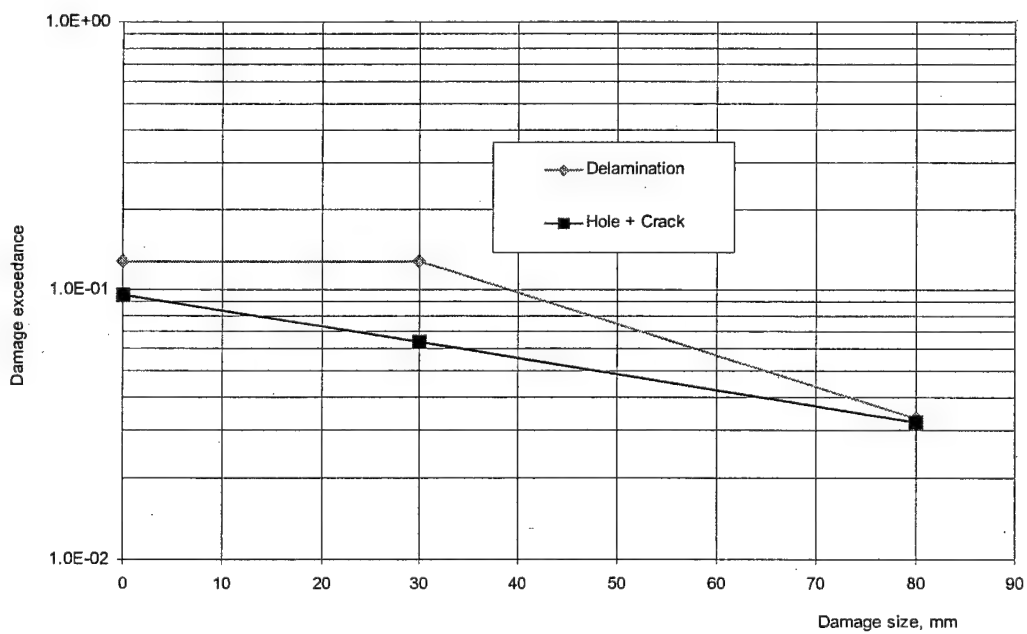


FIGURE 8-14. DAMAGE EXCEEDANCES OF AN-124 LANDING GEAR DOOR  
(per 25,000 flight hours per 0.0225 sq. m)

### 8.2.9 Repairs.

It was assumed that two basic methods of repair are used for each damage type:

- simplified repair applied in airfield conditions and
- special repair at airline maintenance facility.

The second method is applied if some damage is detected during maintenance (carried out at interval of 250 hours of aircraft operation).

The strength restoration factors and variation coefficients for cracks/holes and delamination are shown in table 8-24. These values were estimated by using the typical data obtained at TsAGI as a result of testing the composite structures after repair. There were difficulties in generalizing the available data because residual strength notably depends on the repair method employed. The strength restoration factors can be changed by using advanced repair techniques and selecting the structures repaired.

TABLE 8-24. STRENGTH RESTORATION FACTORS

|               | Field Facility |           | Maintenance Facility |           |
|---------------|----------------|-----------|----------------------|-----------|
|               | Coefficient    | Variation | Coefficient          | Variation |
| Hole + Cracks | 0.9            | 0.115     | 0.95                 | 0.095     |
| Delaminations | 0.9            | 0.115     | 0.95                 | 0.095     |

### 8.2.10 Results of Calculating the TU-204 Aileron Fracture Probability Within the ProDeCompoS Methodology.

The theoretical analysis relied on the initial data described in section 8.2.4; other parameters were taken from table 8-1. Table 8-25 shows the results of calculating the aileron failure probability for 25,000 flight hours (that is, the failure probability per life).

TABLE 8-25. FAILURE PROBABILITY PER LIFE

| Zone With Critical Damage | Aileron Failure Probability |
|---------------------------|-----------------------------|
| Zone A                    | $4.0 \cdot 10^{-7}$         |
| Zone B                    | $1.9 \cdot 10^{-6}$         |
| Zone C                    | $3.5 \cdot 10^{-4}$         |

Thus, the ProDeCompoS evaluates the failure probability as follows:

- $3.5 \cdot 10^{-4}$  for the entire service life of 25,000 flight hours;
- $3.5 \cdot 10^{-8}$  for a flight lasting 2.5 hours, and
- $1.4 \cdot 10^{-8}$  for a flight hour.

### 8.2.11 Parametric Studies Based on TU-204 Aileron Example.

### 8.2.12 Uncertainty Due to Load Extrapolation.

There exists some uncertainty in extrapolating the load exceedance curve into the domain surrounding the observation region, as it concerns the TU-204 aileron, the observed aileron deflection region is limited with the angle  $\varphi = 12^\circ$ .

Figure 8-15 represents three versions of load exceedance curve extrapolation. The extrapolation type (1) corresponds to linear extrapolation of the curve into the domain with  $\varphi > 12^\circ$  in the log plot. This extrapolation is used in the ProDeCompoS as a standard means. The extrapolation (2) assumes the load exceedance curve to be interrupted at  $\varphi = 12^\circ$ . The extrapolation type (3) is the load exceedance curve continuation (on the log plot) to the value corresponding to the ultimate force  $P_{ult}$  ( $\varphi = 53.55^\circ$ ). Various methods are demonstrated in the diagram of figure 8-15.

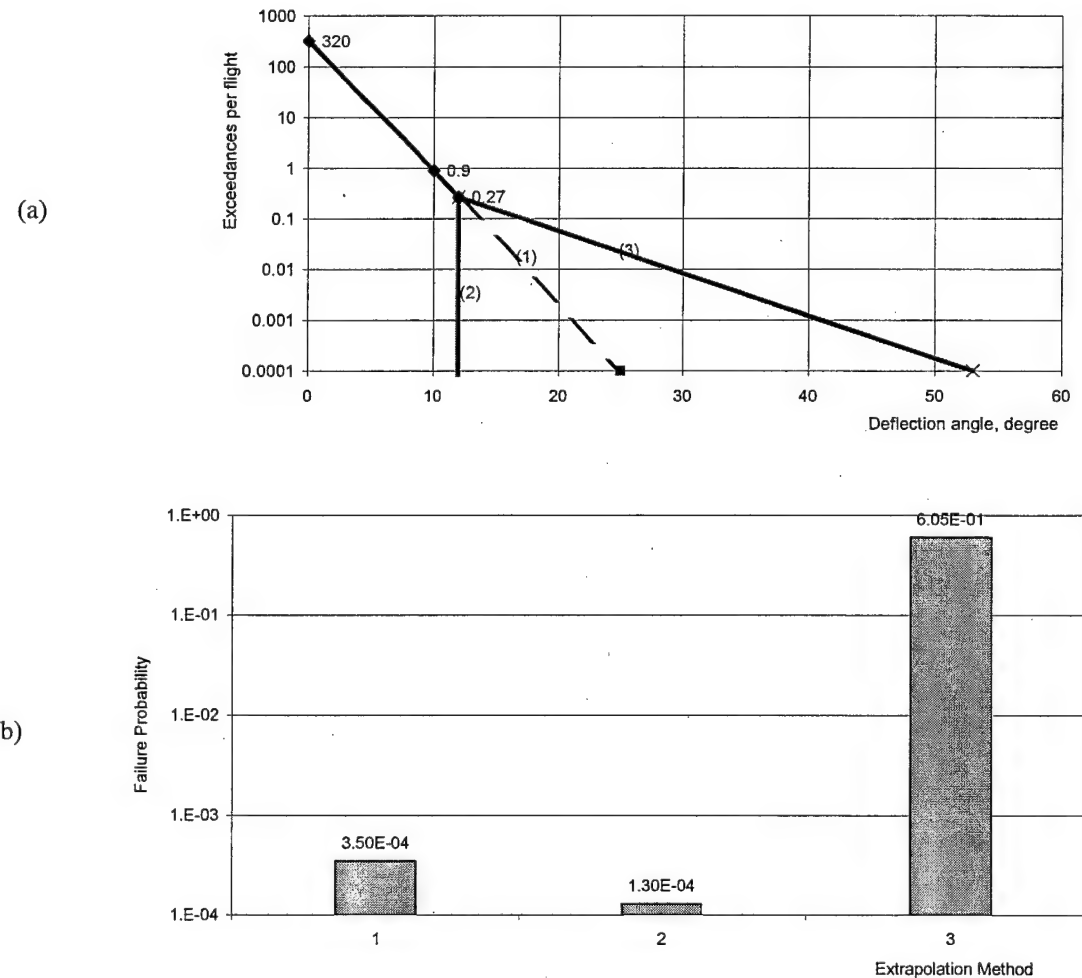


FIGURE 8-15. LOAD EXCEEDANCE EXTRAPOLATION

It is clear that the load exceedance curve extrapolation manner does greatly affect the computation result. This factor is a common weak point in statistical methods of structural mechanics.

### 8.2.13 Extent of Damage.

The TU-204 aileron has been classified as a structural unit with a low damage rate. The computation was based on the observation data for AN-124 landing gear door damage rate. Analytical results for cases when the basis is taken from data about other units in the group are compared:

- wing/fuselage of L-1011 airplane and
- cargo bay door of AN-124 airplane.

The results are depicted as a diagram in figure 8-16.

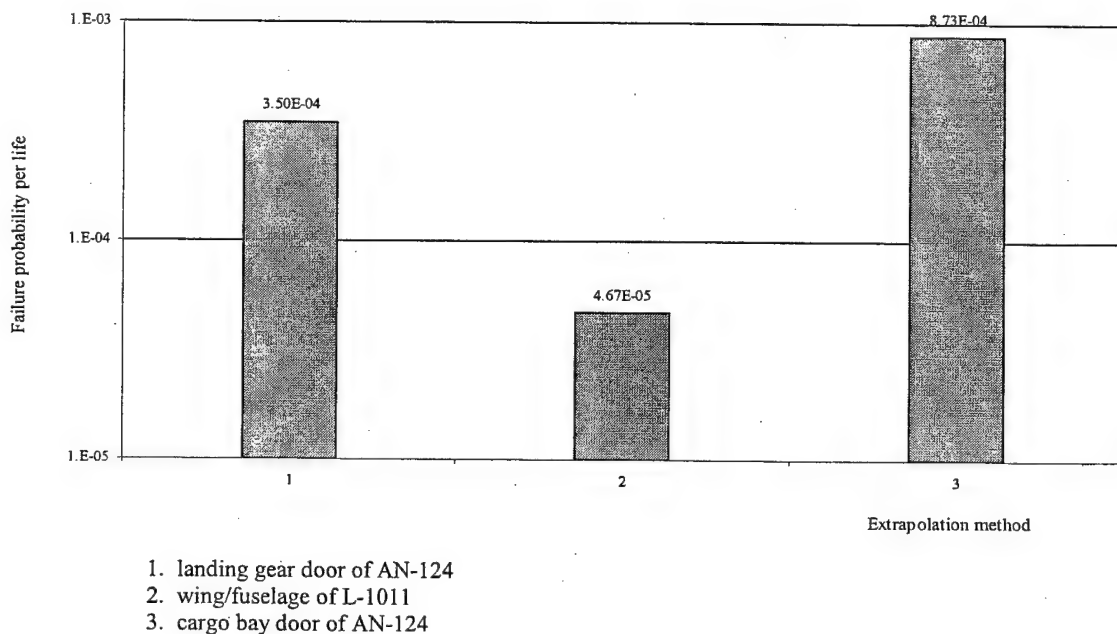


FIGURE 8-16. FAILURE PROBABILITY FOR DIFFERENT LEVELS OF DAMAGE RATE

### 8.2.14 Estimates for Various Service Life Duration.

The calculation for various service life duration while assuming an identical flight duration of 2.5 hours was performed.

- 50,000 flight hours,
- 25,000 flight hours, and
- 12,500 flight hours.

The analytical data is on the straight line in figure 8-17; within the error typical of the Monte-Carlo method.

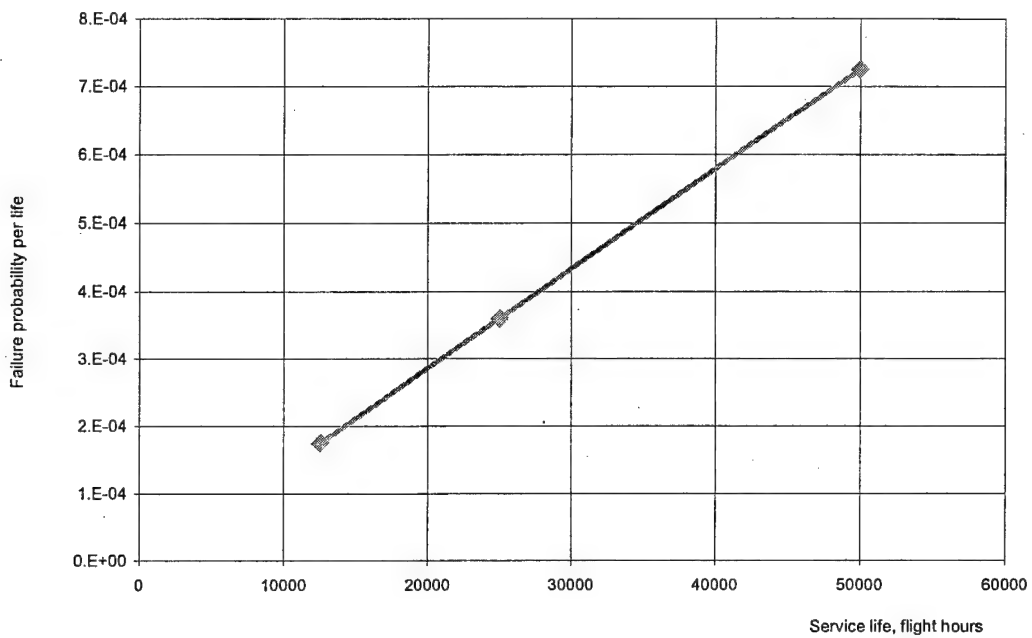


FIGURE 8-17. FAILURE PROBABILITY VS SERVICE LIFE DURATION

#### 8.2.15 The Influence of Inspection Schedule.

The preflight inspection schedule may be a rather serious factor in fracture probability. Figure 8-18 provides results of computation with the assumption that only one inspection is carried out after some number of flights.

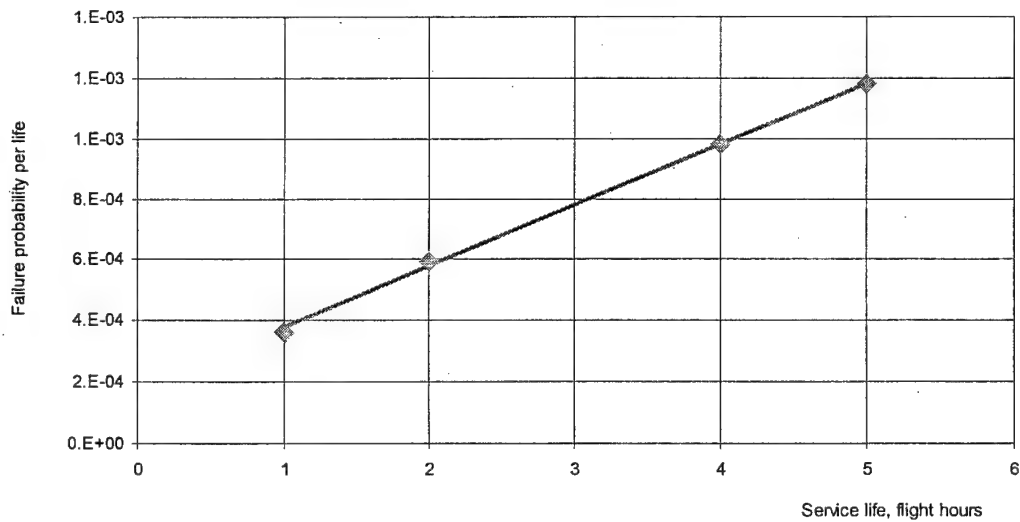


FIGURE 8-18. FAILURE PROBABILITY VS VISUAL INSPECTION SCHEDULE

The calculation indicates that the special (instrumented) inspection is only an auxiliary means for ensuring flight safety, and the inspection frequency only slightly affects the in-flight fracture probability.

#### 8.2.16 The Effect of Repair Quality.

The effect of repair quality may be evaluated by varying the strength restoration coefficients. When computing residual strength and effectiveness of repair, it was assumed that all coefficients are identical (for all damage types, all load types, all repair types, etc). The theoretical data are presented in figure 8-19. One can see that the repair quality is a strong factor in aileron reliability.

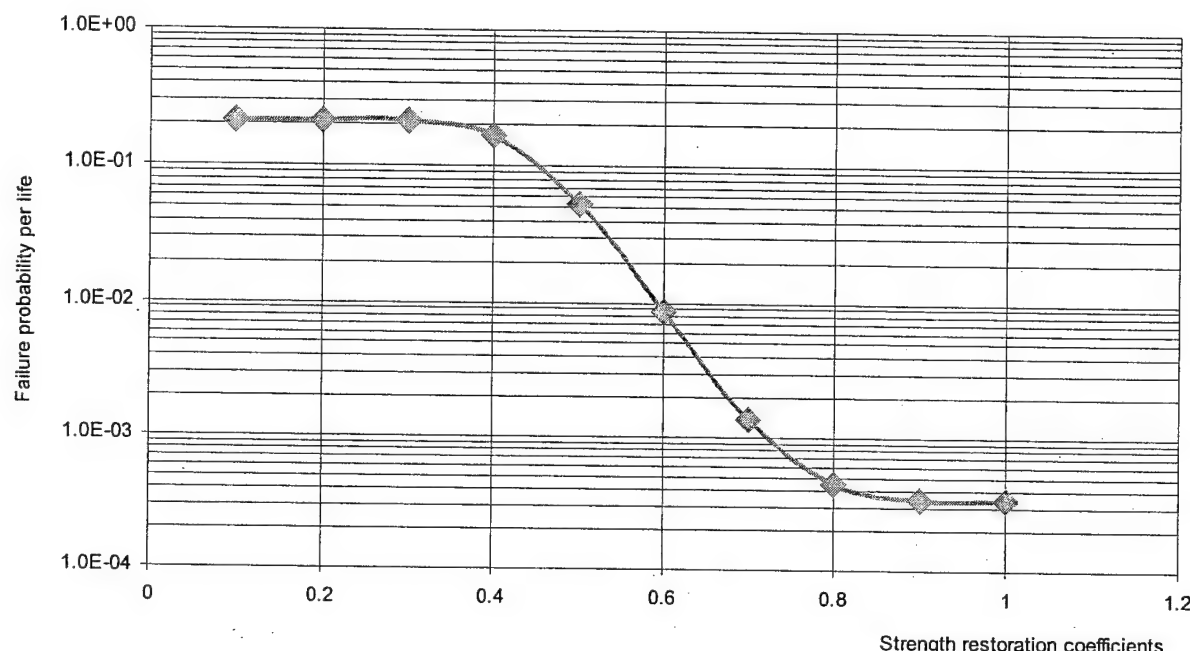


FIGURE 8-19. FAILURE PROBABILITY VS STRENGTH RESTORATION COEFFICIENTS

#### 8.3 LEAR FAN-2100 WING FAILURE PROBABILITY ESTIMATION.

##### 8.3.1 Airplane Under Consideration.

This estimation is made for a twin engine Lear Fan 2100 airplane having the following main characteristics [3]:

- AREAS:
  - Wing main box (semispan)  $4.83 \text{ m}^2 (52 \text{ ft}^2)$
- WEIGHTS:
  - Maximum takeoff  $3310 \text{ kg (7350 lb)}$

- PERFORMANCE:

|  |                                     |
|--|-------------------------------------|
| - Limit maneuver load factor               | 3.5                                 |
| - Limit maneuver load factor (restricted)  | 3.29                                |
| - Limit gust load factor (expert estimate) | 2.9                                 |
| - Safety factor (static test)              | 1.5 · 1.14 = 1.71                   |
| - Life                                     | 15,000 flight hours, 12,274 flights |
| - Three basic mission profiles             |                                     |

### 8.3.2 Spectra Loading.

Cumulative load exceedance curves are used for load spectra characterization in the ProDeCompoS. In case of unrestricted normal load factor, initial maneuver spectrum exceedance curves are used as shown in figure 8-20 [3].

Contribution of the gust load was estimated by combining maneuver load spectrum with the gust load spectrum taken as statistically independent variables. Gust load spectrum was estimated approximately by taking into account three mission profiles [3] and the typical maximum gust load factor for similar Russian aircraft.

Equivalent gust exceedance curves for different altitudes similar to that of 14 Code of Federal Regulations (CFR) Part 25 were used, which were combined in correspondence with the predicted usage of Lear Fan-2100 (three missions). For each mission the number of gust exceedance was determined by formula:

$$F_t = \sum_{i=1}^N F_{ti} \frac{\Delta L_i}{L} \quad (8-1)$$

where  $F_{ti}$  is the gust spectrum exceedance for  $i^{\text{th}}$  segment of mission;  $\Delta L_i$  is the summary distance of  $i^{\text{th}}$  segments;  $L$  is the summary distance covered by aircraft per its life.

Combined gust spectrum exceedance curve for all three missions was determined by the formula:

$$F_t = F_{t(I)} \cdot UF_I + F_{t(II)} \cdot UF_{II} + F_{t(III)} \cdot UF_{III} \quad (8-2)$$

where  $UF_j$  is usage factor for  $j^{\text{th}}$  mission.

Since Lear Fan-2100 geometric and aerodynamic data are not available in reference 3, the value of limit load factor was taken, which is similar to the Russian aircraft  $N_z = 2.9$  corresponding to the maximum gust speed  $U = 15 \text{ m/s}$  at  $V_c$ , which corresponds also to the continuous gust design criteria CFR Part 25, Appendix G. Combined gust frequency of exceedance for Lear Fan three missions nearly corresponds to  $2 \cdot 10^{-5}$  per flight hour at  $U = 15 \text{ m/s}$ . The resulting gust load factor exceedance curve is also shown in figure 8-20.

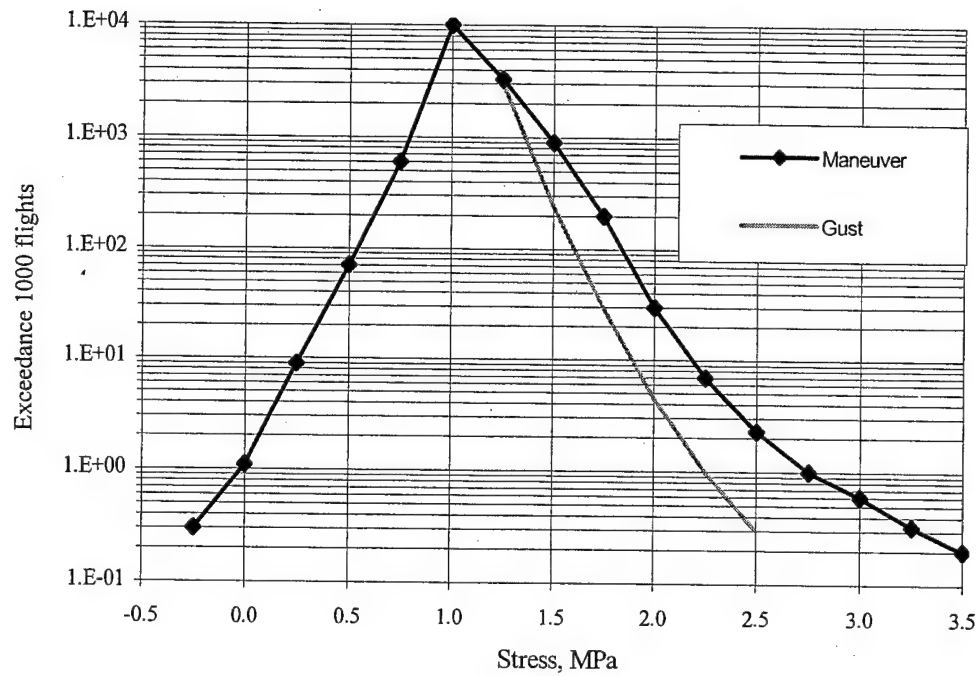


FIGURE 8-20. MANEUVER/GUST SPECTRUM EXCEEDANCE CURVE

In the case of application of maneuver load factor restriction,  $N_z = -3.29$ , the maneuver exceedance curve for positive load factor was modified so that the frequency of exceedance of limit load factor is the same as in an unrestricted case. This curve is shown in figure 8-21.

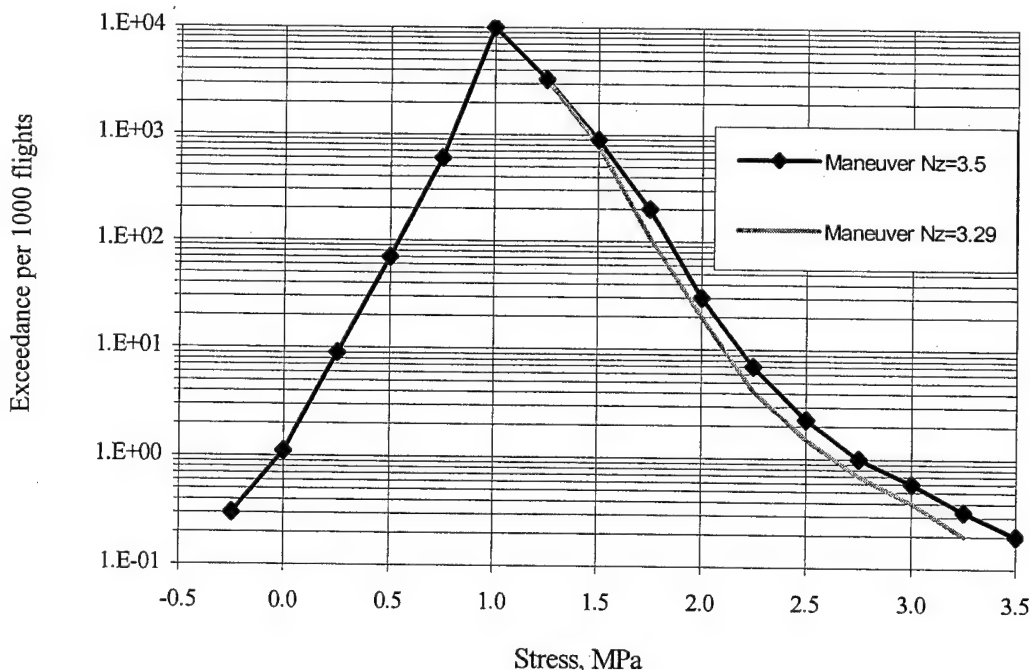


FIGURE 8-21. MANEUVER SPECTRUM EXCEEDANCE CURVE  
(Restricted load factor)

Since the linear extrapolation in semilogarithm scale is used for probability simulation, it becomes very important to determine the last points of exceedance curve properly. If the simple mentioned linear extrapolation is used, the resulting curve is shown in figure 8-22. It is evident that this type of extrapolation will give very low failure probability. So, the probability of ultimate load ( $L.F. = 5.626$ ) exceedance per 15,000 flight hours with this extrapolation is approximately equal to 0.01. Then it was assumed, that the given exceedance curve may be continued as shown in figure 8-22. The slope of the straight line here is selected similar to the typical slope of load factor exceedance for commercial airplanes, used in Russia.

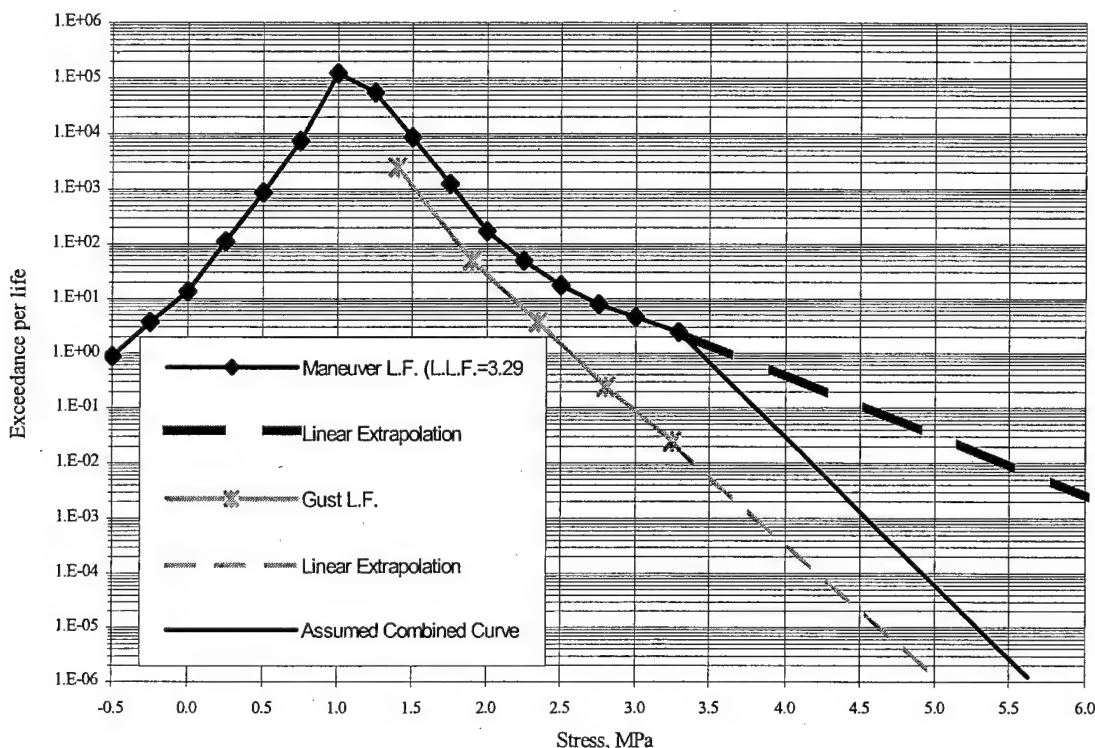


FIGURE 8-22. EXTRAPOLATION OF EXCEEDANCE CURVE

### 8.3.3 Critical Areas.

Only upper and lower composite panels of the wing box structure are considered for failure probability estimation. It is considered that the probability of in-service damage for internal substructure panels is approaching zero. Critical panels located on the upper surface are shown in figure 8-23 and for the lower surface are shown in figure 8-24.

According to the general concept of the ProDeCompoS, the probability of wing box failure is a sum of the conditional probabilities of wing failure determined for the chosen load distribution over the wing surface and under condition that the critical panel may be damaged. In this particular example, only one upbending loading case is considered and only 12 panels may be damaged.

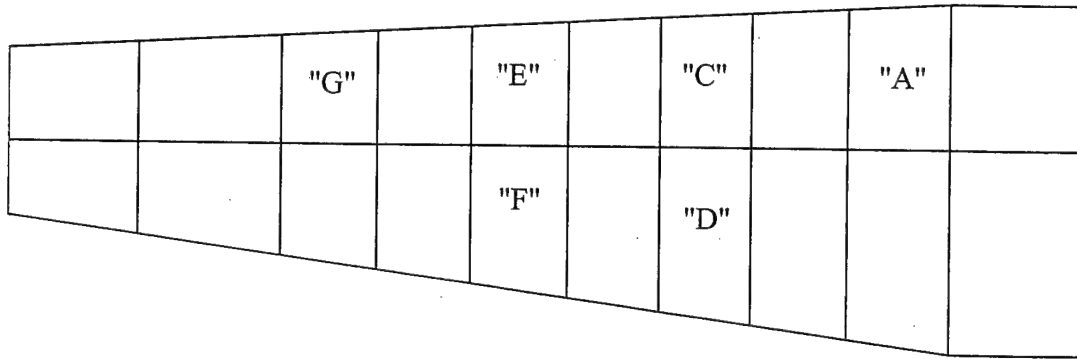


FIGURE 8-23. CRITICAL PANELS ON UPPER WING SURFACE

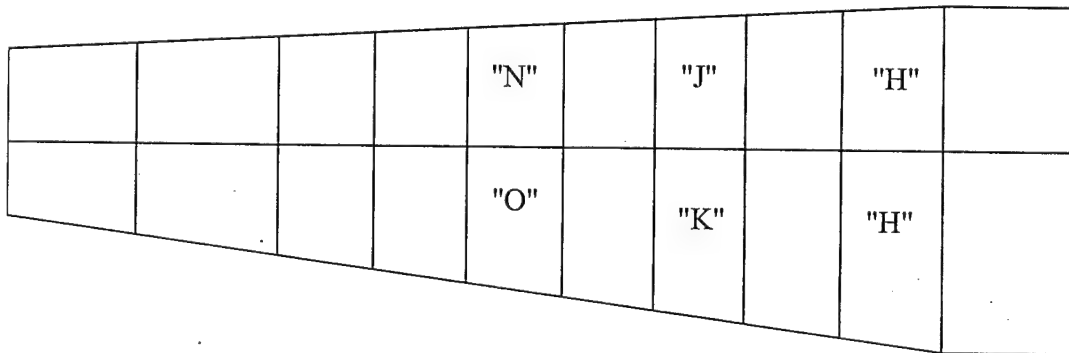


FIGURE 8-24. CRITICAL PANELS ON LOWER WING SURFACE

#### 8.3.4 Damage Occurrences.

Information presented in reference 3 is insufficient for estimation of damage frequency of occurrence for critical areas under consideration. It is necessary to relate the data [3] to the specific location of composite structure and the area of composite structure. It was assumed (expert estimate) that the mean area of composite external surface for considered aircraft is  $30 \text{ m}^2$ . The damages of hole and crack type were combined because the same strength degradation model is used in ProDeCompoS for cracks and holes. The resulting cumulative number of occurrences per Lear Fan-2100 life per 1 m of external surface of composite structure is shown in table 8-26 and in figure 8-25.

TABLE 8-26. CUMULATIVE NUMBER OF OCCURRENCES PER 15,000 FLIGHT HOURS PER  $1 \text{ m}^2$

| Damage Size<br>(mm) | Damage Type    |              |
|---------------------|----------------|--------------|
|                     | Holes + Cracks | Delamination |
| 0.0                 | 0.2425         | 0.2435       |
| 37.5                | 0.132          | 0.219        |
| 75                  | 0.05           | 0.146        |

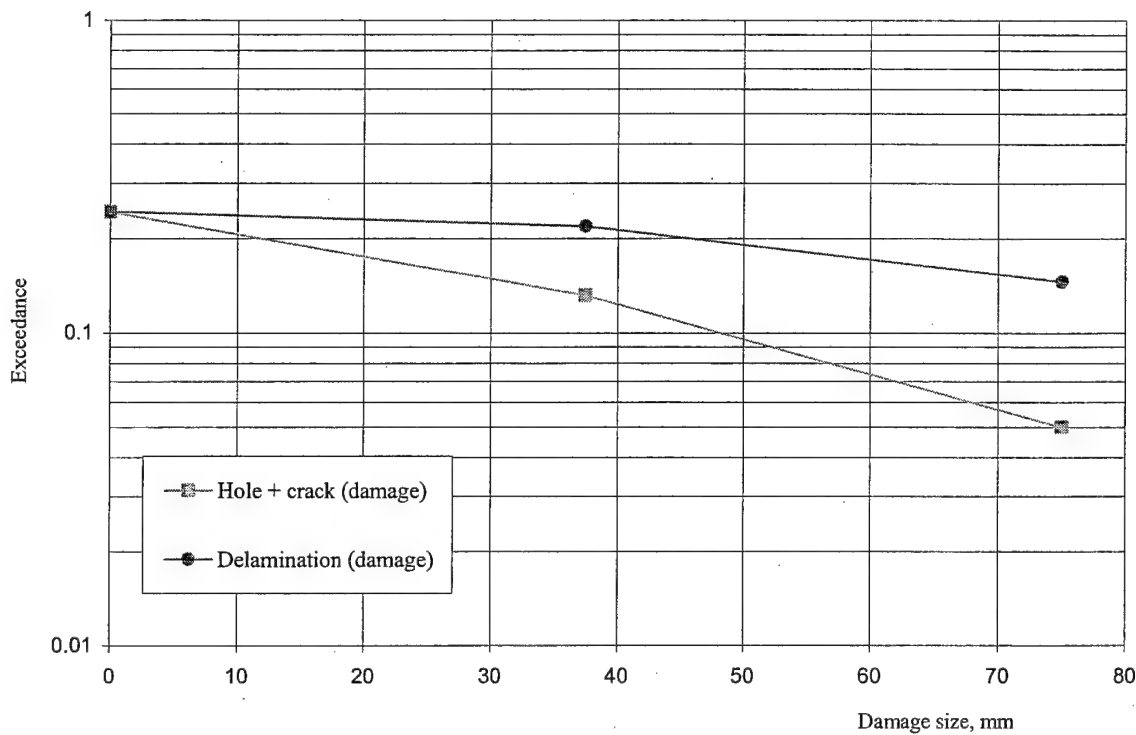


FIGURE 8-25. DAMAGE SPECTRA

The areas of chosen critical panels are shown in figure 8-26. Cumulative numbers of occurrences per Lear Fan-2100 life for critical panels are calculated proportionally to these areas.

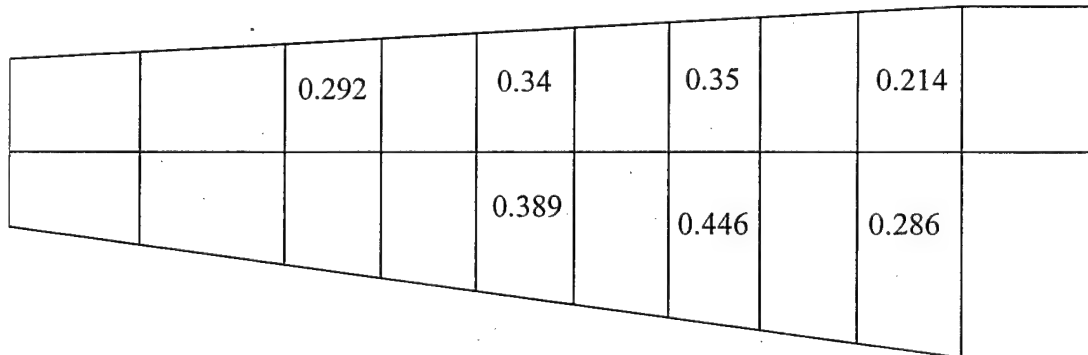


FIGURE 8-26. AREA OF CHOSEN CRITICAL PANELS,  $\text{m}^2$

### 8.3.5 Residual Strength.

Initial static strength characteristics for critical panels of upper and lower skin was taken from, tables 4-5, and 4-6 of reference 3. It is assumed that the main failure mode for upper skin is buckling and for lower skin is tension failure. In table 8-27, the initial static strength characteristics for six upper skin critical panels are shown in terms of limit load factor (LLF) and

failure load factor (FLF). Here the mean failure load factors (MFLF) for panels A, E, F are calculated as:

$$MFLF = LLF \cdot 1.5 \cdot (M.S. @ Static Test RTD + 1) = 3.29 \cdot 1.5 \cdot 1.14 = 5.626 \quad (8-3)$$

For other panels, it is assumed that the value obtained from equation 8-3 should be multiplied by the factor  $FB$  which accounts for the difference between the B allowable value and a mean strength value utilized by ProDeCompoS:

$$MFLF = LLF \cdot 1.5 \cdot (M.S. @ Static Test RTD + 1) \cdot FB \quad (8-4)$$

where:  $FB = (1 - 1.282 \cdot C_v)$ ,  $C_v$  is a coefficient of strength variation.

TABLE 8-27. FAILURE LOAD FACTOR AND COEFFICIENT OF VARIATION FOR  
UPPER WING SURFACE CONDITION—SYMMETRICAL UPBENDING

| Panel ID | Assumed Failure Mode | MS® Static Test RTD* | MFLF* | $C_v, \%$ | Comments    |
|----------|----------------------|----------------------|-------|-----------|-------------|
| A        | Buckling             | +0.14                | 5.626 | 7.0       | Panel No. 1 |
| C        | Buckling             | +0.68                | 9.03  | 7.0       | Panel No. 2 |
| D        | Buckling             | +0.33                | 7.15  | 7.0       | Panel No. 5 |
| E        | Buckling             | +0.14                | 5.626 | 7.0       | Panel No. 3 |
| F        | Buckling             | +0.14                | 5.626 | 7.0       | Panel No. 6 |
| G        | Buckling             | +0.58                | 8.5   | 7.0       | Panel No. 4 |

\* For restricted aircraft (94% of DLL).

Since no information about coefficients of strength variation of Lear Fan-2100 panels was available, their values are taken similar to the Russian-production composite panels (KMU-4e graphite/epoxy material).

In table 8-28, the initial static strength characteristics for six lower skin critical panels are shown. For these panels, it is assumed that the value obtained from equation 8-3 should be multiplied by the factor  $FB$  which accounts for the difference between the B allowable value and a mean strength value utilized by ProDeCompoS.

TABLE 8-28. FAILURE LOAD FACTOR AND COEFFICIENT OF VARIATION FOR LOWER WING SURFACE CONDITION—SYMMETRICAL UPBENDING

| Panel ID       | Assumed Failure Mode | MS® Static TestRTD* | MFLF* | $C_v, \%$ | Comments     |
|----------------|----------------------|---------------------|-------|-----------|--------------|
| H              | Tension              | +1.11               | 10.66 | 4.0       | Panel No. 7  |
| I              | Tension              | +1.37               | 12.3  | 4.0       | Panel No. 10 |
| j              | Tension              | +1.21               | 11.47 | 4.0       | Panel No. 8  |
| K              | Tension              | +1.85               | 14.79 | 4.0       | Panel No. 11 |
| N <sup>1</sup> | Tension              | +1.05               | 10.64 | 4.0       | Panel No. 9  |
| 0              | Tension              | +1.52               | 13.07 | 4.0       | Panel No. 12 |

\* For restricted aircraft (94% of DLL)

Dependencies of residual strength on the damage size were calculated only for up bending load case. Since no information on structural material and layout is presented in reference 3, it was assumed that the both upper and lower skin is made of the graphite/epoxy material KMU-71 (Russia), exhibiting the following properties (monolayer, international unit system kg mm).

$$\begin{aligned}
 E_1 &= 185\,000 \text{ MPa}, E_2 = 6\,400 \text{ MPa}, G = 4\,500 \text{ MPa}, v = 0.25, \\
 \sigma_1^t &= 970 \text{ MPa}, \sigma_1^c = 750 \text{ MPa}, \sigma_2^t = 250 \text{ MPa}, \sigma_2^c = 190 \text{ MPa}, \tau = 62, \\
 \gamma &= 1.55 \text{ g/cm}^3, \delta_m = 0.13 \\
 K_{Ic1} &= 250 \text{ kg/mm}^{3/2}, K_{Ic2} = 10 \text{ kg/mm}^{3/2}, K_{IIC} = 5 \text{ kg/mm}^{3/2},
 \end{aligned}$$

Layup arrangement: [45/-45/90/45/-45/45/-45/0/90/45/-45/0]s, the number of layers is 24. The total thickness of laminate is 3.1 mm.

According to Tsai-Hill criterion the resulting laminate characteristics are as follows:

- Compression

$$\begin{aligned}
 E_x &= 54\,100 \text{ MPa} \\
 s_x^{lim} &= 213 \text{ MPa} \text{ (matrix cgracing)} \\
 s_x^{ult} &= 279 \text{ MPa} \text{ (fiber failure)} \\
 e_x^{ult} &= 0.516\% \\
 K_{Icx} &= 64 \text{ kg/mm}^{3/2}
 \end{aligned}$$

- Tension

$$\begin{aligned}
 E_x &= 54\,100 \text{ MPa} \\
 s_x^{lim} &= 215 \text{ MPa} \text{ (matrix cgracing)} \\
 s_x^{ult} &= 219 \text{ MPa} \text{ (fiber failure)} \\
 e_x^{ult} &= 0.405\% \\
 K_{Icx} &= 64 \text{ kg/mm}^{3/2}
 \end{aligned}$$

The loading of panels is assumed to be uniaxial, which corresponds to the wing upbending without torque, (see figure 8-27). Upper panels are in compression and lower ones are in tension. All the panels are assumed to have the same dimension,  $a = 508$  mm,  $b = 766$  mm.

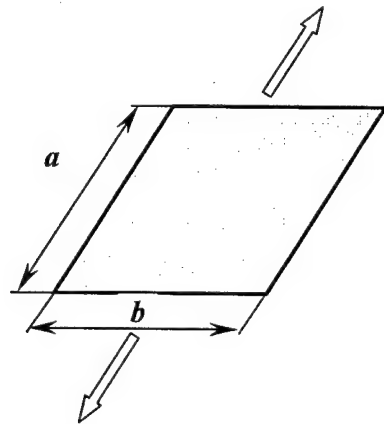


FIGURE 8-27. SCHEMATIC OF PANEL UNDER TENSILE LOAD

### 8.3.6 Residual Strength Degradation of Damaged Panels.

#### a. Upper panels (compression)

The most critical damage is assumed to be a delamination located at the middle of the skin thickness.

A computer program called DELAM was used for residual strength prediction. It was based on equations shown in section 4.2. The results are shown in table 8-29 and in figure 8-28.

The reduction of the residual strength of the wing having a damaged panel was estimated by using the computer program "BOX-C" (wing box strength analysis). Relative residual strength (the ratio of wing box residual strength to the strength of undamaged wing box structure) in the case of different critical upper panels, damage is shown in figure 8-29 for delaminations.

TABLE 8-29. RELATIVE RESIDUAL STRENGTH OF UPPER PANEL VS DAMAGE SIZE

| Damage size, mm            | 1   | 10  | 22  | 23    | 25   | 50    | 100   | 300    |
|----------------------------|-----|-----|-----|-------|------|-------|-------|--------|
| Relative residual strength | 1.0 | 1.0 | 1.0 | 0.934 | 0.79 | 0.198 | 0.050 | 0.0055 |

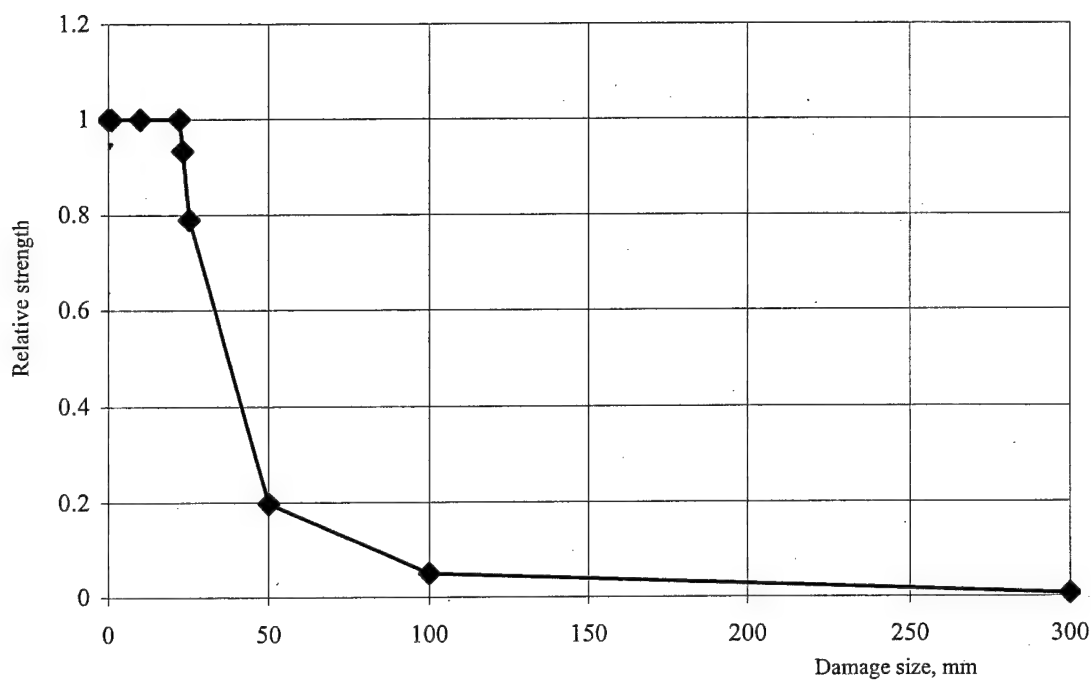


FIGURE 8-28. RELATIVE STRENGTH OF DAMAGED PANELS, LEAR FAN-2100  
(Compression panels)

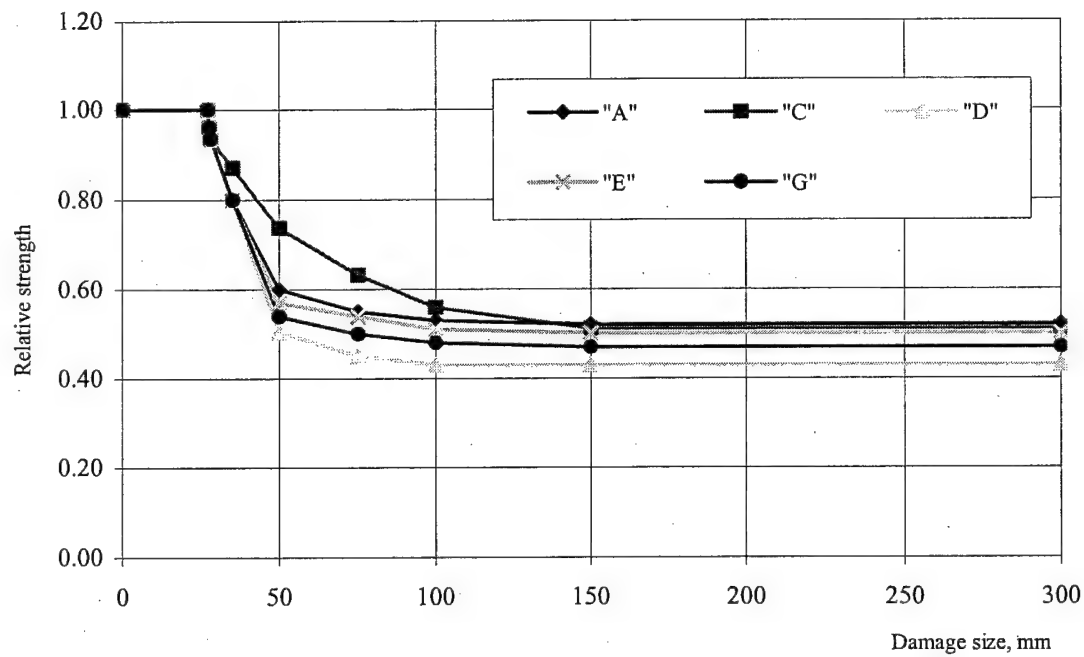


FIGURE 8-29. RELATIVE WING RESIDUAL STRENGTH FOR UPPER SKIN  
PANELS WITH DAMAGE (Compression panels)

b. Lower panels (tension)

The most critical damage is assumed to be a round shape through hole of diameter  $D$ , (see figure 8-30). It is also assumed that:

1. the type I of failure takes place
2. there exists an additional cracking zone of size  $a$  near the hole
3. the strength of laminate with this hole can be determined by equation

$$\sigma_{cr} = \frac{K_{Ic}}{\sqrt{\pi a} \cdot f\left(\frac{a}{D}\right)}$$

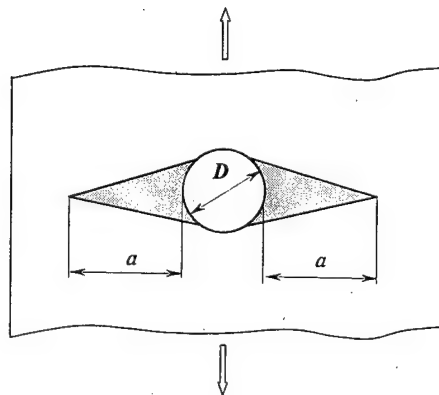


FIGURE 8-30. SCHEMATIC OF PANEL WITH HOLE UNDER TENSILE LOAD

For selected type of material, the SIF is equal to  $85.7 \text{ kg/mm}^{3/2}$ , and it does not depend on the hole size  $D$ .

A computer program called CRACK was used for panel residual strength prediction. CRACK is based on equations found in section 4.1. The results are shown in table 8-30 and in figure 8-31.

TABLE 8-30. RELATIVE RESIDUAL STRENGTH OF LOWER PANEL VS DAMAGE SIZE

| Damage size, mm            | 1     | 2     | 3     | 4     | 5     | 10    | 20    | 50    |
|----------------------------|-------|-------|-------|-------|-------|-------|-------|-------|
| Relative residual strength | 0.866 | 0.775 | 0.707 | 0.654 | 0.612 | 0.481 | 0.361 | 0.232 |

The reduction of the strength of wing having damage panels was estimated by the computer program BOX-C. The theory behind BOX-C is described in section 5. Relative residual strength in case of different critical lower panels with damage is shown in the figure 8-32 for holes/cracks. It is also assumed that delaminations do not influence the residual strength in tension. So the strength for all these damages is constant. The same data (table 8-30) were also used for holes/cracks in upper panels (compression).

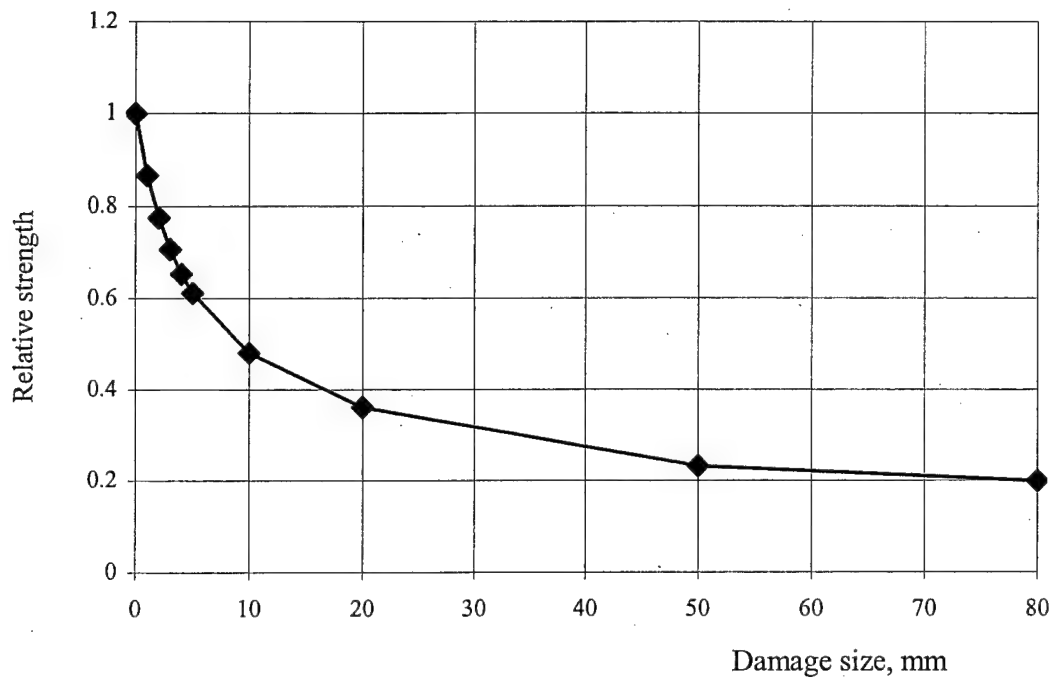


FIGURE 8-31. RELATIVE STRENGTH OF DAMAGED PANEL OF LEAR FAN-2100 WING (Tension panels)

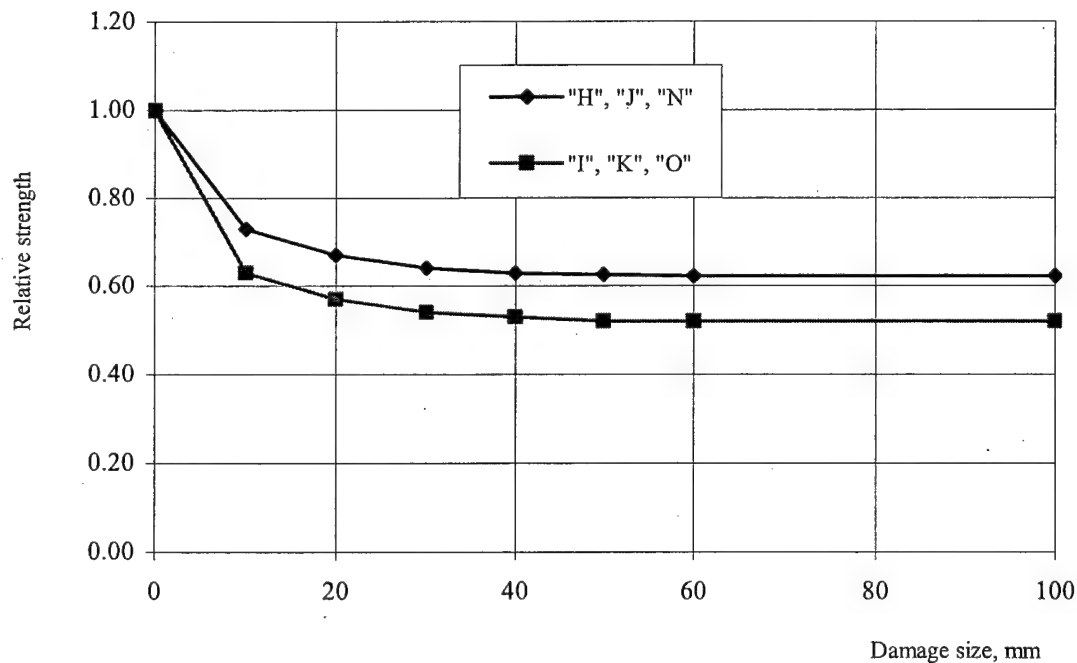


FIGURE 8-32. RELATIVE WING RESIDUAL STRENGTH FOR LOWER SKIN PANELS WITH DAMAGE

### 8.3.7 Probability of Damage Detection.

No information on the probability of damage detection was found in reference 3. It was assumed that two basic methods of inspection are used for each type of damage: preflight visual inspection and some special inspection method applied during maintenance. The latter method is applied ones per each 100 hours of aircraft operation (FAA requirement). Probabilities of damage detection for holes/cracks and delaminations are shown in figures 8-7 and 8-8, respectively.

The reduction of the residual strength of wing having a damaged panel was estimated by the computer program BOX-C. Relative residual strength in case of different critical lower

### 8.3.8 Repairs.

No information concerning the types and effectiveness of repairs prescribed for Lear Fan-2100 is available in reference 3. It was assumed that two basic methods of repair are used for each type of damage: simplified repair applied in airfield conditions and special repair on airline maintenance facility. The latter method is applied if some damage is detected during maintenance (each 100 hours of aircraft operation). The corresponding strength restoration factors and their coefficients of variation for holes/cracks and delaminations are shown in table 2-7. These values were estimated by using the typical data obtained in TsAGI as a result of testing the different repaired composite structures.

### 8.3.9 Lear Fan Wing Box Analysis/Results.

The 12 critical panels of the Lear Fan wing box are presented in tables 8-27 and 8-28 and were utilized along with

- one load case (upbending): combined maneuver + gust induced load spectra (figure 8-22);
- operational damages: damage size spectra (figure 2-7);
- frequency and resolution of two inspection methods: probability of damage detection (see figures 8-7 and 8-8);
- residual strength of damaged structure (figures 8-29 and 8-32);

to obtain ProDeCompoS input file.

The output structural failure risk estimates (probability of failure) for the restricted load factor are presented in the table 8-31 in terms of upper skin risk and lower skin risk for buckling failure mode and tension failure mode, respectively. Noncritical panels contribution to the cumulative risk of wing box is negligible compared to the critical panels.

TABLE 8-31. PROBABILITIES OF FAILURE FOR THE RESTRICTED LOAD FACTOR

| Location   | Failure Mode         |                       | SFPR (Single Flight)  |
|------------|----------------------|-----------------------|-----------------------|
|            | Buckling             | Tension               |                       |
| Panel A    | $5.5 \cdot 10^{-4}$  |                       |                       |
| Panel C    | $1.68 \cdot 10^{-6}$ |                       |                       |
| Panel E    | $9.5 \cdot 10^{-4}$  |                       |                       |
| Panel G    | $5.9 \cdot 10^{-6}$  |                       |                       |
| Panel D    | $2.63 \cdot 10^{-4}$ |                       |                       |
| Panel F    | $2.74 \cdot 10^{-3}$ |                       |                       |
| Panel H    |                      | $<10^{-7}$            |                       |
| Panel J    |                      | $1.0 \cdot 10^{-6}$   |                       |
| Panel N    |                      | $<10^{-7}$            |                       |
| Panel T    |                      | $1.520 \cdot 10^{-6}$ |                       |
| Panel K    |                      | $1.0 \cdot 10^{-6}$   |                       |
| Panel O    |                      | $1.0 \cdot 10^{-7}$   |                       |
| Upper skin | $4.51 \cdot 10^{-3}$ |                       | $3.67 \cdot 10^{-7}$  |
| Lower skin |                      | $3.62 \cdot 10^{-6}$  | $2.94 \cdot 10^{-10}$ |

#### 8.4 SUKHOI SU-29 COMPOSITE WING FAILURE PROBABILITY ESTIMATION.

##### 8.4.1 Airplane Under Consideration.

This estimation is made for aerobatics category one-engine SU-29 airplane having the following main characteristics:

- External dimensions
  - Wing span 8.2 m
  - Length 7.29 m
  - Height Overall from Ground 2.74 m
- Areas
  - Wing  $12.24 \text{ m}^2$
- Weights and thrust
  - Maximum T.O. 1205 kg
  - Empty Weight 735 kg
  - Fuel 260 liters

- Performance

|  |                                 |
|--|---------------------------------|
| - Maximum dive speed $V_D$             | 450 km/hour                     |
| - Limit positive maneuver load factor  | 12.0                            |
| - Limit negative maneuver load factor  | -9.0                            |
| - Safety factor                        | $1.5 \cdot 1.25 = 1.875$        |
| - Service Life                         | 1,000 flight (250 flight hours) |
| - Maximum aerodynamic lift coefficient | 1.26                            |
| - Maximum dynamic pressure             | 976.6 kg/m <sup>2</sup>         |

#### 8.4.2 Spectra Loading.

Cumulative load exceedance curves are used for load spectra characterization in ProDeCompoS. In case of unrestricted normal load factor, initial maneuver spectrum exceedance curves are used as shown in figure 8-33. Two design loading cases are considered for wing: upbending case and downbending case.

The physical limit of aerodynamic lift corresponding to the maximum lift coefficient,  $C_{zmax}$ , is very close to the limit load. The maximum attainable load factor at design weight 1205 kg is equal to L.L.F = 12.5. It may be exceeded only in case of maximum diving speed exceedance. The probability of this event is very small. According to reference 21 the coefficient of variation of maximum speed per life is less than 4%. This was taken into account when the resulting curve (see figure 8-33) was drawn.

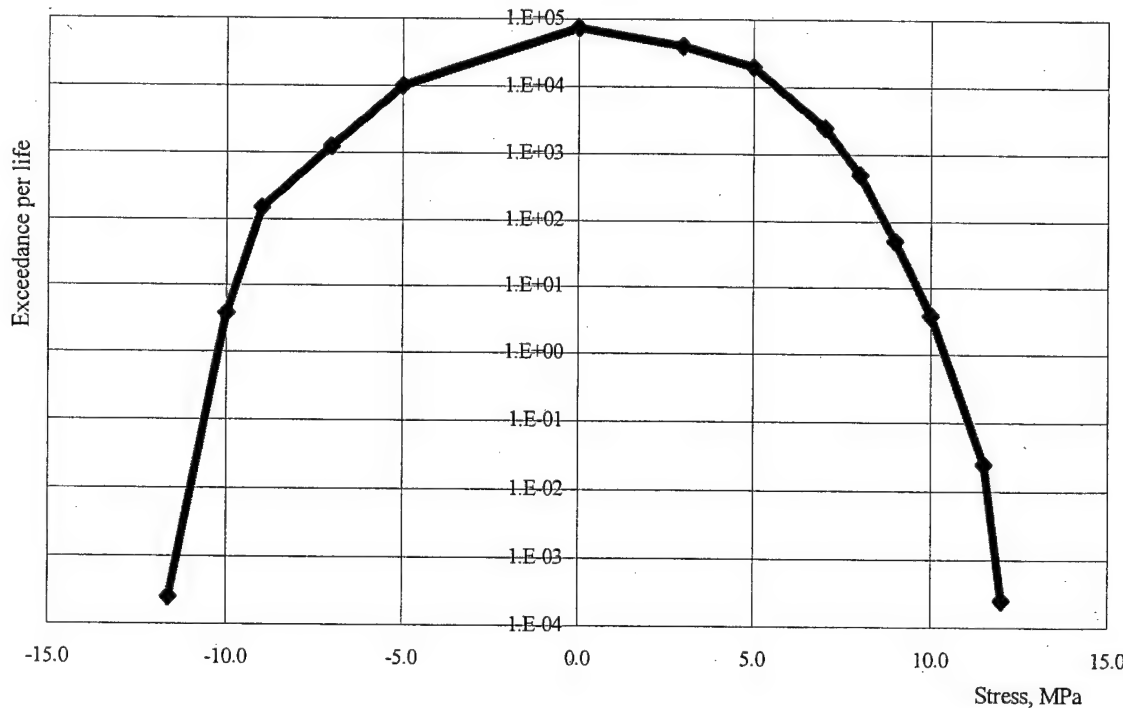


FIGURE 8-33. MANEUVER SPECTRUM EXCEEDANCE CURVE

#### 8.4.3 Critical Areas.

Only upper and lower composite panels of the wing box structure are considered for failure probability estimation. It is considered that the probability of in-service damage for internal spars and ribs is approaching zero. Critical panels located on upper and lower surfaces are assumed to be similar. They are shown in figure 8-34. In this particular example two loading cases and eight panels are considered.

#### 8.4.4 Damage Occurrences.

Information presented in reference 4 is used for estimation of damage frequency of occurrence for critical areas. Damage occurrence curves obtained for wing-fuselage fairing aramide/epoxy honeycomb panels were used. The same strength degradation model as used in ProDeCompoS for cracks and holes was assumed. The resulting cumulative number of occurrences per SU-29 life per  $1 \text{ m}^2$  of external surface of composite structure is shown in table 8-32 and in figure 8-35.

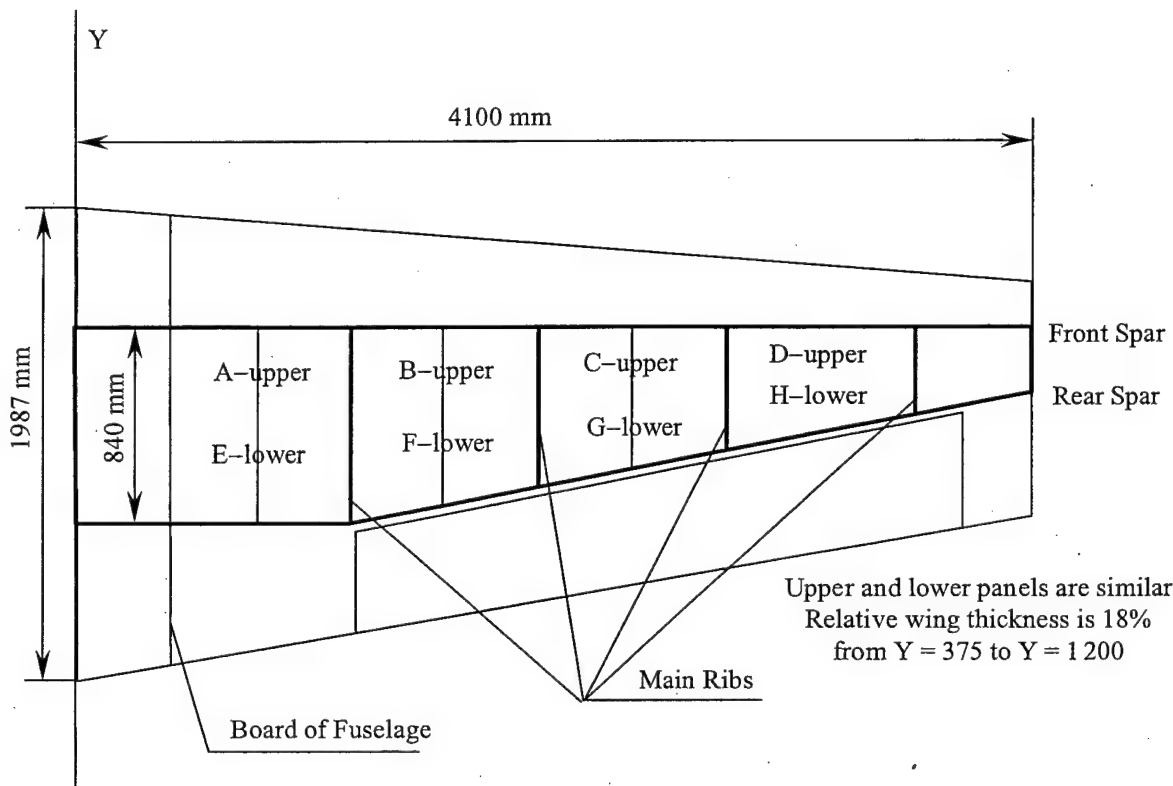


FIGURE 8-34. CRITICAL PANELS ON UPPER/LOWER WING SURFACES

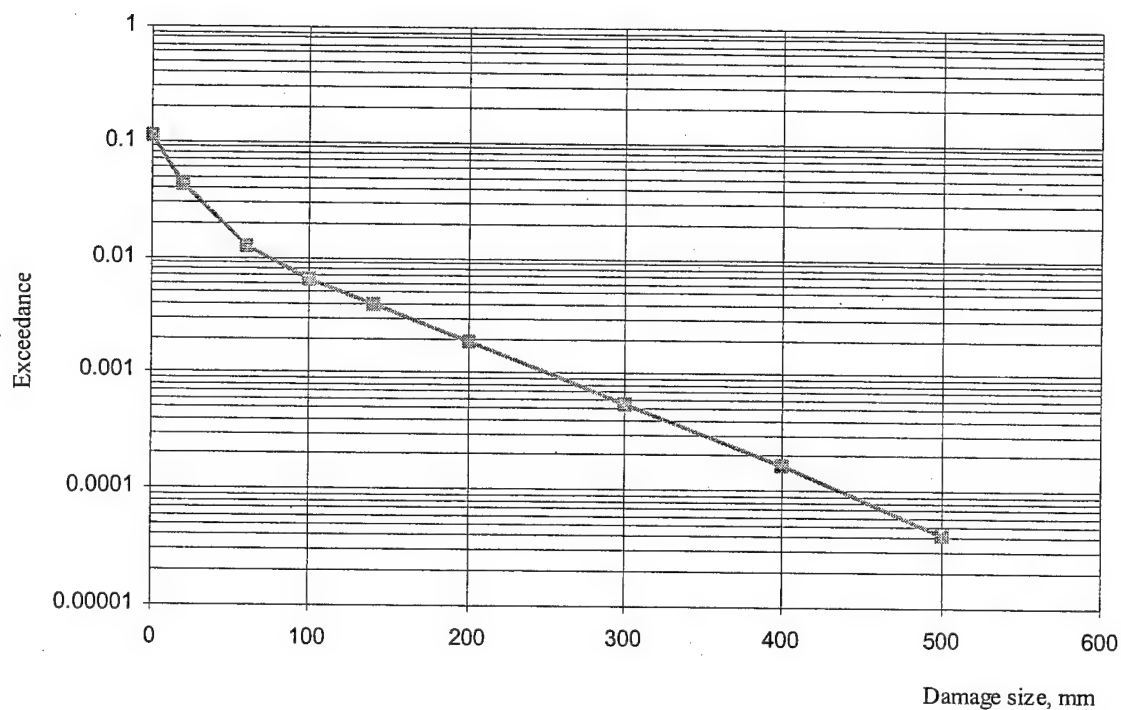


FIGURE 8-35. DAMAGE SPECTRA

TABLE 8-32. CUMULATIVE NUMBER OF OCCURRENCES PER  
250 FLIGHT HOURS PER 1 m<sup>2</sup>

| Damage Size<br>(mm) | Damage Type    |              |
|---------------------|----------------|--------------|
|                     | Holes + Cracks | Delamination |
| 0.0                 | 0.1125         | 0.1125       |
| 20                  | 0.0433         | 0.0433       |
| 60                  | 0.01275        | 0.01275      |
| 100                 | 0.0066         | 0.0066       |
| 140                 | 0.0039         | 0.0039       |
| 200                 | 0.00185        | 0.00185      |
| 300                 | 0.00055        | 0.00055      |
| 400                 | 0.000165       | 0.000165     |
| 500                 | 0.000043       | 0.000043     |

The areas of chosen critical panels are shown in figure 8-36. Cumulative numbers of occurrences per SU-29 life for critical panels are calculated proportionally.

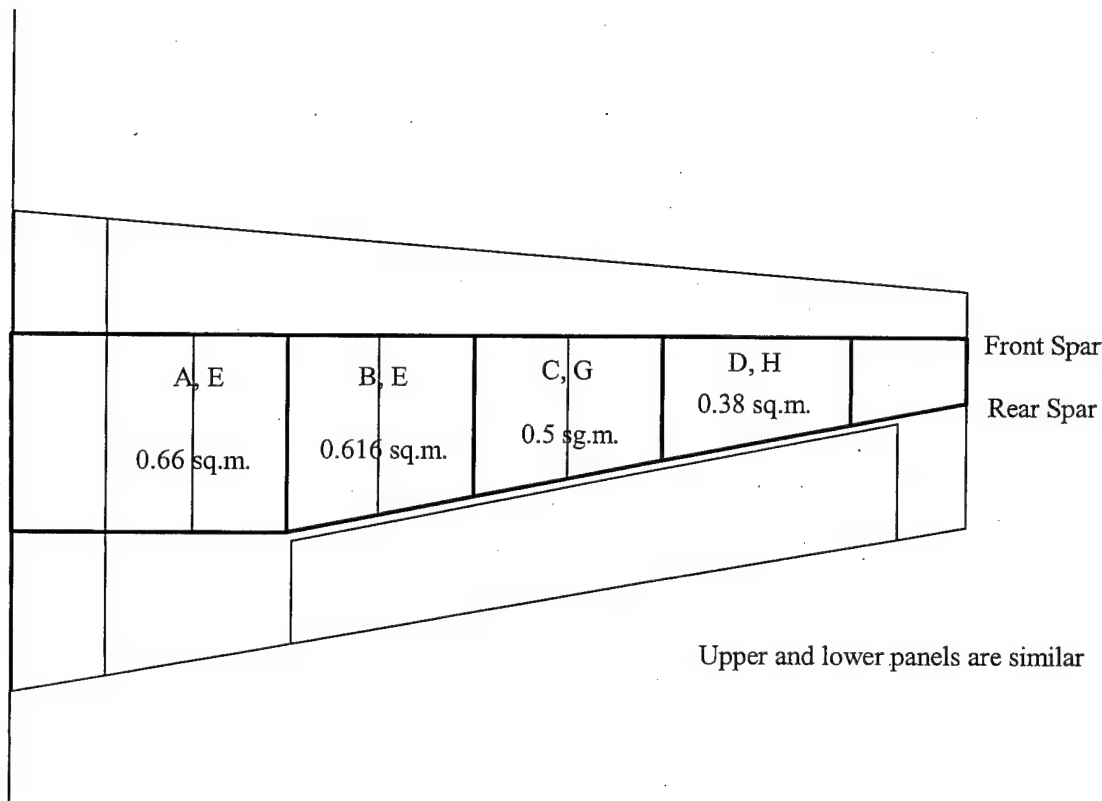


FIGURE 8-36. AREA OF CHOSEN CRITICAL PANELS,  $\text{m}^2$

#### 8.4.5 Residual Strength.

Initial static strength characteristics for critical panels of upper and lower skin were obtained from Sukhoi Design Bureau. It is assumed that for an upbending case, the main failure mode for upper skin is buckling, for lower skin is tension failure and for downbending case they are vice versa.

Both upper and lower panels are of honeycomb structure. The skins are made of the aramide/epoxy material SVM (Russia) and honeycomb core is made of PSP materials (paper Russia).

The properties of skins: Fabric CBM, martix UP-2227 (Organit-10T, Aramide/epoxy SVM/UP-2227). Layup arrangement: [0/90], the number of layers is two. The total thickness of laminate is 0.26 mm.

- Monolayer characteristics

$$\begin{aligned}
 E_1 &= 28\,000 \text{ MPa}, E_2 = 28\,000 \text{ MPa}, G = 3\,000 \text{ MPa}, \nu = 0.33, \\
 \sigma_1^t &= 560 \text{ MPa}, \sigma_1^c = 390 \text{ MPa}, \sigma_2^t = 440 \text{ MPa}, \sigma_2^c = 300 \text{ MPa}, \tau = 70 \text{ MPa}, \\
 \gamma &= 1.25 \text{ g/cm}^3, \delta_m = 0.13
 \end{aligned}$$

- Laminate characteristics

$E_x = 28\ 000 \text{ MPa}$  (exper.  $27\ 700 \text{ MPa}$ ),  $E_y = 28\ 000 \text{ MPa}$ ,  $G = 3\ 000 \text{ MPa}$ ,  $\nu = 0.33$ ,  
 $\sigma_x^t = 440 \text{ MPa}$  (exper.  $45.3 \text{ MPa}$ ),  $\sigma_y^t = 440 \text{ MPa}$ ,  $\sigma_x^c = 300 \text{ MPa}$  (exper.  $29.2 \text{ MPa}$ ),  
 $\sigma_y^c = 300 \text{ MPa}$ ,  $\tau = 70$ ,  $\delta_m = 0.13$

for  $\sigma_x^t \ C_v = 13.4\%$

$\sigma_x^c \ C_v = 15.3\%$

$E_x \ C_v = 5.2\%$ .

- Honeycomb core PSP-2.5, thickness 8 mm,  $G_{xz} = 50 \text{ MPa}$ ,  $G_{yz} = 25 \text{ MPa}$ .

The loading of panels is assumed to be biaxial, which corresponds to the wing upbending with torque, (see figure 8-37). Upper panels are in compression and shear and lower ones are in tension and shear.

A computer program called COMPOSITE package was used for strength prediction. The results are:

- margin of safety for A panel is 0.84;
- margin of safety E panel is 1.5.

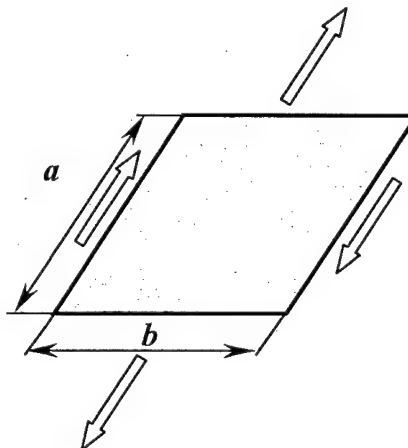


FIGURE 8-37. LOADING OF PANEL

The distribution of margins of safety (MS) for panels is shown in table 8-33. The initial static strength characteristics for four upper skin critical panels are shown in terms of FLF. Here the MFLF for panels are calculated by using the equations 8-3 and 8-4 of example No. 3. The results of the calculation, same for the downbending case, is shown in table 8-34.

TABLE 8-33. FAILURE LOAD FACTOR AND COEFFICIENT OF VARIATION FOR  
UPPER/LOWER WING SURFACE CONDITION—SYMMETRICAL UPBENDING

| Panel ID | Assumed Failure Mode | MS     | MFLF  | $C_v, \%$ | MS/FLF if Buckling is a Failure Mode |
|----------|----------------------|--------|-------|-----------|--------------------------------------|
| A        | Compression          | +1.25  | 40.5  | 15.0      | -0.65/6.3                            |
| B        | Compression          | +1.5   | 45.0  | 15.0      | -0.61/7.0                            |
| C        | Compression          | +1.25  | 40.5  | 15.0      | -0.65/6.3                            |
| D        | Compression          | +1.75  | 49.5  | 150       | -0.57/7.7                            |
| E        | Tension              | +2.125 | 56.25 | 13.0      |                                      |
| F        | Tension              | +2.75  | 67.5  | 13.0      |                                      |
| G        | Tension              | +2.26  | 58.5  | 13.0      |                                      |
| H        | Tension              | +3.5   | 81.   | 13.0      |                                      |

TABLE 8-34. FAILURE LOAD FACTOR AND COEFFICIENT OF VARIATION FOR  
UPPER/LOWER WING SURFACE CONDITION—SYMMETRICAL DOWNBENDING

| Panel ID | Assumed Failure Mode | MS    | MFLF  | $C_v, \%$ | MS/FLF if Buckling is a Failure Mode |
|----------|----------------------|-------|-------|-----------|--------------------------------------|
| A        | Tension              | +3.17 | 56.25 | 13.0      |                                      |
| B        | Tension              | +4.0  | 67.5  | 13.0      |                                      |
| C        | Tension              | +3.33 | 58.5  | 13.0      |                                      |
| D        | Tension              | +5.0  | 81.0  | 13.0      |                                      |
| E        | Compression          | +2.0  | 40.5  | 15.0      | -0.53/6.3                            |
| F        | Compression          | +2.33 | 45.0  | 15.0      | -0.48/7.0                            |
| G        | Compression          | +2.0  | 40.5  | 15.0      | -0.53/6.3                            |
| H        | Compression          | +2.67 | 49.5  | 15.0      | -0.43/7.7                            |

#### 8.4.6 Residual Strength Degradation of Damaged Panels.

##### a. Compression (Shear) Panels

The most critical damage is assumed to be a delamination between the skin and core. A computer program called DELAM was used for residual strength prediction. The results are shown in table 8-35 and in figure 8-38.

TABLE 8-35. RELATIVE RESIDUAL STRENGTH OF UPPER PANEL VS DAMAGE SIZE

| Damage size, mm            | 10  | 20  | 25   | 30    | 50   | 100   |
|----------------------------|-----|-----|------|-------|------|-------|
| Relative residual strength | 1.0 | 1.0 | 0.84 | 0.583 | 0.21 | 0.052 |

With respect to another panels (B, C, D), the same dependencies are assumed.

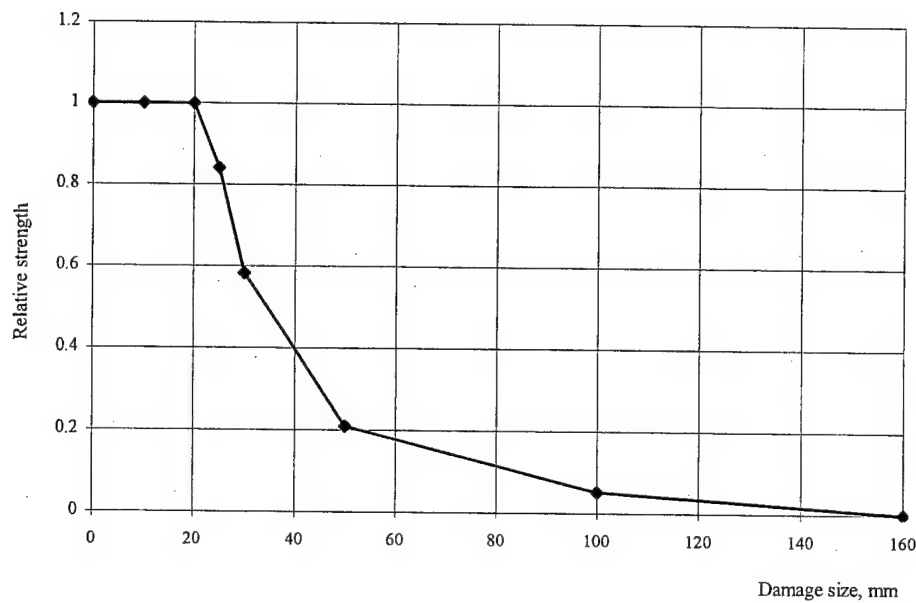


FIGURE 8-38. RELATIVE STRENGTH OF DAMAGED PANELS, SU-29  
(Compression panels)

According to the information received from Sukhoi designer, the SU-29 wing was designed without taking into account the contribution of skins. Therefore, reduction of the panel strength due to damage does not influence the wing load carrying capability. So, if the failure probability is defined as a probability of the loss of wing load carrying capability, it may be assumed that the latter is constant.

b. Panels Under Tension

The most critical damage is assumed to be a round shape through hole of diameter  $D$ , (see figure 8-39). The same assumption as in example of Lear Fan is used here. A computer program called CRACK was used for panel residual strength prediction. The results are shown in table 8-36 and in figure 8-40.

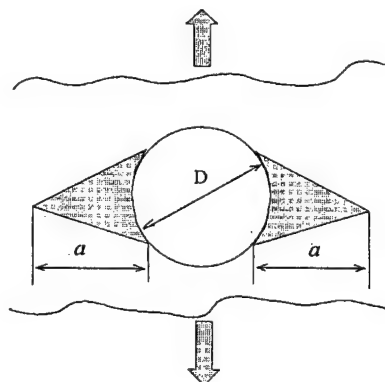


FIGURE 8-39. LOADING OF OPEN-HOLED PANEL

TABLE 8-36. RELATIVE RESIDUAL STRENGTH OF PANEL UNDER TENSION VS DAMAGE SIZE

|                            |       |       |       |       |       |
|----------------------------|-------|-------|-------|-------|-------|
| Damage size, mm            | 1     | 2     | 5     | 10    | 20    |
| Relative residual strength | 0.847 | 0.757 | 0.598 | 0.469 | 0.353 |

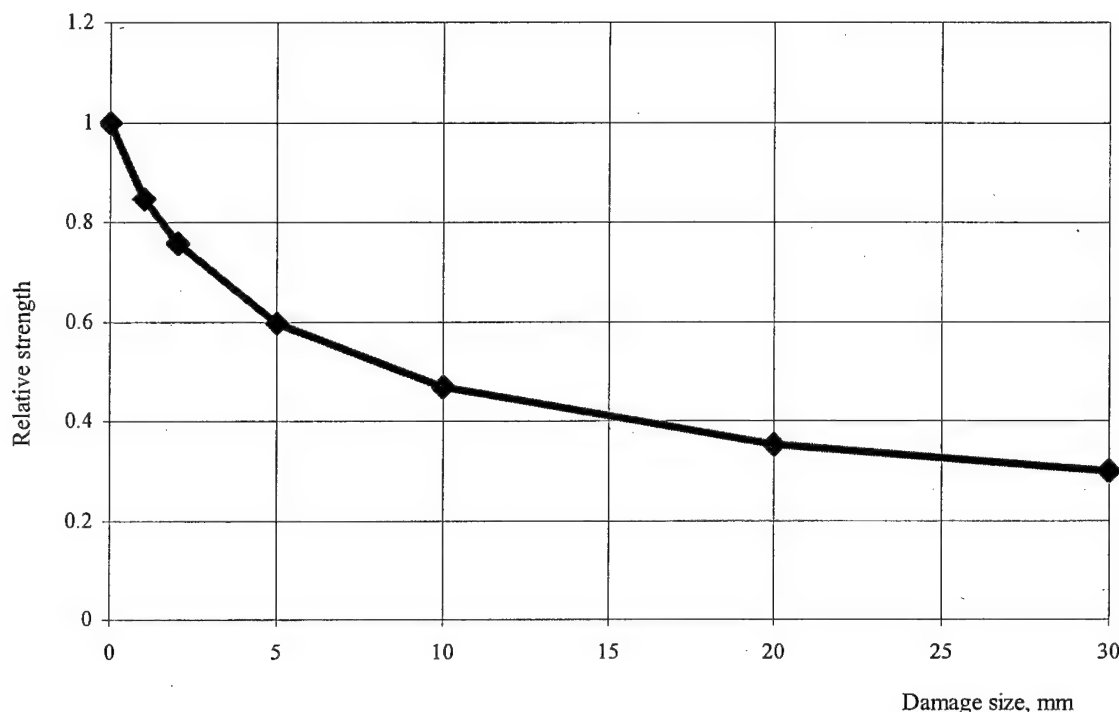


FIGURE 8-40. RELATIVE STRENGTH OF DAMAGED PANEL OF SUKHOI SU-29 COMPOSITE WING (Tension panels)

Wing load carrying capability is also assumed to be independent of the skin panel damage.

#### 8.4.7 Probability of Damage Detection.

It was assumed that the same two methods of inspection (as in first example) are used for each type of damage: preflight visual inspection and some special inspection method applied during maintenance. The latter method is applied once per each 100 hours of aircraft operation. Probabilities of damage detection for through damages and delaminations are shown in figures 8-7 and 8-8, respectively.

#### 8.4.8 Repairs.

It was assumed that two basic methods of repair are used for each type of damage: simplified repair applied in airfield conditions and special repair on airline maintenance facility. The latter method is applied if some damage is detected during maintenance (each 100 hours of aircraft

operation). The corresponding strength restoration factors and their coefficients of variation for holes/cracks and delaminations are in table 2-7.

#### 8.4.9 SU-29 Wing Box Analysis/Results.

The eight critical panels of SU-29 wing box presented in tables 8-33 and 8-34 were used along with:

- two load case (upbending, downbending): maneuver induced load spectra (see figure 8-34),
- operational damages: damage size spectra (see figure 8-36);
- frequency and resolution of two inspection methods: probability of damage detection (see figures 8-7 and 8-8);
- residual strength of damaged structure, to obtain ProDeCompoS input file.

Since the damages are assumed not to influence the wing strength, the structural failure risk is determined by spars, ribs, etc., which are assumed to be protected from in-service damages. The output structural failure risk estimates (conditional probability of undamaged wing failure) are presented in table 8-37, if compression/shear failure mode and tension failure modes are taken into account.

TABLE 8-37. CONDITIONAL PROBABILITIES OF WING SKIN FAILURE

| Location | Failure Mode |         |
|----------|--------------|---------|
|          | Buckling     | Tension |
| Panel A  | 0.028        |         |
| Panel B  | 0.024        |         |
| Panel C  | 0.021        |         |
| Panel D  | 0.013        |         |
| Panel E  |              | 0.028   |
| Panel F  |              | 0.024   |
| Panel G  |              | 0.021   |
| Panel H  |              | 0.013   |

## 9. ESTIMATES OF RELIABILITY OF FAILURE PROBABILITY CALCULATION ON THE BASIS OF STATISTICAL SIMULATION.

Statistical simulation is useful in obtaining quantitative estimates for various problems in engineering. In particular, the method has been used successfully when selecting the design conditions for airframes made of composite materials. The method includes multiple simulation of the aircraft loading process by means, firstly, of a math model of the loading process and, secondly, of determining the failure probability  $\beta \approx h = m_f/m$ , where

$\beta$ —is the failure probability depending on aircraft operation conditions and structural strength

$h$ —is the relative occurrence rate of failure

$m_f$ —is the total number of failure events during the series of numerical experiments

$m$ —is the total number of loading process realizations in the series

In this computation, two kinds of error appear:

1. Errors caused by the finite number  $m$  of realizations in the math model adopted; this is the classical problem in mathematical statistics, and approaches to evaluating the likely deviations  $h$  from  $\beta$  are known.
2. Errors caused by weak points of the very model including the limited amount of the initial statistical data (such as distribution laws of random values; values of essential parameters; the degree of correspondence between the mathematical process and real loading); these problems are not considered in classical statistics and reliability theory and must be resolved by utilizing engineering methods for concrete situations.

### 9.1 ESTIMATE OF FAILURE PROBABILITY COMPUTATION RELIABILITY FOR A PARTICULAR STATISTICAL MODEL.

#### 9.1.1 Confidence Intervals; Determining the Necessary Number of Realizations in Simulation.

The probability (or the extent of risk)  $\beta$  is determined on the basis of  $x_i(t) = P_{maxi}^e - P_i^f$ , where

$x_i \geq 0$  — corresponds to failure in an  $i^{th}$  realization,

$x_i < 0$  — corresponds to absence of failure in the  $i^{th}$  realization,

$P_{maxi}^e$  — is the extreme value of external load, and

$P_i^f$  — is the structural strength.

During simulation, the number  $m_f$  of realizations in which failure occurs is counted first and, secondly, the total number  $m$  of realizations. The relative frequency,  $h = m_f/m$ , is the unbiased estimate of  $\beta$  as for a random event with two possible results. The number  $m$  is finite, and  $h$  is a

random value with asymptotically ( $m \rightarrow \infty$ ) normal distribution with the following parameters:

the mean value  $\bar{h} = \beta$ , dispersion  $\sigma_h^2 = \frac{\beta(1-\beta)}{m}$ .

In this case, it does not matter what is the origin of the random value  $x_i$ ; of importance is only the fact that there exists statistical stability which is ensured by constancy of the set of factors, which takes place in the simulation. This means that the general population of random value  $x_i$  exists; and their set of realizations is a random sample with the extent  $m$ .

This is the basis for establishing the confidence interval for a particular confidence level (that is, the probability of the random quantity  $h$  being in the confidence interval) depending on the total number of realizations during statistical simulation. Consider hereafter the two-sided confidence interval symmetric with respect to the general mean value and corresponding to the confidence interval  $\bar{\alpha} = 1 - \alpha$ :

$$\Delta\beta = \beta_2 - \beta_1 = 2U_{1-\alpha/2} \cdot \sigma_h = 2U_{1-\alpha/2} \cdot \sqrt{\frac{\beta(1-\beta)}{m}}$$

where  $U_p$  is the quintile of the normal distribution with zero mean and unit dispersion (root mean square deviation). This provides the confidence interval:

$$\Delta\beta = \beta_2 - \beta_1 = 2U_{1-\alpha/2} \cdot \sigma_h = 2U_{1-\alpha/2} \cdot \sqrt{\frac{\beta(1-\beta)}{m}}$$

For a prescribed confidence level  $\alpha$  is a function of the general mean value  $\beta$  and the total number of realizations  $m$ . The relative error is

$$\frac{\Delta\beta}{\beta} = 2U_{1-\alpha/2} \cdot \sqrt{\frac{1-\beta}{\beta \cdot m}} \quad \text{or} \quad m = \frac{4 \cdot U_{1-\alpha/2}^2 (1-\beta)}{\left(\frac{\Delta\beta}{\beta}\right)^2 \cdot \beta}$$

In computing the failure probability the error in  $\beta$  is not required to be very small. Deviations by a factor of 1.5 or 2 would be suitable; an essential deviation for  $\beta$  is one order of magnitude. Therefore, to determine  $m$ , it suffices to adopt  $\Delta\beta/\beta \leq 0.5$ . Note also that the exact value of the general mean,  $\beta$ , is unknown. In the case of simulation in accordance with the loading simulation method of, the mean value,  $\beta$ , is estimated preliminarily on the basis of a finite number of realizations; the number, the prescribed accuracy in  $\Delta\beta/\beta$ , and the confidence level  $\bar{\alpha}$  dictate the necessary number  $m$  which is obeyed in the final computation.

For example, assume  $\bar{\alpha} = 0.9$ ;  $\Delta\beta/\beta = 0.5$ ; and  $\beta \sim 0.0015$ . Calculation provides

$$m \approx 16 \cdot (1.64)^2 \frac{0.9985}{0.0015} \approx 28646. \text{ And at } \bar{\alpha} = 0.95, m \approx 40915.$$

### 9.1.2 Establishing the Parameters of Probabilistic Model.

Statistical simulation of fracture of a composite aircraft is based on determination of random quantities,  $P_{max}^e$  and  $P_i^f$ , that have some prescribed distribution functions,  $\Phi_{max}(x) = e^{-F_t(x) t}$  and  $\Phi_f(x)$ , over a certain temporal (in-service) interval  $\Delta t$ ; here,  $F_t(x)$  is the load exceedance per operation hour.

- The function of distribution of failure loads,  $\Phi_f(x)$ , is established upon analyzing statistical data on testing of specimens, structural components, and full-size airframes. As for structures made of metallic materials, the amount of test data is rather great; and parameters of the function  $\Phi_f(x)$  can be evaluated reliably. However, for composite structures the extent of systematized statistical data is much less, so the statistical simulation relies upon two distribution functions—the normal (Gaussian) law and the Weibull distribution; their parameters are defined on the basis of suitable materials. Using various functions,  $\Phi_f(x)$ , provides differing values of  $\beta$ . For example, for the SU-29 airplane the values of failure probability are presented in table 9-1.

TABLE 9-1. CALCULATED FAILURE PROBABILITIES USING DIFFERENT DISTRIBUTION PROPERTIES FOR COMPOSITE MATERIAL STRENGTH

| Kind of analysis                          | Normal   | Weibull  |
|---|----------|----------|
| Analysis for intact structure             | 0.001336 | 0.005312 |
| Simulation allowing for in-service damage | 0.001421 | 0.005356 |

The distribution parameters, normal and Weibull, have been determined on the basis of testing of airplane wing structure elements ( $\gamma_f = 0,15$ ). The less the  $\gamma_f$  values, the more notable the relative difference. The failure probability included in table 9-1 is the mean value for ten sets of analyses in accordance with the simulation algorithm implemented in ProDeCompoS. Values corresponding to the various distribution laws differ by a factor of about 4. This is a difference which cannot be neglected. In addition, it must be taken into account that current theories on composites do not provide substantiation of the type of distribution function  $\Phi_f(x)$ ; so the analyses should be conducted for the two types of distribution, and thereafter the distribution parameters must be refined as additional strength test data become available.

- The distribution function for extreme loads,  $\Phi_{max}(x) = e^{-F_t(x) t}$ , is determined through exceedance of external loads  $F_t(x)$  per flight hour. The most reliable method for deriving the load  $F_t(x)$  exceedance curves is to use measured loads from regular and test flights. The load exceedance is known to depend, first of all, on allowable in-service conditions; therefore, the data can be generalized for airplanes of various classes. However, there appears to be the following errors in defining  $F_t(x)$  for new designs:

- the generalized exceedance curves do not allow for individual features of the new design; these can only be evaluated upon a first stage of real operation;
- the external load exceedance curves may be derived from results of testing within the allowable loads:  $P^e < P_{reg} \approx P^{lim}$ , where  $P^{lim}$  is the standardized limit load (figure 9-1).

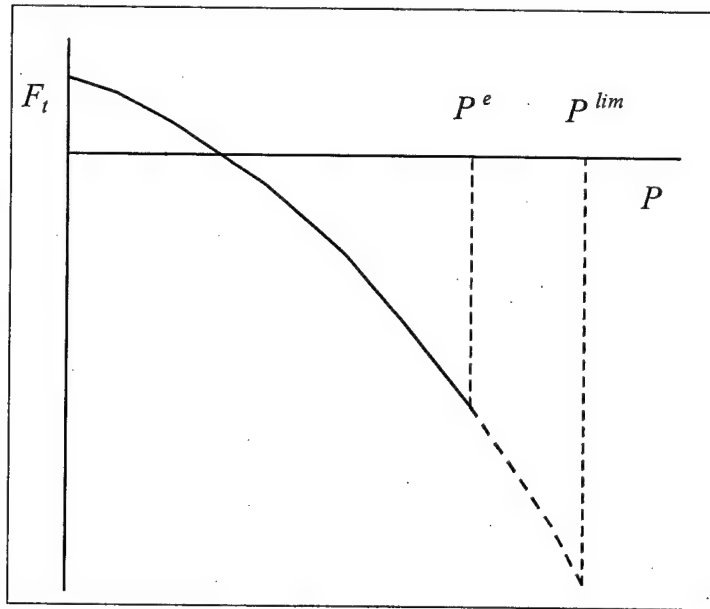


FIGURE 9-1. LOAD EXCEEDANCE CURVE

It is known that the failure probability  $\beta$  is mainly governed by the high loads which are comparable with or higher than  $P^{lim}$ ; therefore, the  $F_t(x)$  curves have to be extrapolated to the larger loads. This also means that it is not reasonable to use the usual criteria when selecting an theoretical distribution function describing the extreme loads. Rational methods for extrapolating  $F_t(x)$  for various loads have been proposed in reference 20 on the basis of experimental data.

- The maneuvering loads (and load factors) for airplanes with manual control are:

$$F_t(x) = -\frac{a}{t_{serv}} \cdot \ln \left[ \Phi \left( \frac{x/n_{lim} - 1}{\gamma} \right) \right]$$

where  $t_{serv}$  – is the airplane service life expressed in hours,

$a$  – is the matching multiplier chosen so that the experimental points for maximum loads be on the extrapolated portion of the curve,

$\Phi$  – is the normal distribution function,

$n_{lim}$  – is the limit load factor stated in Operations Manual for the airplane, and

$\gamma \approx 0,07$  – is the variance coefficient for the extreme loads near  $n_{lim}$ .

- The maneuvering loads for airplanes with automatic control systems ensuring  $P^{lim}$  is not to be exceeded. The extrapolation for this case is shown in figure 9-2.

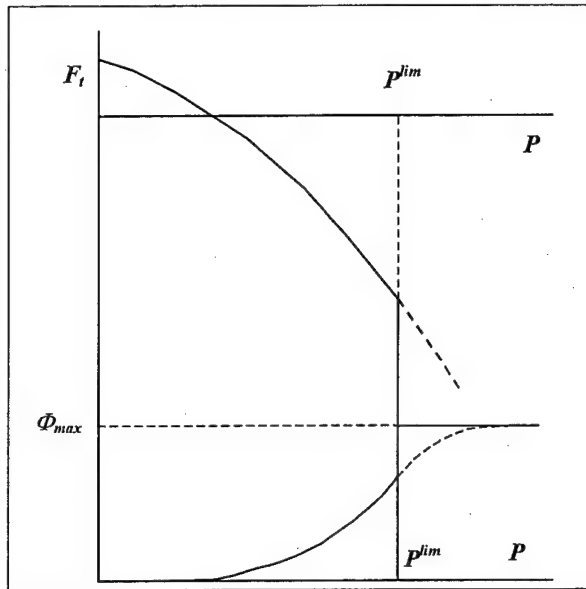


FIGURE 9-2. LOAD EXCEEDANCE CURVE WITH EXTRAPOLATION  
WHEN  $P^{lim}$  CANNOT BE EXCEEDED

- Occurrence rate curves for effective wind gusts should be extrapolated to the limiting values of  $W_{eff}$ . If  $W_{eff} \geq W$ , then adopt  $F_L(x) \rightarrow 0$ .

Numerical estimates demonstrate that errors associated with which statistical model is adopted are greater than errors caused by the finite number of realizations during simulation. These errors could be reduced by:

- improving the model,
- resorting to more appropriate extrapolation of load occurrence rate curves, and
- choosing the distribution function for strength of composite aircraft structures.

## 9.2 RELIABILITY OF FAILURE PROBABILITY COMPUTATION TAKING INTO ACCOUNT OF VARIATIONS IN PARAMETERS OF STATISTICAL MODEL.

### 9.2.1 Scatter Caused by Selection of the Initial Value for Beginning the Simulation.

To determine the failure probability of the structure, the total number of iterations is specified at the initial simulation stage—prior to the first failure of the structure. Data from this stage are

used to estimate the necessary number of structural lives to be simulated for obtaining the failure probability at a prescribed accuracy. The initial values for simulation are taken at random; therefore, the estimated numbers of the necessary number of structural lives will also be random, as will the final probability. To estimate the statistical parameters of the simulation module, a series of 1000 analyses of failure probability was carried out at a certain accuracy and constant initial data. The results are presented in table 9-2.

TABLE 9-2. MEAN VALUES AND STANDARD DEVIATIONS OF FAILURE PROBABILITIES

| Accuracy | Mean Value | Standard Deviation | Variation |
|----------|------------|--------------------|-----------|
| 0.223    | 0.0130     | 0.0037             | 28%       |
| 0.0223   | 0.0122     | 0.00013            | 1.1%      |

Figure 9-3 shows the cumulative distribution function for the failure probability; here, normal distribution axes are assumed.

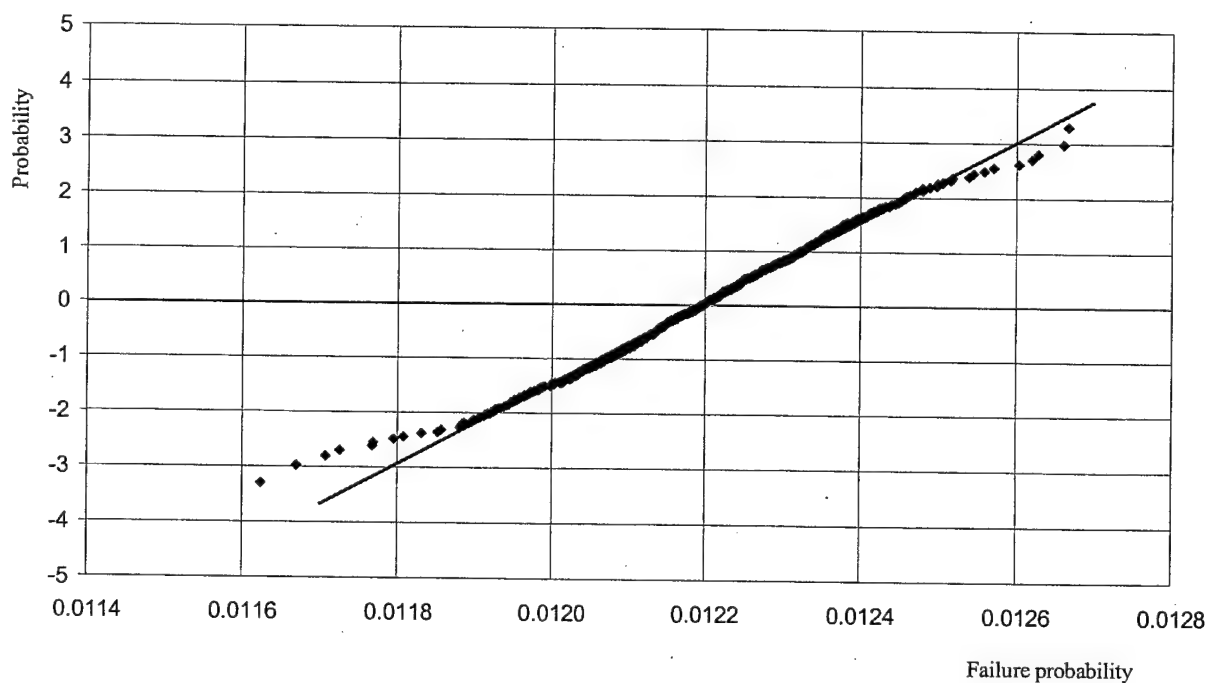


FIGURE 9-3. CUMULATIVE DISTRIBUTION FUNCTION OF THE FAILURE PROBABILITY DUE TO UNCERTAINTY IN INITIAL VALUE FOR SIMULATION

Shape of the functions in figure 9-3 confirms the conclusion that the failure probability calculated by ProDeCompoS is Gaussian distribution. The calculation shown was at the allowable error of 0.0223.

### 9.2.2 Variability in Failure Probability Due to Uncertainty in Load-Stress Transfer Coefficient.

The occurrence rates of the load factors at the airplane center of gravity are obtained during operation of the airplane or its predecessor. The load factors are multiplied by a coefficient that transfers the load factor into stresses for the structural zones under study. The load-stress transfer coefficient is derived by either the finite-element analyses or strain measurement during full-size structure test. Thus, the error in load-stress computation is directly related to errors inherent in the methods adopted to determine these transfer coefficients. By experts' estimation, the error of the methods is around 10%. Therefore, the further simulation was based on the assumption that the load-stress transfer coefficient is a random quantity featuring the uniform distribution over the range from 0.9 to 1.1 of the mean value. This means that basic loads were multiplied by a random value uniformly distributed between 0.9 and 1.1; and the occurrence rates were unchanged.

The variation was carried out 100 times. The distribution of failure probability obtained has the following characteristics: the mean value of 0.0125, the dispersion of 0.00214, and the variance coefficient of 17%. Figure 9-4 demonstrates realizations of the random load-stress transfer coefficient and the respective normalized failure probability (failure probability divided by the mean value).

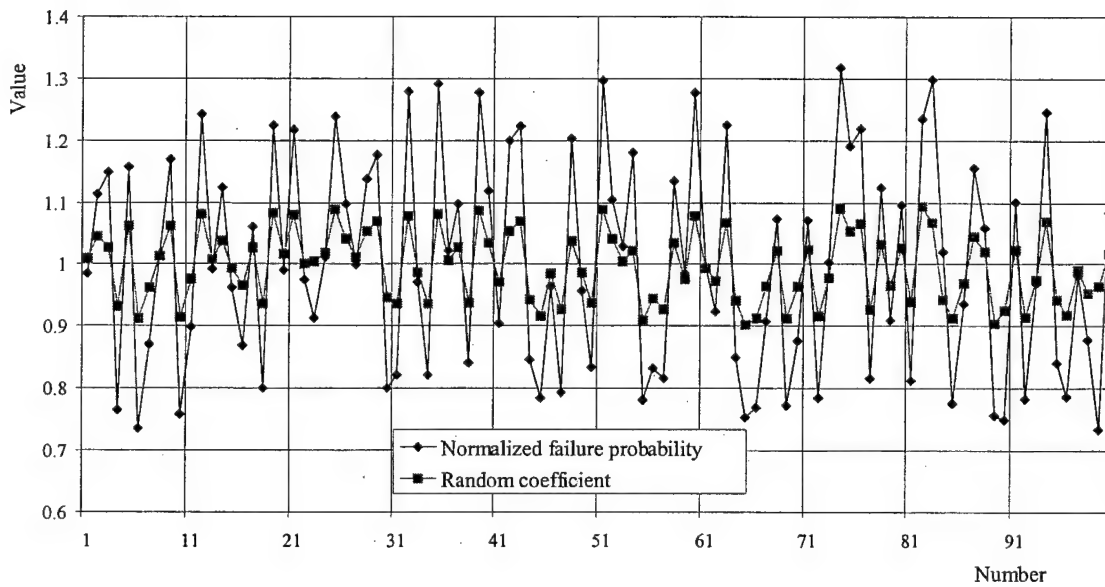


FIGURE 9-4. RANDOM LOAD-STRESS TRANSFER COEFFICIENT AND ITS RESPECTIVE FAILURE PROBABILITY VS NUMBER OF THE REALIZATION

Figure 9-5 depicts dependence of the failure probability mean value on the load-stress transfer coefficient which is the multiplier for loads in the load-occurrence rate function. To evaluate the dependence, the coefficient was specified from 0.8 to 1.2 in increments of 0.05. At each value, ten analyses were conducted, and their results were the basis for computing the failure probability mean values. The function is nonlinear because the greater load decreases the critical damage size (nonlinear), whereas the decrease in the size increases the damage occurrence probability.

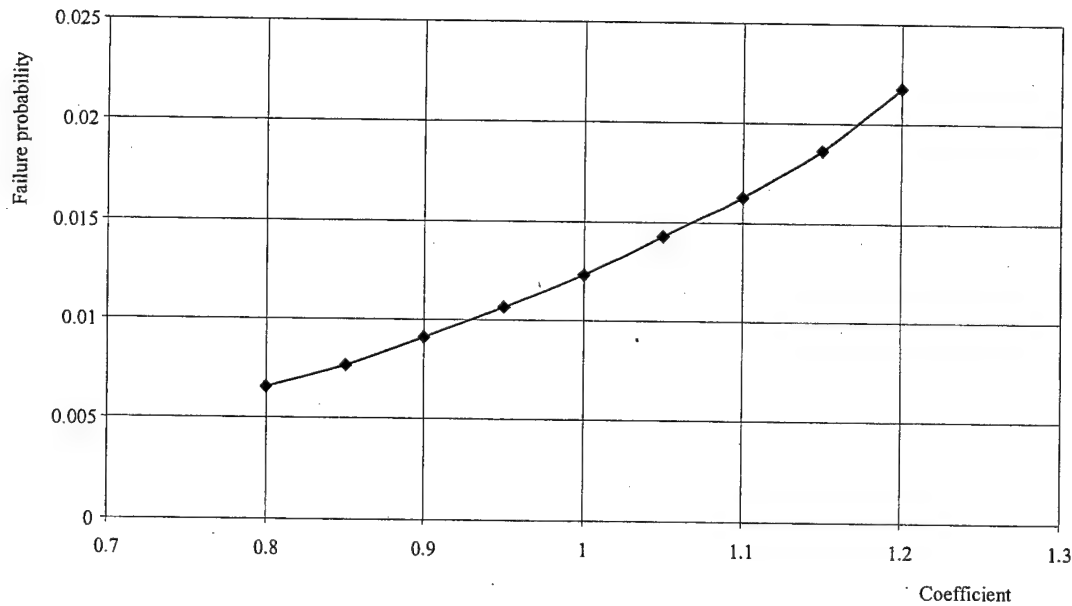


FIGURE 9-5. RELATIONSHIP BETWEEN FAILURE PROBABILITY AND LOAD-STRESS TRANSFER COEFFICIENT

Figure 9-6 shows the relationship between the failure probability and load-stress transfer coefficient.

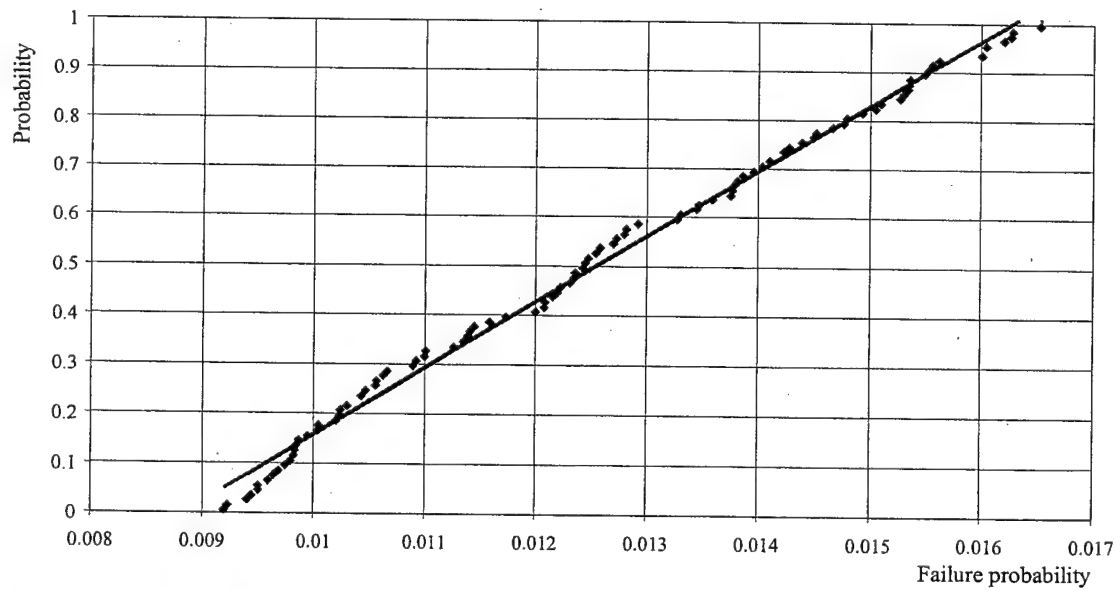


FIGURE 9-6. CUMULATIVE DISTRIBUTION FUNCTION OF FAILURE PROBABILITY DUE TO UNCERTAINTY IN LOAD-STRESS TRANSFER COEFFICIENT

Figure 9-6 dependence was approximated with a linear function on the basis of the Least Squares Method. The correlation coefficient,  $r^2$ , for the failure probability realization and the linear approximation is 0.995. This could be due to the fact that over the 0.9-1.1 interval, the relation of the failure probability to the load-tress conversion coefficient is almost linear (see figure 9-5),

whereas the failure probability scatter at a fixed load-occurrence rate is insignificant as compared with the variation in the case of loads being changed over the interval mentioned. The empirical data were checked out for their correspondence to the uniform distribution by using the  $n\omega^2$  criterion; it turns out that the hypothesis cannot be rejected if the significance level  $\alpha$  is higher than 0.1. The above considerations make it possible to conclude that, with the assumption about the load occurrence rate variation model, the failure probability distribution is uniform.

### 9.2.3 Variability in Failure Probability Due to Uncertainty in the Structural-Size Coefficient.

The damage occurrence rate is determined by processing the in-service data on damages per unit time (such as an hour or the service life) per unit surface area. ProDeCompoS multiplies the rate by the area of the structural zone for which the failure probability is computed. Dimensions of the zone are established by finite-element methods, and the error is about 10%, as mentioned in description of load occurrence rate variability. The structural-size coefficient is defined as a multiplier to the dimensions of a structural zone (or area) uniformly distributed between 0.9 and 1.1.

The variation was carried out 200 times. The distribution obtained has the following characteristics: the mean value of 0.0122, the dispersion of 0.000458, and the variance coefficient of 3.8%. Figure 9-7 demonstrates realizations of the random structural-size coefficient and the corresponding normalized failure probability (failure probabilities divided by the mean value).

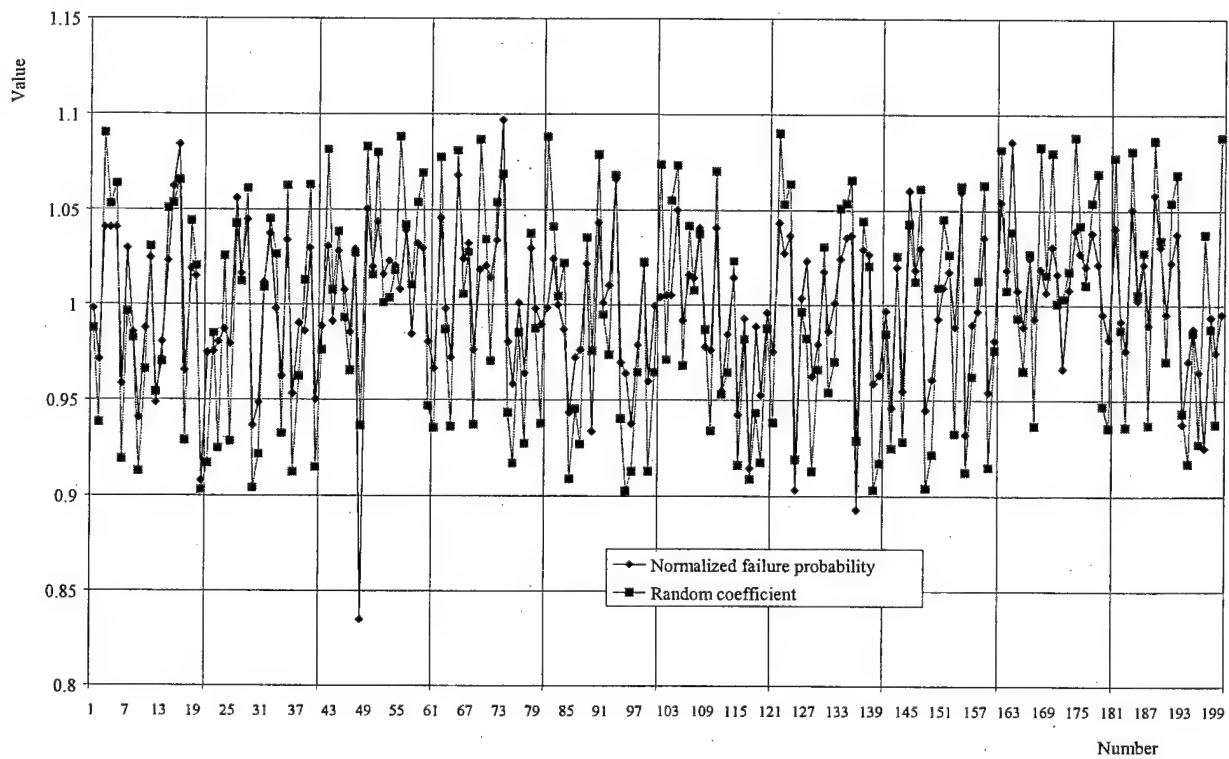


FIGURE 9-7. RANDOM STRUCTURAL-SIZE COEFFICIENT AND ITS RESPECTIVE FAILURE PROBABILITY VS NUMBER OF THE REALIZATION

Figure 9-8 depicts dependence of the failure probability mean value on the structural-size coefficient which is the multiplier for occurrence rates in the damage size/occurrence rate function. The dependence is plotted in the same way as the one in figure 9-4. The linear function is a natural result here, because the failure probability at a certain value of the size coefficient (in accordance with the failure model used) must be proportional to the product of the coefficient and the probability at the basic occurrence rate of damage sizes.

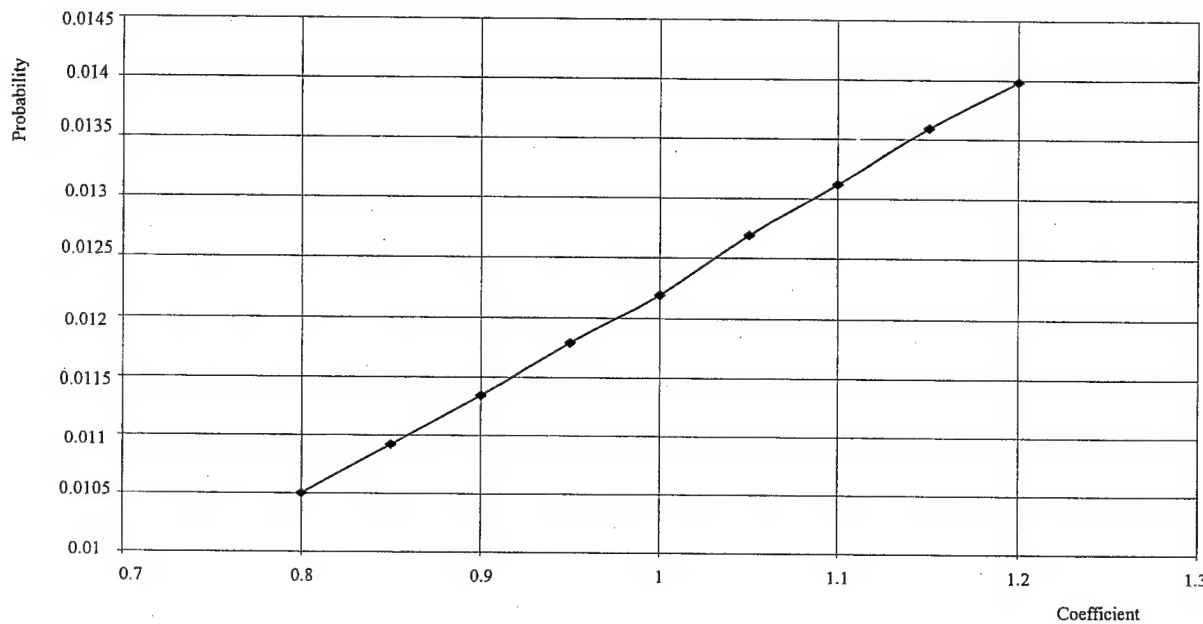


FIGURE 9-8. RELATIONSHIP BETWEEN FAILURE PROBABILITY AND STRUCTURAL-SIZE COEFFICIENT

Figure 9-9 shows the failure probability at uniform division of axes, and figure 9-10 represents the same function in normal axes.

The functions of figures 9-9 and 9-10 were approximated with linear functions by using the Least Squares Method. The correlation coefficient,  $r^2$ , for the failure probability realization and the linear approximations is 0.951 and 0.992 for the uniform and normal divisions. In the beginning, section 8 explains that the failure probability calculated by ProDeCompoS at a fixed occurrence rate of the damage size is Gaussian distribution. If one can take into account this circumstance and the features of the influence of the damage size/occurrence rate variation on the probability, then the strict conclusion is that the failure probability distribution at the assumptions on distribution of the random coefficient must be a mix of normal distributions with uniformly distributed values of parameters. However, the damage size occurrence rate varies within a rather narrow interval; figure 9-10 empirical distribution may well be approximated with the normal function. By utilizing the Anderson-Darling criterion, the normal distribution hypothesis does not contradict the sample at the significance level  $\alpha = 0.111$ .

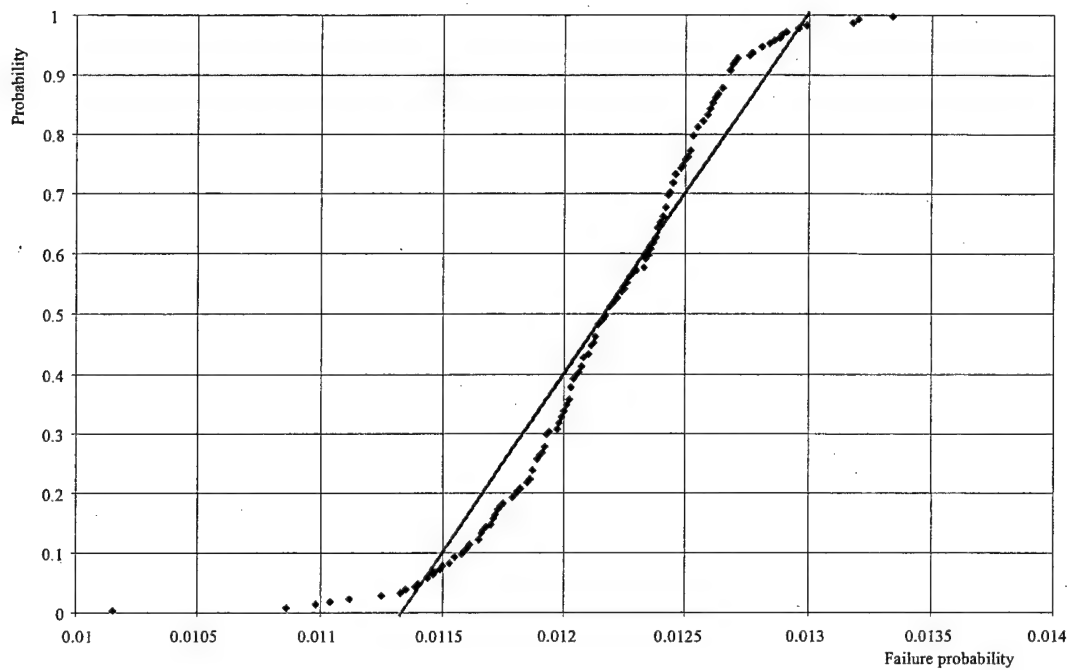


FIGURE 9-9. CUMULATIVE DISTRIBUTION FUNCTION OF FAILURE PROBABILITY DUE TO UNCERTAINTY IN STRUCTURAL-SIZE COEFFICIENT  
(Uniform probability scale)

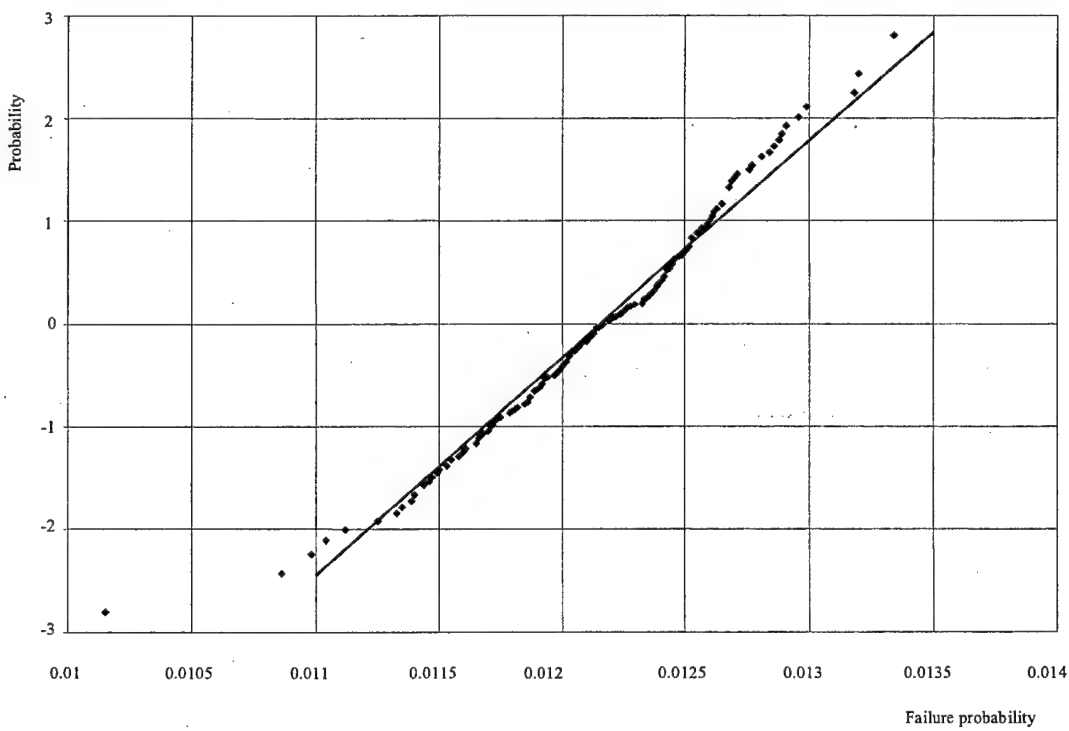


FIGURE 9-10. CUMULATIVE DISTRIBUTION FUNCTION OF FAILURE PROBABILITY DUE TO UNCERTAINTY IN STRUCTURAL-SIZE COEFFICIENT  
(Normal probability scale)

#### 9.2.4 Variability in Failure Probability Due to Uncertainty in Static Strength.

Static strength is usually determined by experiments with a set of specimens, and it is a random quantity. Its variability depends on the total number of test specimens. Static strength is assumed to have a normal distribution. Therefore, the coefficients for multiplying the basic values of static strength were established as realizations with a Gaussian distribution whose parameters are 1 and  $\gamma/\sqrt{n}$ , where  $\gamma$  is the static strength variance coefficient and  $n$  is the total number of specimens tested. The present research was based on assumption that static strength is determined by testing ten specimens.

The variation was carried out 100 times. The distribution obtained has the following characteristics: the mean value of 0.0123, the dispersion of 0.00124, and the variance coefficient of 10%. Figure 9-11 demonstrates realizations of the random coefficient (with the normal distribution) and the corresponding normalized failure probability (failure probabilities divided by the mean value).

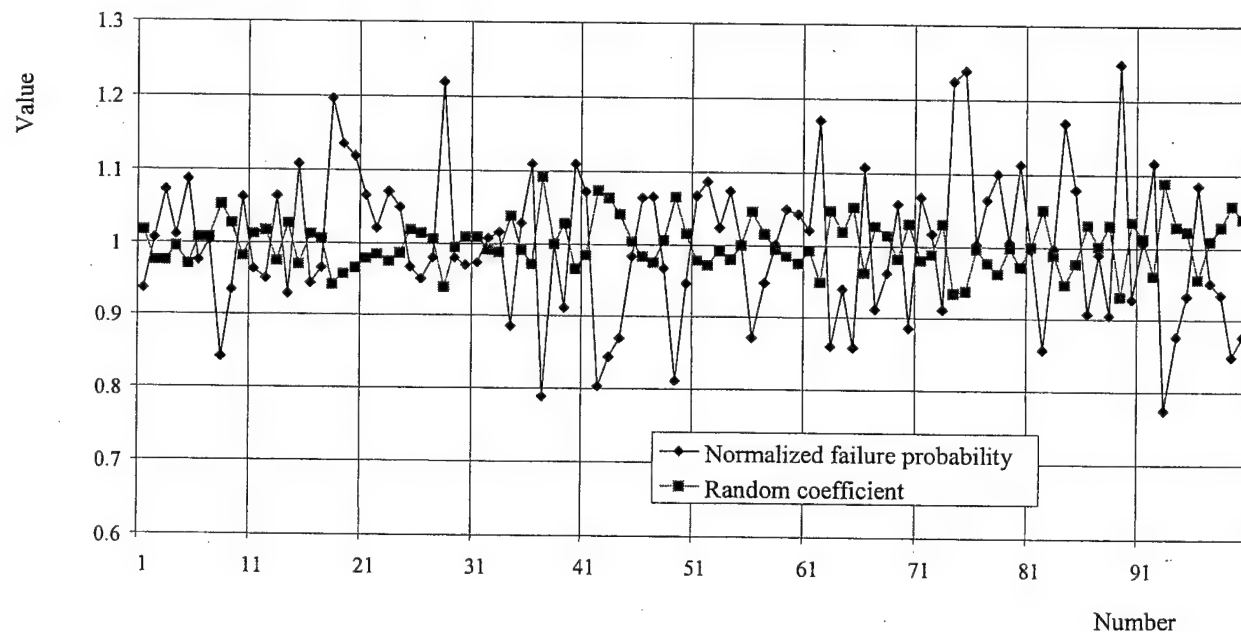


FIGURE 9-11. RANDOM STATIC-STRENGTH COEFFICIENT AND THE RESPECTIVE FAILURE PROBABILITY VS NUMBER OF THE REALIZATION

Figure 9-12 depicts dependence of the failure probability on the static-strength coefficient which is the multiplier for static strength in the damage size/residual strength function. The dependence is determined in the same way as that in figure 9-5.

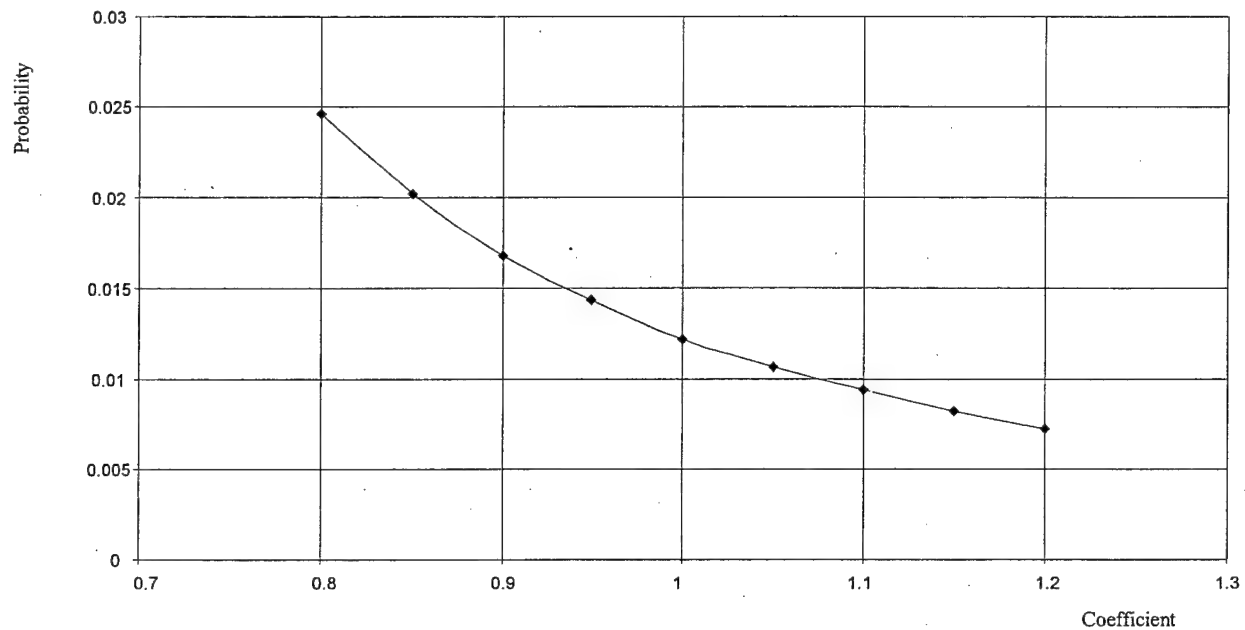


FIGURE 9-12. RELATIONSHIP BEWTEEN FAILURE PROBABILITY AND STATIC-STRENGTH COEFFICIENT

Figure 9-13 shows the failure probability at uniform division of axes and figure 9-14 represents the same function in normal axes.

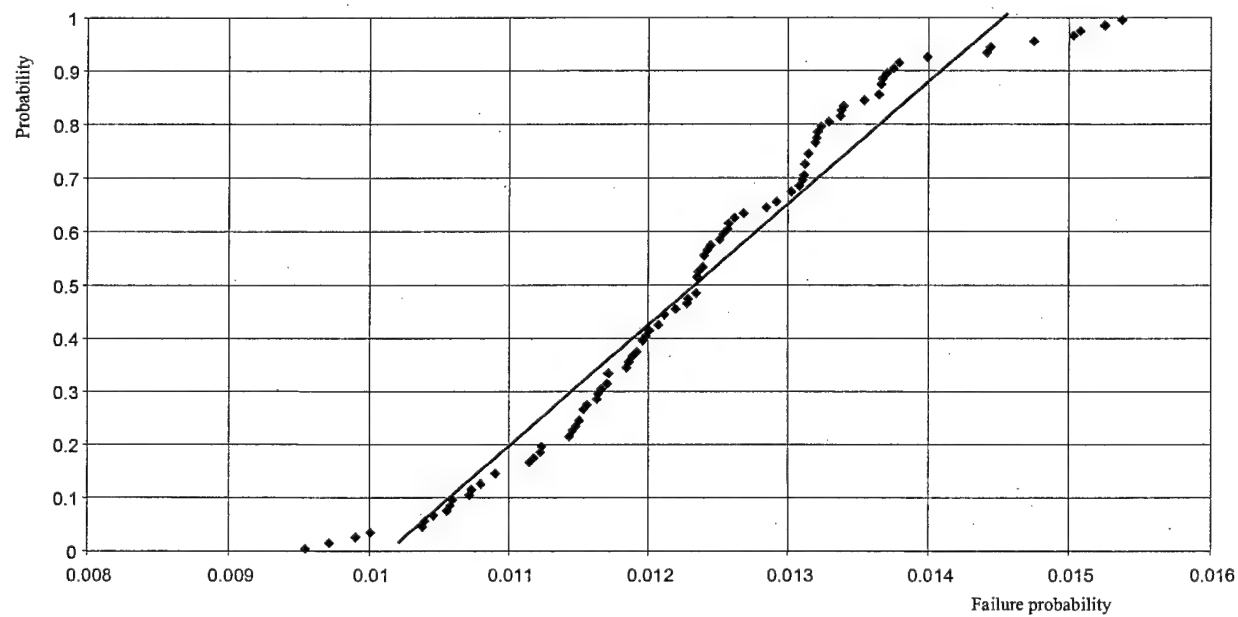


FIGURE 9-13. CUMULATIVE DISTRIBUTION FUNCTION OF FAILURE PROBABILITY DUE TO UNCERTAINTY IN STATIC-STRENGTH COEFFICIENT  
(Uniform probability scale)

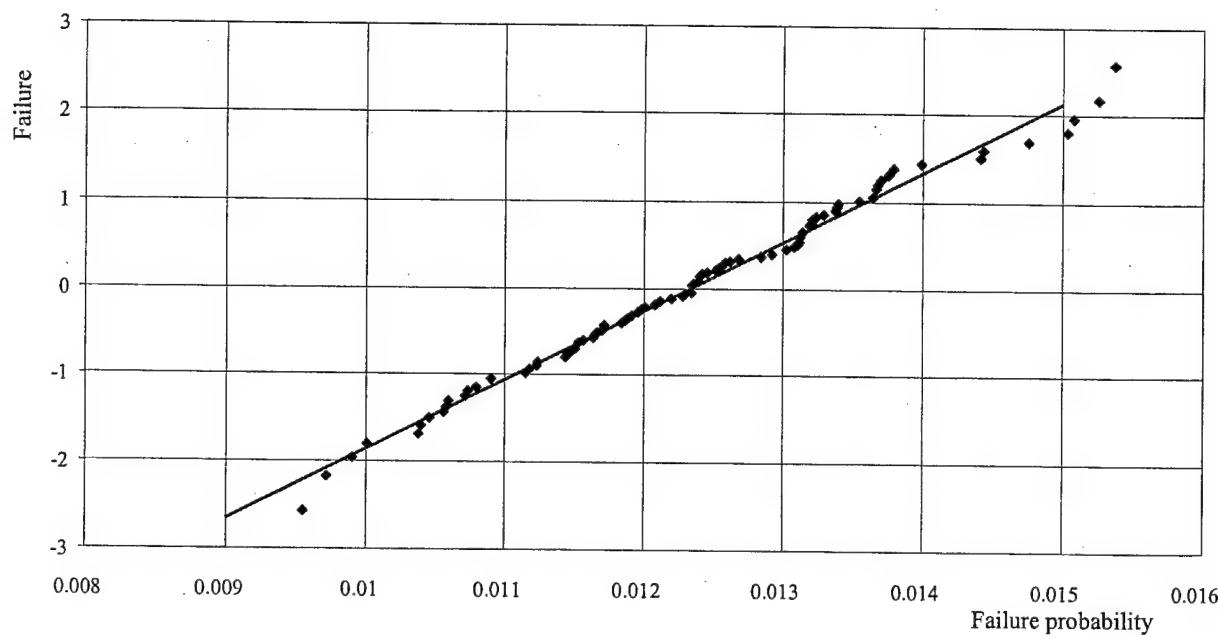


FIGURE 9-14. CUMULATIVE DISTRIBUTION FUNCTION OF FAILURE PROBABILITY DUE TO UNCERTAINTY IN STATIC-STRENGTH COEFFICIENT  
(Normal probability scale)

The functions shown in figures 9-13 and 9-14 were approximated with linear functions by using the Least Squares Method. The correlation coefficient,  $r^2$ , for the failure probability realization and the linear approximations is 0.95 and 0.99 for the uniform and normal divisions, respectively. Since the distribution of the multiplier for basic strength is normal, the generalized distribution of failure probability must also be normal as a mix of normal distributions with the uniformly distributed mean value and identical dispersion values. On the basis of the Anderson-Darling criterion, the normal distribution hypothesis does not contradict the sample at the significance level  $\alpha = 0.573$ .

#### 9.2.5 Variability in Failure Probability Due to Uncertainties in the Coefficients of Load-Stress Transfer, Structural Size, and Static Strength.

The failure probability was computed 100 times, simultaneously varying the coefficients for load-stress transfer, structural size and static strength. The sample obtained shows the following characteristics: the minimum of 0.00804, the maximum of 0.01745, the mean value of 0.01241, the standard deviation of 0.00250, and the variance coefficient of 20.1%.

Figures 9-15 and 9-16 show the cumulative distribution function of failure probability in uniform, normal probability scales, respectively.

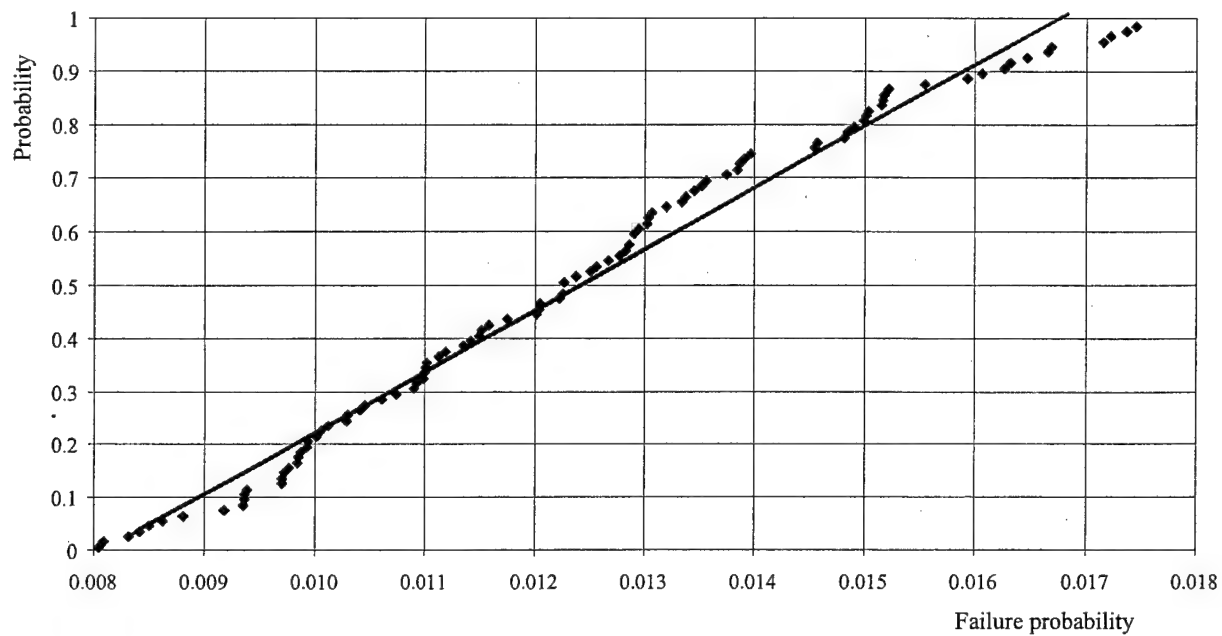


FIGURE 9-15. CUMULATIVE DISTRIBUTION FUNCTION OF FAILURE PROBABILITY DUE TO UNCERTAINTIES IN LOAD-STRESS TRANSFER, STRUCTURAL SIZE, AND STATIC STRENGTH (Uniform probability scale)

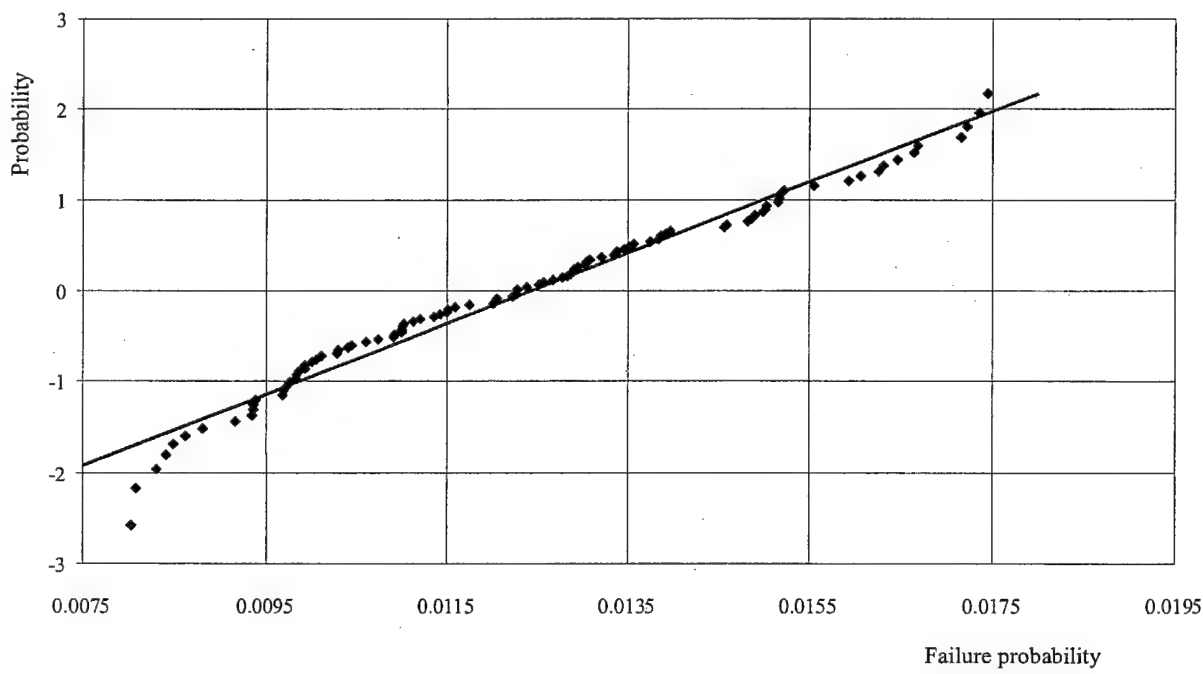


FIGURE 9-16. CUMULATIVE DISTRIBUTION FUNCTION OF FAILURE PROBABILITY DUE TO UNCERTAINTIES IN LOAD-STRESS TRANSFER, STRUCTURAL SIZE, AND STATIC STRENGTH (Normal probability scale)

It is very difficult to substantiate a particular distribution of the failure probability estimate. As seen visually, the empirical distribution is better described by the uniform function (see figure 9-15) than by the normal function (see figure 9-16). Hypotheses were validated by using the Anderson-Darling criterion for the normal distribution and by using the  $n\omega^2$  criterion for the uniform distribution  $F(x) = (x-a)/b$ ; it has been found that the normal distribution hypothesis does not contradict the sample at the significance level  $\alpha = 0.056$ , and the uniform distribution at  $\alpha > 0.25$ . With this, the uniform distribution would be preferred. Parameters of the uniform distribution are  $a = 0.008105$  and  $b = 0.0086155$ . The theoretical value of failure probability varies by a factor of 2.063. At a probability of 0.9, the failure probability estimate is from 0.00864 to 0.0163.

\* \* \*

For the ProDeCompoS system, an analyses was conducted that made it possible to determine the failure probability range as a function of reliability of initial data. The analyses allow designers to evaluate the laws of distribution of  $\beta$  at various types of distribution of major parameters. The estimates suggest the value of  $\beta$  provided by ProDeCompoS is rather reliable for designers to judge the strength of a structure.

## 10. CONCLUSIONS.

The methodology of the ProDeCompoS which evaluates the statistically based probabilistic design to improve structural efficiency of damage tolerant composite aircraft structures, was described. It includes databases and application programs that form an automated complex. The use of ProDeCompoS was demonstrated by calculating the reliability of four composite components: a highly maneuverable MiG-29 fin, a transport TU-204 aileron, a business jet Lear Fan-2100 wing, and an aerobatic SU-29 wing.

The robustness of ProDeCompoS was evaluated by a method which estimated the spread and confidence intervals for failure probability. The method was demonstrated in the analysis of the MiG-29 fin. The analysis showed that the reliability estimates are quite stable for the range of expected variations of input data.

## 11. REFERENCES.

1. A. Ushakov, A. Kuznetsov, A. Stewart, and I. Mishulin, "Probabilistic Design of Damage Tolerant Composite Structures," final report under Annex 1 to Memorandum of Cooperation AIA/CA-71 between the Federal Aviation Administration (FAA) and Central Aerohydrodynamic Institute (TsAGI), Moscow, 1996.
2. A. Ushakov, "A Framework for Ensuring Damage Tolerance of Polymeric Composite Airframes Through the Proper Design Philosophy and Manufacturing Methods," Doctoral Thesis, Moscow, 1991 (in Russian).
3. P.M. Gary and M.G. Riskalla, "Development of Probabilistic Design Methodology for Composite Structures," Vought Aircraft Company, DOT/FAA/AR-95/17, August 1997.
4. Yu. A. Stuchalkin, A.V. Stewart, and A.E. Ushakov, "Characteristics of Certification of Composite Structures," Chapter 7, *Topics in Composite Materials in Aerospace Design*, Ed. G.I. Zagainov, Chapman & Hall Publishers in Science, Technology, Medicine, and Business, London, 1995.
5. Ya. S. Borovskaya, S.M. Naumov, V.F. Panin, and Yu. G. Chernov, "Study on Strength Characteristics of Adhesive-Bonded Structures With Honeycomb Core Upon Repair," *Design and Structural Analysis of Airframes*, Trudy TsAGI, No. 2629, 1997 (in Russian).
6. J.H. Myhre and C.E. Beck, "Repair Concepts for Advanced Composite Structures," *Journal of Aircraft*, Vol. 16, No. 10, 1979.
7. C. Bullock, "Repairing Composite Structures," *Interavia*, N. 4, 1983.
8. R.H. Stone, "Field-Level Repair Materials and Processes," SAMPE28, National Symposium Proceedings, 1983.
9. H. Wicker, "Composite Structures Repair," ICAS Proceedings, Vol. 2, 1982.
10. A. Ushakov, "Strength Analysis of Carbon Fiber Reinforced Plastic Skin With Cutouts Subjected to Uniaxial Loading," *Design Stress Analysis and Testing of Structures Made of Composite Materials*, TsAGI, Moscow, 1984, Issue 11 (in Russian).
11. Yu. P. Trunin and A.E. Ushakov, "Some Problems of Evaluating and Ensuring Damage Tolerance of Aircraft Composite Structures," *Design Stress Analysis and Testing of Structures Made of Composite Materials*, TsAGI, Moscow, 1984, Issue 10 (in Russian).
12. M.E. Waddoups, J.R. Eisenmann, and B.E. Kammski, "Macroscopic Fracture Mechanics of Advanced Composite Materials," *Journal of Composite Materials*, Vol. 5, No 10, 1971.
13. J.M. Whitney and R.J. Nuismer, "Stress Fracture Criteria for Laminated Composites Containing Stress Concentrations," *Journal of Composite Materials*, Vol. 8, 1974.

14. K.H. Lo, E.M. Wu, and D.Y. Komshi, "Failure Strength of Notched Composite Laminates," *Journal of Composite Materials*, Vol. 17, IX, No. 5, 1983.
15. R.B. Pipes, R.C. Wetherhold, and J.W. Giblespie, "Notched Strength of Composite Materials," *Journal of Composite Materials*, Vol. 13, 1979.
16. J.W. Mar, "Fracture, Longevity, and Damage Tolerance of Graphite/Epoxy Filamentary Composite Materials," *Journal of Aircraft*, 1, Vol. 21, No. 1, 1984.
17. O.L. Bowie, "Analysis of an Infinite Plate Containing Radial Cracks Originating From the Boundary of an Internal Circular Hole," *Journal of Mathematics and Physics*, Vol. 35, 1956.
18. R. Peterson, "Stress Concentration Factors," Mir, Moscow, 1977 (in Russian).
19. Yu. G. Odinokov, "Structural Analysis of Airplanes," Mashinostroenie, Moscow, 1973 (in Russian).
20. A.V. Stewart, V.M. Chizhov (TsAGI), and M.Yu. Legnyov (MFTI), "Extrapolation of Load Occurrence Rate Curves for Computing the Airframe Fracture Probability," TVF, No. 6, 1998 (in Russian).
21. Selikhov, A.E. and V.M. Chizhov, "Probability Approach to Airplane Structural Analyses," Mashinostroyeniye, Moscow, 1987 (in Russian).